Model Systems for Self-Assembly

Universiteit Utrecht

Cover design: Daniela Kraft.

ISBN 978-90-393-5435-3
Subject headings: Colloids / patchy particles / colloidal micelles / depletion interaction / Pickering emulsions / colloidal phase transfer / thermodynamic stability / virus assembly.

Model Systems for Self-Assembly

Model systemen voor zelf-ordening

(met een samenvatting in het Nederlands)

Modellsysteme für Selbstassemblierung

(mit einer Zusammenfassung in Deutsch)

Proefschrift

ter verkrijging van de graad van doctor aan de
Universiteit Utrecht op gezag van de rector magnificus,
prof. dr. J. C. Stoof, ingevolge het besluit van het
college voor promoties in het openbaar te verdedigen
op 1 november 2010 des middags te 2.30 uur

door

Daniela Jutta Kraft

geboren op 5 februari 1983 te Würzburg

Promotor: Prof. dr. W. K. Kegel

Het in dit proefschrift beschreven onderzoek werd gefinancierd door het gebied chemische wetenschappen (CW) van de Nederlandse Organisatie voor Wetenschappelijk Onderzoek (NWO).

Contents

List of publications

This thesis is based on the following publications:

- Daniela J. Kraft, Wessel S. Vlug, Carlos M. van Kats, Alfons van Blaaderen, Arnout Imhof and Willem K. Kegel, *Self-Assembly of Colloids with Liquid Protrusions*, Journal of the American Chemical Society, 131(3), pp 1182-1186 (2009). This work was highlighted in Science: *A Colloidal Erector Set*, Science, 323, p. 855 (2009). (Chapter 2 and 5)
- Daniela J. Kraft, Jan Groenewold and Willem K. Kegel, *Colloidal Molecules with Well-Controlled Bond Angle*, Soft Matter, 5(20), pp 2823-3825 (2009). (Chapter 3)
- Daniela J. Kraft, Jan Hilhorst, Maria A.P. Heinen, Andrei V. Petukhov and Willem K. Kegel, *Patchy Polymer Particles with Tunable Anisotropy Dimensions*, accepted for publication in the special issue "Clusters in Complex Fluids" of the Journal of Physical Chemistry B. (Chapter 4)
- Daniela J. Kraft, Ran Ni, Michiel Hermes, Kisun Yoon, David Weitz, Alfons van Blaaderen, Marjolein Dijkstra and Willem K. Kegel, *Experimental Observation of Colloidal Micelles*, in preparation. (Chapter 6)
- Daniela J. Kraft, Julius W. J. de Folter, Bob Luigjes, Sonja Castillo, Stefano Sacanna, Albert P. Philipse and Willem K. Kegel, *Conditions for Equilibrium Solid-Stabilized Emulsions*, The Journal of Physical Chemistry B, 114, pp. 10347-10356 (2010). (Chapter 7)
- Daniela J. Kraft, Bob Luigjes, Julius W. J. de Folter, Albert P. Philipse and Willem K. Kegel, *Evolution of Equilibrium Pickering Emulsions: A Matter of Time Scales*, The Journal of Physical Chemistry B, 114, pp. 12257-12263 (2010). (Chapter 8)
- Daniela J. Kraft, Albert Philipse and Willem K. Kegel, *Equilibrium Pickering Emulsions from Carboxylic acids*, in preparation. (Chapter 9)
- Daniela J. Kraft, Willem K. Kegel and Paul van der Schoot, *Kinetic Zipper Model for Self-Assembly of Tobacco Mosaic Virus*, to be submitted. (Chapter 10)

Other papers by the author:

- Daniela J. Kraft, Roger D. Bengtson, Boris N. Breizman, D. G. Chavers, Chris C. Dobson, J Jone and V T Jacobson, *Analysis of multifrequency interferometry in a cylindrical plasma*, Review of Scientific Instruments, 77, 10E910 (2006).

1

General Introduction

1.1. Self-Assembly

Order spontaneously emerging from chaos is one of the most fascinating features of biological and physical systems in nature. Rippled sand dunes, crystallization of liquids upon freezing, the formation of schools of fish or flocks of birds, the assembly of virus particles from protein molecules and genetic information encoded in nucleic acid molecules, and the swirling spirals of chemical reactions (Turing patterns) are just a few of the compelling systems where order spontaneously emerges from a more disordered system consisting of small interacting building units. In the above examples, the building blocks were sand grains, atoms or molecules, a single fish or bird, the protein and nucleic acid molecules, and the chemical species taking part in the reactions, respectively. Such systems are called self-organized or self-assembled, depending on whether energy is required to maintain the order.

Definitions for the processes of self-assembly and self-organization vary across the sciences, and efforts to extract the common elements that allow to define and distinguish these concepts are still ongoing. [**1, 2**] Halley and Winkler recently suggested to differentiate the two concepts on thermodynamic grounds, with self-organization being a nonequilibrium process, and self-assembly implying a spontaneous process that strives to achieve thermodynamic equilibrium. More detailed, their definition of self-assembly is:

> Self-assembly is a nondissipative structural order on a macroscopic level, because of collective interactions between multiple (usually microscopic) components that do not change their character upon integration into the self-assembled structure. This process is spontaneous because the energy of unassembled components is higher than the self-assembled structure, which is in static equilibrium persisting without the need for energy input." [**2**]

In contrast, self-organization is a spontaneous dissipative nonequilibrium process requiring constant input of energy to maintain the formed structural order. Order between multiple components occurs through positive and negative feedbacks and combinations thereof, often involving fluctuations, bifurcations and multiple stabilities. [**2**] Example for self-organized pattern formation are the Rayleigh-Bénard convection cells created when a thin layer of oil is heated from below. [**3, 4**], the Turing patterns of chemical reaction-diffusion systems, or the ripples of sand dunes blown by the wind. However, some processes that exhibit order spontaneously may be a combination of self-assembly and self-organization, and hence the distinction is not always straightforward.

This thesis focusses on self-assembling systems, where larger structures are spontaneously formed from building blocks while lowering the free energy of the system.

1.2. Model Systems for Self-Assembly

Many self-assembling processes are taking place on length scales inaccessible to direct *in situ* observation of the structural changes. Then, information on the type and strength of the interactions between building blocks, and their assembly dynamics have to be deduced indirectly, for example by light scattering, electron microscopy, or macroscopic observation. Two examples are the assembly of proteins and genetic information into identical functional virus particles, and the formation of vesicles and micelles from surfactants dispersed in a solvent. Fully assembled virus particles are roughly between 25 nm (poliovirus) and 300 nm (tobacco mosaic virus), but can extend up to 1 μm (ebola virus) in length. Their building blocks are proteins that form the virus capsid and nucleic acid that gets encapsulated in the capsid during the assembly. Both are much smaller than the overall virus size, typically a few nm. Amphiphilic molecules such as surfactants or copolymers, which consist of hydrophilic and hydrophobic parts, readily assemble into larger structures in aqueous solutions driven by their amphiphilic nature. These structures include micelles, inverse micelles, vesicles, and bilayers, which range from a few nm to a few μm in size.

Both for the viruses as well as for surfactants, the building blocks are not visible in techniques such as light or confocal microscopy, and hence their assembly into the equilibrium structures needs to be deduced indirectly from light scattering or electron microscopy. Recent advances in cryo-electron microscopy also allow for a direct view of vitrified solutions. Yet, the technique is (still) time-consuming, and for gaining insights into assembly dynamics many samples in close need to be prepared. Furthermore, the interactions between protein molecules of a virus are varied and complex, and computationally expensive free energy landscape calculations aid in comprehension, but cannot differentiate which interactions are sufficient for the assembly and which are redundant. Model systems that capture the main features of the building blocks and the assembly are hence viable tools for understanding the underlying physical principles of the assembly. Such models can be theoretical, as well as computational or experimental when simplified building blocks with few, controlled interactions are used. In this thesis, all three approaches are employed to gain insights into various self-assembling systems.

Colloids as experimental model systems

In experimental model systems for self-assembly, the challenges present in the natural systems such as the small scale or complex interactions can be overcome or simplified. A straightforward choice for building blocks that are both directly visible by techniques such as light and confocal microscopy, yet are small enough to experience thermal fluctuations, are colloidal particles. The term colloid refers to particles with at least one of their dimensions being on the order of 1 nm to 1 μm that are dispersed in a continuous medium. Their shape and properties, such as the type and strength of their

interactions, are available in a wide variety, making them the perfect choice for studying naturally occurring self-assembling systems as well as using them as building blocks for new, rationally designed self-assembling structures. Due to these tunable properties, colloidal spheres have also been termed "artificial atoms". The challenge for properly modeling or controlling the assembly lies in finding colloidal particles with compatible shape and interactions.

Anisotropic colloidal particles with "patchy" interactions

The simplest colloidal shapes, such as spheres and platelets, are often insufficient to model the complex building blocks in nature. For example, amphiphilic molecules consist of hydrophobic and hydrophilic moieties, and proteins of tobacco mosaic virus are wedge shaped. Artificial assemblies of colloidal particles, for example colloidal crystals with desirable photonic or mechanic properties, have been proven to be prohibitively difficult to achieve from uniform spheres that commonly crystallize in a face centered cubic (fcc) or hexagonal close packed (hcp) crystal structure. While the last decades focused on studying mainly these basic colloid shapes, the prospect of creating nanostructures as well as macroscopic crystals "made-to-order" as predicted by recent computer simulations,[**5, 6, 7, 8, 9, 10**] has triggered renewed interest into development of colloidal particles with controlled anisotropic shapes and interactions.[**11, 12**]

To extend the possible structures two approaches are conceivable: (1) directional, site-specific interactions, and (2) anisotropic colloidal particles, or a combination of both. For crystallization prearranged clusters of colloidal spheres may suffice to achieve new crystal structures even in the absence of additional interactions. In analogy with spherical colloids and atoms, such clusters consisting of spherical particles have also been termed "colloidal molecules".[**13**] For more complex arrangements or crystals build up of unit cells not easily achievable by present synthesis techniques, site-specific interactions need to be added. As many interactions, such as Van-der-Waals, electrostatic, and depletion forces are centrosymmetric, site-specificity of the interactions have to be integrated on the particles level. To break their symmetry, colloidal particles with specific sites that for example strengthen or weaken the interaction have to be used. These colloidal particles with discrete, attractive or repulsive sites are also called "patchy" particles. [**14, 15**] The number, size and location of the patches are expected to determine the self-assembled structure. Yet, truly patchy particles with flexible number and position of patches are still elusive. Two realizations of patchy colloids based on liquid protrusions (**Chapter 2 and 3**) and site-specific depletion interaction strengths (**Chapter 6**) are presented in this thesis. Furthermore, synthetic methods for making anisotropic particles that may be employed in self-assembly are presented.

Theoretical models for self-assembly

Colloidal particles are not only used as a model system for other self-assembling processes, but they themselves may take part in self-assembly unique to colloidal particles, which in turn may require a model for a better understanding. Such a system is presented in **Part 2** of this thesis. Here, mixtures of aqueous dispersions of colloidal particles and a particular oil lead to the spontaneous formation of oil droplets covered with the solid particles. The intriguing observations of the stability of these emulsions lead us to investigate the underlying physics of the stability. By systematically varying the different components, a model for these solid-stabilized emulsions is proposed, which initiated more advanced theoretical studies.

Where colloidal model systems are yet to be developed, theoretical models can further understanding of complex forms of self-assembly. Variation of the different parameters of the theoretical model may help to identify the key components required for the assembly more easily than with a colloidal model system where each variation of a parameter requires different particles and experimental conditions. With these basic requirements extracted from theory, simplified colloidal model systems may be developed more straightforwardly. One example of a complex, yet fascinating self-assembly process are virus particles, which spontaneously form from proteins that build up the virus capsids and nucleic acid that encodes the amino acid sequence of the protein. The interactions on a molecular level between proteins, and protein and nucleic acid are so varied that a theoretical model is well-suited to reduce this complexity to the relevant physical quantities, and unravel this captivating self-assembly process. Yet, knowledge about the basic physics underlying virus assembly is not only interesting from a fundamental point of view, but may also allow for the development of a colloidal model system in the future. The main function of the virus capsid is to protect and transport genetic information between cells and hosts. Colloidal models of spherical or elongated virus capsids could be used as small containers that encapsulate and release substances in a controlled fashion, for example for drug delivery. We develop a model for self-assembly of the earliest discovered virus, the rod-like tobacco mosaic virus, in **Chapter 10**.

1.3. Scope of this Thesis

This thesis is organized in four parts dealing with different models for and aspects of self-assembly.

Part 1 focuses on synthetic aspects of anisotropic patchy particles and colloidal molecules. In **Chapter 2** and **3**, a synthetic method for assembling colloidal spheres into clusters by making use of liquid patches on the particle surface, so called protrusions, is presented. While the synthesis itself is a self-assembling process, the clusters obtained through it may again be used in self-assembly studies, as building blocks in

crystallization and in finite sized patchy interactions. The obtained colloidal molecules are highly symmetric (**Chapter 2**), or have a well-controlled bond angle (**Chapter 3**). By controlling the stability of the liquid protrusions, the number of patches on each colloidal particle can be influenced. Through adsorption of secondary nucleated particles at the seed particle surface, roughness anisotropy can be introduced to the colloidal molecules (**Chapter 4**). Last, we investigate the long-term assembly of colloids with liquid protrusions into Pickering emulsions. (**Chapter 5**).

In **Part 2**, we use the roughness anisotropic colloidal particles introduced in Part 1 to make patchy particles for self-assembly. Here, we show that depletion interaction is surface roughness dependent and for particles with one patch leads to the spontaneous formation of clusters reminding of surfactant micelles. The similarities between the observed colloidal clusters and surfactant micelles are discussed and quantified by a theoretical model, and the experimental results are compared to computer simulations (**Chapter 6**).

Part 3 is dealing with self-assembling, thermodynamically stable Pickering emulsions. In **Chapter 7** the requirements for their formation and stability are investigated, and a model containing the minimally required components and conditions is developed. We find an intricate dynamic equilibrium to be present in these emulsions due to a chemical process taking place on a distinctly different timescale than the formation of the emulsions (**Chapter 8**). At last, we apply the knowledge obtained in **Chapter 7** to create particle stabilized emulsions from fatty acids (**Chapter 9**).

In **Part 4**, a theoretical model for the self-assembly of tobacco mosaic virus (TMV) particles from protein subunits and TMV RNA is developed. The model is solved analytically for equilibrium conditions, and numerically for the assembly and disassembly dynamics. The results from the model are compared with experimental data available in literature (**Chapter 10**).

Part 1

Synthesis of Colloidal Molecules

2

Synthesis of Highly Symmetric Colloidal Molecules via Self-Assembly of Colloids with Liquid Protrusions

Abstract

A facile and flexible synthesis for colloidal molecules with well-controlled shape and tunable patchiness is presented. Cross-linked polystyrene spheres with a liquid protrusion were found to assemble into colloidal molecules by coalescence of the liquid protrusions. Similarly, cross-linked polymethylmethacrylate particles carrying a wetting layer assembled into colloidal molecules by coalescence of the wetting layer. Driven by surface energy a liquid droplet on which the solid spheres are attached is formed. Subsequent polymerization of the liquid yields a wide variety of colloidal molecules with tunable patchiness. Precise control over the topology of the particles has been achieved by changing the amount and nature of the swelling monomer as well as the wetting angle between the liquid and the seed particles. The overall cluster size can be controlled by the seed size as well as the swelling ratio. Use of different swelling monomers and/or particles allows for chemical diversity of the patches and the center. For low swelling ratios assemblies of small numbers of seeds resemble clusters that minimize the second moment of the mass distribution.

2.1. Introduction

Anisotropic particles that resemble molecules or have an integrated patchiness are of great interest in the field of colloid and material science [**14, 15, 11, 13**]. They may be used as basic building blocks for hierarchical self-assembly [**16**], which is expected to facilitate and expand the range of possible colloidal structures such as clusters,[**14, 17, 7, 8**] liquid [**18**] and crystal phases. [**19**] They are likely candidates to succeed in the search for new materials with custom made properties as they may mimic molecular self-assembly through shape and directional interactions. [**7, 20, 21**]

Different methods are known to create colloidal molecules as well as patchy particles. Colloidal clusters can be made in a controlled way by evaporating toluene droplets in water containing colloids in the oil phase. [**22**] Upon evaporation, the capillary forces pack the colloids into clusters whose topology only depends on the number of spheres they contain. The cluster structures were found to minimize the second moment of the mass distribution. [**23**] Addition of a second type of smaller colloids to the droplets created binary colloidal clusters. The surrounding smaller colloids did not affect the configurations of the larger colloids. [**24**] However, the number of small colloidal particles per cluster cannot be controlled in the emulsification step, resulting in polydisperse particles. Sonicating UV-curable oil drops with adsorbed colloidal particles lead to similar clusters with a central body comprised not of colloids but of polymerizable oil. [**25**] Again, due to the emulsification step this approach does not provide control over the size of the center. The polydisperse shapes are a major drawback for model systems where monodisperse colloids with controlled shape and patchiness are required. Here, we take a different approach to make colloidal molecules by starting from colloidal particles with liquid protrusions. This new method provides unique control over the obtained colloidal shapes.

Sheu et al. [**26, 27**] found that heating monomer-swollen cross-linked polystyrene spheres of a few micrometer causes phase-separation of the monomer from the seed particle in form of an aspherical protrusion from the particle. Covering the seed particle surface with a hydrophilic layer of vinyl acetate or acrylic acid allowed Mock et al. [**28**] to extend this technique to smaller colloids of about 250 nm.

Here, we show that delaying the polymerization of the liquid protrusions leads to coalescence of the droplets upon collision, thereby creating colloidal molecules in a simple one-step synthesis. Our new technique allows for tuning the topology from colloidal clusters to patchy particles via adjustment of the swelling ratio and hydrophilicity of the particle surface. This uniquely provides precise control over the shape and patchiness of the resulting particles. We demonstrate the generality of the method by conducting the synthesis both for polystyrene and polymethylmethacrylate and by using different swelling monomers.

2.2. Experimental

2.2.1. Colloidal particles

Synthesis of monodisperse cross-linked polystyrene spheres Monodisperse cross-linked polystyrene spheres (CPS) were prepared using an emulsion polymerization procedure described previously [**28**]. All components were used as received.

A 1 liter round bottom flask equipped with a PTFE stir bar was placed in an 80°C oil bath. 400 mL deionized water was charged into the reactor and allowed to reach bath temperature. Then 47 mL (42.3 g) styrene (99% purity, Merck) and 0.500 g sodium dodecylsulfate (BDH) dissolved in 50.0 mL of deionized water were added, followed by 50 mL of rinse water. To cross-link the latex colloids 1.39 mL (1.27 g) of divinylbenzene (DVB, 55% mixture of isomers, tech. grade) was added yielding a cross-linking density of 3% w/w. The ingredients were allowed to mix and reach the temperature of the oil bath for one hour. Addition of 1.55 g potassium persulfate dissolved in 75.0 mL deionized water initiated the reaction. Polymerization was allowed to continue for 24 hours. The resulting colloidal CPS suspension had a weight fraction of 7% w/w. The sphere radius was determined by TEM to 113 nm with a polydispersity of 3.4%.

Vinyl-acetate coating of cross-linked polystyrene spheres A part of the CPS suspension was consequently coated with vinyl acetate (surface coverage $3.56{\cdot}10^{-21}\mathrm{g/nm}^2$ in order to increase the hydrophilicity of the surface. For this a round bottom flask equipped with a PTFE stir bar was immersed in an oil bath at 80° C. It was charged with 200 mL of the colloidal polystyrene solution and allowed to reach bath temperature for 1 hour. Addition of vinyl acetate took place in four steps spaced by 15 minutes, each containing 25% of the total mass of 135 mg of vinyl acetate. With the first addition of vinyl acetate 5.05 mL potassium persulfate (1 g/150 g Millipore water) were charged to the reaction vessel for initiation. Polymerization was allowed to continue for 24 hours after the last addition. The sample was purified by washing it three times with Millipore water and redispersed by addition of 1.33 g sodiumdodecylsulfate (SDS) in 80 mL water. The final suspension of about 400 mL contained 2.6% w/w polystyrene spheres by weight measurement of 1 mL. The radius was determined to 111.1 nm with a polydispersity of 2.5% by TEM.

Synthesis of monodisperse cross-linked PMMA spheres Monodisperse cross-linked polymethylmethacrylate (PMMA) spheres were prepared using a surfactant free emulsion polymerization procedure according to a modified procedure of Paquet et al. [**29**]. A 250 mL round bottom flask equipped with a reflux cooler was filled with 90 mL of deionized water and 0.24 g of potassium persulphate (0.01 M KPS) and magnetically stirred. The flask was put in a thermostatted oil bath at 80.0°C and kept

at that temperature for 30 minutes to allow for radical formation of the KPS. A separate vial was filled with 10.0 g of monomer, which consisted of a mixture of methyl methacrylate (MM) and methacrylic acid (MA) in a weight ratio of 90:10, 0.1 g (1% w/w) cross-linking agent ethylene glycol dimethacrylate (EGDMA), and 47.4 μL of 1-dodecanethiol (DDM). The content of the vial with the monomer mixture was added to the round bottom flask under vigorous stirring. The polymerization was allowed to proceed for 2 hours. The resulting seed particles measured 220 nm in radius by scanning electron microscopy (SEM).

Commercial cross-linked polystyrene spheres Sulfated 1.88 μm polystyrene spheres, cross-linked with 5% divinylbenzene were ordered from Magsphere Company and used at 3% w/w concentrations for synthesis of colloidal molecules.

2.2.2. Characterization

Density Gradient Centrifugation Colloidal molecules could be separated into distinct bands by use of density gradient centrifugation. After separation, each band was washed three times by centrifugation and redispersation in deionized water.

Microscopy Polymerized samples were imaged using a scanning electron microscope (SEM XL FEG 30). The PS and PMMA particles were sputter coated with 4 nm platinum/paladium and gold, respectively, prior to imaging. Light microscopy was performed with a Zeiss Axioplan microscope using an oil immersion lens (NA=1.4, 100x magnification). Pictures were captured with a Basler scout camera.

2.2.3. Synthesis of Colloidal Molecules

For each of the experiments with CPS seeds varying volumes of the seed suspensions were added to a glass flask equipped with a magnetic PTFE-coated stir bar. We define the amount of monomer $m_{monomer}$ added to the suspension divided by the polymer mass present in the seed solution as the swelling ratio

$$S = \frac{m_{monomer}}{m_{seed\ polymer}}. \tag{2.1}$$

Additionally, 1% w/w SDS was added to the 1.88 μm CPS samples. All samples were stirred vigorously during swelling for about 1-2 days and subsequently placed in an 80°C oil bath. Heating causes phase separation of the monomer taken up by the cross-linked polymer network resulting in the formation of a droplet on the colloidal surface [**28, 30, 31**]. The hydrophilicity of the surface determines the wetting angle between the monomer and the colloidal surface. The less favorable it is for the monomer to wet the surface, the more aspherical the protrusion is to the extent of forming a separate droplet.

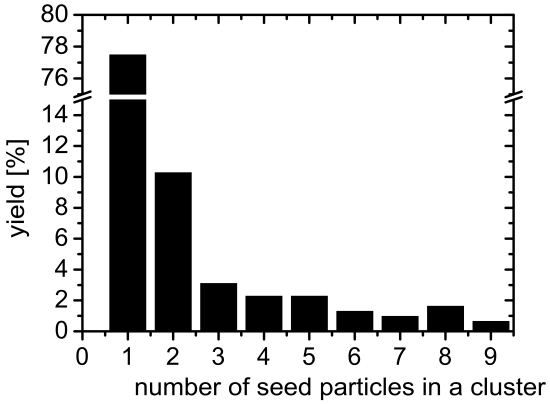

Figure 2.1. Yield of clusters of N seed particles for swelling ratio ($S = 3.4$), such as shown in Figure 2.3A.

For CPS seed particles 222 nm in size we have never observed more than one protrusion on the particles. For the larger colloidal particles of 1.88 μm we sometimes found secondary protrusions, which are significantly smaller than the primary protrusion. However, they were only present if polymerization was induced after short coalescence times. The formation of more than one protrusion is an unfavorable state in terms of surface energy, and protrusions on the surface of one seed particle coalesce over time. Yet, if stabilized sufficiently multiple protrusions obtained in a controlled fashion can be utilized to make anisotropic particles as well, see Chapter 4. We expect that coalescence of protrusions on larger seed particles takes place on a longer time scale compared to that on the smaller particles due to their larger diameter.

After the formation of a droplet on the colloid surface the samples were taken out of the oil bath and left stirring for several days. During this period colloidal molecules were formed. Subsequent polymerization was carried out at 80°C by addition of hydroquinone (0.75 mM, 99% purity, Riedel), a water soluble inhibitor, and azobisisobutyronitrile (0.94 mg AIBN dissolved in 0.046 mL styrene per mL of seed suspension) after heating for about one hour. Polymerization was allowed to continue for 24h. The syntheses typically yielded about 10% dimers and another 12% of higher multimers after a coalescence time of 24h (see Figure 2.1.

For the formation of PMMA colloidal molecules a similar procedure was followed with a shorter clustering time. A 250 mL round bottom flask equipped with a PTFE-coated stir bar and a reflux condenser was used. 60 mL of a diluted (2.5% v/v) and washed seed dispersion in water was added to the flask along with 0.01 g of AIBN. The flask was put in a thermostatted oil bath at 80°C and allowed to reach bath temperature in 30 minutes. Then a 24.44 g MM/MA mixture (10 % w/w MA), 0.1123 g EGDMA, 71.1 μL DDM and 0.1805 g AIBN were added dropwise at a rate of 1 drop every 3

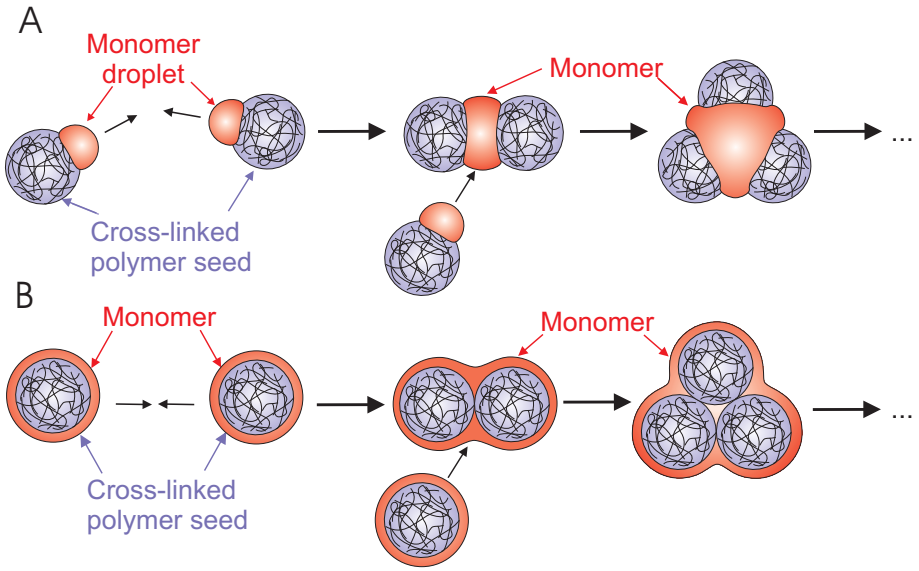

Figure 2.2. Schematic of merging of (A) liquid protrusions or (B) wetting layers yielding colloidal molecules.

seconds under vigorous stirring. When the monomer addition was complete (typically 30 minutes) the reaction was allowed to proceed for another 2 hours. The coagulum that formed was removed and the remaining particles were cleaned by centrifugation and redispersion in deionized water.

In the case of PMMA seed particle protrusions were not observed, but the particles grew from a 220 nm to 335 nm radius. Small clusters formed if the monomer was a mixture of MM and MA containing at least 5% MA. The number as well as the size of clusters increased with the MA percentage. Also, a higher percentage of MA in the seed particles favored cluster formation. We found that 10% MA in both the seed and the swelling monomer was a suitable value to obtain clusters in good yield: about 16% dimers and 16% of higher multimers were found.

From the formation mechanism it is expected that the distribution of multimers shifts to higher cluster sizes N the longer the coalescence is allowed to continue. This means that there is no unique distribution of clusters as it depends on the rate of formation. In the beginning mainly monomers, dimers and trimers are expected, whereas at later stages larger clusters should prevail.

2.3. Results and Discussion

2.3.1. Topology of clusters

Each batch of colloidal particles made by this method contained a distinct variety of colloidal molecules comprised of different numbers of seed spheres. They are formed by merging of the liquid droplet upon collision as is shown schematically in Figure 2.2. The size of the protrusion can be chosen by the wetting properties of the seeds and by

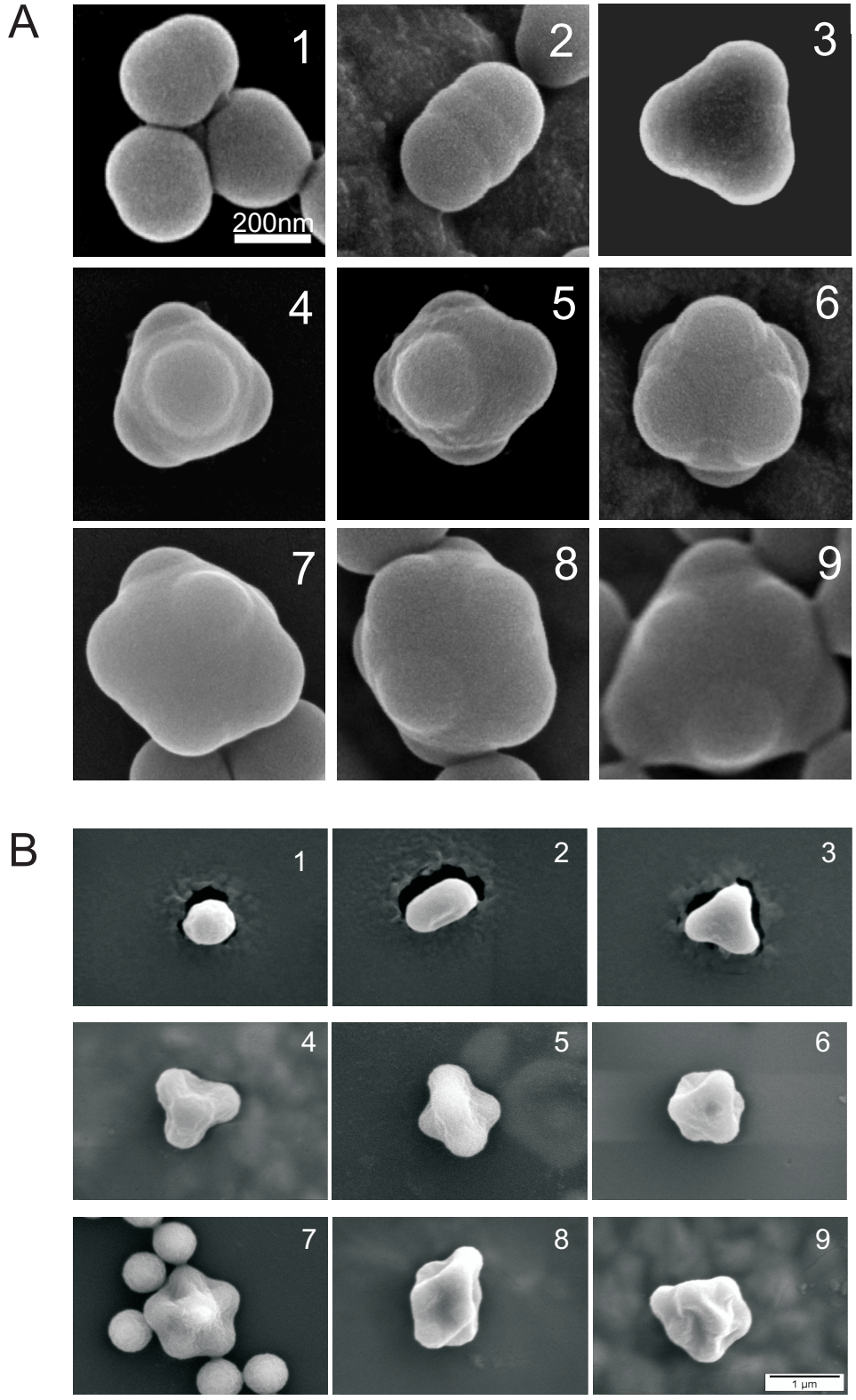

Figure 2.3. Scanning electron micrographs of colloidal molecules for N=1 to N=9 created by merging of liquid protrusions. A) Vinyl acetate coated polystyrene spheres with $R_{seed} = 111$ nm used as seed particles, swelling ratio 3.4. B) PMMA seed particles of radius $R_{seed} = 220$ nm with a wetting layer consisting of methacrylic acid/methyl methacrylate.

the swelling ratio, yielding colloidal molecules that ranged from cluster-like particles up to patchy spheres. A representative example of colloidal molecules ($N = 1 - 9$) made from vinyl acetate coated CPS spheres swollen with styrene ($S = 3.4$) is shown in Figure 2.3A. In this case a distinct protrusion was present as can be seen for the case $N = 1$. Also, each cluster of N seeds has a unique central body with a volume roughly equal to N times the protrusion volume. In the case of PMMA seeds a protrusion or a central droplet were not observed, while the particles had grown significantly. Clusters were formed nonetheless as is shown in Figure 2.3B for $N = 1 - 9$. From these images it is apparent that clusters have become enveloped in an outer skin. Thus, we conclude that the PMMA seeds cluster due to merging of a wetting layer of monomer covering the whole seed surface.

Interestingly, all colloids with a given number of seed particles have identical geometry, supporting the idea of minimization of the second moment of the mass distribution, as will be discussed in the next section. The particles could be separated according to their weight by density gradient centrifugation (Figure 2.4).Within each band, only a single type of colloidal molecule with unique topology was found. In the top band, colloids with one protrusion were found. In the second, third and subsequent bands, colloidal molecules with two, three and many seed particles were present, respectively. Spherical clusters containing a large number of spheres on the surface ($N \approx 10^2 - 10^4$) are known as colloidosomes and were found up to a size of 14μm for high swelling ratios (see Chapter 5). The unpolymerized clusters could be observed by light microscopy using larger, 1.88μm, styrene swollen (S=3) and heated polystyrene spheres as shown in Figure 2.5. They exhibit the same colloidal clusters as CPS seeds 222 nm in size (Figure 2.3). This further shows that the technique is not restricted to a specific seed size, nor is induced by polymerization of the sample.

2.3.2. Control of Particle Anisotropy via Swelling Ratio

A facile way to influence the topology of the resulting colloids is the swelling ratio. A higher swelling ratio results in a larger liquid protrusion after heating as can be seen from the SEM pictures of polymerized colloids for $N = 1$ in Figure 2.6. Note that for swelling ratios $S = 1.1$ and $S = 3.4$ (Figure 2.6A, B) the seed particle is larger than the protrusion, whereas for $S = 5.6$ (Figure 2.6 C) the protrusion is larger than the seed sphere. After merging the protrusion volume determines the size of the liquid center of the resulting colloids (Figure 2.6, $N = 2$ and 3). With an increasing swelling ratio the relative size of the seed particle compared to the droplet shrinks gradually changing the shape of the colloidal molecules from cluster-like to spheres with patches. Manoharan et al. created colloidal clusters by evaporating toluene droplets in water with colloids adsorbed to the oil-water interface. [**22, 32**] Upon evaporation the capillary forces pack the colloids into clusters identical for a given number of spheres and

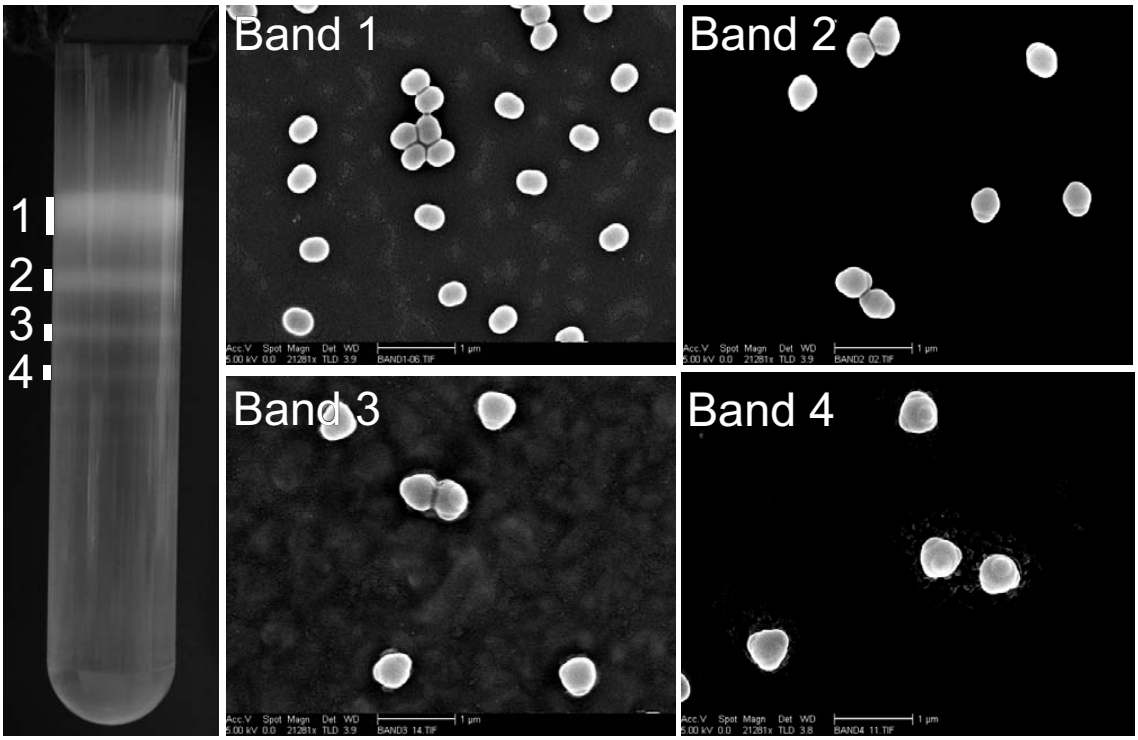

Figure 2.4. A) Density gradient centrifugation in a 3%-9% wt/wt Ficoll 400 gradient in 1% wt/wt Pluronic F127/millipore water yields bands that each contain one type of colloidal molecules each. From top to bottom we find (B) monomers, (C) dimers, (D) trimers, (E) tetramers etc. as shown in the SEM pictures.

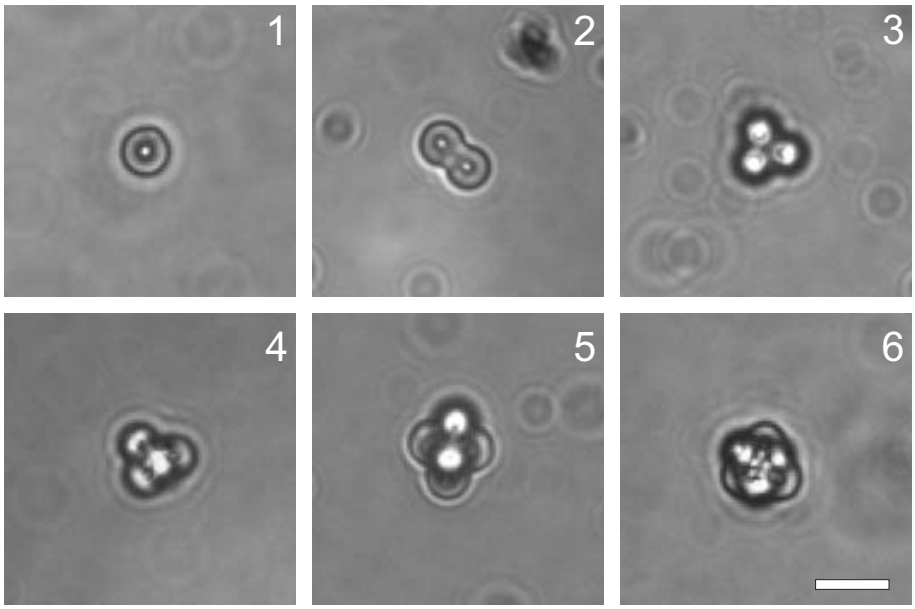

Figure 2.5. Light microscope images of colloidal molecules for N=1 to N=6; CPS seeds with a diameter of 1.88 μm, swelling monomer was styrene (S = 3.2). Scalebar is 5 μm.

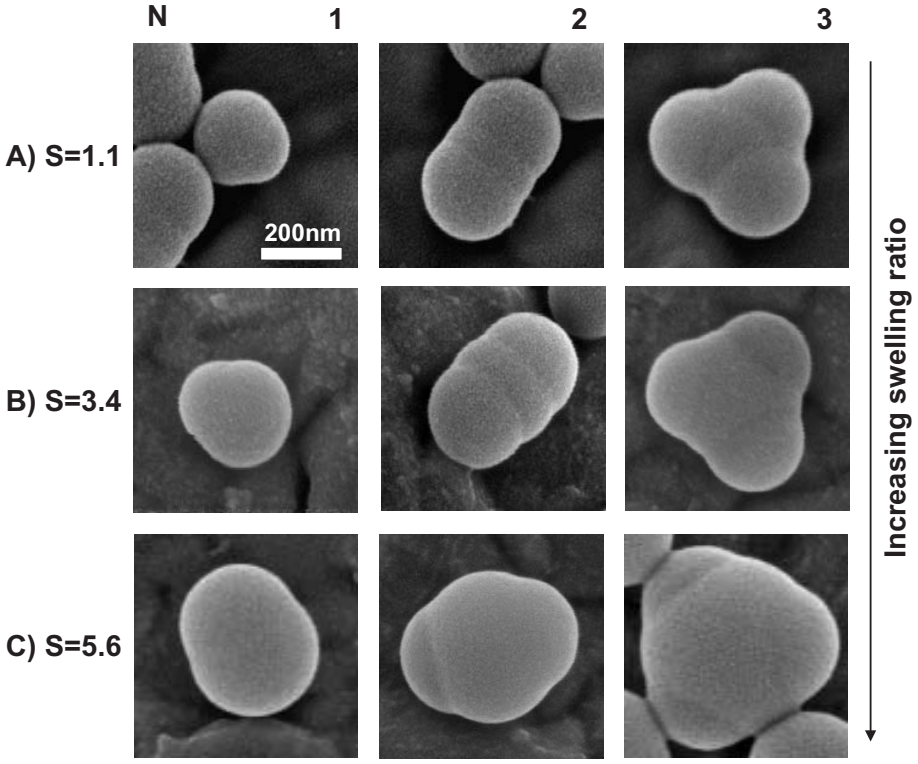

Figure 2.6. Swelling vinyl acetate coated polystyrene spheres of $R_{seed} = 111$ nm with different amounts of styrene changes the geometry of the resulting multimers. SEM pictures show clusters of N=1-3 polystyrene spheres with swelling ratios 1.1, 3.4, 5.6.

that minimize the second moment of the mass distribution, $M_2 = \sum_{i=1}^{N} |\vec{r}_i - \vec{r}_0|^2$, where $\vec{r}_i$ is the center coordinate of the ith sphere and $\vec{r}_0$ is the center of mass of the cluster. [**23**] In our colloidal system spheres are attached to an oil-water interface as well. At low swelling ratios interfacial tension compresses the spheres to form clusters partially immersed in a liquid droplet. This may be comparable to the late stage of droplet evaporation. Despite the extra oil contained in the center this explains why we still find the same arrangement of seed spheres inside the liquid center as Manoharan et al.. [**22**] Defining the center of the sphere as a vertex of a polyhedron we find for the lowest order configurations (Figure 2.3): line segment ($N = 2$), triangle ($N = 3$), tetrahedron ($N = 4$), triangular dipyramid ($N = 5$), octahedron ($N = 6$), pentagonal dipyramid ($N = 7$), snub disphenoid ($N = 8$) and triaugmented triangular prism ($N = 9$) (Figure 2.3).

2.3.3. Control of Particle Anisotropy via the Wetting Angle

The seed particles determine the resulting patch size both by their own diameter as well as by the wetting angle between the liquid protrusion, the aqueous phase and the polymer seed particle. Adjustment of either the liquid or the polymer wetting

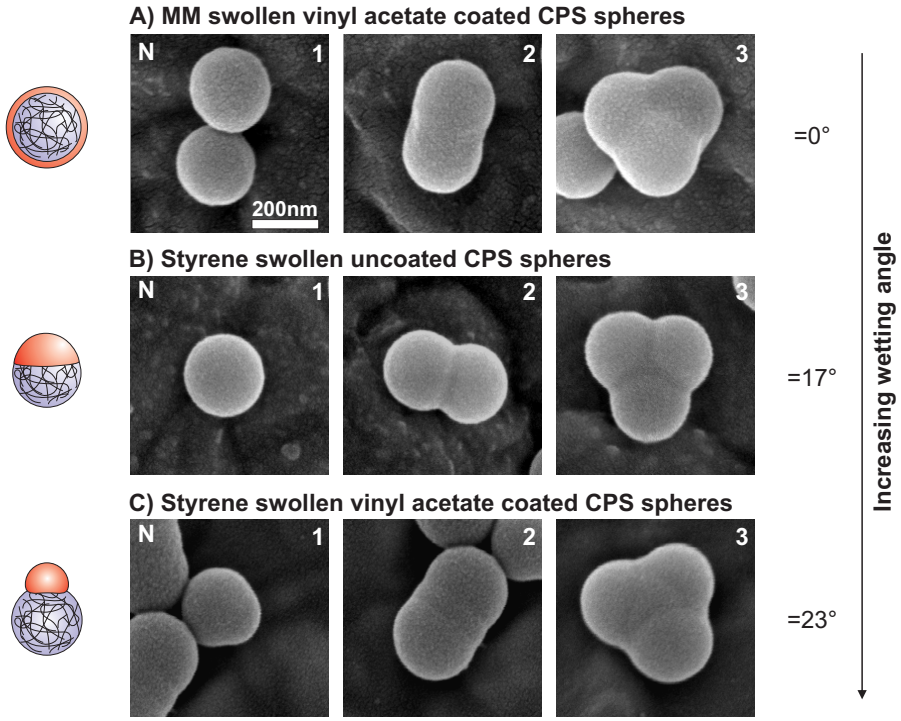

Figure 2.7. A larger wetting angle creates colloidal molecules with a more pronounced delineation between the liquid center and the seed particles. The wetting angle increases from top to bottom, using a hydrophilic monomer, methyl methacrylate ($S = 3.3$), and styrene on uncoated and vinyl acetate coated polystyrene spheres ($S = 1.1$).

properties therefore affects the shape of the colloidal molecules. This can be done by use of different seed particles, coatings, swelling monomers and different amounts of surfactant. Both acrylic acid and vinyl acetate coatings are known to render polystyrene seeds more hydrophilic leading to more pronounced protrusions [**28**]. The same can be observed for the synthesis of colloidal molecules. Uncoated polystyrene spheres exhibit a smaller wetting angle of $\theta = (17 \pm 3)°$(Figure 2.7B) than vinyl acetate coated polystyrene spheres when swollen with styrene (Figure 2.7C), which have a wetting angle of $\theta = (23 \pm 2)°$. Even this small difference in wetting angle leads to a clear influence on the shape of the resulting colloidal particles. Different swelling monomers also lead to different wetting angles between the droplet, seed particle and aqueous phase, as can be seen in Figure 2.7. Complete wetting, i.e. $\theta = 0°$, of vinyl acetate coated polystyrene spheres can be achieved by swelling the seeds with a more hydrophilic monomer, methyl methacrylate, leading to polymethylmethacrylate covered CPS clusters (Figure 2.7A). The latter case leads to identical looking clusters as the one made from PMMA seeds (Figure 2.3B), where no protrusions were formed because of a complete wetting of the MM/MA mixture on the PMMA particle.

An advantage of using PMMA as seeds is that those particles can be both refractive index and density matched which makes them suitable for confocal microscopy studies on concentrated suspensions. Use of different monomers to swell the seed particles may also give rise to different chemical properties of the colloidal body and the patches. This could be used to create spheres with sticky patches. [**31**]

2.4. Conclusions

We have shown that colloids with liquid protrusions spontaneously merge forming colloidal molecules that range from cluster-like particles up to the size of colloidosomes. The presented technique uniquely allows for tuning of the colloidal shape via the size of the seed particles, swelling ratio and hydrophilicity of the polystyrene or polymethylmethacrylate surface. Chemical properties can be altered by use of different monomers and subsequent modification. Combining all of the above a wide variety of colloidal molecules with varying patchiness was obtained.

Acknowledgements

I thank Eric Mock for experimental insights, Hans Meeldijk and Chris Schneijdenberg for support during electron microscopy. Carlos van Kats and Wessel Vlug are thanked for their contribution on PMMA colloidal molecules, and introduction to density gradient centrifugation. I would furthermore like to thank Jan Groenewold, Arnout Imhof and Alfons van Blaaderen for useful discussion. This chapter is based in part on the unedited author's version of a Submitted Work that was subsequently accepted for publication in The Journal of the American Chemical Society, copyright American Chemical Society after peer review. To access the final edited and published work, see http://pubs.acs.org/doi/abs/10.1021/ja8079803

Appendix - Density gradient centrifuation

A 12 mL linear gradient ranging from 3% to 9% w/w Ficoll 400 in 1% w/w Pluronic F127/millipore water was prepared with a gradient mixer. For this, two solutions of 3% and 9% w/w Ficoll 400 and 1 % w/w Pluronic F127 in millipore water were filled in the two compartments of the gradient mixer (see Figure 2.8B). The solution with higher density is layered in the compartment with the outlet and continuously stirred. The outlet is connected to a tube that via a peristaltic pump transfers the Ficoll solution to the centrifugation tube. To carefully layer the solutions on top of each other without disturbing the gradient a pipette with a slightly bend tip was used. For a picture of the setup, see Figure 2.8. Samples were carefully layered on top and centrifuged for 12 minutes at 116,000g and 20°C with a Beckmann Optima L60 Ultracentrifuge yielding up to 10 clearly separated bands. The bands were taken out with a pipette with a bent tip connected to a peristaltic pump.

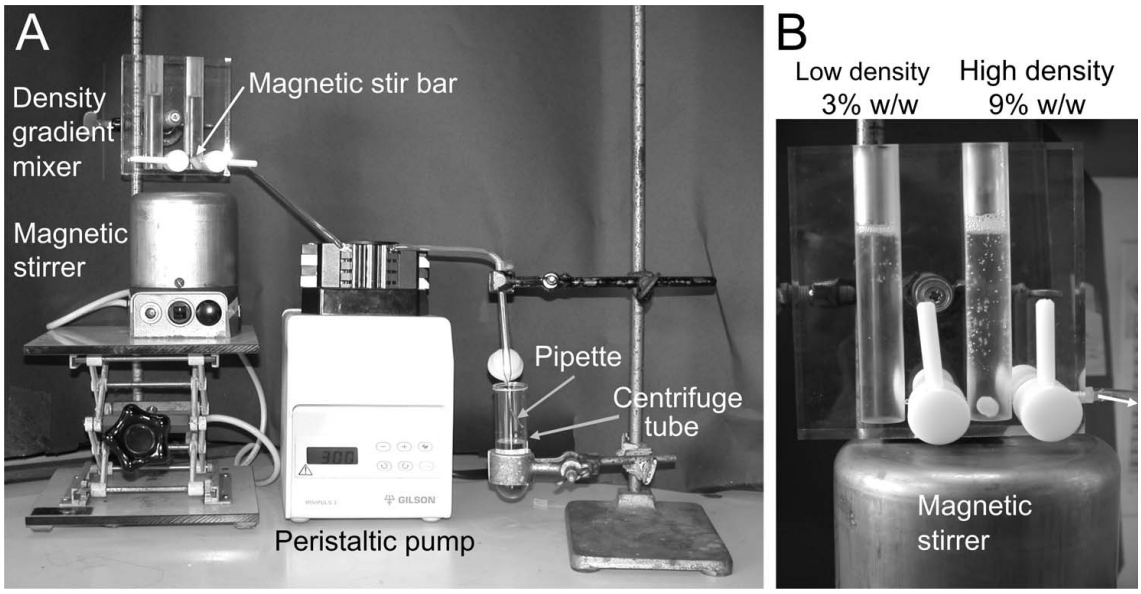

Figure 2.8. (A) Setup for preparation of the Ficoll density gradient for cluster separation according to their weight. (B) Enlarged view of the density mixer of (A).

3

Asymmetric Colloidal Molecules by Fusion of Colloids with Liquid Protrusions

Abstract

We present a straightforward technique to synthesize asymmetric colloidal molecules with uniform and well-controlled bond angles. The new method makes use of coalescence of liquid protrusions on polystyrene spheres. The bond angle between the seed particles and central sphere can be chosen as desired by adjusting the size of the liquid protrusion. The surprising uniformity of the colloidal molecules comprised of small numbers of seed particles is proven by comparison with 3D models. Considering different origins for this uniformity we conclude that the asymmetric and unique shape is induced by aggregation inside the liquid droplets upon polymerization. This technique offers a new and simple way to make a wide variety of asymmetric colloidal molecules in a reproducible and controlled fashion.

3.1. Introduction

The prospect of using colloidal particles as building blocks for colloid and material science has been a driving force to extend colloidal syntheses to a variety of shapes and materials.[**11, 34, 16**] Colloidal particles with rationally designed topologies may lead to precise control over the macroscopic assemblies of the particles.[**15**] Specifically, colloidal particles with shapes resembling space-filling models of molecules are expected to exhibit complex behavior similarly to molecules or even beyond. Taking the analogy between colloidal spheres and atoms further, such colloids are termed colloidal molecules.[**15, 13**] Simulations have predicted that these are likely candidates to form intriguing new fluid and crystal phases[**35, 18, 36, 19**] as well as finite superstructures such as rings, shells, chains and clusters. [**14, 20, 7, 8**] These crystals may form a new category of materials with novel properties, such as optical band gaps.[**21**]

Several methods have been proposed to create highly symmetric colloidal molecules [**22, 37, 24, 38, 39, 40, 33**] as well as simple asymmetric shapes such as snowman particles,[**26, 27, 30, 31, 41, 42**] or confetti-like particles[**43**]. To date only few methods either based on emulsification[**44**] or controlled aggregation[**45**] have been reported to produce more complex asymmetric arrangements. Due to the lack in control over the size and composition of particle containing emulsion droplets, it is still prohibitively difficult to obtain uniform clusters from emulsification methods. Snyder et al.[**45**] recently obtained colloidal trimers from different materials by a multi-step method of aggregation and partial polymer coating. Here, we introduce a new one-step technique to produce uniform, asymmetric colloidal molecules such as colloidal water and ammonia by coalescence of liquid protrusions attached to polystyrene particles.

3.2. Experimental

3.2.1. Colloidal seed particles

Polystyrene spheres of 220 nm diameter Cross-linked polystyrene spheres (CPS) of 111 nm radius (polydispersity of 2.5%) and cross-link density of 3% were synthesized via an emulsion polymerization as described in Chapter 2.2.1. Two samples of the CPS suspension were consequently coated with vinyl acetate (surface coverage $\sigma = 3.56 \cdot 10^{-21}\mathrm{g/nm^2}$) to render the surface more hydrophilic. Despite using the same coating procedure two batches with different wetting angles between the CPS seeds and the swelling styrene were obtained, namely $\theta = 23°$ and $\theta = 30°$. The final colloidal suspensions had a weight fraction of 2.6% w/w in aqueous solution.

Polystyrene spheres of 2.2 μm Polystyrene spheres with cross-link density of 1.5% w/w were synthesized as described in Chapter 6.2.

3.2.2. Synthesis of Colloidal Molecules

In a typical experiment 5 mL of CPS seed suspensions and varying volumes of the swelling monomer were added to a glass flask equipped with a magnetic PTFE-coated stir bar. During swelling all samples were stirred vigorously for about 2-3 days and subsequently placed in an 80°C oil bath. Heating causes the cross-linked polymer network to shrink resulting in the formation of a droplet of the swelling monomer on the colloidal surface.[**26, 27, 28, 33**] Surface energy between the monomer and the water phase as well as hydrophobicity of the seed particles favors the formation of one single protrusion (see also Chapter 4 on colloids with multiple protrusions). The hydrophilicity of the seed particle surface as well as the surfactant determines the wetting angle between the monomer and the colloidal surface. The less favorable it is for the monomer to wet the surface, the more aspherical the protrusion is to the extent of forming a separate droplet. The samples were left stirring in the oil bath for several days for increasing the number of coalesced colloids. Subsequent polymerization was carried out at 80°C by addition of a water soluble inhibitor, hydroquinone (0.75 mM, 99% purity, Riedel), and initiated with azobisisobutyronitrile (0.94 mg AIBN dissolved in 0.046 mL styrene per mL of seed suspension). Polymerization was allowed to continue for 24 h.
The samples containing micron-sized polystyrene colloids were prepared slightly different (see also Chapter 6.2. A swelling emulsion containing styrene, divinylbenzene, V65B (2,2'-azodi (2,4'-dimethylvaleronitrile), initiator) and TMSPA (3-(trimethoxysilyl) propyl acrylate, Sigma Aldrich) was emulsified with 1% w/w aqueous polyvinylalcohol solution and added to the seed dispersion. Protrusion formation occurs instantaneously after mixing with the seed dispersion. Polymerization in an 75°C oil bath was allowed to continue for 20 h.

3.2.3. Transfer of colloidal particles from aqueous solution to styrene

An aliquot of the polystyrene seed suspension was centrifuged and redispersed in ethanol twice, then centrifuged and redispersed in styrene to test for colloidal stability in styrene.

3.2.4. Characterization

Density Gradient Centrifugation For separation of colloidal molecules of different mass density gradient centrifugation was employed in a 3 to 9% w/w Ficoll 400 in 1% w/w Pluronic F127 in MilliQ water gradient. Centrifugation was performed for 12 mins at 20,000 rpm in a Beckmann Optima L60 ultracentrifuge. After having taken out the bands with a pipette with bend tip we washed them three times with MilliQ water to remove remains from the density gradient.

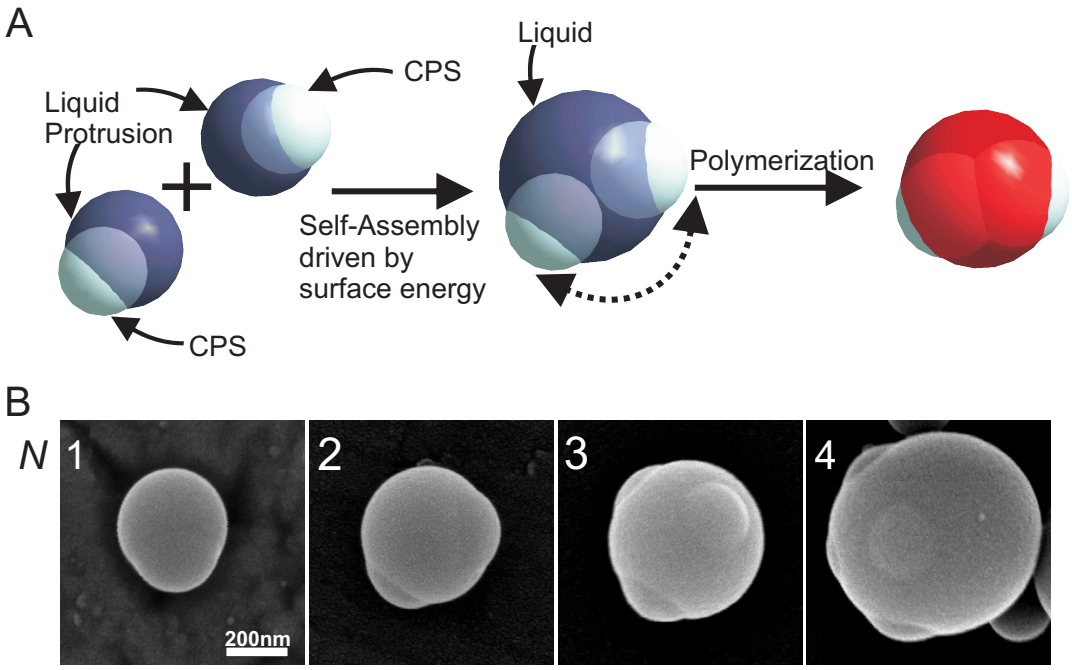

Figure 3.1. (A) Crosslinked polystyrene colloids (CPS) with liquid protrusions self-assemble into colloidal molecules by fusion of the liquid protrusion. The process is driven by minimization of the surface energy between the protrusions and the water phase. If the seed particles are not restricted inside the fused protrusions, they are expected to be randomly distributed over the surface. (B) After polymerization we observe colloidal molecules with a controlled bond angle by scanning electron microscopy. Assemblies consisting of two and three seed particles resemble water ($N = 2$) and ammonia-like ($N = 3$) molecules, respectively.

Microscopy Polymerized samples were imaged using a scanning electron microscope (SEM XL FEG 30, Philips). The PS particles were sputter coated with platinum/palladium prior to imaging. Electron micrographs were digitally post-processed to optimize brightness and contrast for print. Seed particles in styrene were imaged with a transmission electron microscope (Tecnai 10, Philips) after drying on a polymer coated copper grid.

Dynamic Light Scattering Dynamic Light Scattering measurements were done by a Malvern Zetasizer Nano NS at 173° and 13° (wavelength: 620 nm).

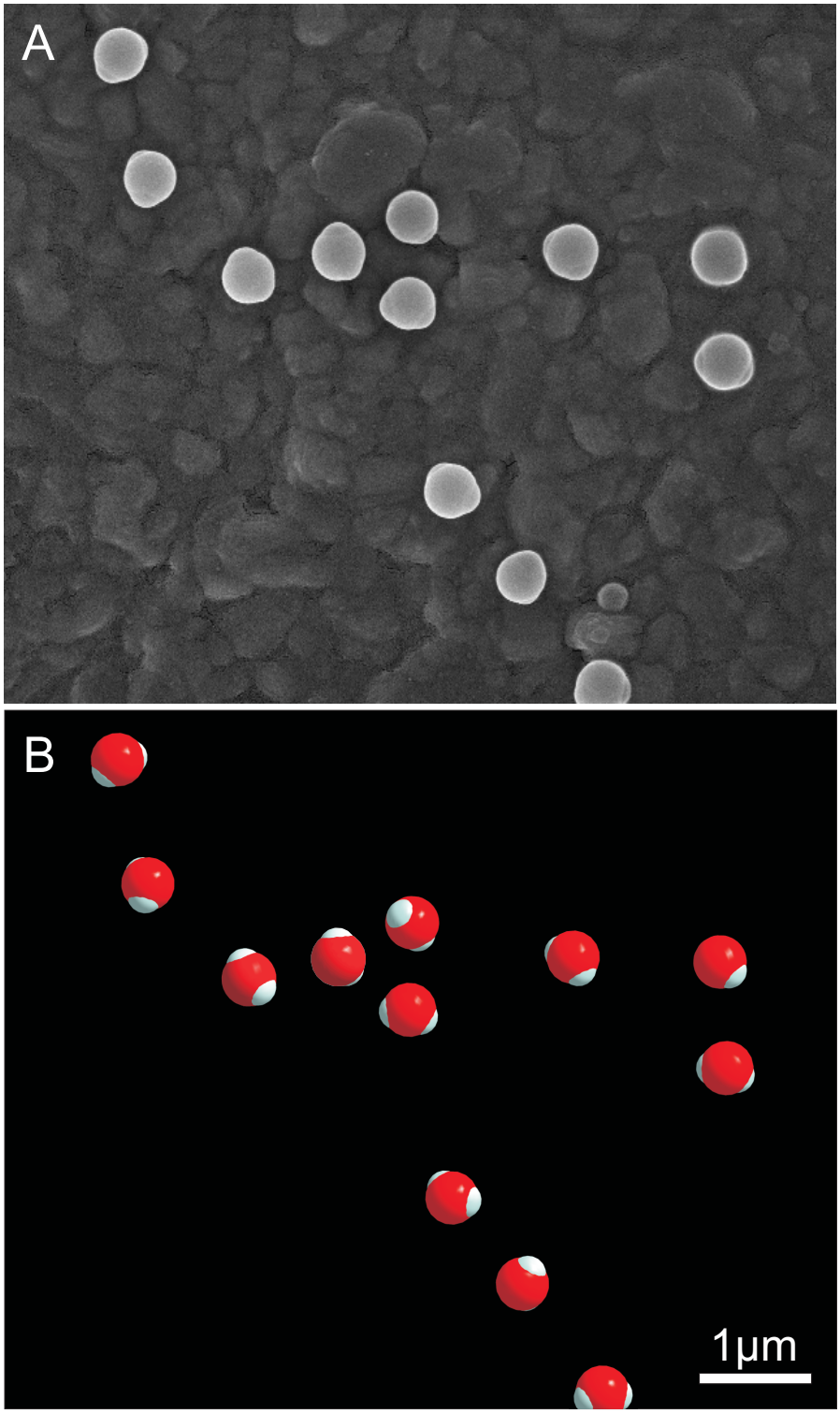

Figure 3.2. A) Scanning electron micrograph of water-like colloids in the second band after density gradient centrifugation. B) Turning a 3D model constructed from the EM image reproduces all observed views of the colloidal particles in the SEM image indicating that the assembly produces uniform colloidal particles with a fixed bond angle of 139°.

3.3. Results and Discussion

3.3.1. Formation of Asymmetric Colloidal Molecules

Raising the temperature of monomer-swollen cross-linked polymer particles causes phase separation of the monomer from the polymer seed in form of liquid protrusions.[**26, 27, 28**] Subsequently, the seed colloids can bind by fusion of the attached liquid protrusions to form colloidal molecules (Figure 3.1A).[**33**] The wetting angle between the seed particles and the monomer phase as well as the extent of the swelling provides precise control over the shape and size of the protrusions and hence, the final topologies of the colloidal molecules. In previous experiments[**33**] the volume of the liquid protrusions was small, restricting the movement of the seed particles inside the fused protrusions. This resulted in highly symmetric clusters as well as large droplets with many attached seed particles (Chapter 2 and 5).

Here, we chose a high degree of swelling, which induced liquid protrusions larger than the original seed particles (see $N = 1$, Figure 3.1B). Fusion of such protrusions leads to large droplets with attached seed particles that are expected to move freely over the surface. Surprisingly, we observed well-defined seed particle positions for assemblies of small numbers of seed particles after polymerization. For each assembly of N seed particles we found one type of asymmetric colloidal molecule with a unique bond angle. Representative examples of the obtained colloids from cross-linked polystyrene spheres (CPS) are shown in Figure 3.1B. Clusters comprised of two CPS seed particles resembled water molecules, whereas three seed particles formed colloids resembling ammonia molecules.

3.3.2. Proof of Uniformity in Shape by Use of 3D Models

To elucidate that the obtained colloidal particles are exhibiting a single, unique shape we employed separation of the assemblies by density gradient centrifugation (DGC) and imaged the obtained fractions by scanning electron microscopy (SEM). The fraction containing dimers, trimers and tetramers are shown in Figure 3.2, Figure 3.3 and Figure 3.4, respectively. We modeled the shape of the water-like arrangements ($N = 2$) as shown in Figure 3.5 A. By only rotating this model, that means changing the view point, we could reproduce all colloids observed within one DGC band, convincing us that the obtained colloidal particles are exhibiting an unique shape (Figure 3.2 B).
The 3D models were constructed according to the wetting angle, α, and the radius of the seed particles, r, and the droplet, R, as shown in Figure 3.5 C. Agreement between model and experiment required slightly interpenetrating seed particles. Similarly, for trimer clusters the seed particles partially overlapped inside the center (Figure 3.5 B) forming a unilateral triangle immersed in the protrusion body. In both cases the particles interpenetrated by about 18% of their original size. This 'soft' behavior can be understood considering that the polymer network of the seeds was only cross-linked

by 3% w/w divinylbenzene, and that the swelling monomer inherently is a good solvent for the polymer. The bond angle α of a particle with two seeds can be calculated as seen in Figure 3.5 C, via

$$\alpha = \sin^{-1}(r'/c) \tag{3.1}$$

$$= \sin^{-1}(r'/\sqrt{(r^2 + R^2 - 2rR\cos\theta)}). \tag{3.2}$$

r' is half the distance between two seed centers. In analogy, we define a bond angle β for colloidal molecules with three seeds as the angle between the center of the coalesced protrusions and any two seed particles. As shown in Figure 3.2 and Figure 3.3 all colloidal arrangements consisting of two and three seed particles could be described well with those models.

3.3.3. Control over Bond Angle

Variation of the amount of styrene allows for adjustment of the volume of the protrusions and therefore the radius of the central body of the colloidal molecules. We define the swelling ratio as the volume of the fused protrusions over the volume of one seed particle. Since the particles were always found to be overlapping inside the center an increased liquid volume changes the angle α (Figure 3.5C) between the centers of the seed particles and the center of the liquid droplet. As shown in Figure 3.6, increasing the actual swelling ratio, S, (volume of the protrusion per volume of seed particle) from $S = 0.52$ (top row) to $S = 1.70$ (bottom row) changes the dimer angle from $\alpha = 180°$ to $\alpha = 100°$. Similarly, for trimer particles the angle between any two seed particles and the liquid center changes from $\beta = 180°$ to $\beta = 80°$ (Figure 3.6, right columns). As only one unique angle is found within each batch of particles this procedure provides a unique opportunity to create colloidal "water" (dimer) and colloidal "ammonia" (trimer) at any desired angle. The smallest obtainable angle is only restricted by the maximum volume of monomer that can be taken up by the seed particles.

To demonstrate that the shape can further be influenced by the wetting angle between the seeds and the fused protrusions,[**33**] we used CPS with a wetting angle of $\theta = 30°$ as shown in the last row of Figure 3.6. All other pictures show CPS seeds with a wetting angle of $\theta = 23°$. The larger wetting angle clearly increases the extent to which the seed particles protrude from the droplet, yielding an even richer variety in shapes. At larger wetting angles, asymmetric assemblies can be obtained even with small protrusions, as long as the seed particles are not restricted to move inside the droplet. The particles with a higher wetting angle were interpenetrating by only 11% compared to 18% for the ones with a low wetting angle.

As exemplified in Chapter 2, the synthesis is independent of the seed particle size. In Figure 3.7 some examples of asymmetric colloidal molecules from polystyrene are

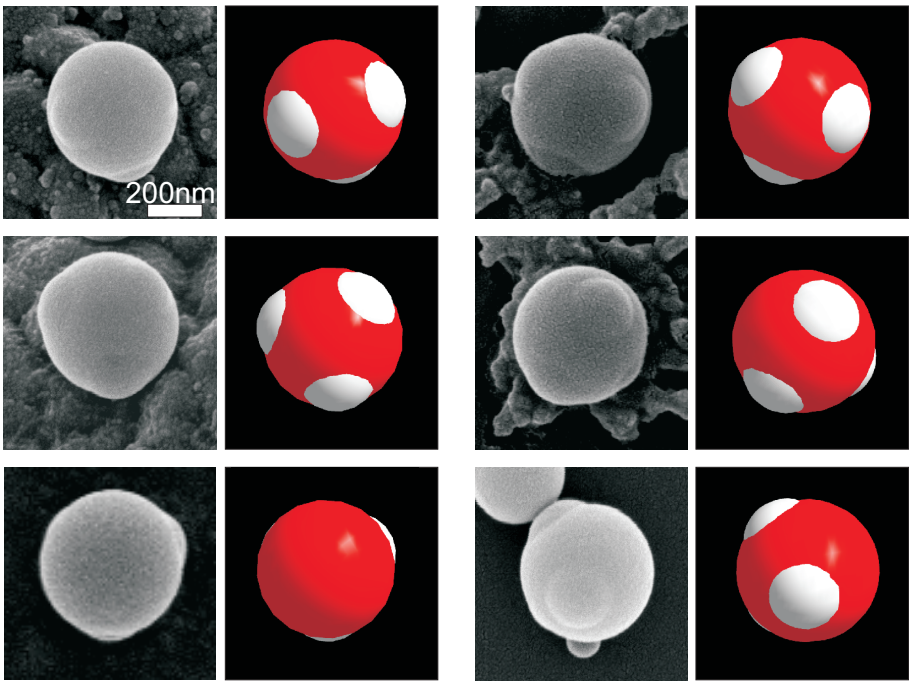

Figure 3.3. Colloidal polystyrene particles with three patches resembling ammonia molecules and their respective view of the 3D model. The angle between any two seed particles (white) and the center (grey) is 101°. The wetting angle between seed particles and the center is 23°

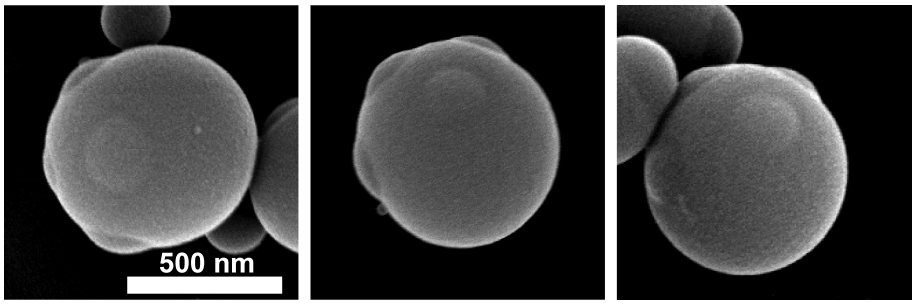

Figure 3.4. Colloidal molecules with four integrated seed particles also show uniform shapes.

shown. Again, the bond angle is determined by the wetting angle between the seed particle, the aqueous phase and the protrusion, as well as the size of the protrusions.

3.3.4. Origin of Uniformity in Shape

To elucidate the underlying physical mechanism of local attraction between the seed particles we consider different possible contributions. Charged polystyrene particles adsorbed at a styrene water interface are accompanied by an asymmetric ion cloud that forms a dipole moment perpendicular to the interface.[**46, 47**]

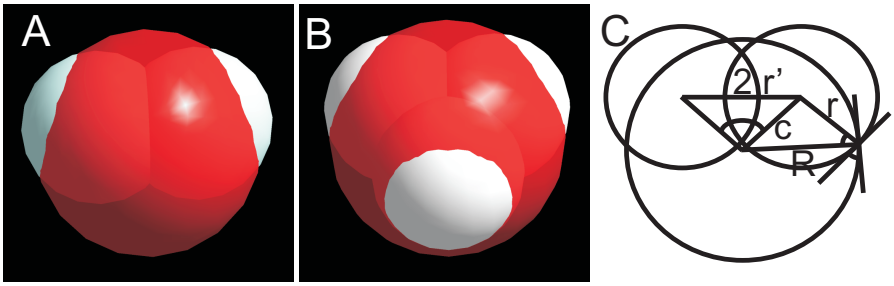

Figure 3.5. Transparent 3D models of the A) dimers and B) trimers showing that the white seed particles are interpenetrating each other by 18% inside the protrusion body (depicted in grey). C) Schematic representation of a dimer. The bond angle α can be calculated from the wetting angle θ and the seed and center radius, r and R, respectively.

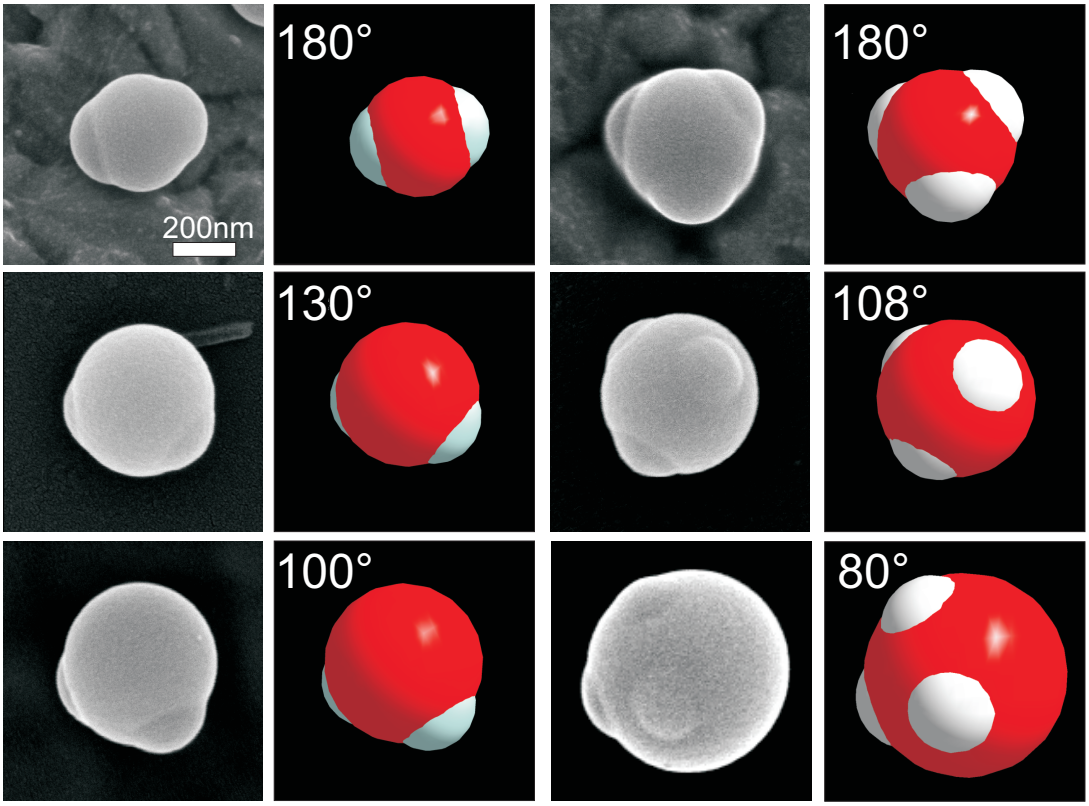

Figure 3.6. Increasing the volume of the liquid protrusions with respect to the seed volume in the system decreases the bond angle between the seed particles and the center. For a swelling ratio of 0.52 (top row) we find bond angles of $\alpha = 180°$ and $\beta = 180°$ for assemblies comprising two and three seed particles, respectively. For a swelling ratio of 1.7 (bottom row) the bond angles change to $\alpha = 100°$ for assemblies of two and $\beta = 80°$ for assemblies of three seed particles.

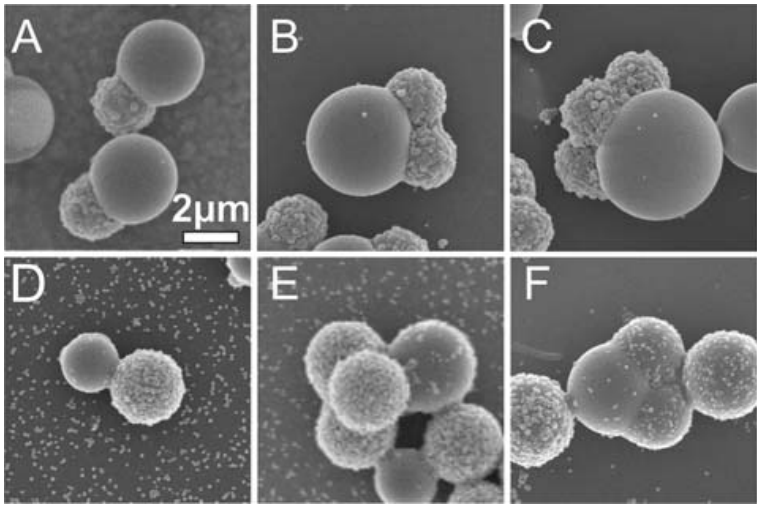

Figure 3.7. Scanning electron micrographs of asymmetric colloidal molecules made from rough polystyrene seeds (see Chapter 6 at swelling ratio 4 (A-C), 2 (D,E) and 3.5 (F).

Dipole-Dipole interactions

Straightforward calculations reveal that two dipoles attached to a spherical surface have minimum repulsive interaction energy at maximum separation. That is, the seed particles should be placed on opposite ends of the droplets. Experimental observations do not agree with this seed arrangement and we therefore conclude that dipole-dipole interactions are not playing a major role.

Van-der Waals forces

If van der Waals forces caused attraction between the particles, aggregation is expected to occur upon transfer from water to styrene. We washed a small quantity of vinyl-acetate coated polystyrene particles twice with ethanol and styrene. Immediately after preparation the sample looked macroscopically stable and remained so for over three months without precipitation. Transmission electron micrographs of dried samples do not show aggregation in three dimensions but two-dimensional layers of seed particles (Figure 3.8). Dynamic Light Scattering measurements yielded a size of $R = 195 \pm 32$ nm, and proved furthermore that only swelling, but not aggregation occurred in styrene. Steric stabilization provided by vinyl-acetate polymers grafted to the interface could explain this behavior. Van der Waals forces are thus not responsible for the observed attraction between seed particles.

Depletion interaction

Another possible candidate is depletion interaction. Upon polymerization polymers are formed inside the droplet which could induce attractive interactions by depletion forces.

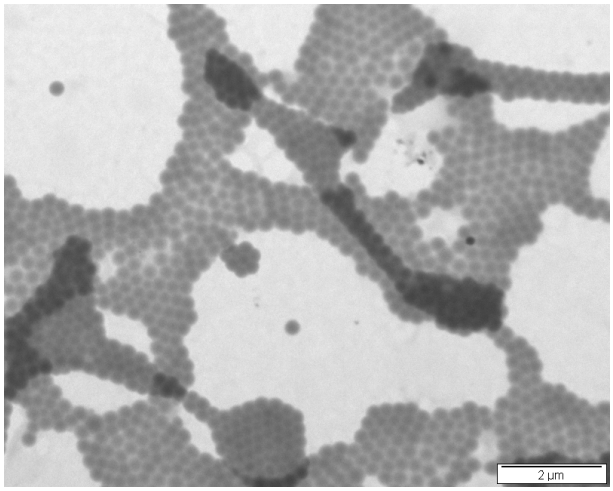

Figure 3.8. Transmission electron micrograph of cross-linked polystyrene seed particles in styrene. The particles form 2D layers indicating that no 3D aggregation takes place upon transfer to styrene.

This mechanism has been seen in other systems such as Pickering emulsions[**48**] and requires that diffusion of colloids on the droplet surface happens on a much faster time scale than polymerization of the whole droplet. To get an estimate of the time it takes a particle to diffuse from one side of the droplet to the other, we simplify the system in the following way: the seed particle can diffuse on a two dimensional spherical surface of radius R with a diffusion coefficient assumed to be given by $D = k_B T/(6\pi\eta r)$.[**49**] Here, $\eta = 3.75 \cdot 10^{-4} Pa \cdot s$ is the viscosity of styrene at 80°C [**50**] as the seeds are mainly immersed into styrene. k_B is the Boltzmann constant and T the temperature during synthesis. We then obtain for the diffusion time from one side of the sphere to the other

$$t_d = \frac{\langle x^2 \rangle}{4D} = \frac{3(\pi R)^2 \pi \eta r}{2k_{\mathrm{B}}T}. \tag{3.3}$$

For dimer and trimer particles as shown in the third row of Figure 3.6, this yields diffusion times of $t_d(R = 250\ \mathrm{nm}) = 68$ ms, and $t_d(R = 320\ \mathrm{nm}) = 0.11$ s, respectively. However, for large droplets with hundreds of adsorbed seed particles, we find that the seed particles aggregate locally, but do not maximize the number of contacts on a global length scale (Figure 3.9). This indicates that the seed particles can indeed move freely over the droplet surface before polymerization. However, diffusion across such a droplet takes an estimated $t_d(R = 2\mu\mathrm{m}) = 4.36$ s and may explain why it is not possible for the seed particles to rearrange quickly enough upon polymerization. Assemblies of seed particles intermediate in size between this assembly and the colloidal molecules show a transition of global to local aggregation of the seed particles on the surface (Figure 3.10). Polymerization thus happens on the timescale on the order of seconds: too fast for rearrangement of the spheres on large droplets, but slow enough for the seeds in

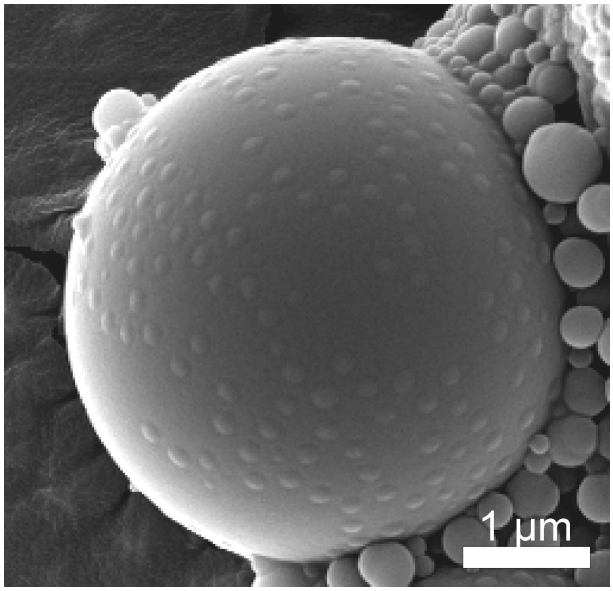

Figure 3.9. Large droplet consisting of several hundreds of fused protrusions with seed particles attached to the interface. The seed particles aggregate locally on the surface. Globally, however, the number of contacts between the seeds is not maximized indicating that polymerization is taking place on a shorter time scale than the rearrangement of the seed particles due to depletion attraction.

small assemblies to respond to depletion attraction induced by the formation of polymers.

3.3.5. Variation of the Synthesis - Colloidal Molecules with a Cavity

During polymerization of the liquid protrusions, a variation of the outcome can be achieved: after radical initiation polymerization of the liquid protrusions gradually progressing from the outside inwards. That way, a polymerized shell and a liquid core is formed. Dropping the temperature to room temperature polymerization ceases and the liquid core is preserved. Leaching out the inner styrene core, for example by evaporation, yields dimples in the protrusions, both with singgle protrusions as well as for fused protrusions (Figure 3.11). The colloidal molecules obtained may be employed in controlled self-assembly processes, for example in lock-key colloids organized by depletion interaction[**51**], as a branching piece (Figure 3.11C). The branching angle can be controlled via the bond angle of the colloidal molecules. The cavity size is tunable by the degree of polymerization of the shell [**51, 52**] and the overall protrusion size. Integrating roughness on the round site of dimers with cavity renders them also useful as terminating particles in lock-key chains.

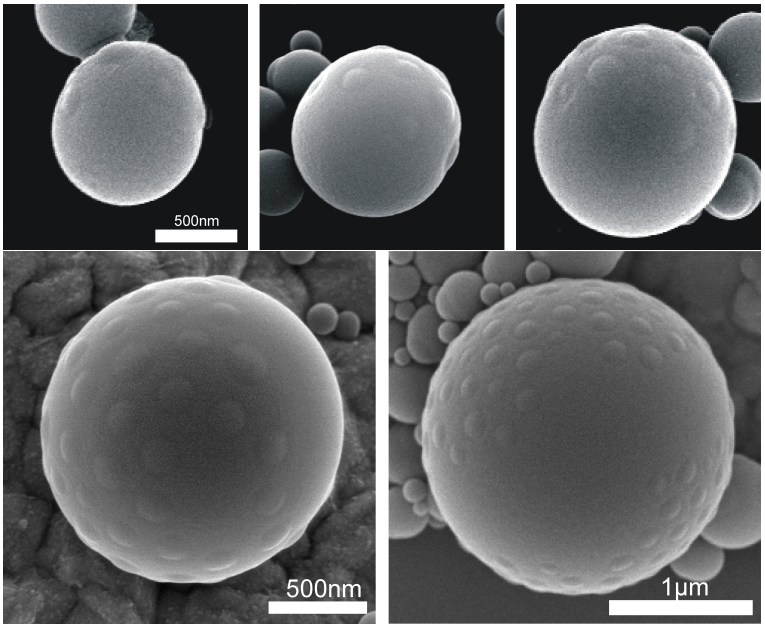

Figure 3.10. Assemblies of seed particles intermediate in size between the colloidal molecules (consisting of only few seeds) and the large assembly shown in Figure 3.9. On the surface of the droplets consisting of the fused protrusions seed particles aggregate due to polymerization. With an increase in droplet size, particle aggregation at the surface gradually changes from a global to a local optimization.

3.4. Conclusions

In conclusion, we have presented a new and facile synthesis method for preparing colloidal molecules with well-controlled bond angles. The choice of the size of the liquid protrusion and the wetting angle allows for uniform particles with a bond-angle "made to order". Utilizing polymerization induced depletion interaction we find reproducible shapes for small assemblies. The technique can be easily extended to other seed polymers or swelling monomers due to its underlying generality[**31, 33**] providing a simple method to produce asymmetric colloidal molecules for studying collective behavior as well as self-assembly. Further modification is possible by introducing cavities in the protrusions, leading to new building blocks for self-assembly.

Acknowledgments

I would like to thank Dr. Paul van der Schoot, Dr. Jan Groenewold and Jan Hilhorst for useful discussions, as well as Hans Meeldijk and Chris Schneijdenberg for support during electron microscopy. Kisun Yoon is thanked for experimental insights into synthesis of large cross-linked polystyrene spheres. This chapter is based in parts on the

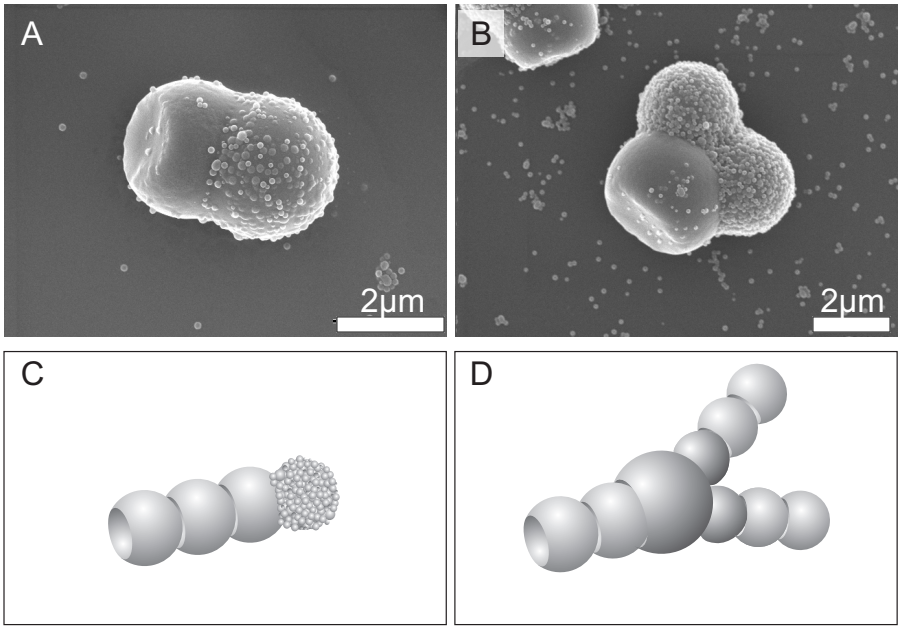

Figure 3.11. A) and B) SEM images of colloidal molecules with a cavity prepared by partial polymerization of the protrusions and removal of the remaining liquid core. The resulting colloids have a cavity that can be used as a "key" site in lock-key recognition systems. C) With one rough side these colloids can be used as starting points of colloidal chains (refer also to Chapter 6), and, B) colloidal molecules with cavity and multiple seed particles may be employed for branching of the depletion induced assembly.

4

Patchy Polymer Particles with Tunable Anisotropy Dimensions

Abstract

We present the synthesis of polymer colloids with continuously tunable anisotropy dimensions: patchiness, roughness, and branching. Our method makes use of controlled fusion of multiple protrusions on highly cross-linked polymer particles produced by seeded emulsion polymerization. Carefully changing the synthesis conditions we can tune the number of protrusions, or branching, of the obtained particles from spheres with one to three patches to raspberry-like particles with multiple protrusions. In addition to that, roughness is generated on the seed particles by adsorption of secondary nucleated particles during synthesis. The size of the roughness relative to the smooth patches can be continuously tuned by the initiator, surfactant, and styrene concentrations. Seed colloids chemically different from the protrusions induce patches of different chemical nature. The underlying generality of the synthesis procedure allows for application to a variety of seed particle sizes and materials. We demonstrate the use of different sized polyNIPAM (poly-N-isopropylacrylamide), as well as polystyrene and magnetite filled polyNIPAM seed particles, the latter giving rise to magnetically anisotropic colloids. The high yield together with the uniform, anisotropic shape make them interesting candidates for use as smart building blocks in self-assembling systems.

4.1. Introduction

Anisometric colloids with site-specific properties, so called patchy particles, are promising candidates for building blocks intended for bottom-up assembly of functional materials. [**14, 16, 54**] Patchy particles offer unique control over the assembled structures due to their locally confined interactions between specific patches. Because most colloidal pair interactions by themselves are isotropic and centrosymmetric, directionality in the attraction is implemented most easily on the particle level, for example, by anisotropic shapes and/or patterning. By introducing sites on the colloids that site-specifically attract or repel, patchy interactions can be obtained.[**55, 56, 57, 58, 59**]

To categorize particle anisotropy, Glotzer and Solomon recently suggested a conceptual framework of key anisotropy dimensions,[**11**] such as aspect ratio, branching, roughness and patchiness. Along each dimensionality axis the extent of the anisotropy gradually increases. In self-assembly it is desirable to be able to tune the key anisotropy dimensions of colloidal building blocks continuously, for example by a simple adjustment of the synthesis parameters. Despite the wide variety of patchy particles available today, the particle fabrication techniques for synthesis of complex colloids are limited either in their variability and uniformity of shapes and patchiness, the yields of uniform particles or the separation of particles from the templates.[**12**] The yield is usually restricted by either the batch volume or the time consuming separation of different patchy particles. Here, we present a simple, straightforward technique for making anisotropic, patchy polymer particles that resemble colloidal molecules.[**13**] The synthesis allows for continuously variable anisotropy dimensions: branching, roughness and patchiness, while maintaining a high yield of the desired colloidal particle type and being scalable in overall particle size.

Seeded emulsion polymerization techniques have successfully been employed in the fabrication of various anisotropic polymer particles.[**26, 27, 28, 31, 40, 60**] Typically, cross-linked polymer spheres suspended in an aqueous environment are swollen with hydrophobic monomers, such as methyl methacrylate or styrene. Upon relaxation of the stretched polymer network the swollen polymer spheres phase separate, yielding a liquid protrusion consisting of monomer. This relaxation can be induced by temperature elevation as well as long swelling times. The obtained particles were mainly reported to be dimers,[**26, 27, 28, 31, 60, 61**] but also popcorn-like [**43**] and, after merging of liquid protrusions on different seed particles, colloidal molecules.[**33, 53**] Yet, it remains cumbersome to obtain complex particle shapes due to the requirement of multiple fabrication steps [**40, 62**], and patchiness is generally not straightforwardly integrated. Moreover, systematic approaches to fabricate complex patchy particles in high yields are desirable.

In this chapter, we employ the controlled formation of multiple protrusions on highly cross-linked polymer spheres for making uniform anisotropic colloidal particles with patches in high yields. By increasing the stabilization of the protrusions with surfactants, intra- and inter-particle merging of the liquid protrusions is controlled, and gradually one, two, three or multiple protrusions are obtained. Adsorption of secondary nucleated particles on the seed particle surface adds "roughness" to the obtained particles in contrast to the smooth protrusions. Employing depletion interactions may lead to site-specific attraction between the patches, as was explored for flat surfaces.[**63, 64, 65, 66**] We address the following anisotropies that can be continuously tuned: (1) Branching, or, the number of protrusions on the particle surface. (2) Patchiness, which can be induced in two ways: (a) chemically different materials for the seed particles and the protrusions, and, (b) roughness, that is the relative size of the adsorbed secondary particles to the smooth protrusions. (3) Size and material: the generality of our synthesis method is demonstrated by use of polyNIPAM (poly-N-Isopropylacrylamide), polystyrene and magnetite filled polyNIPAM seed particles of different sizes. PolyNIPAM particles are temperature sensitive microgels that decrease in size above a specific volume phase transition temperature.

4.2. Materials and Methods

4.2.1. Seed Particle Synthesis

polyNIPAM spheres

We synthesized several batches of cross-linked polyNIPAM spheres for use as seed particles. PolyNIPAM spheres of 581 and 945 nm (at 25°C) were made according to the method described by Pelton and Chibante. [**67**] In a typical synthesis, 1.4 g of N-Isopropylacrylamide (NIPAm, Aldrich, 97%) and 40 mg of N,N′-Methylenebisacrylamide (BIS, Sigma, for electrophoresis >98%, corresponding to a cross-linking density of 2.9 % w/w) were dissolved in 100 mL of water (Millipore) in a 250 mL three necked flask. This mixture was heated to 70°C under nitrogen flow and left to stir for 1 hour before adding 40 mg of Potassium persulfate (KPS, Acros Organics, 99+%) to initiate the reaction. The mixture was left to react for 3 hours. The resulting dispersion was centrifuged and redispersed in water at least three times before use. polyNIPAM particles of 256 nm (3% w/w cross-linking density) and 327 nm (2.5% w/w cross-linking density) were grown by adding sodium dodecyl sulphate (SDS, Brunswig) to an otherwise similar reaction mixture.[**68**] The resulting dispersions were dialyzed against Millipore water for four days, during which the dialysate was exchanged four times. The diameter of the final polyNIPAM spheres as a function of temperature as measured by Dynamic Light Scattering is shown in Figure 4.1.

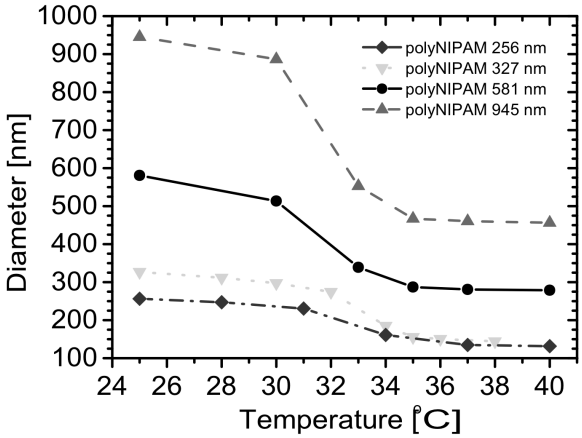

Figure 4.1. Dynamic Light Scattering measurement of polyNIPAM colloidal size as a function of temperature for different polyNIPAM spheres.

Magnetite filled polyNIPAM spheres

Magnetite filled polyNIPAM particles were prepared using the method described by Zhang et al. with minor modifications.[**69**] In the first step, polyNIPAM particles were prepared by dissolving 1.0 g of NIPAM, 14 mg of BIS, 32 mg of SDS and 0.3 mL of acrylic acid (AA, Sigma-Aldrich, 99%) in 95 mL of water. This mixture was heated to 70C under nitrogen flow and left to stir for 1 hour before adding a solution of 22 mg of KPS in 5 mL water (8 mM in reaction mixture) to initiate polymerization. The mixture was left to react for 3 hours and subsequently purified by dialysis overnight. 13 mL of the resulting dispersion was diluted to 200 mL with water and the pH was increased by addition of 1 M potassium hydroxide solution (KOH, Merck, p.a.) solution, until the pH was 7. Then, 1.05 g of iron sulphate ($FeSO_4 \cdot 7\,H_2O$, Merck, p.a.) was added and the mixture was left to stir overnight. The resulting mixture was dialyzed under a nitrogen atmosphere, and added to a round bottom flask equipped with a mechanical stirrer. 0.109 g of sodium nitrite ($NaNO_2$, Sigma-Aldrich) was added, and subsequently 12.5 mL of 25% ammonia solution (Acros Organics, p.a.) was quickly added under vigorous stirring. This mixture was stirred for 3 hours, after which the particles were rinsed by repeated centrifugation and redispersion in water. The final particle suspension consisted of 597±61 nm diameter polyNIPAM spheres with magnetite particles. For a transmission electron micrograph of the seed spheres, see Figure 4.2.

Cross-linked polystyrene spheres with different vinyl acetate coating densities

Polystyrene particles cross-linked with 18% w/w divinylbenzene (DVB, Aldrich, 55% mixture of isomers, undistilled) were synthesized as described in Chapter 2 according to Mock et al. [**28**]. The polystyrene spheres were 226.5 nm ±7.9% in diameter as

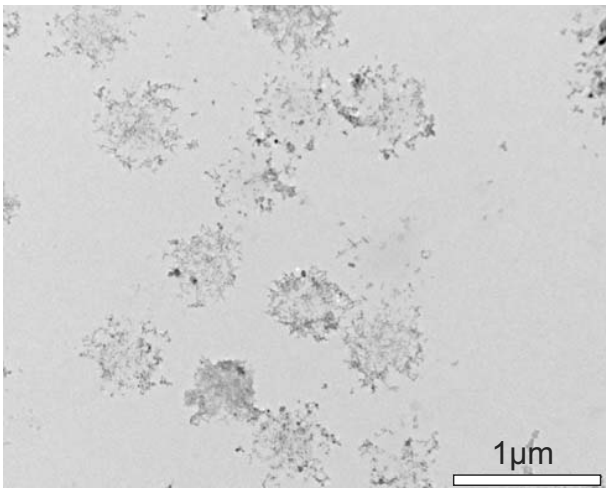

Figure 4.2. Transmission electron micrograph of magnetite filled polyNIPAM seed particles. Due to the large contrast difference between polyNIPAM and magnetite, the polyNIPAM is hardly visible compared to the magnetite colloidal particles.

measured by TEM. After synthesis, dialysis against demiwater was performed for 5 days during which the dialysate was changed 6 times.

A hydrophilic coating of vinyl acetate was applied to aliquots of this cross-linked polystyrene dispersion at different coating densities as described in Chapter 2 and ref. [**28**]. We applied a nominal surface coating density, $\sigma = VA \cdot 3.610^{-21}$ g/nm^2, with VA varying between 1 and 10. After coating, the particle suspensions were dialyzed against demi-water for 24 h with the dialysate being changed 4 times.

4.2.2. Synthesis of Anisotropic Patchy Particles

polyNIPAM seed particles

Typically, 5 mL of a 1% w/w solution of colloidal polymer spheres was swollen with 143 μL distilled styrene and 129 μL aqueous sodium dodecyl sulfate (SDS, 32 mg/mL water) at 25 or 32°C (polystyrene and polyNIPAM, respectively) for 24 h. For polyNIPAM, the swelling temperature was chosen around the volume phase transition temperature [**67**] to enhance swelling with the hydrophobic monomer. For polyNIPAM sizes as a function of temperature, see Figure 4.1. After heating to 80°C for 30 minutes, initiation was induced by addition of 460 μL of 20 mg/mL azobisisobutyronitrile (AIBN, Aldrich) in styrene, and allowed to continue for 24 h. Variations to the synthesis were carried out as described in the text. Before imaging, the colloidal samples were washed by repeated centrifugation to remove secondary particles nucleated during synthesis.

Polystyrene seed particles

Typically, 2 mL of a 1% w/w suspension of vinyl-acetate coated polystyrene seeds was swollen with varying amounts of styrene in the presence of SDS for 24 h. We define the

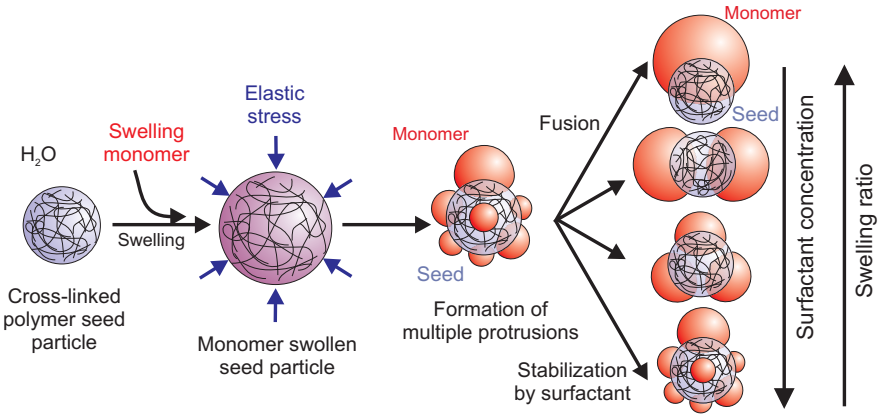

Figure 4.3. Schematic of the synthesis technique and systematic influence of several factors on the resulting patchy particles.

relative amount of styrene with the swelling ratio, $S = m_{styrene}/m_{polymer}$, and the SDS concentration in multiples of the cmc, that is, $c_{cmc} = 2.6$ mg/mL. Then, 0.88 mL of a 0.32 g/mL aqueous hydroquinone suspension was added and the vial was immersed in a constant temperature bath at 80°C. Initiation was induced by addition of 0.12 mL of a 2% w/v AIBN in in styrene, and allowed to continue for 24 h.

4.2.3. Characterization

Diluted samples of colloidal dispersions were imaged using a scanning electron microscope (SEM XL FEG 30) or a transmission electron microscope (TEM, Technai 12, Philips). For SEM the colloidal particles were sputter coated with 4 nm platinum/palladium prior to imaging.

4.3. Results and Discussion

4.3.1. Branching Anisotropy

A schematic illustration of our synthesis technique is depicted in Figure 4.3. The cross-linked polymer seed particles suspended in an aqueous environment are swollen for 24 hours with a hydrophobic monomer, styrene, in the presence of sodium dodecyl sulfate (SDS). We define the swelling ratio to be the monomer mass added to the unswollen seed particle mass, or, $S = m_{monomer}/m_{polymer}$. The swelling of the polymer sphere creates a visco-elastic stress on the polymer network, which can be released by phase separation of the previously taken up monomer into one or more liquid protrusions attached to the seed particles. The liquid protrusions can be prevented from merging by employing surfactants, which decrease the driving force for fusion by lowering the interfacial tension. Relaxation of the polymer chains strongly depends on the temperature as well as the swelling time [**26, 30**], but also on the internal seed particle morphology. A higher cross-linking density in the seed particle network was shown to

lead to the formation of multiple protrusions after network relaxation. [**26, 27**] This was attributed by Sheu et al. to inhomogeneities in the network, which tend to localize the contraction force during swelling. [**26**] Until now, the number and position of the multiple protrusions was rather uncontrolled and the formation of more than one protrusion therefore undesirable. Here, we demonstrate how we can control the number of protrusions by controlling their stability against fusion with the concentration of anionic surfactant.

After formation of multiple protrusions on the surface, the interfacial tension between the droplets and the aqueous phase determines the driving force for merging. The larger the interfacial tensions, the larger the surface free energy and the stronger the driving force to minimize the total interfacial area (Figure 4.3). High surfactant concentrations prevent the droplets from coalescing, thus yielding raspberry- or popcorn-like particles. At lower surfactant concentrations, first, multiple protrusion appear during phase separation as well, but subsequently fuse into less droplets driven by interfacial energy (Figure 4.3). For very low surfactant concentrations, a single protrusion is formed eventually. At slightly higher surfactant concentrations, the polymer particles develop two protrusions, and with increasing surfactant concentration a gradual transition from single, to double, triple and multiple protrusions occurs. Scanning electron micrographs of polyNIPAM particles exhibiting one, two, three, or multiple protrusions are shown in Figure 4.4A-D. Note, that the smaller spherical particles visible in the electron micrographs are not due to unfused protrusions, [**70**] but originate from adsorption of secondary particles nucleated during polymerization onto the seed particles as proven below. Thereby, the seed particles can easily be distinguished from the larger protrusions. The assignment of "seed" and "protrusions" to the respective parts of the particle will be explained later.

The gradual change of the fractions of monomers, dimers and trimers with the surfactant concentration, independent of the seed particle size, is shown in Figure 4.4F. The different number of protrusions at equal surfactant concentrations can be ascribed to the higher cross-linking density of the smaller 256 nm polyNIPAM particles. At a SDS concentration of 0.83 mg/mL formation of multiple protrusions was observed. Similar observations of a gradual transition from one to multiple protrusions were made for larger polyNIPAM seed particles, and polystyrene spheres (Figure 4.5). Figure 4.5 shows that the transition from no clearly discernible (Figure 4.5A) or one (Figure 4.5B) to multiple protrusions occurs with increasing surfactant concentrations. The difference between Figure 4.5 A and B lies in the coating density of the seed particles. The seed particles displayed in Figure 4.5A has a nominal vinyl acetate coating of $VA = 2$ (where VA is defined through the surface coating density $\sigma = VA \times 3.6 \cdot 10^{(}-21)\mathrm{g/nm^2}$), whereas in Figure 4.5B a coating of $VA = 6$ was applied. Clearly, the number of protrusions on polystyrene seed particles is increasing with a higher coating density of the

seed particle surface with vinyl acetate. Most likely, the polyvinyl acetate polymers grafted to the seed particle surface are stabilizing the liquid protrusions, analogous to the surfactant SDS, and therefore, a higher coating density has a similar effect on the number of protrusions as an increased SDS concentration. Again, the transition from single to multiple protrusions occurs gradually with an increasing vinyl acetate coating density, see Figure 4.6D.

By careful adjustment of the synthesis conditions, the number of protrusions, or the degree of branching, and therefore, the particle shape can be selectively chosen to be uniform. The anisotropy dimension "particle branching" can be smoothly tuned "to-order" by the surfactant concentration, while still maintaining high particle yields of over 90% selectivity in shape (Figure 4.4).

4.3.2. Chemical Anisotropy

On top of the branching anisometry of the particles, patchiness is induced in two ways: firstly, by a different chemical composition of the protrusions, namely polystyrene, and the seed polyNIPAM particle. Transmission electron micrographs of double protruded particles of 945 nm show a clear contrast between the center and the protrusions (Figure 4.7A), indicating chemically different compounds. Yet, the contrast of the center is darker than what is commonly observed for polyNIPAM particles, indicating the presence of linear, non cross-linked polystyrene molecules. Before polymerization of the protrusions, we infrequently observe fusion of protrusions of different seed particles[**33, 53**] yielding intriguing angled colloidal particles such as shown in Figure 4.7B and C. The contrast difference in electron microscopy together with the observation of inter-particle fused protrusions corroborates our assignment of "protrusions" and "seed particle" to the respective parts of the anisotropic particles.

4.3.3. Patchiness through Roughness Anisotropy

Secondly, patchiness can also be integrated into the surface properties of the particles: in excess of surfactant, secondary particles nucleate in the aqueous phase during polymerization, and subsequently adsorb at the polyNIPAM seed surface uncovered by the protrusions. The adsorbed smaller secondary particles render the center of the anisometric particles rough, in contrast to the smooth protrusions (Figure 4.4 and Figure 4.9). Adsorption of secondary particles in contrast to, for example, formation of smaller protrusions is convincingly supported by electron micrographs of unwashed colloidal dispersions (Figure 4.11F). The size ratio of the roughness and the protrusions can be altered by the initiator and the surfactant concentration, as well as the amount of swelling monomer. Higher initiator concentrations induce more radicals upon heating, and therefore smaller secondary particles, that is, less roughness (Figure 4.9B). Similarly, higher surfactant concentrations lead to smaller secondary particles.

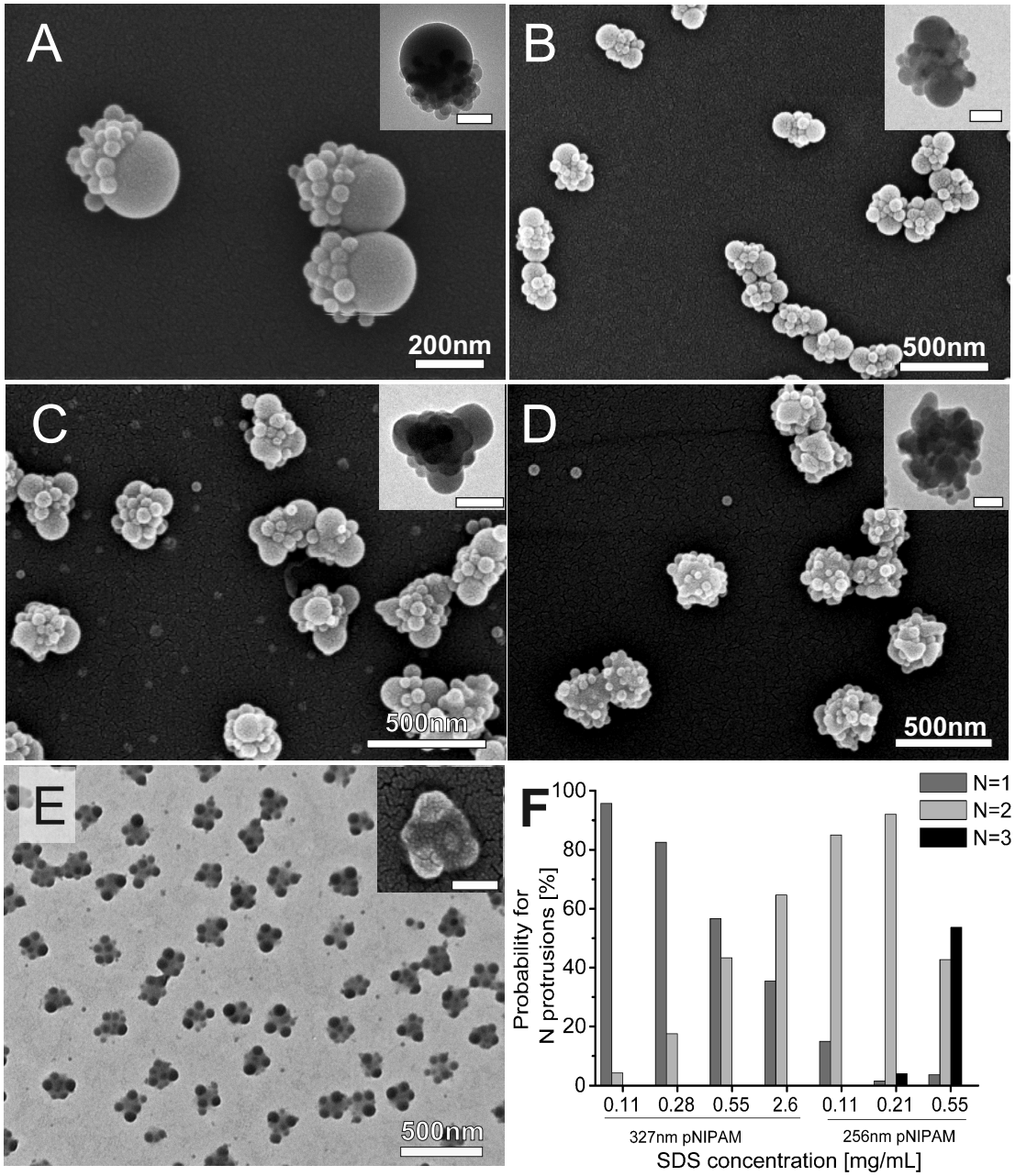

Figure 4.4. The number of protrusions, or patches, can be systematically changed from A) one to B) two, C) three or D) multiple by increasing the surfactant sodium dodecyl sulfate (SDS) concentration. Here, 7.5 μL styrene per mg polyNIPAM was used. Note that the seed particles are covered with secondary nucleated particles, whereas the protrusions are smooth larger spheres. E) If only 2.5 μL styrene per mg polyNIPAM is used for swelling, many more small protrusions occur at the same surfactant concentration as in B). F) Statistics for gradual transition from single to triple protrusions with surfactant concentration. Two different seed particles of 327 and 256 nm have been employed as indicated. Scalebars in the insets are 100 nm.

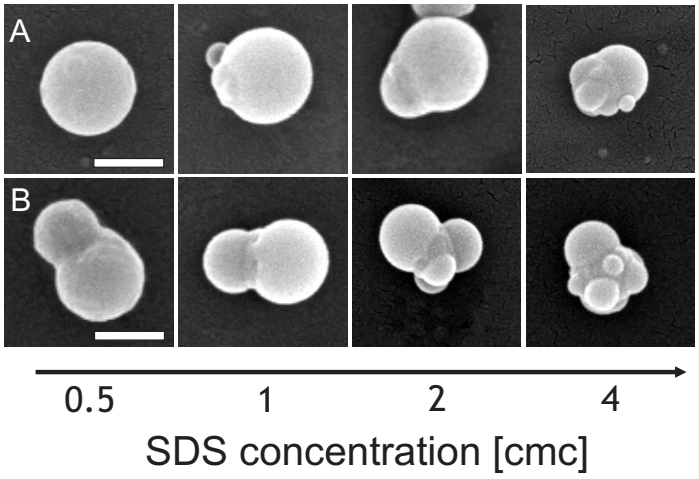

Figure 4.5. The number of protrusions, or patches, on highly cross-linked PS spheres is influenced by the SDS concentration during synthesis. A) PS seed particles with vinyl acetate coating $VA = 2$, and B) $VA = 6$, and swelling ratio $S = 7$. Scale bars are 300 nm.

Integration of roughness in the particles is an option: by reducing the surfactant concentration nucleation of secondary particles can be suppressed as shown exemplarily for polyNIPAM seed particles of 945 nm in 4.12D. Equivalently, addition of an inhibitor in the aqueous phase may be employed.

The larger the volume of the swelling monomer is compared to the volume of the polymer particles, the larger the protrusions after phase separation are, limited by the maximum swelling volume of the seed particles. When polyNIPAM spheres of 256 nm diameter are swollen with 2.5 μL styrene per mg particles, they exhibit multiple, on average 5.7 ± 1.4, small protrusions (Figure 4.4E) after phase separation. Increasing the swelling volume leads to fusion of the protrusions on the surface during phase separation, possibly due to steric hindrance at the interface. Interestingly, larger swelling volumes (≥ 5 μL) lead to two protrusions at these synthesis conditions, independent of the exact swelling amount (Figure 4.4C and 4.11).

Polystyrene seeds show this effect of fusion of the protrusions of one seed particle even more clearly. Figure 4.6 A and B show colloids obtained for A) swelling ratio $S = 2$, and B) $S = 7$ at different vinyl acetate coating densities. Especially for higher coating densities ($VA = 6, 8$), the number of protrusions decreases for higher swelling ratios. The decrease is due to fusion of the initially multiple protrusions on the surface, because they cannot all be accommodated on the seed particle surface at a larger protrusion size.

When increasing the swelling of 327 nm polyNIPAM seeds from 2.4 μL to 21.45 μL styrene per mg seed particles the size of the single and double protrusions increases from 240 $\pm$ 11 nm to 314 $\pm$ 11, and from 205 $\pm$ 14 nm to 267 $\pm$ 15 nm, respectively.

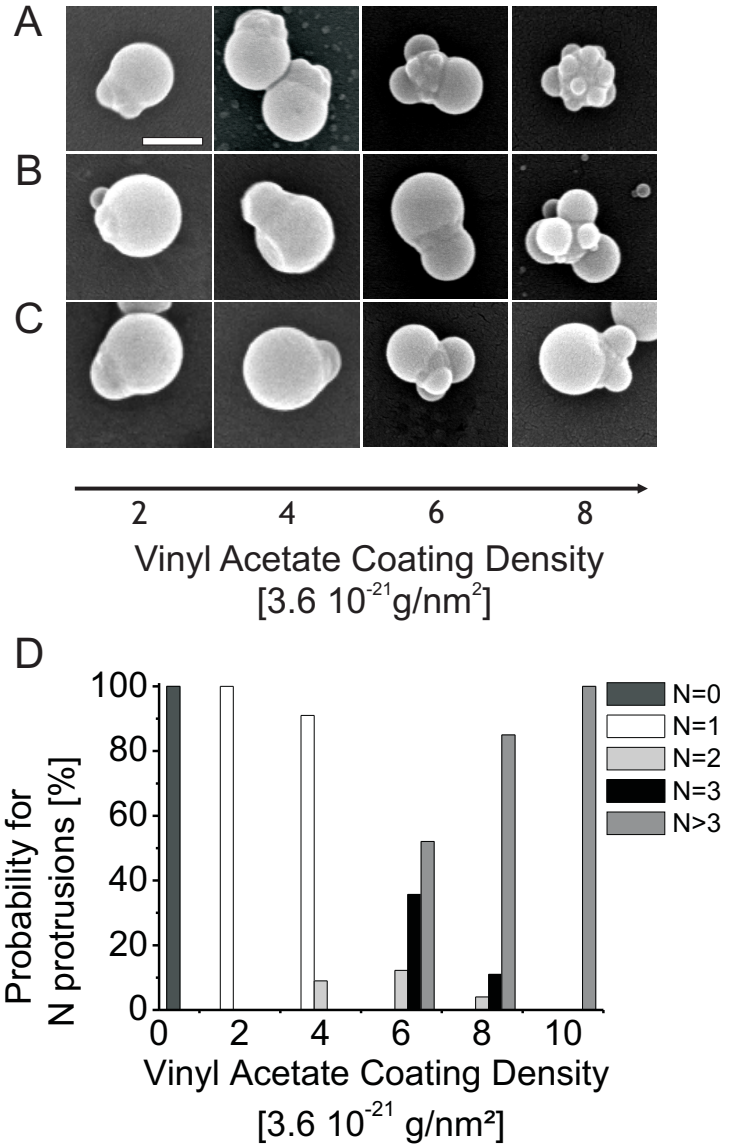

Figure 4.6. SEM images of colloids obtained by variation of the coating density of the seed particles with vinyl acetate, and swelling ratio A) S=2 (SDS concentration c_{SDS} = 1.1× cmc, where c_{cmc}=2.36 g/L) , B) S = 7 (c_{SDS} = 1.1×cmc) and C) S = 7 (c_{SDS} = 2.0×cmc). D) The fractions of colloidal particles with N protrusions are continuously tunable by the coating density (S = 2, c_{SDS} = 1.1×cmc).

Despite the ninefold increase in swelling volume, the protrusion volume only doubles, indicating a maximum swelling volume of the seed particles. Excess styrene is converted into secondary nucleated particles, whose average size depends on the amount of styrene present in the system (Figure 4.9C and 4.11). At very large styrene volumes popcorn-like colloidal particles are obtained again, though two main protrusions may still be

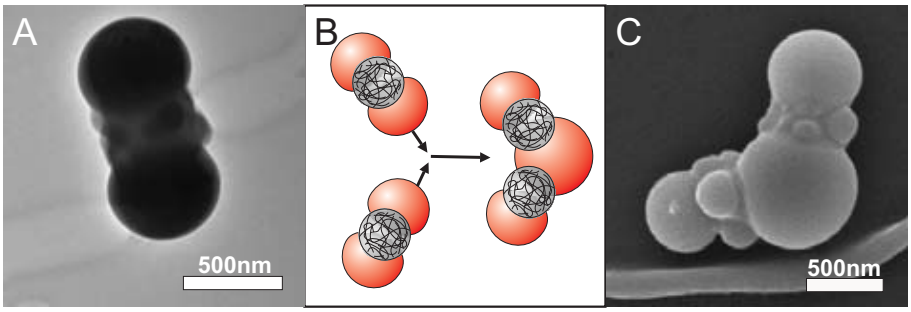

Figure 4.7. A) TEM reveals that polyNIPAM spheres of 945 nm with two polystyrene protrusions consist of chemically different seeds (center) and protrusions. The lower contrasts is evidence of polyNIPAM, whereas the higher contrast indicates polystyrene. B) Before polymerization, the still liquid styrene protrusions may undergo interparticle fusion, into complex angled colloidal molecules. C) SEM micrograph of two fused double protruded particles.

discerned. Note also that the volume of two double protrusions is 1.07 times the volume of a single protrusion, corroborating the formation of one or multiple protrusions from the same swelling volume per seed particle. For calculating these numbers we assumed spheres for single protrusions, and spherical caps for double protrusions.

Therefore, the anisotropy dimension "surface roughness" is continuously tunable with the initiator and surfactant concentration, and yield particle patchiness together with the smooth protrusions. In combination with depletion interaction induced by polymers smaller than the roughness dimension, site-specific interactions can be induced, see also Chapter 6.[**65, 66, 63, 64**]

Highly cross-linked polystyrene seeds turned rough during the synthesis of the multiple protrusions without adsorption of secondary nucleated particles. A possible reason for this may be unreacted cross-linkers in the seed particles that lead to local crimping of the seed particles after the protrusion synthesis. We can utilize this by making colloidal molecules with rough seed particles and smooth protrusions, as depicted in Figure 4.8. Roughness can also be introduced by employing rough seed particles in the synthesis (see Chapter 6).

4.3.4. Versatility of the method

Due to its underlying generality the technique can be applied to a wide variety of seed sizes and materials given significant cross-linking of the polymer network to induce multiple protrusions. To demonstrate the versatility of our fabrication method, we used 256, 327, 581, and 945 nm polyNIPAM spheres, as shown in Figures 4.9 and 4.12. The anisotropic colloids obtained for all seed sizes exhibited the smoothly changeable anisotropies upon variation of the synthesis conditions as described above. An overview of representative shapes obtained for different seed particles can be found in Figure 4.12. First experiments on magnetite filled polyNIPAM seed particles show that also

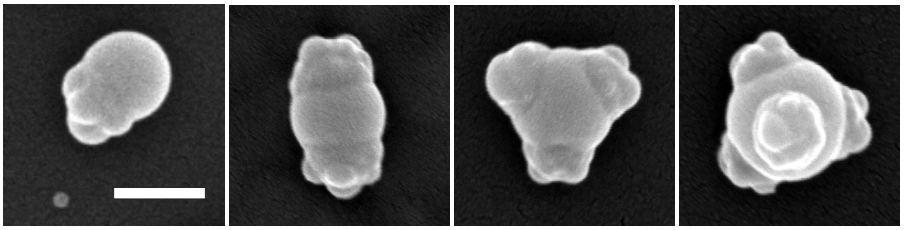

Figure 4.8. By fusion of their liquid protrusions, the highly crosslinked polystyrene seeds can also form colloidal molecules. SEM images show colloidal molecules from $N = 1-4$ fused protrusions with the rough seed particles arranged symmetrically at the outside (S=7, VA=4, c_{SDS} = 4×cmc). Scale bar is 300 nm.

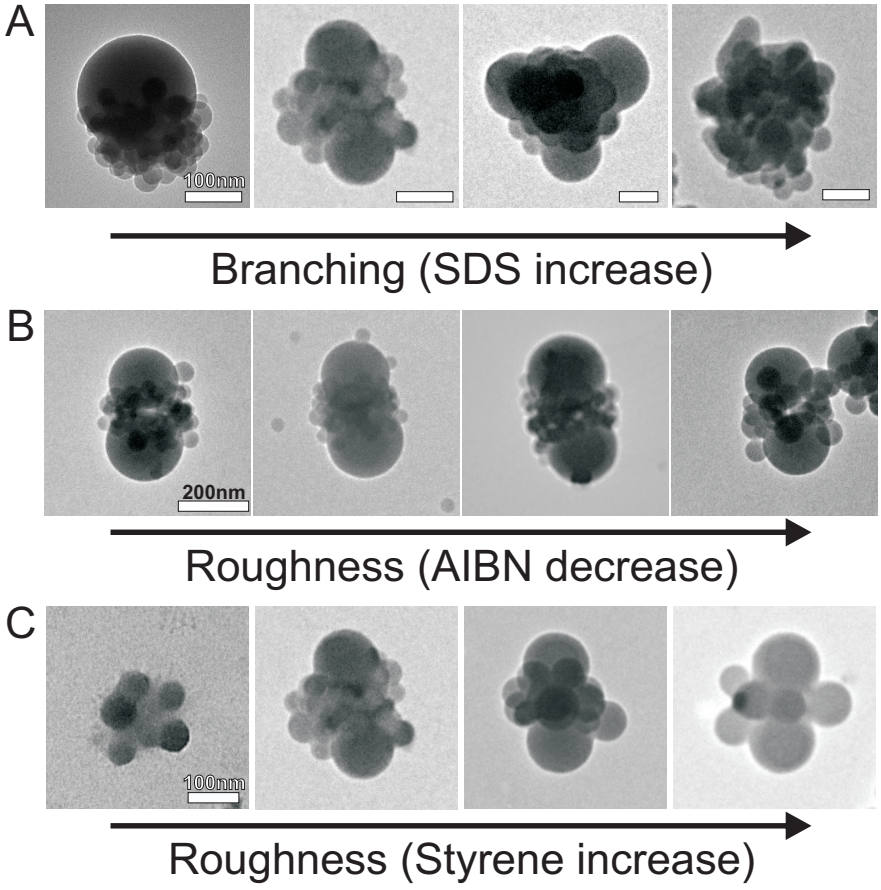

Figure 4.9. Continuously changeable anisotropy dimensions: A) Branching of the particles, or the number of protrusions, by increasing the SDS concentration (256 nm pNIPAM seeds, see also Figure 4.4 for SEM images). Scale bar is 100 nm. B) Site specific roughness induced by adsorption of secondary particles onto the center: variable by the AIBN concentration (20 mg/mL left to 4 mg/mL right; 327 nm pNIPAM seeds) or C) styrene concentration (2.5, 5, 10 and 15 μL styrene per mg pNIPAM; 256 nm pNIPAM seeds).

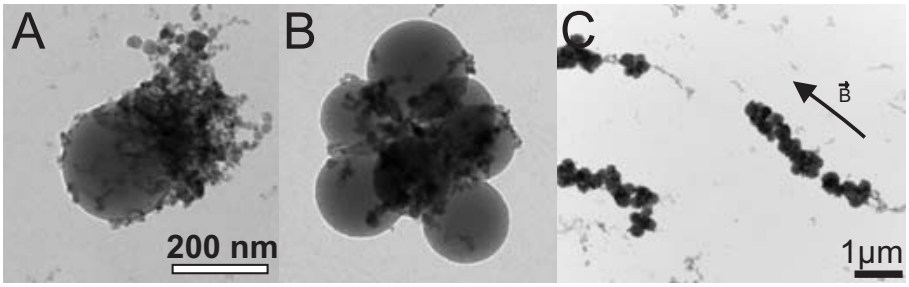

Figure 4.10. TEM micrographs of magnetite containing polyNIPAM seed particles with A) one polystyrene and B) multiple polystyrene protrusions. C)TEM micrograph of magnetite filled polyNIPAM colloids with multiple styrene protrusions dried in the presence of a magnet. Arrow indicates direction of the magnetic field.

magnetic anisotropy can be integrated (Figure 4.10A and B). The polyNIPAM cores contain significantly more magnetite particles compared to the protrusions. Note that again the polystyrene protrusions (grey spheres in Figure 4.10 A and B) have a much stronger contrast than the polyNIPAM seed particles, making them in fact invisible except for the magnetite particles located inside them. Hence, in Figure 4.10A the lower grey sphere is associated with the polystyrene protrusion, whereas the sphere consisting of small magnetite particles is associated with the polyNIPAM seed particle. In Figure 4.10 B, multiple polystyrene protrusions are located around the polyNIPAM seed particle, which again is not visible due to the low contrast. The magnetite particles at the center of the colloid allow for assignment of the center as the polyNIPAM seed particle.

When a diluted sample is dried on top of a magnet, the particles align centered along the field direction (Figure 4.10C). Magnetic anisotropy opens up the possibility to guide assembly of the particles by combining magnetic fields as well as patchy interactions. We are confident that the synthesis can easily be extended to other polymer particles and sizes.

4.4. Conclusions

In summary, we presented a new method to make anisotropic polymer particles in a simple one step synthesis based on the formation of multiple protrusions by seeded emulsion polymerization. Changing the stabilization of the protrusions by the amount of surfactant allows for control over the final number of protrusions, or branching anisotropy of the particles. The adsorption of smaller polymer particles during polymerization onto the uncovered polyNIPAM cores adds roughness to the complexity of the obtained colloidal particles. The relative roughness can be continuously altered by the initiator

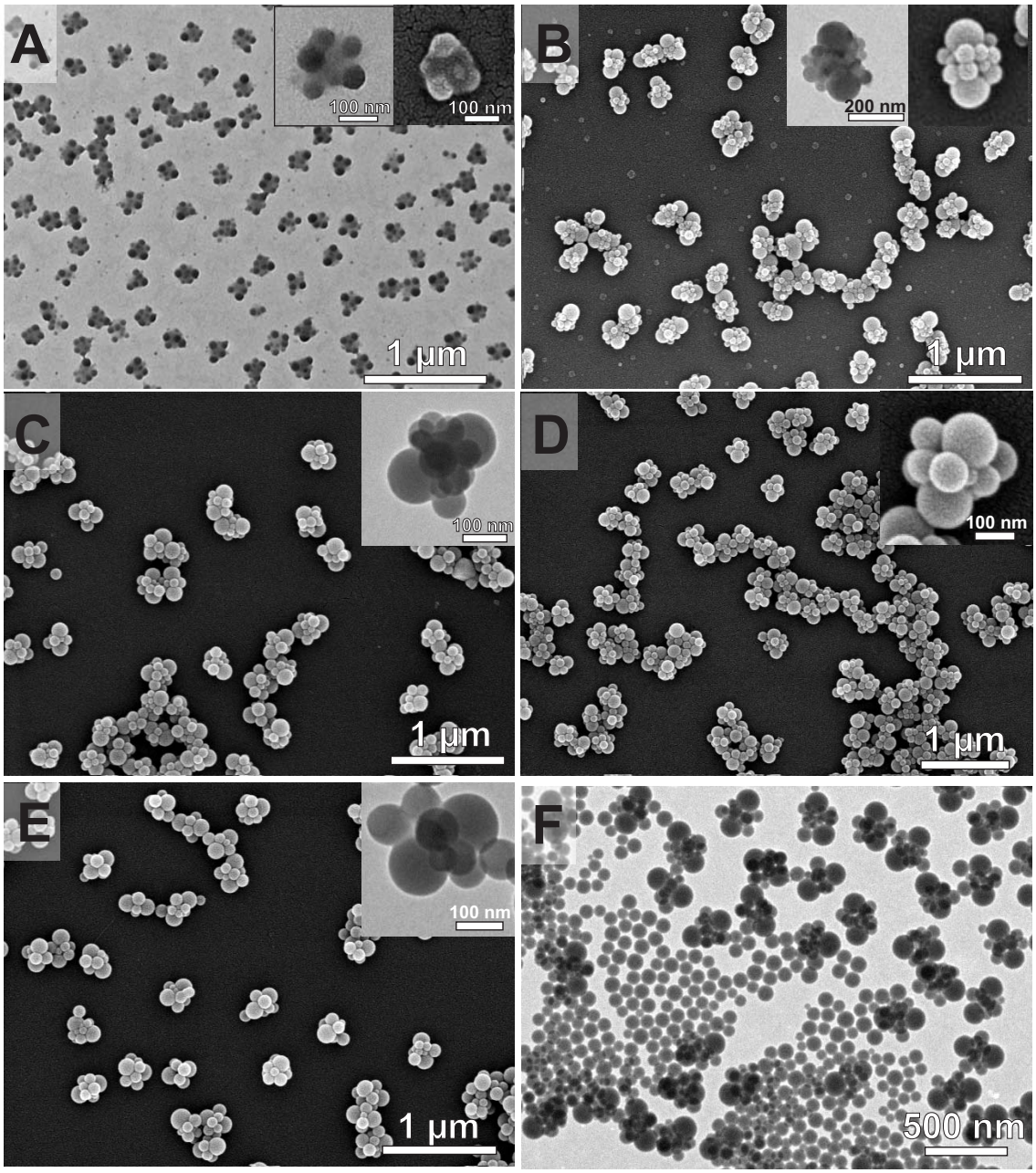

Figure 4.11. TEM and SEM pictures of anisotropic colloids obtained from 256 nm polyNIPAM seed spheres at increasing styrene volume (A-E). Swelling concentrations in μL styrene per mg polyNIPAM used were A) 2.5, B) 5, C) and F) 10, D) 15 and E) 25. For low swelling ratios multiple small protrusions are observed. Upon growth of the protrusions at larger styrene volumes, the number of protrusions remains two independent of the styrene volume, while the secondary nucleated particles that attach at the pNIPAM center grow in size. F) TEM micrograph of sample as obtained from solution. Secondary nucleated polystyrene particles visible in the left bottom corner of the image agree in size with the smaller spherical particles attached to the polyNIPAM seeds between the protrusions.

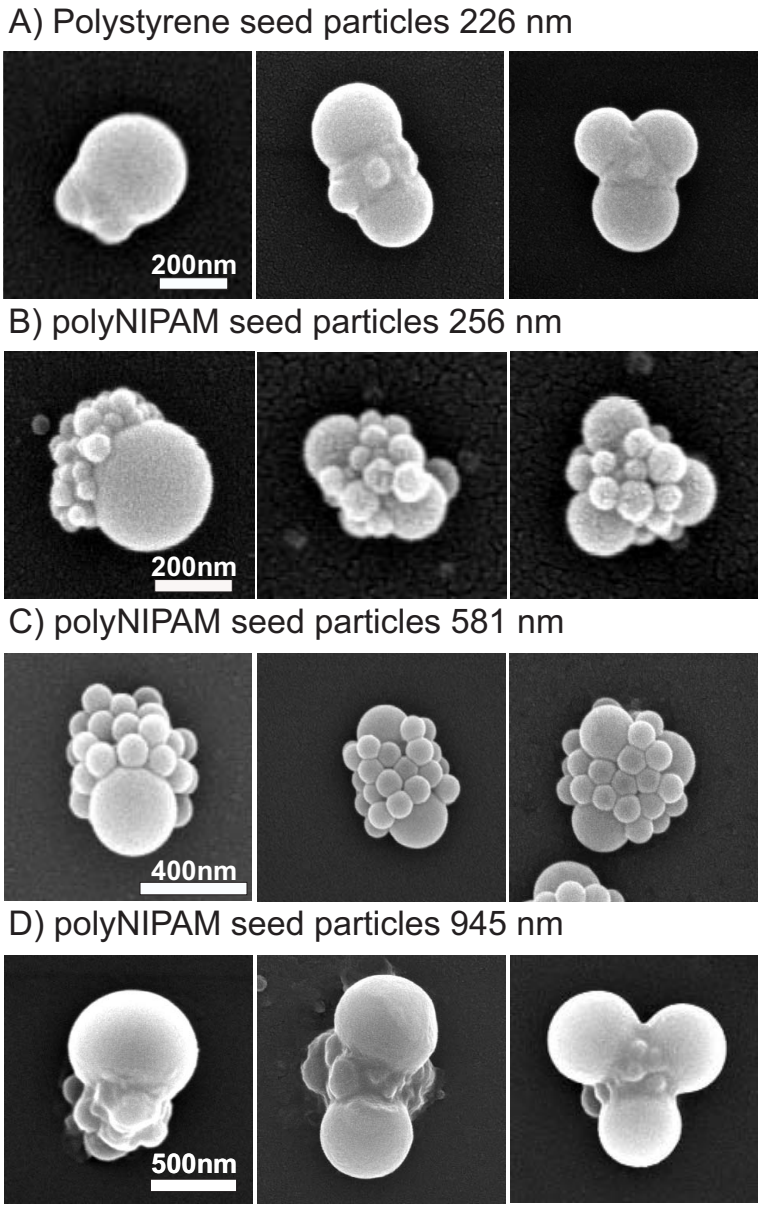

Figure 4.12. SEM micrographs of anisotropic colloids obtained from swelling different seed particles with styrene.

and surfactant concentration and the amount of swelling monomer. Chemical anisotropy is integrated through polyNIPAM centers and polystyrene protrusions. Unique for this synthesis is the high yield in combination with the control over the particle topology. The generality of the approach has been demonstrated by using different sizes of cross-linked polyNIPAM, polystyrene and magnetite filled polyNIPAM as seed particles, and should be easily extendable towards other polymer particles.

Acknowledgments

Jan Hilhorst and Sandy Heinen are thanked for the many experiments and discussions on the synthesis described in this chapter. Matijs Hoogenraad is thanked for experiments on polystyrene colloids, Bob Luigjes, Richard Daniëls, Simone Droog, and Nico Hommels for help with magnetite filled seed particle synthesis, and Dr. Andrei Petukhov and Vera Abramova for useful discussions. This chapter is reprinted with kind permission from [**71**].

5

Bottom-up Assembly of Solid-Stabilized Emulsions by Fusion of Liquid Protrusions on Polymer Particles

Abstract

We investigate the self-assembly of colloids with liquid protrusions over long times. Fusion of the liquid protrusions of many colloidal particles leads to the formation of droplets with colloids attached to the interface, also called Pickering emulsions. We can follow this "bottom-up" assembly into micron-sized emulsion droplets by employing fluorescent colloidal polystyrene particles. The size of the emulsion droplets can be described by the mechanism of the assembly process: the droplet radius of N merged liquid protrusions scales with N times the volume of a liquid protrusion, and the wetting properties of the colloidal spheres. The colloids on the interface are found to be arranged in a hexagonal fashion with excess disclinations present for stress relief. We explore the possibilities of a self-sharpening process in the droplet size distribution from geometric considerations, and experimentally by employing *in situ* sectioning of polymerized emulsion droplets as well as assemblies where the droplet has been removed. In the latter case we find collapsed spherical clusters consisting of jammed particles for small N, and shells consisting of multiple layers of particles.

5.1. Introduction

Self-assembly of colloidal particles at oil-water interfaces is driven by the large energies associated with the reduction of the energetically unfavorable bare oil-water interface. This assembly process can be utilized to stabilize fine dispersions of oil droplets in water, and vice versa, with colloidal particles. [**72, 73, 74**] Stability against coalescence is provided by the mechanical barrier formed by the particles, but is only of kinetic, and not thermodynamic nature. Hence, for the formation of most solid-stabilized emulsions, also called Pickering emulsions, a fine dispersion of one phase into the other has to prepared by mechanical means, such as shaking or shear, before colloidal particles can adsorb at the droplet interface. This "top-down" approach of emulsion formation is limited by the minimum droplet size obtainable from mechanical methods, and generally is in the size range of tens of microns.

Assembling Pickering emulsions from "bottom-up" opens up the possibility of accessing a much smaller size range, and, with it, applications for the smaller emulsion droplets. Examples include the fabrication of hierarchical colloidal particles for use in colloidal assembly,[**75, 76, 77**] or as a template for making capsules with controlled permeability. [**78, 79, 80**] Starting from cross-linked polystyrene spheres with liquid protrusions [**33, 53**], we prepare Pickering emulsions by fusion of the liquid protrusions. We investigate the arrangement of colloidal particles at the interface, and the droplet size as a function of synthesis parameters. We also present first studies on preparing multi-layered micron-sized shells by removal of the droplet template.

5.2. Experimental

5.2.1. Rhodamine labelled polystyrene colloids

Cross-linked vinyl-acetate coated polystyrene spheres 222 nm in diameter were synthesized as described in the experimental section of Chapter 2. Five milliliter of this polystyrene suspension was swollen with 0.5 mL 1 mM rhodamine B in dichloromethane (CH_2Cl_2, Acros Organics) and 1.0 mL 17 mg/g aqueous sodium dodecylsulfate (SDS, Prolabo) for 3 days while stirring with a magnetic PTFE bar. Then, the suspension was continued stirring with an open cap for 6 h to evaporate the CH_2Cl_2. Polystyrene colloids with rhodamine dye were obtained.

5.2.2. Bottom-up assembly of Pickering emulsions and Shells

Typically, an 0.5 mL aliquot of the polystyrene dispersion was swollen with styrene at various swelling ratios $S = m_{styrene}/m_{polystyrene}$ and 0.4 mL 17 mg/g aqueous SDS for 24 h. The swollen seed dispersion was subsequently heated to 80°C for 2h to induce the formation of liquid protrusions, and then stirred at room temperature to induce coalescence of the liquid protrusions. The samples were either polymerized to obtain solid Pickering emulsions, or injected in EtOH for removal of the emulsion droplet.

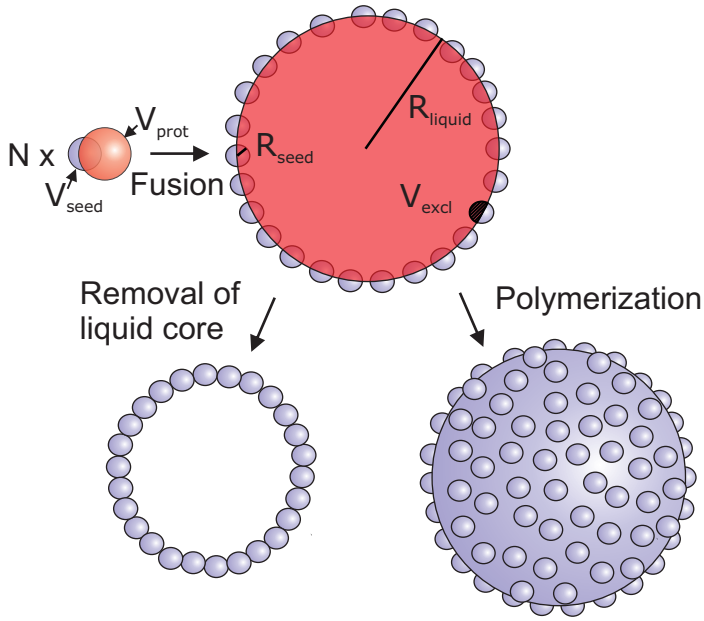

Figure 5.1. Schematic drawing to illustrate the "bottom-up" assembly of Pickering emulsions by fusion of protrusions on polystyrene seed particles. The liquid droplets with seed particles attached to the interface, can be polymerized for imaging with electron microscopy. Alternatively, the liquid template may be removed to obtain shells made from the polymer seed particles.

Polymerization of the samples was initiated by 40 μL azoisobutyronitril (AIBN, 0.02 g/mL styrene) per mL particle suspension. For removal of the liquid core, 100 μL of the swollen, heated, and coalesced suspension was injected in 10 mL EtOH. Alternatively, an aliquot of the sample was left stirring with the cap of the flask removed to evaporate the styrene for one week. To enhance the stability of potential shells of colloidal particles formed by removal of the liquid droplet, samples were also stored in an autoclave above the glass transition temperature of polystyrene at 110°C for 30 minutes. The obtained clusters were sedimented by gravity and redispersed in water several times.

5.2.3. Characterization

Scanning electron microscopy Samples of diluted polymerized particle dispersions were dried on polymer-coated copper grids, and sputter coated with 4 nm platinum/palladium prior to imaging with a scanning electron microscope (SEM XL FEG 30, Philips).

(cryo-) Focused Ion Beam - Scanning Electron Microscopy (FIB-SEM) Copper grids with dried particle dispersions were imaged at room temperature with a focused ion beam - scanning electron microscop (Nova Nanolab 600, FEI, Netherlands).

The samples can be gradually sectioned in situ with a focused ion beam (FIB), and subsequently imaged by (high resolution) scanning electron microscopy (SEM). Sectioning conditions used were 30kV, 0.3 nA for the rough cut, and 5 kV, 0.12 nA for the final polishing step.

For preparing aqueous samples for cryo-FIB-SEM, droplets of the suspension were placed in between two copper rivets (dimensions 4.5 x 3 mm, BAL-TEC AG, Liechtenstein, sealed by Tissue-Tex), and plunge-frozen in LN_2 (liquid nitrogen) slush. Samples were then transferred under vacuum to the cryostatic preparation chamber (Quorum Technologies, PP2000T, United Kingdom). In the preparation chamber a fractured surface was created at -160°C by breaking off the copper rivet. The surface is coated with platinum for 60 s under argon atmosphere. After increasing the temperature to -140°C, the samples are transferred to the cryo stage in the microscope chamber, where they can be sectioned with FIB and imaged with SEM. Sectioning conditions used were 30kV, 0.3 nA.

5.3. Results

5.3.1. Bottom-up Assembly of Pickering emulsions

Clusters assembled through fusion of liquid protrusions on seed particles are not limited to aggregates of a few seed particles as described in Chapters 2 and 3, but may grow into micron-sized droplets with solid seed particles attached at the interface. For more details on the formation of liquid protrusions on polymer particles, see Chapters 2, 3 and 4. Given that the liquid protrusion carried by each seed particle is sufficiently large, a substantial number of seed particles can be accommodated at the interface of the droplet created by merging of their respective liquid protrusions (Figure 5.1). The resulting particle-covered droplets are in fact Pickering emulsions (see also Chapters 7, 8 and 9, [**72, 73**]) assembled in a "bottom-up" fashion. Contrary to Pickering emulsions described in Part 3, these "bottom-up" Pickering emulsions are not thermodynamically stable, and may be at most kinetically stabilized against coalescence by the dense layer of polystyrene spheres at the interface.

We can follow the assembly of these large objects directly with confocal microscopy by employing rhodamine swollen polystyrene spheres as seed particles. Before and after swelling with styrene, the 220 nm seed particles are barely visible with confocal microscopy, as shown in Figure 5.2A and B, respectively. The absence of larger fluorescent objects indicates that assembly has not commenced yet, and hence, that protrusions are only induced on the seed particles after heating to 80°C. Indeed, after heating the swollen samples for 2 h, micron-sized fluorescent objects are visible by confocal microcopy (Figure 5.2C). Polymerization of the merged styrene droplets allows for direct imaging of the Pickering emulsion droplets with a scanning electron microscope (Figure 5.1). Examples of the solidified particle-stabilized emulsions are shown

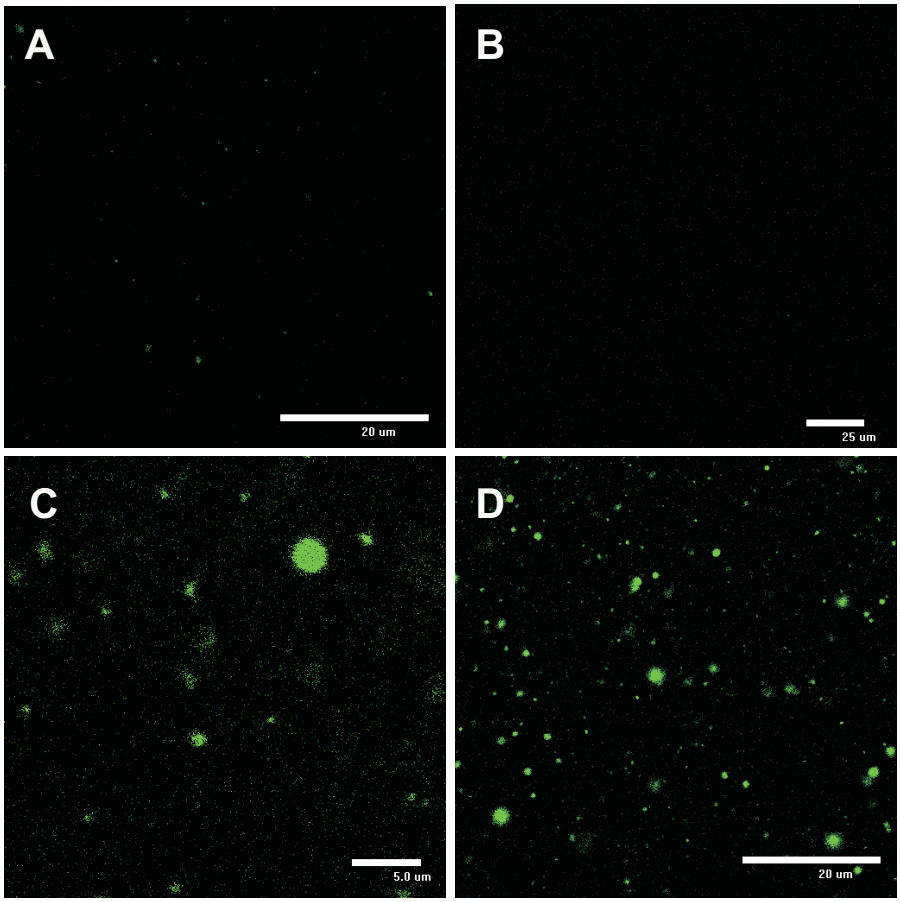

Figure 5.2. Confocal microscope images of A) polystyrene seed particles containing rhodamine dye, B) fluorescent polystyrene spheres swollen with styrene for 24 h, C) styrene swollen and heated polystyrene seeds after 2 h coalescence time, D) after evaporation of styrene for a week.

in Figure 5.3. The small spheres partially emerging from the large spherical assembly are the seed particles. The larger sphere, which they are attached to, is made up of the merged protrusions.

This assignment of seed particles and merged protrusions is supported by sectioning through polymerized Pickering emulsions with a focused ion beam (FIB), which allows for a look inside the spherical assemblies. We found the inside to be solid and made up of a material comparable to that of the adsorbed seed particles (Figure 5.3, right column), which is deduced from the low contrast between the seed particles and the droplet. The latter is of course no surprise since the polystyrene seed particles were swollen with styrene to induce the liquid styrene protrusions. After merging into larger droplets, polymerization converts the styrene emulsions to polystyrene. The low contrast makes a distinction between seeds and droplet on the inside very difficult. From SEM images, we can nevertheless investigate the arrangement of the seed particles at the interface.

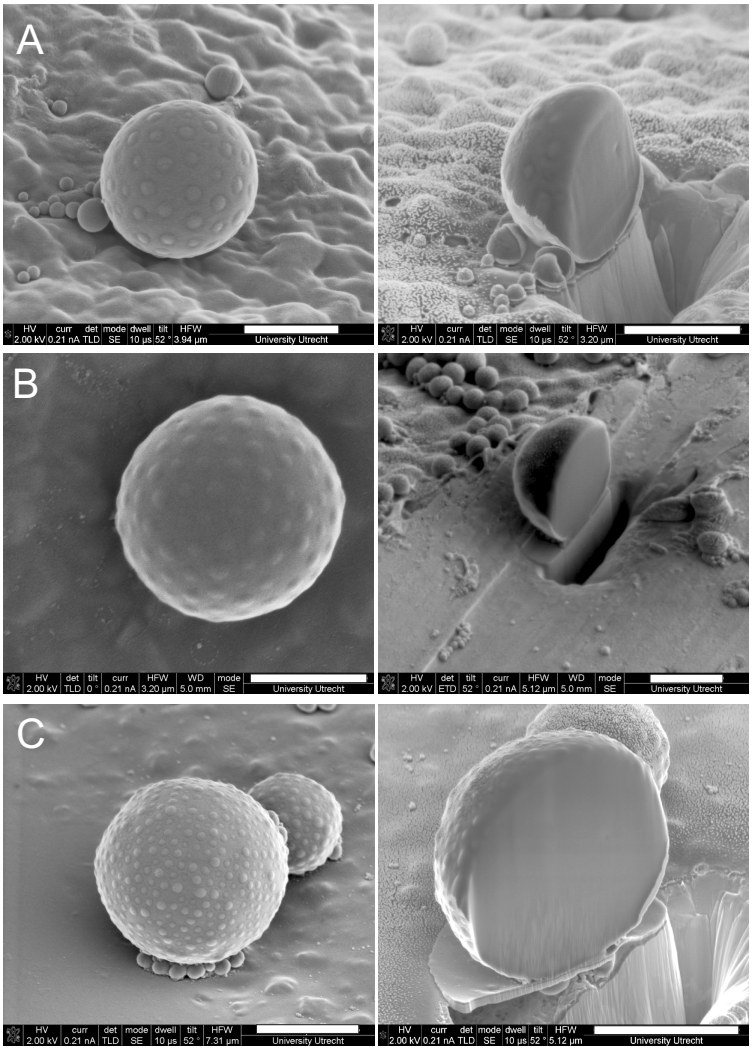

Figure 5.3. Polymerized Pickering emulsions from bottom-up assembly by merging of liquid styrene protrusions on polystyrene seed particles. Three examples of emulsion droplets before (left) and after (right) sectioning by a focused ion beam. Scale bar is 1 μm in A) and B), and 2 μm in C).

5.3.2. Seed Arrangement on the Droplet Surface

As can be seen in the left column of Figure 5.3, the seed spheres adsorbed at the interface of the fused protrusions are partially immersed in the liquid droplets, with only a small cap exposed to the aqueous phase. At high densities of seed colloids at the surface, the particles even touch inside the liquid droplet. Although there is still interfacial area unoccupied, adsorption of another seed particle and protrusion is then prevented, unless the energy costs for deformation of the spherical droplet interface are lower than the gain in energy by the adsorption. Even more so, in small aggregates, the colloidal spheres were found to partially overlap after polymerization (Figure 3.5). For highly covered droplets as shown in Figures 5.3 and 5.4A, the seed particles are

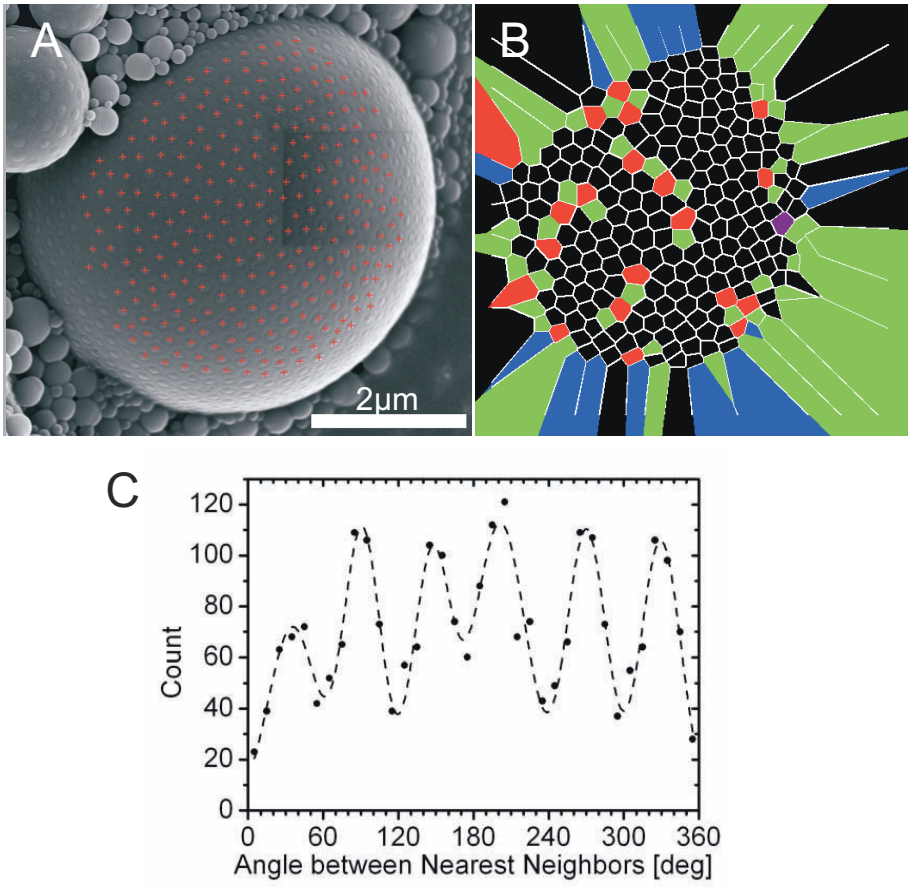

Figure 5.4. Short range order is visible at high swelling ratio. Scanning electron micrographs: A) Polymerized Pickering emulsion droplet with seed particle positions specified by crosses. B) Voronoi construction from image in A). Number of nearest neighbors are indicated by color: 5, green; 6, black; 7, red; 8, purple. Excess dislocations in chains of 5-7-5-7... defects are visible and known to reduce elastic strain. C) Nearest neighbor angle distribution of seeds on the interface.

ordered at the interface. To quantify this short range order, the seed positions are determined, and from that the nearest neighbor angle distribution of the spheres in the center of the 2D projection is calculated. Six peaks with an average distance of $60 \pm 3.6°$ confirm hexagonal arrangement of the seed particles (Figure 5.4C). Furthermore, there are chains of excess dislocations in the form of 5-7-5-7-..-5 defects visible in the Voronoi plots besides single five fold disclinations. These excess dislocations are expected for systems with R_{liquid}/(interparticle spacing) > 5 (5.4C)[**81**] and known to relieve elastic strain on the surface by forming high angle grain boundaries [**82**].

In Chapter 3, we showed that electrostatic repulsion between the charge-stabilized spheres was negligible compared to depletion induced by polymerization of the droplet. This was deduced from observations on colloidal molecules (Figure 3.6) and sparsely

covered emulsion droplets (see Figure 3.9). There, the seed particles are not found at maximum distance from each other after polymerization, but in cluster at the interface that exhibit local short-ranged ordering. However, before polymerization, together with surface packing constraints electrostatic repulsions may still play a role [**83, 84**] in the seed arrangement at the interface.

5.3.3. Droplet Size as a Function of the Number of Integrated Seed Particles and Swelling Ratio

The "bottom-up" assembly process for these Pickering emulsions implies that the droplet size is set by the number of merged protrusions, the swelling ratio S, and the wetting angle of the colloidal seed particles. We assume that each integrated seed particle contributes a volume $V_{prot} = S{\cdot}V_{seed}$, where V_{seed} is the volume of a seed particle, to the central liquid core (see also Figure 5.1). Then, for N assembled particles and protrusions, the total liquid volume of the fused protrusions is given by

$$V_{liquid} = N \cdot S \cdot V_{seed}. \tag{5.1}$$

Furthermore, the volume that the immersed part of the seed particles takes up in the liquid core can be approximated by a spherical cap as:

$$V_{excl} \approx N \cdot \frac{\pi}{3} R_{seed}^3 \,(2-z)\,(1+z)^2 \qquad \text{if } N \gg 1, \tag{5.2}$$

where z is the immersion depth of the seed particles into the liquid droplet normalized to the seed radius R_{seed}. Hence, an expression for the radius of the particle-covered droplet as a function of the swelling ratio S and number of integrated seeds, N, is:

$$\begin{aligned} R_{liquid} &= \frac{3}{4\pi}\left(V_{liquid} + V_{excl}\right)^{1/3} && (5.3)\\ &\approx \left(\frac{3}{4\pi}N\right)^{1/3}\left[SV_{seed} + \frac{\pi}{3}R_{seed}^3(2-z)(1+z)^2\right]^{1/3} && (5.4)\\ R_{liquid}/R_{seed} &= N^{1/3}\cdot\left[S + \frac{1}{4}\,(2-z)\,(1+z)^2\right]^{1/3}. && (5.5) \end{aligned}$$

To determine the total number of seed particles adsorbed onto a droplet, we scale the number of particles visible on SEM micrographs with the surface on which they are located to the surface of the droplet, presuming that the coverage with seed particles is homogeneous.

Experimental data for vinyl acetate coated CPS Pickering emulsions ($z = 0.16$) is in good agreement with this simple model as presented in Figure 5.5), despite the fact that the nominal swelling volume calculated from the swelling ratio does not equal the actual volume of the single protrusions. However, in the course of the experiment, monomer taken up by the liquid droplets due to diffusion compensates for the initial shortage. The good quality of the fit is another indication that the solid-stabilized emulsions form by merging of liquid protrusions.

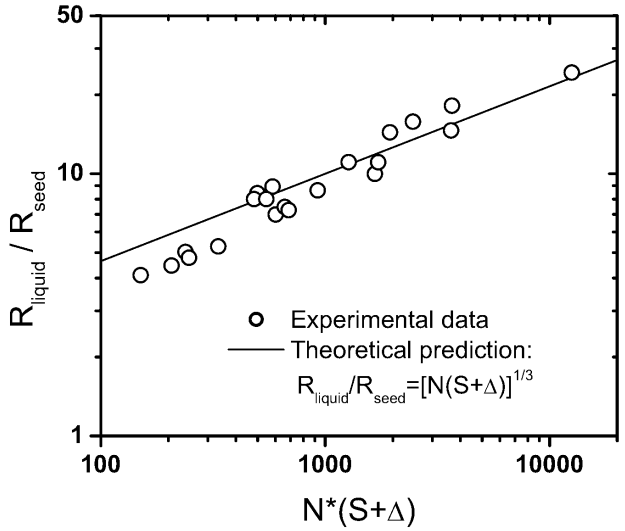

Figure 5.5. The emulsion droplet size can be described as a function of the swelling ratio, S, and the number of swollen seeds, N, by $R_{liquid}/R_{seed} = [N \cdot (S + \Delta)]^{1/3}$, where $\Delta = 1/4 \cdot (2-z)(1+z)^2$. Experimental data shown is for droplets covered with vinyl acetate coated polystyrene spheres of $R_{seed} = 111$ nm and $z = 0.16$.

5.3.4. Self-Sharpening Droplet Size

Furthermore, qualitative observations were made with respect to the maximum size of the colloidal assemblies. Small liquid protrusions limit the number of seed particles that can attach to the interface of the merged droplets. Hence, for low swelling ratios mainly monomers, dimers and trimers were found. On the other hand, large liquid protrusions can form droplets stabilized by many seed particles. Considering that the droplet surface grows with the number of seed particles $N^{2/3}$, while the area occupied by the seed particles increases with N, we conclude that the system cannot grow beyond a critical size N_{max}. At this maximum number of integrated seed particles, the following condition has to be fulfilled:

$$N_{max} A_{sphere,excl} = \sigma A_{liquid}, \tag{5.6}$$

where $A_{sphere,excl}$ is the interfacial area covered by one seed sphere, A_{liquid} is the total surface of the droplet of merged liquid protrusions, and σ is the maximum surface coverage, defined as the surface area occupied by seed particles divided by the total surface area of the droplet. The maximum number of seeds at which no additional seeds can be integrated is thus given by:

$$N_{max} = 4\sigma^3 \cdot (z^2 - 1)^{-3} \cdot \left(2 + 4S - 3z + z^3\right)^2. \tag{5.7}$$

Therefore, we expect this bottom-up self assembly process to be self-sharpening in the droplet size distribution. [**85**] Quantitatively, we indeed observed that larger protrusion as well as longer assembly times promote the formation of larger particle-stabilized droplets. Yet, even after five days of coalescence time, no limiting droplet size could be found, and often, small clusters of 1-5 colloidal particles were observed next to the Pickering emulsions droplets with several hundreds of integrated particles. Apparently, the assembly process furthers the growths of a few large assemblies instead of a uniform size increase of all clusters.

To investigate this further, we have a taken closer look at the SEM micrographs of the particle stabilized droplets (Figure 5.3). The colloidal particles at the interface are immersed in the droplet at different immersion depths, z. The reasons for this variation in the immersion depth could be an inhomogeneous coating with vinyl-acetate, but also effects of polymerization. During polymerization, the styrene droplet with density $\rho_S = 0.909$ g/cm^3 shrinks upon conversion to the more dense polystyrene ($\rho_{PS} = 1.05$ g/cm^3. Styrene is certainly a good solvent for polystyrene, which allows for an overlap of the polystyrene spheres inside the droplets, as demonstrated in Chapter 3. The good solubility together with the droplet size decrease during polymerization could lead to the apparent different immersion depths seen in SEM micrographs. For densely covered droplets, it could be favorable to immerse some colloids deeper into the styrene liquid to accommodate more colloidal particles. In the extreme case, some particles may fully migrate to the styrene phase. However, no indications for this were found in FIB sectioned polymerized Pickering emulsions, but the low contrast between colloids and droplet phase make it difficult to find such fully immersed particles. Yet, we can conclude that the polystyrene particles insufficiently stabilize the emulsion droplets to halt coalescence at high surface coverages. [**85**]

5.3.5. Shells and Clusters by Removal of the Liquid Droplet

So far, we have convinced ourselves that the colloidal molecules and Pickering emulsions are seed particles organized at the interface of a liquid droplet created by merging of their liquid protrusions. The liquid styrene droplet, whose size is correlated with the number of adsorbed seed particles, acts as a template to organize the colloidal spheres. By injecting of a small quantity of cluster suspension into ethanol, which is a solvent for both water and styrene, we remove this droplet template. Gradually, the droplet is dissolved in ethanol, leading to an increased surface coverage, and, eventually to a collapse of the colloidal layer at the interface into clusters. Confocal microscope images confirm the presence of spherical assemblies after removal of the template (Figure 5.2). However, some non-spherical half-moon shaped objects were seen as well. Combined use of SEM and FIB allows for imaging of the clusters and their insides.

Intriguingly, assemblies made up of a few hundreds of seed particles become spherical clusters after removal of the template, with closely packed seed spheres at the surface (Figure 5.6, left column). However, when we cut the clusters open with a focused ion beam, we find that they are not hollow, but consist of jammed spheres, see Figure 5.6, right column. Most likely, seed spheres at the interface of the droplet were not closely packed and collapsed upon removal of the template. For large numbers of seed particles, hollow spaces are observed in the collapsed structures, that possibly originate from locally jammed particles that form stable cavities. For even larger assemblies, extending over more than 5 μm after removal of the liquid droplet, we find hollow spherical structures, see Figure 5.7. The shell consists of multiple layers of jammed particles that stabilize the cavity sufficiently to prevent further collapse as observed for smaller assemblies (Figure 5.6). Hence, the size of the original droplet template, which is of course connected with the surface coverage with colloids, plays a role in determining the outcome of the cluster suspensions after the templates were removed. The larger Pickering emulsions form a more dense coverage with colloidal particles, and form stable shell-like clusters upon removal of the droplet. Smaller emulsion droplets were not sufficiently densely covered, and instabilities upon removal of the droplet template lead to a collapse into spherical, but not hollow, aggregates. From these observations on hollow spherical structures, we can deduce, that probably no or only few seed particles migrated to the styrene phase, otherwise we would have found a particle network inside the larger structures as well.

Stabilization of the colloidal particles while the template is still present may lead to uniform, single layer shells after dissolution in ethanol. Preliminary experiments on heating aqueous cluster suspensions in an autoclave above the glass transition temperature of styrene for 30 minutes, did not improve the shell stability, possibly due to the fat that the layer of particles is not close-packed at the interface.

Last, we confirm that the collapse of shells into spherical assemblies of jammed seed particles is not induced by drying. For this, we examined plunge-frozen cluster dispersion with cryo-FIB-SEM. With a focused ion beam, cross-sections of the frozen aqueous dispersion were prepared, and the obtained interfaces were imaged with SEM. In Figure 5.8, SEM images of cross-sections of a dispersion of clusters after removal of the droplet template are shown. Clusters of particles are visible in the frozen aqueous surrounding, with small clusters exhibiting jammed spherical aggregates of seed particles. Larger clusters exhibit a small cavity in the center of multiple layers of seed particles, similar to the observations on medium (Figure 5.6) to large clusters (Figure 5.7).

5.4. Conclusions

In this chapter, we have investigated the "bottom-up" assembly of particle stabilized emulsion droplets by employing the merging of liquid protrusions on the surface of

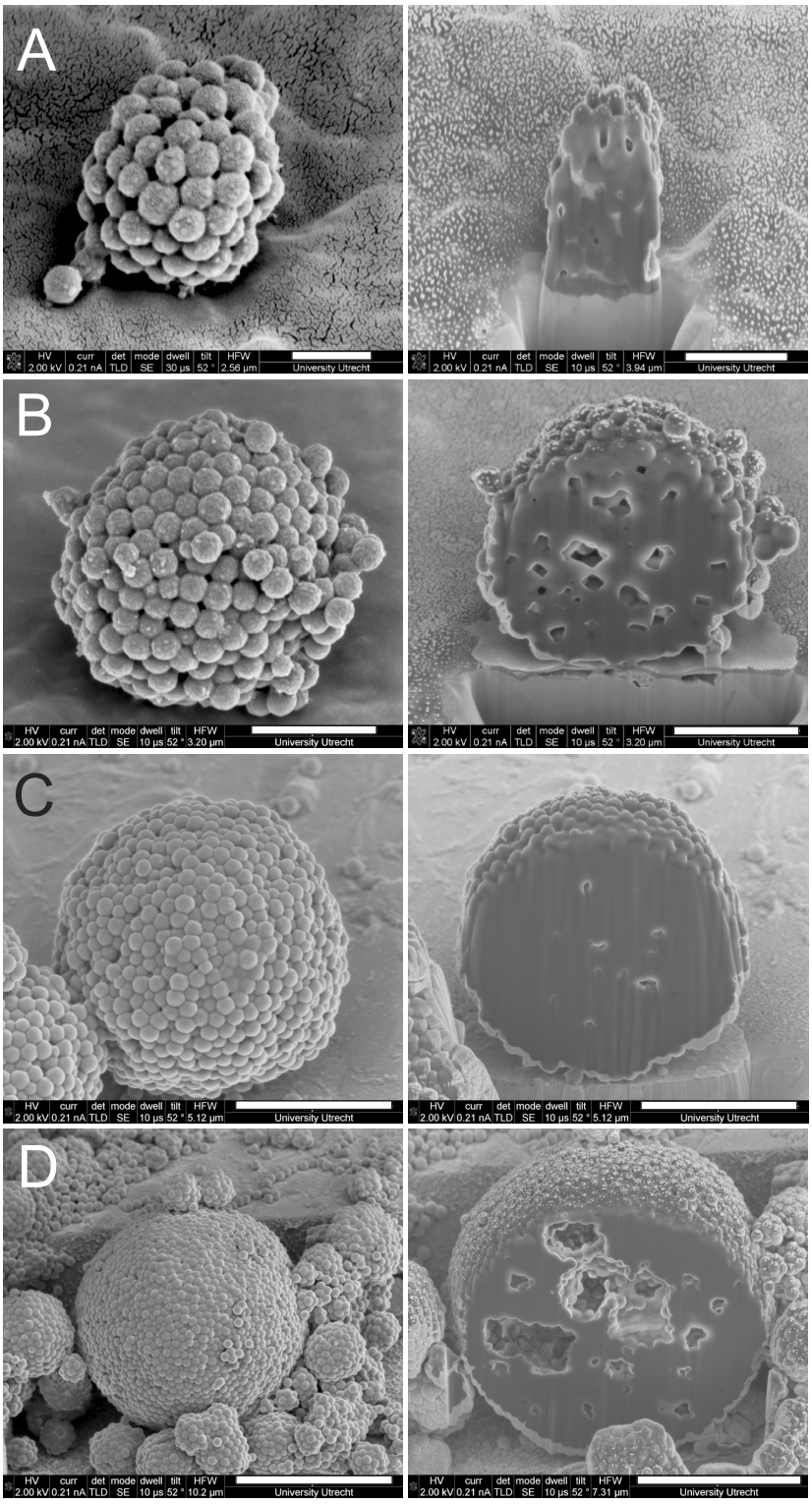

Figure 5.6. After removal of the droplet of the Pickering emulsions, clusters of polystyrene particles are observed. Smaller spherical clusters consist of individual particles, whereas larger clusters have cavities stabilized by jammed particles. Scale bars are A) 500 nm, and 1 μm, B) 1 μm, C) 2 μm, and D) 4 μm and 3 μm.

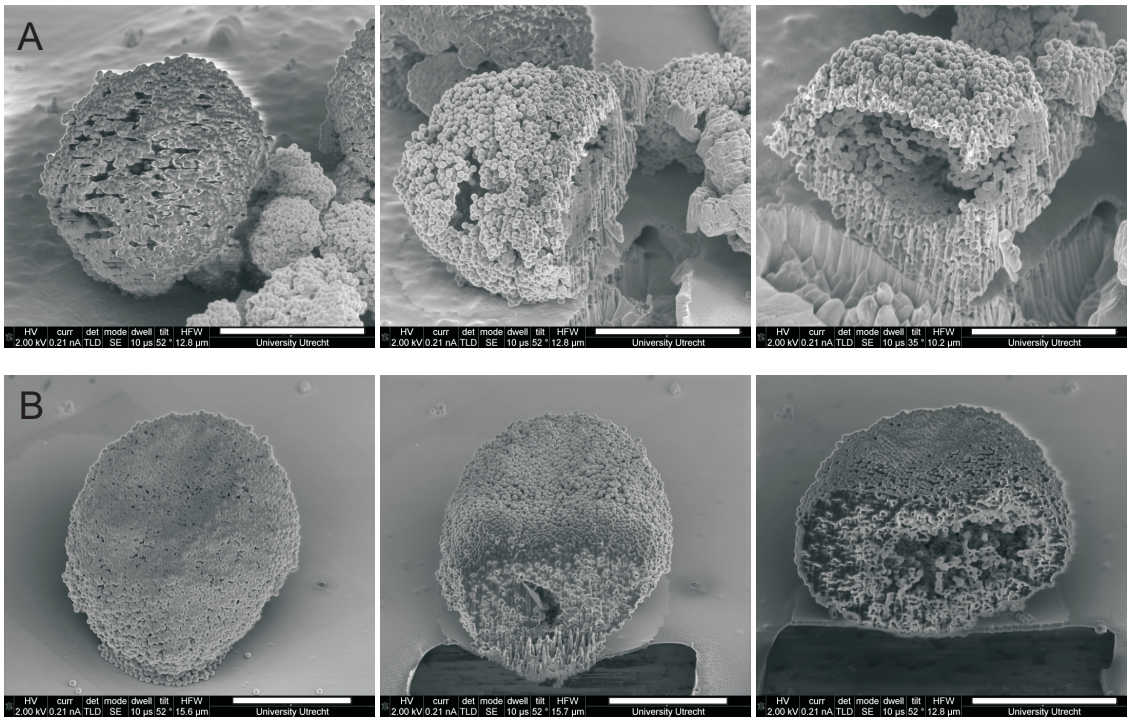

Figure 5.7. SEM images of two large assemblies consisting of a multilayer shell and cavity that were sectioned with Focused Ion Beam. Left to right: intact clusters, one sectioning step, second sectioning step. Scale bars are 5 μm, except for A) very right: 4 μm.

polystyrene particles. The "bottom-up" assembly technique offers the advantage of accessing smaller droplet sizes compared to the commonly "top-down" prepared Pickering emulsions. The latter are prepared from mechanically breaking up emulsions, limiting the attainable droplet sizes to the micrometer range.

The droplet sizes may in principle become more monodisperse over time through a self-sharpening process. While the free surface area of the droplets grows with the number of integrated seed particles, N, as $N^{2/3}$, the surface area occupied by the colloidal seeds grows as N. The maximum droplet size is then expected to depend on the swelling ratio, the wetting angle, and the maximum surface coverage. The size of the observed droplets can be well described from these geometric considerations, and depends both on the swelling ratio, the wetting angle, and the number of assembled seed particles.

The seed particles which occupy the droplet interface are at dense coverages found to exhibit short-range ordering, which was quantified by calculating the nearest neighbor angle distribution. As expected for colloidal particles on droplets, defects and excess dislocations were observed.

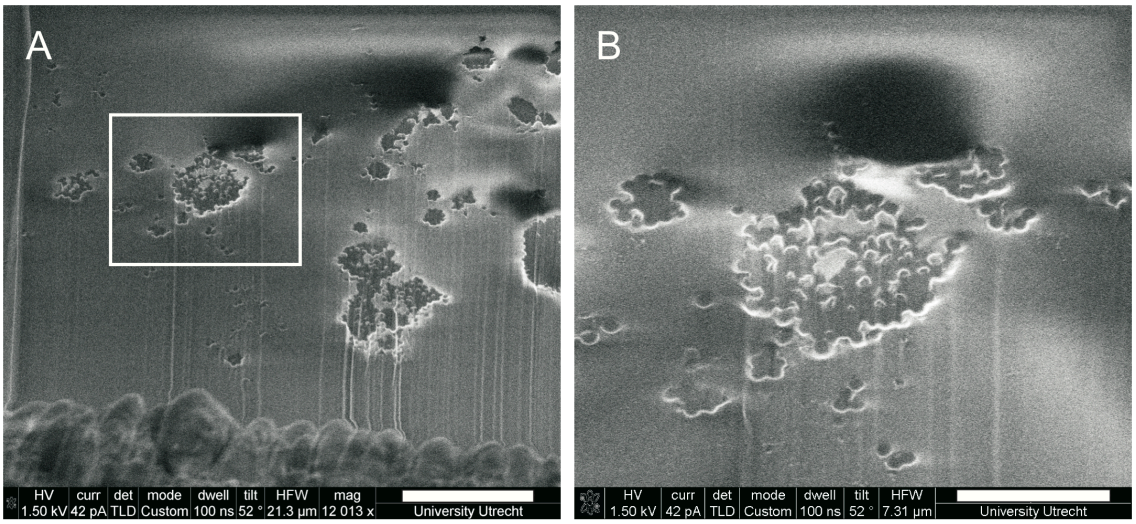

Figure 5.8. A, B) Cryo-SEM images of plunge-frozen cluster suspensions after removal of the liquid droplet. Spherical assemblies of colloidal particles immersed in the frozen aqueous phase are visible. Smaller aggregates consist of jammed particles, whereas larger spherical structures are made up of many particles surrounding cavities. B) Enlarged inset of A), which shows a hollow spherical shell of particles in the middle, and smaller aggregates around it. Scale bar is 5 μm for A, and 2 μm for B.

Removing the liquid droplet by transferring the clusters to ethanol allows for making spherical clusters of seed particles. Low numbers of seed were found to form dense clusters, whereas larger assemblies formed stable multilayered shells with cavities.

Acknowledgements

I thank Matthijs de Winter for performing the (cryo-)FIB SEM on the colloidal golf balls and shells, and Arie Verkleij for discussion and kind permission for measurement time at the FIB SEM. Volkert de Villeneuve is thanked for help with the analysis of the colloidal golf balls with IDL. This chapter is based in parts on the unedited author's version of a Submitted Work that was subsequently accepted for publication in The Journal of the American Chemical Society, copyright American Chemical Society after peer review. To access the final edited and published work, see http://pubs.acs.org/doi/abs/10.1021/ja8079803.

Part 2

Colloidal Micelles

6

Experimental Observation of Colloidal Micelles

Abstract

We present a general way for producing patchy colloidal particles by making use of the surface roughness specific strength of the depletion interaction. Site-specific attraction, or patchiness, is obtained by employing polystyrene dimers consisting of one sphere with a smooth surface, and another one decorated with smaller spherical particles. By careful adjustment of the concentration of a depletant, we are able to control the strength of the depletion potential such that only the smooth sides of the colloidal particles become attractive. We find that the rough polystyrene particles with one smooth patch act like colloidal surfactants, and assemble into micelle-like structures. The experimentally obtained cluster distribution can be reproduced by computer simulations. A theoretical framework originating from surfactant micelles is adapted to describe the colloidal micelles.

6.1. Introduction

Patchy particles are colloidal particles with distinct attractive sites, so called patches, that have been envisioned to lead to self-assembly into pre-determined, complex structures. [**14, 15, 11, 86**] There are numerous examples of experiments on patchy particles conducted by simulations,[**14**] which predict promising applications for such particles, for example in the controlled assembly into new clusters,[**54, 17, 87**] liquid phases, [**9**] and crystal structures. [**6, 88, 10**] They may furthermore be used as models for self-assembling systems, such as surfactants and viruses, that in contrast to their equivalent in nature are observable *insitu* during assembly and disassembly. Yet, an experimental realization of truly patchy particles is still not at hand.

The reasons for this are that the synthesis of colloidal particles that may be used in *in vitro* experiments lags far behind the possibilities of simulations when it comes to the particle patch topology, and specifically, the placement of site-specific attractive spots. Experimental systems showing side specific colloidal interactions include the assembly of spherical particles with opposite hemispheres, so called Janus particles, for example dipolar, [**89**] amphiphilic,[**57**] partially magnetic, [**59**] and metallodielectric spheres. [**58**] For an overview on Janus particle synthesis and assembly, see a recent review by Shan Jiang [**90**]. Yet, the controlled distribution of small patches on the surface has proven to be experimentally challenging, often being restricted to very specific geometries and producing uniform particles only in low yields.[**12**]

In Chapters 2, 3, and 4, we have presented new synthetic approaches to fabricate colloidal particles with distinctly distributed patches. The synthesis presented in Chapter 4 furthermore allows for high quantities of particles with the desired number of patches and topology. However, the essential next step is to modify the procedure such that the patches become locally attractive sites on the colloidal particles. A tunable interaction strength and reversibility are furthermore desirable properties for the study of equilibrium structures that might be formed by these patchy particles.

Here, we present the synthesis and assembly of particles with one attractive patch by employing the influence of surface roughness on the strength of the depletion interaction. First, we describe the synthesis of particles with rough and smooth sides in high yields. Next, we induce site-specific depletion attraction by addition of a non-adsorbing polymer smaller than the roughness on the colloidal particles, which we show to result in attraction between the smooth sides of the colloids only. At larger depletant concentrations, the patchy particles assemble into colloidal micelles, with a well-defined peak in the cluster distribution. The position of the peak for two different polymer sizes seems to Experimental observations are well-matched by Monte-Carlo simulations. We discuss the similarities and differences with surfactant micelles by applying micelle theory to our colloidal micelles.

6.2. Experimental

6.2.1. Synthesis of polystyrene dimers with a rough and a smooth side

Linear polystyrene spheres (LPS). Monodisperse linear polystyrene spheres of 1.42 μm in diameter were synthesized by dispersion polymerization. For this 126 mL ethanol (200 Proof), 14 mL deionized water, 10 mL styrene (Reagant Plus, Sigma Aldrich), 0.136 g asobisisobutyronitrile (AIBN) and 5.0 g polyvinylpyrrolidone (PVP, K30, $M_w = 40$ kg/mol) were measured into a 200 mL round bottom flask, closed with a rubber septa and sealed with Teflon tape. To commence polymerization, the flask was immersed in a 75°C oil bath with its axis of rotation at roughly a 60° angle. Polymerization was carried out for 20 h while rotating the flask at 60 rpm.

Cross-linking of the polystyrene spheres. Typically, an aliquot of a 10% w/w linear polystyrene dispersion was washed with methanol and redispersed in 10% w/w aqueous polyvinyl alcohol (PVA, M_w= 89-98 kg/mol) twice. After a third centrifugation step the pellet was redispersed with 1% w/w aqueous PVA such that the obtained colloidal dispersion had a weight fraction of approximately 20% w/w. For cross-linking the polystyrene particles, a procedure by Kim et al. was followed.[**31**] A swelling emulsion consisting of 1% w/w aqueous PVA solution (M_w= 89-98 kg/mol) and 20%v/v styrene containing 1.5% v/v divinylbenzene, 10% v/v TMSPA (3-(trimethoxysilyl)propyl acrylate , Sigma Aldrich) and 2% w/w V65B (2,2'-azodi (2,4'-dimethylvaleronitrile), initiator)) was prepared either by tip sonication (Branson Sonifier 150, speed 8 for 2 min), or by homogenization (UltraTurrax 20, 8000 rpm for 4 min). The volume of the swelling emulsion was chosen such that a swelling ratio of 4 was achieved, where we define the swelling ratio as $S = m_{monomer}/m_{polymer}$. Polymerization was carried out for 24 h while rotating in a 70°C oil bath. The final cross-linked particles were 2.41 $\pm$0.04 μm in diameter. During this step, the surface of the particles became corrugated by adsorption of polystyrene particles nucleated during polymerization, as depicted in Figure 6.2B. The diameter of these secondary particles was 0.18 μm. The dispersions of cross-linked polystyrene spheres were washed by centrifugation and redispersion in 1 % w/w aqueous PVA solutions three times.

Protrusion formation. To obtain smooth protrusions on the cross-linked polystyrene seed particles, the previous step was repeated.[**26, 27, 28, 31**] A 20% w/w colloidal dispersion of cross-linked polystyrene seed particles (CPS) was swollen with an emulsion consisting of 1% w/w aqueous polyvinyl alcohol solution (M_w= 89-98 kg/mol) and styrene containing 1.5% v/v divinylbenzene and 2% w/w V65B. The protrusions formed

by phase separation induced by an overswelling of the particles [**91**] have a smooth surface. They were polymerized by tumbling in an oil bath at 70°C for 10 h. The volume of the protrusions relative to the seed particles is determined by the swelling ratio S.

For colloids with protrusions smaller than the seed particles, the seed dispersion was swollen with a 10% w/w emulsion (swelling ratio $S = 2$). The final particles have a protrusion radius of 1.11±0.06 μm (smooth side) and a seed radius of 1.46±0.06 μ m (rough side). The total length is 4.9±0.12 μm. A SEM image of the obtained particles is shown in Figure 6.2C. We term these colloidal particles R(1.5)S(1.1) colloids, after the sizes of the rough and smooth side. Furthermore, large rough spheres of radius 1.6±0.1 μm are employed in the experiments.

To fabricate colloids with protrusions larger than the seed particles a 20% w/w swelling emulsion with swelling ratio $S = 4$ was employed. The final anisotropic particles have a protrusion radius of 1.66 μm (smooth side) and a seed radius of 1.20 μm (rough side). The total particle length is 4.70±0.15 μm. A scanning electron micrograph (SEM) is shown in Figure 6.2D. We refer to these colloids as R(1.2)S(1.7) colloids.

Both colloidal dispersions were washed by centrifugation until all secondary nucleated particles were removed. They were redispersed in 0.3% w/w aqueous polyvinyl alcohol solution (M_w=30-50 kg/mol).

A schematic of the synthesis of polystyrene dimers with a rough and a smooth side is depicted in Figure 6.2.

6.2.2. Sample Preparation

Coating of the glass capillaries. To prevent the particles to adsorb at the glass slide in the presence of depletant, a coating was applied to the glass capillaries.[**64**] For this, a pipette tip was connected to 50 mm borosilicate glass capillaries via elastic tubing and PTFE tape. Successively, 0.5 mL 1 M aqueous KOH (Merck), 0.5 mL millipore water, 0.5 mL 1% w/w aqueous polyethyleneimine (Fluka, $M_w = 60$kg/mol, 50% aqueous solution), 0.5 mL millipore water, 0.5 mL 1% w/w aqueous dextran sulfate sodium salt (Acros Organics) and 0.5 mL millipore water were run through the capillaries. To remove excess polymer and salt, the capillaries were then placed in Millipore water for 10 mins and dried with nitrogen gas.

Microscope sample preparation The samples were prepared by mixing of aqueous solution of polymer, colloidal dispersion, 20 mM NaCl (unless stated otherwise), and millipore water. All components contained 7.7 mM sodium azide (extra pure, Acros Organics) to prevent bacterial growth. The colloidal volume fraction was chosen to be 0.3% w/w. For depletion interaction, dextran polymers of $M_w = 110$kg/mol (Fluka) and $M_w = 500$kg/mol (Sigma Aldrich) were dissolved in 7.7 mM aqueous sodium azide

(NaN_3). After preparation, the samples were filled in the capillaries and sealed with UV sensitive glue onto microscope slides. To prevent sedimentation the microscope samples were rotated on stage (VWR) at 10 rpm.

6.2.3. Characterization

Microscopy. Polymerized samples were imaged using a scanning electron microscope (SEM XL FEG 30, Philips). The dried samples of particles were sputter coated with 4 nm platinum/palladium prior to imaging. Light microscopy was performed with a Zeiss Axioplan microscope using an oil immersion lens (NA=1.4, 100x magnification). Pictures were captured with a Basler scout camera and saved to disk using Streampix.

Dynamic light scattering (DLS). To measure the polymer sizes, DLS was performed with a Malvern Zetasizer ZS at a scattering angle of 173°.

Zetapotential. The surface-, or zetapotential, of the dimers was measured by laser Doppler electrophoresis with a Malvern Zetasizer ZS.

6.3. Results and Discussion

6.3.1. Surface Roughness Specific Depletion Potential

Depletion attraction arises in dispersions of colloidal particles when a second, smaller type of non-adsorbing colloid or macromolecule, also termed depletant, is introduced in the suspension. The center of mass of the depletant cannot approach the larger colloidal particles closer than its radius r_p, restricting the volume available to the depletant (see Figure 6.1). The volume around the colloidal particles unavailable to the depletant is called the exclusion volume. When two large colloids come closer together than the diameter of the depletant, $2r_p$, their exclusion volumes overlap and the volume accessible to the depletant increases by the amount of this overlapping volume ΔV. The volume available to the depletant, and hence its entropy, increase, which reduces the free energy of the system by:[**92, 93, 94**]

$$u_{AO} = -\Pi \Delta V = -\rho_p k_B T \Delta V. \tag{6.1}$$

Here, Π is the osmotic pressure caused by the depletant, $\rho_p = n/V$ is the number density of the depletant, k_B is Boltzmann's constant and T is the temperature. The depletion potential increases with larger depletant concentrations and with larger overlap volumes.

For smooth spheres with a radius R_s at a distance r, the overlap volume in the presence of a depletant of size r_p is simply given by the volume of the two spherical

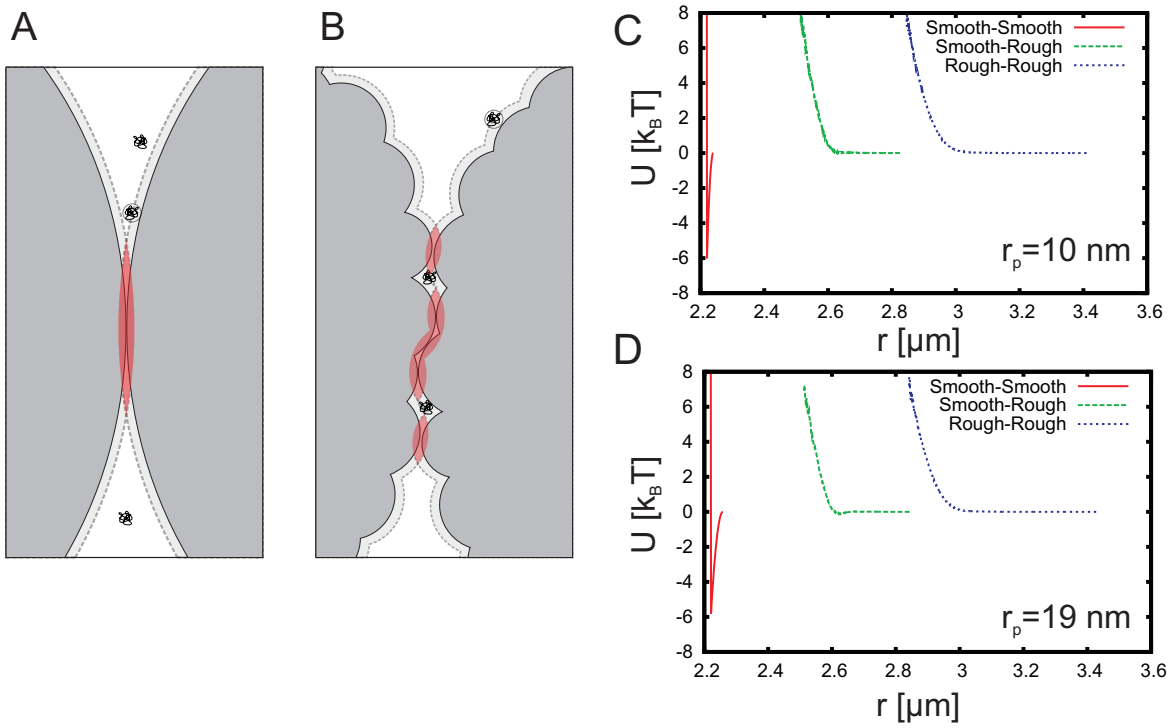

Figure 6.1. The roughness specific depletion interaction. In the presence of small depletants (here depicted as polymers with radius r_p) colloidal particles are surrounded by a layer inaccessible to the depletant (dotted line). If colloidal particles approach such that their excluded volumes overlap, the depletant gains entropy resulting in a net attraction between the colloids. The arising attraction is called the depletion potential and is proportional to the overlapping excluded volume (shaded regions). For two rough spheres (B) the overlap volume is restricted to the overlapping regions of the roughness, whereas for smooth particles (A), the overlap volume is given by the large spherical caps. Note that although the shaded areas in this 2D projection may look equally large for the rough and the smooth particles, their 3D overlap volumes are significantly smaller, because they extend out of the paper much less than the smooth particles. Simulated depletion potential [**95**] between two smooth, two rough and one smooth and one rough side for the R(1.5)S(1.1) colloids, and polymer of size C) r_p=10 nm ($\rho_p = 0.025$), and D) r_p=19 nm ($\rho_p = 0.038$) as a function of the distance of the centers of mass of the colloids, r.

caps (Figure 6.1):

$$\frac{u_{AO,sphere}(r)}{k_BT} = \begin{cases} \infty & \text{for} \quad r < 2R_s \\ -\frac{4}{3}\pi\rho_p(R_s+r_p)^3\left[1-\frac{3}{4}\frac{r}{R_s+r_p}+\frac{1}{16}\left(\frac{r}{R_s+r_p}\right)^3\right] & \text{for} \quad 2R_s < r < 2(R_s+r_p) \\ 0 & \text{for} \quad r > 2(R_s+r_p) \end{cases} \tag{6.2}$$

Introducing roughness on a colloidal surface can significantly affect the overlap volume between two such rough particles, and thus the depletion potential. The extent of the reduction of the depletion potential depends on the ratio of the size of the roughness, h, and the diameter of the depletant, $2r_p$.[**65, 66, 63, 64**] For platelets, the depletion potential was found to be decreased if small particles with diameter h, such that $2r_p/h < 1$, were adsorbed at the platelet surface. [**65**] Similarly, cylinders with smooth top and bottom, and a rough side where found to attract specifically with their flat surfaces.[**63, 64**] Surface roughness induced by just a few large asperities led to a considerably smaller overlap volume, and thus, weaker depletion interactions, because of the large overlap volumes involved in two touching flat surfaces. [**66**] If the depletant is larger than the asperities, the surface roughness is effectively smoothed out, and aggregation occurs as if they were smooth particles with a size larger by the asperity height h. Although rough surfaces were generally found to significantly reduce the depletion potential, asperities aligned in a complementary fashion may increase the overlap volume compared to flat surfaces, thereby increasing the depletion force.

In case of spherical particles, the effect of roughness on the depletion potential is not straightforward to predict. Computer simulations by Hermes and Dijkstra showed that a similar suppression of the depletion potential is possible for smooth spheres decorated with smaller spheres. [**95**] The strongest reduction of the attraction can be achieved by intermediate coverages with small spheres, that is, for 33-44 % and 122-144% of close packing. For lower coverage with small spheres, the large smooth spheres may still touch as in the absence of the small spheres, and for a dense coverage, the roughness is effectively reduced by a factor 2 because the small spheres are then in contact with each other.

6.3.2. Particles with Attractive Patches

We employ a surface roughness specific depletion potential to make patchy particles with distinct attractive sites. Our patchy particles are anisotropic polystyrene dimers, that consist of one rough and one smooth sphere. These "rough-smooth" particles are prepared by seeded emulsion polymerization. We obtain roughness on cross-linked polystyrene seed particles through adsorption of smaller polystyrene spheres at the surface during the cross-linking step. Using these rough seeds in an emulsion polymerization yields seed particles with a smooth protrusion after phase separation (see also Chapters 2, 3, and 4), [**26, 31, 33**]). The synthesis protocol is sketched schematically in Figure 6.2. We prepared two systems of rough-smooth particles: one dispersion with colloidal particles where the rough side is larger than the smooth side (R(1.5)S(1.1) particles), and another with colloidal particles where the smooth side is larger than the rough side (R(1.2)S(1.7) particles). The numbers in brackets indicate the radii of

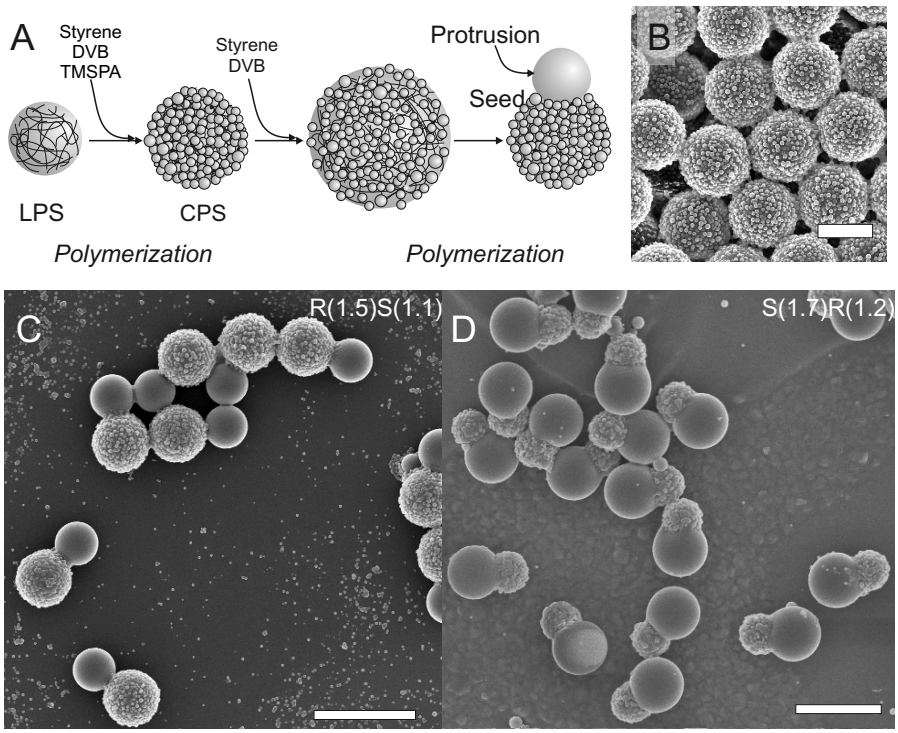

Figure 6.2. Synthesis of patchy particles. A) Schematic representation of synthesis of dimers consisting of a rough and a smooth side. Linear polystyrene spheres are swollen with an emulsion consisting of styrene, divinylbenzene (DVB), and 3-(trimethoxysilyl)propyl acrylate (TMSPA). During polymerization, secondary nucleated particles adsorb to the interface rendering it rough. SEM image of the rough spheres is shown in B (Scale bar is 2 μm). A second swelling step with an emulsion consisting of styrene and DVB yields rough particles with a smooth protrusion. C) and D): polystyrene particles with site specific roughness fabricated by using different swelling volumes (C) $S = 2$ (R(1.5)S(1.1) particles) and D) $S = 4$ (R(1.2)S(1.7) particles). Scale bars are 5 μm.

the respective rough (R) and smooth (S) parts of the colloidal particles. The average diameter of the smaller spheres that provide the roughness is 182±40 nm for the R(1.2)S(1.7) and 187±30 nm for the R(1.5)S(1.1) particles.

SEM images show that the small particles are partially immersed into the seed particle (Figure 6.2B), effectively creating roughness by one hemisphere. For reduction of the depletion potential between the rough sides, the depletant therefore needs to be chosen smaller than the radius of the small spheres, or $h = 90$ nm. In computer simulations, it was found that the depletion potential is suppressed more strongly for depletants that are significantly smaller than the roughness inducing small spheres, [**95**] and hence, we chose nonionic dextran polymers with diameters $d_{110k} = 15.8 \pm 2.5$nm (molecular weight $M_w = 110$kg/mol) and $d_{500k} = 38 \pm 16$nm ($M_w = 500$kg/mol) as depletant. For

these depletant sizes, spherical models of smooth and rough spheres, whose size and roughness were modeled after the R(1.5)S(1.1) colloids, were employed by Hermes and Dijkstra [**95**] to calculate the effective pair potential between two smooth, two rough and one smooth and one rough side. The results are shown in Figure 6.1C and D. An attraction of roughly 6 k_BT between the smooth sides of the R(1.5)S(1.1) colloids can be obtained while attraction between the rough and smooth sides, and two rough sides is negligible.

The site-specific patchiness of our roughness anisotropic colloids in the presence of dextran polymer is illustrated in Figures 6.5B and F for R(1.5)S(1.1) colloids, and 6.9B and C for for R(1.2)S(1.7) colloids, respectively. The R(1.2)S(1.7) colloids shown in Figure 6.5A become attractive with their larger, smooth sides upon addition of the depletant, forming small clusters with the rough, small spheres sticking to the outside. Even in the absence of the surface roughness, preferential binding between the large spheres of the dimers is expected due to the inherently larger overlap volume between the large compared to the smaller sides. However, also the R(1.5)S(1.1) colloids with a smaller smooth side specifically attract at their smooth sides while binding between their rough sides is absent (Figure 6.5B). Bonds between smooth sides are indicated by white arrows in Figure 6.5B, and a bond between a smooth and a rough side of two R(1.5)S(1.1) colloids is specified by a black-white arrow. The distinction between bonded and un-bonded colloids is based on short movies, of which a snapshot is shown in Figure 6.5B. Dextran polymer with radii $r_p = 8$ nm (Figure 6.5B) and $r_p = 19$ nm (Figure 6.5F), both significantly smaller than the roughness, induced binding specifically between the smooth sides. This site specific attraction confirms the significant reduction of the depletion potential between two rough sides, even though the rough sides are larger than the smooth ones. In fact, the depletion potential is reduced so strongly that rough spheres 3.2±0.19 μm in diameter in the suspensions do not aggregate, neither with each other, nor with the rough-smooth colloids. We indicated some of the rough spheres with a black arrow in Figure 6.5.

To illustrate that R(1.5)S(1.1) particles can spontaneously leave these depletion induced clusters snapshots of a movie of an unbinding event are shown in Figure 6.3. This unbinding event occurred in a sample containing a polymer with r_p=19 nm at a concentration of $\rho_p = 0.4\rho_{overlap}$ during roughly 10 mins of observation time. Here, $\rho_{overlap} = (4\pi r_p^3/3)^{-1}$ is the overlap concentration of the polymer. Considering the time frame necessary to observe such an event, we estimate the attractive depletion potential to be on the order of a few k_BT.

Employing equations 6.1 and 6.2 for this experiment, ($r_p = 19$ nm, $\rho_p = 0.4\rho_{overlap}$), yields an attractive potential at contact of roughly $-40k_BT$. We plotted the depletion potential as a function of the distance between two smooth spheres in Figure 6.4. At such a high contact value, spontaneous breaking of bonds between particles is not

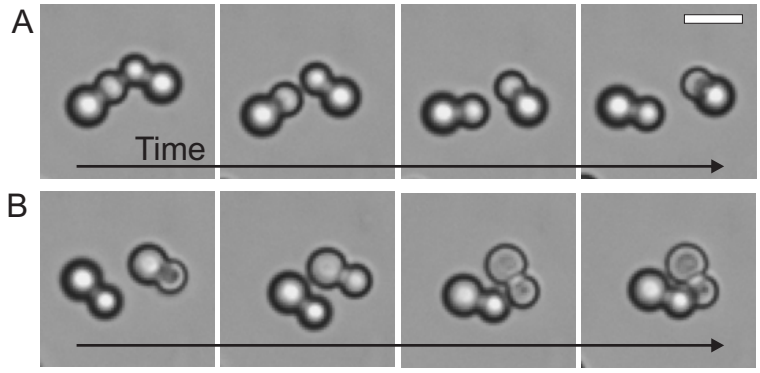

Figure 6.3. Snapshots from a movie showing A) an example of spontaneous unbinding of a dimeric cluster. B) A little bit later, the colloidal particles form a bond between their smooth small sides again. Dextran polymer with radius r_p=19 nm was used at a concentration of $\rho_p = 0.4\rho_{overlap}$. Scale bar is 2 μm.

expected, since the probability for such an event scales as $\exp[u/(k_BT)]$, where $u < 0$ is the bond energy. The range of the depletion potential is roughly the diameter of the depletant (Figure 6.4), and hence on the order of 8 and 19 nm for the polymers with molecular weight M_w = 110 kg/mol and M_w = 500 kg/mol, respectively. For such a short ranged attraction, a screened electrostatic repulsion between the particles may significantly decrease the depletion potential. We take the screened Coulomb potential to be:[**96**]

$$u_{el}(x) = \frac{\Psi^2 R^2}{\lambda_B r} \exp[-\kappa(x - 2R], \tag{6.3}$$

where R is the radius of the smooth side of the colloids, $\Psi = 0.6\ k_BT$ is the zetapotential of the R(1.5)S(1.1) particles measured by laser doppler electrophoresis, $\lambda_B = 0.71$ nm is the Bjerrum length in water, and κ is the inverse of the Debye screening length, and r is the distance between the centers of the two particles. At 20 mM NaCl, $\kappa \approx 0.5$ nm^{-1}. The Asakura-Oosawa potential (AO) is plotted together with the screened Coulomb repulsion (C) in Figure 6.4. For polymer concentrations at which clustering was observed, the minimum of the total potential (tot) is roughly -5 k_BT for the polymer with 8 nm radius (Figure 6.4 A), and -17 k_BT for polymer with 19 nm radius (Figure 6.4 B). Clearly, screened Coulomb repulsion significantly reduces the short-ranged depletion potential. The values obtained for the minima of the potential energies are in better agreement with the observation of spontaneous unbinding events, though -17 k_BT is still much larger than the few k_BT we estimated. However, the minimum of the potential energy strongly depends on value of the zetapotential, namely as $u_{el} \propto \Psi^2$, with small variations leading to significantly different minimum energies. We can conclude that screened Coulomb repulsion can explain the differences between contact values calculated using an Asakura-Oosawa potential and the observed unbinding events.

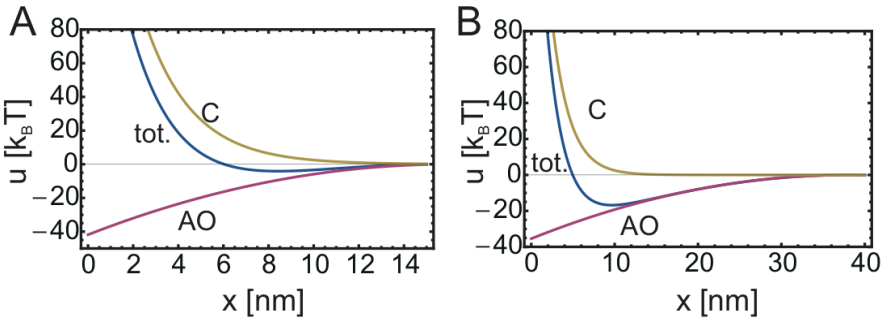

Figure 6.4. A short-ranged screened Coulomb repulsion (C) reduces the Asakura-Oosawa (AO) depletion potential considerably, yielding an overall potential (tot) with an absolute minimum energy to be much smaller. Potential energies are plotted as a function of the distance x between surfaces of the two spheres. A) shows the potentials for r_p=8 nm and $\rho_p = 0.2\rho_{overlap}$, and B) for r_p=19 nm and $\rho_p = 0.4\rho_{overlap}$.

6.3.3. Colloidal Micelles

While varying the strength of the depletion potential, the rough-smooth colloidal particles spontaneously organized into clusters of micellar type, in which the attractive part constitutes the core of the aggregate. The strength of the depletion potential is not only determined by the overlap volumes of the colloidal particles, but also is proportional to the polymer concentration, see equation 6.1. Whereas the overlap volumes are set by the shape of the colloidal particles, the polymer concentration allows for tuning the difference in attraction between two rough and two smooth sides of the R(1.2)S(1.7) and R(1.5)S(1.1) particles. At low polymer concentrations, no attraction between the colloidal particles is observed as shown in Figures 6.5A and 6.9A for $\rho_p(r_p = 8\text{ nm}) = 0.16\rho_{overlap}$ and $\rho_p(r_p = 19\text{ nm}) = 0.32\rho_{overlap}$.

For colloidal particles with smaller smooth side (R(1.5)S(1.1)), an increase in the polymer concentration to $\rho_p = 0.19\rho_{overlap}$ (r_p=8 nm) or $\rho_p = 0.35\rho_{overlap}$ (r_p=19 nm) leads to small clusters, consisting mainly of two to three colloids (Figure 6.5B). The binding between the particles occurs selectively at their smaller smooth sides. White arrows in Figure 6.5B indicate binding between smooth sides, the black/white arrow indicates binding between a rough and a smooth side.

At a slightly higher polymer concentration ($\rho_p = 0.22\rho_{overlap}$ (r_p=8 nm) and $\rho_p = 0.37\rho_{overlap}$ (r_p=19 nm)), the average number of particles in a clusters grows with the attractive depletion potential, while site specific patchiness is maintained. Figure 6.5C and E shows light microscopy images of clusters obtained for polymers with radii r_p=8 nm and r_p=19 nm, respectively. Representative images of the clusters containing $n = 1$ to $n = 15$ R(1.5)S(1.1) particles are presented in Figure 6.7A in comparison with simulation results in Figure 6.7B. Intriguingly, these clusters are reminiscent of micelles,

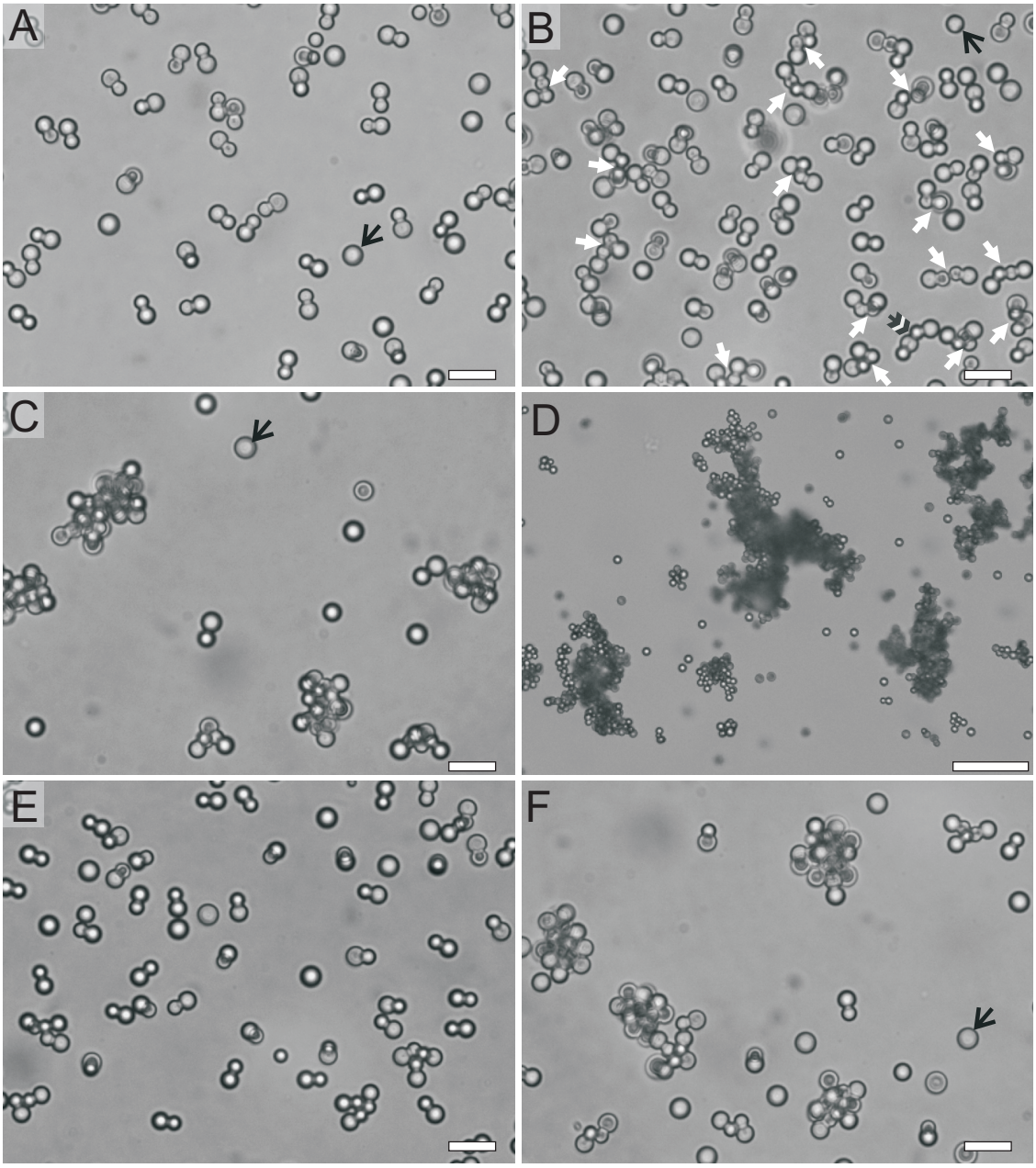

Figure 6.5. Light microscopy images of R(1.5)S(1.1) colloids with small smooth side and dextran polymer at different concentrations at 20 mM NaCl. Polymer radius $r_p = 8$ nm and concentration A) $\rho_p = 0.16\rho_{overlap}$, B) $\rho_p = 0.19\rho_{overlap}$. Black/white arrow indicates binding between smooth and rough sides of the particles, and white arrows binding between smooth sides of the R(1.5)(S(1.1) particles. C) Polymer concentration $\rho_p = 0.22\rho_{overlap}$, and D) $\rho_p = 0.24\rho_{overlap}$. E) c_{NaCl}=0 mM, $\rho_p = 0.22\rho_{overlap}$, and F) r_p=19 nm: $\rho_p = 0.37\rho_{overlap}$. Black arrows indicate large rough spheres. Scale bars are 10 μm, except for D), where the scale bar is 40 μm.

where the R(1.5)S(1.1) colloids specifically bind at their smooth attractive sides inside the clusters just like the lyophilic parts of surfactants attract each other. The rough sides of the particles are facing towards the outside of the clusters similar to the hydrophilic head groups. Therefore, we term these clusters colloidal micelles.

At even higher polymer concentrations, also the rough sides of the R(1.5)S(1.1) colloidal particles become attractive, and the site specificity of the attraction is lost (see Figure 6.5D). While the stronger attraction between the smooth sides still favors binding between them over binding between rough sides, no discrete clusters are observed due to the not negligible interactions between the rough sides. At very high polymer concentrations, diffusion limited aggregation occurs. Surprisingly, a quite subtle change in the polymer concentration from $\rho_p = 0.16\rho_{overlap}$ to $\rho_p = 0.24\rho_{overlap}$ (r_p= 8 nm), and $\rho_p = 0.32\rho_{overlap}$ to $\rho_p = 0.45\rho_{overlap}$ (r_p= 19 nm) causes a transition from unaggregated, free colloids, via finite-sized colloidal micelles of patchy particles to randomly aggregated clusters.

The selectivity of the depletion potential for smooth surfaces at intermediate polymer concentrations can be demonstrated even more convincingly by the use of rough spheres with a diameter larger than the rough side of the R(1.5)S(1.1) particles, namely 3.2 μm. The large rough spheres, indicated by a black arrow in Figure 6.5C are clearly excluded from the clusters despite their larger diameter. This exclusion of rough spheres strongly confirms the patchy attraction between the smooth sides of the R(1.5)S(1.1) particles.

This sensitive dependence of the cluster formation on the attractive potential has also been observed in Monte Carlo simulations performed by Ni et al.* The system is modeled as an ensemble containing $N = 1000$ dimers in a volume V with ideal polymer of density ρ_p.The site-specifically attractive particles are modeled with dimers consisting of one attractive sphere of size R_s interacting by an Asakura-Oosawa potential (see eq. (6.2)), and one sphere of size R_r with hard-sphere repulsion potential. Interactions between the two different spheres are also presumed to be hard sphere repulsions. This is a simplification of the effective potential consisting of a contribution from screened Coulomb repulsions and Asakura-Oosawa depletion attraction. To take the neglected electrostatic repulsions into account, depletion potentials with contact values around $u = -10k_BT$ were employed, much lower than in the experimental situation. Monte Carlo simulations in a canonical ensemble (NVT) are used to calculate the probability distribution of the cluster size. Since the attraction between particles is very steep, cluster moves were employed to further equilibration.

Snapshots of the Monte Carlo simulations for R(1.5)S(1.1) particles and either of the polymer sizes are presented in Figure 6.6.* Despite the electrostatic interactions being neglected, the rescaled depletion attraction between the smaller spheres of the

*Snapshots of Monte Carlo simulations were kindly provided by Ran Ni, Michiel Hermes and Marjolein Dijkstra.

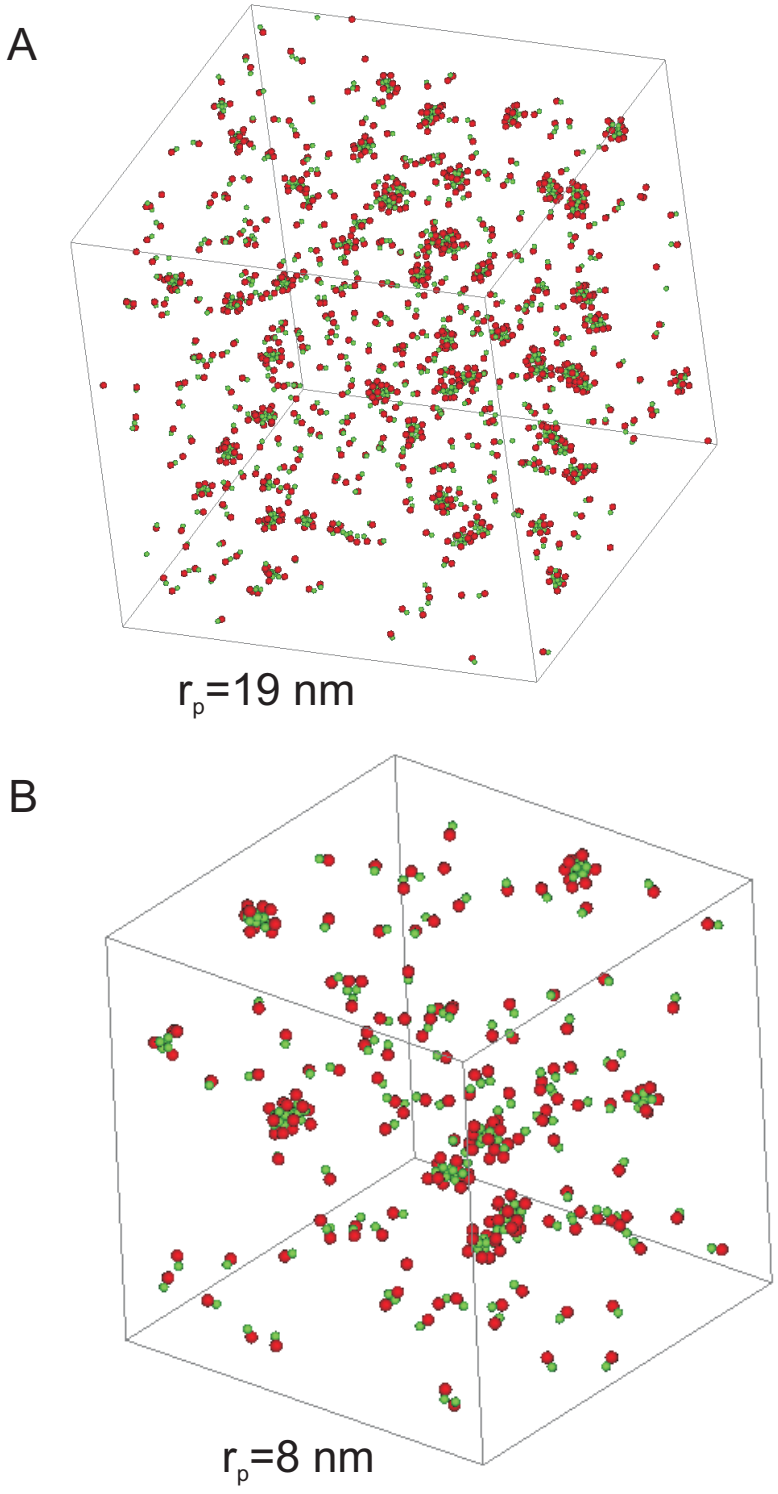

Figure 6.6. Snapshots of Monte Carlo simulations performed by Ni et al. on dimers with one attractive sphere (green) and one hard sphere (red) modeled after the R(1.5)S(1.1) colloids used in experiments. An attractive Asakura-Oosawa potential between the green spheres of the dimers is induced by polymers of radius A) $r_p = 8$ nm, and B) $r_p = 19$ nm. Micelle-like clusters are visible next to single colloids.

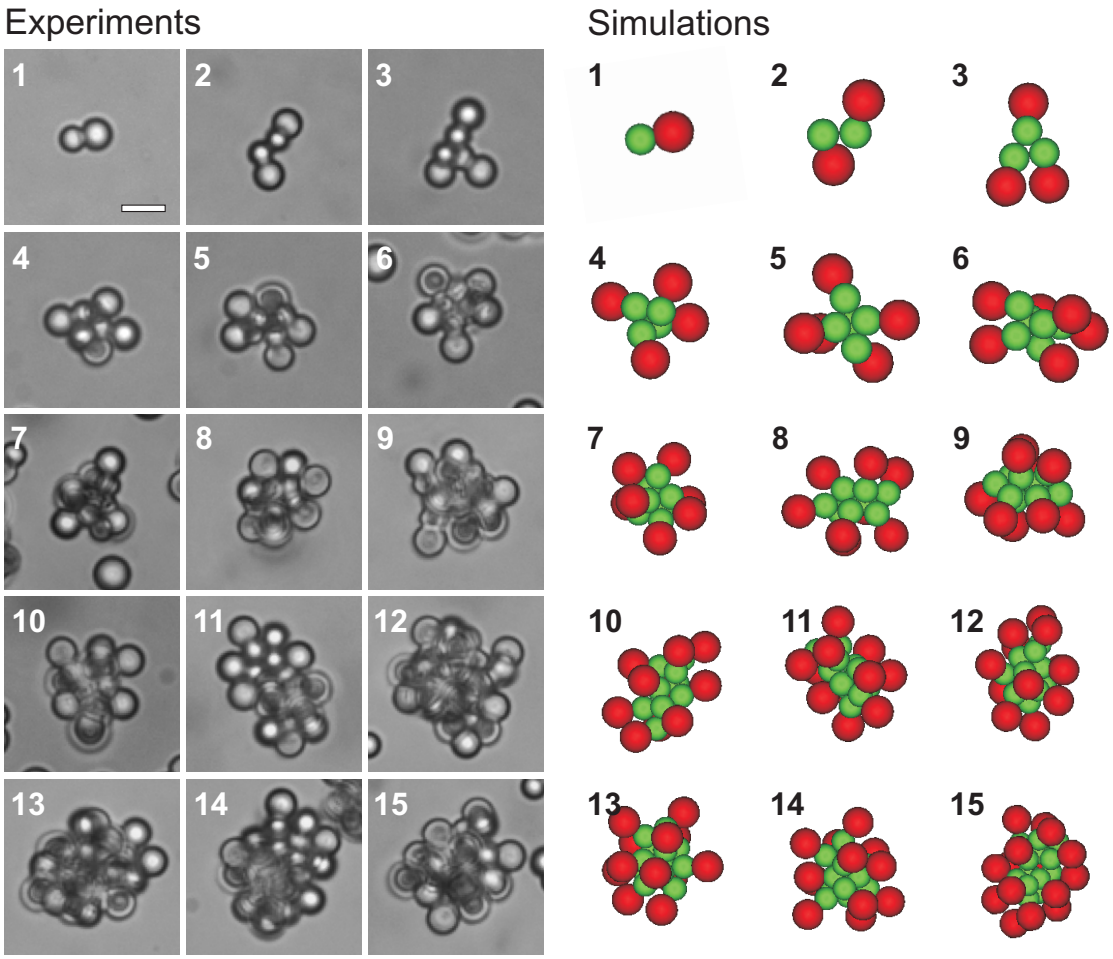

Figure 6.7. Colloidal micelles. Typical cluster shapes obtained from colloids with attractive small smooth, and large rough (non-attractive) side containing n=1 to n=15 patchy particles. On the left side, experimentally observed clusters are presented. The right side shows clusters obtained from Monte Carlo simulations on dimers consisting of one sphere with hard sphere potential (red) and an attractive sphere interacting by a depletion potential (green). In experiments and simulations, the smaller attractive sides are located at the core of the clusters, reminiscent of micelles. Scale bar is 5 μm.

dimers suffices to obtain excellent agreement between simulations and experiments. This implies that the observed clusters are robust with respect to the details of the interaction potentials, and may be obtained by means of other attractive potentials as well.

The clusters obtained in experiments and simulations are but one representation of a multitude of possible realizations. In equilibrium, one expects the clusters to sample many configurations consistent with a maximum number of contacts. For small number of colloids in a cluster ($n < 5$), there exists only one configuration of the attractive sides

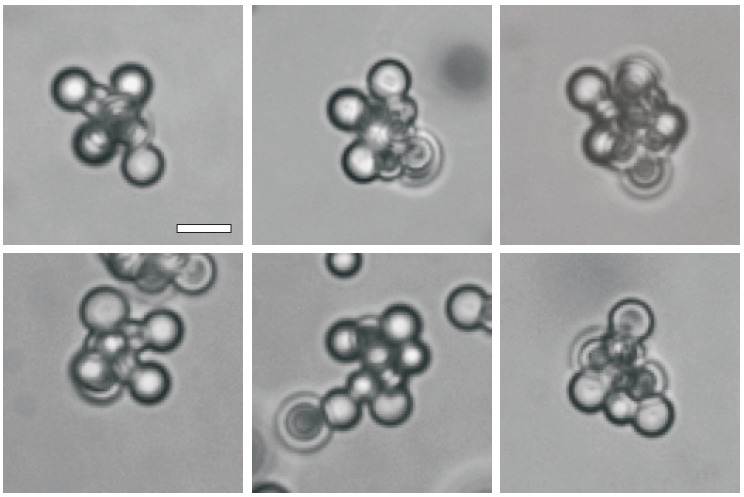

Figure 6.8. Light microscopy images of clusters consisting of five colloids with small smooth and large rough side. Clearly, the colloidal particles touch at their smaller smooth sides, while the large sides are the outside of the clusters. Scale bar is 5 μm.

of the dimers that has minimum bond energy. [**97**] Hence, entropy affects only the outer, rough sides of the colloids, as illustrated for clusters containing five R(1.5)S(1.1) particles in Figure 6.8. For $n = 1 - 5$, it is still possible to distinguish the arrangement of the smooth sides inside the micellar clusters. Their arrangement agrees with clusters of spheres interacting by a short-range depletion potential, [**97**] and are also obtained from simulations. For $n > 5$, cluster "isomers" with equal bond energy are likely to exist and transformed into one another by breaking and forming bonds.[**57, 97**] It is difficult to distinguish such cluster isomers due to large rough spheres that surround the smaller smooth spheres on the inside. Simulation studies may help in shedding light onto the arrangement of the attractive sides inside larger clusters in the future. Finally, we note that the larger clusters become more elongated, due to the steric restrictions imposed by the rough spheres at the outside. With increasing number of colloids n, the clusters can't continue to grow in a spherical fashion. The formation of for example a Bernal spiral,[**98**] where each colloidal particles still forms 6 bonds, may be a possible large n structure, expected for higher colloid volume fractions as reported elsewhere for single sphere colloids. [**99, 100**]

Similarly, an increasing polymer concentration leads to site-specific binding between the smooth sides of colloids with a smaller rough side. In the experiments, we employed R(1.2)S(1.7) colloids. At or below a polymer concentration of $\rho(r_p = 8\ nm) = 0.16\rho_{overlap}$ particles are free in solution. A slight increase to $\rho(r_p = 8\ nm) = 0.19\rho_{overlap}$ leads to binding between the larger, smooth sides of the colloids. Interestingly, we often found three to five colloids arranged in a linear fashion as shown in Figure 6.9B. Larger polymer concentrations lead to clustering of the R(1.2)S(1.7) colloids with their

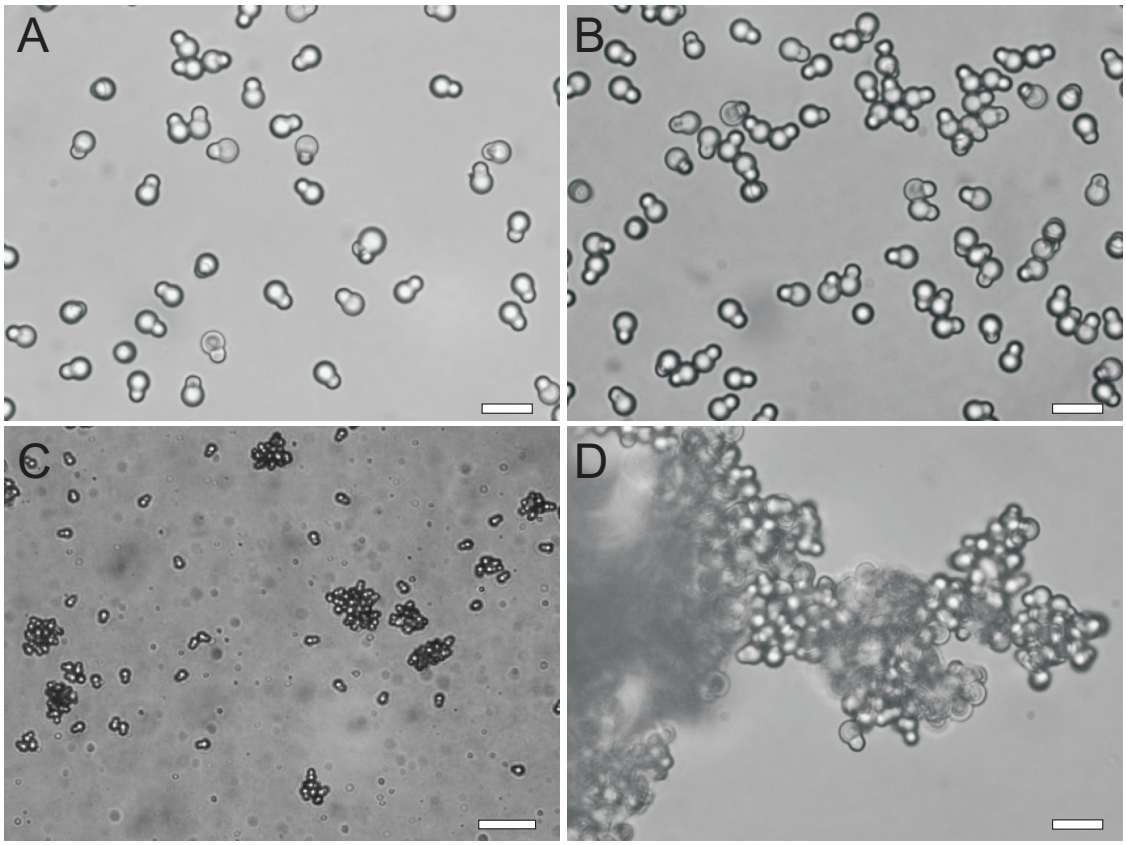

Figure 6.9. Light microscopy images of R(1.2)S(1.7) colloids with large smooth side and dextran polymer at different concentrations at 20 mM NaCl. Polymer radius r_p = 8 nm and concentration A) $\rho_p = 0.16\rho_{overlap}$, B) $\rho_p = 0.19\rho_{overlap}$. C) r_p = 19 nm and $\rho_p = 0.19\rho_{overlap}$, and D) r_p=8 nm and $\rho_p = 0.22\rho_{overlap}$. Scale bars are 10 μm in A, B, and D, and 20 μm in C.

small rough sides at the outside of the cluster (Figure 6.9C). Above $\rho(r_p = 8\ nm) = 0.22\rho_{overlap}$, the rough sides take part in the clustering as well, as shown in Figure 6.9D. Site-specificity in the attraction is lost as a consequence.

To quantify our observations on the cluster sizes for different polymer concentrations we determined the sizes of at least 100 clusters per sample to obtain a cluster size distribution. We defined the probability to observe a cluster as $P(n) = N(n)/(\sum_{n=1}^{n_{max}} N(n))$, where $N(n)$ is the total number of observed clusters containing n colloids in a sample. In the absence of polymer, or at low polymer concentrations ($\rho_p(r_p = 8$ nm$) = 0.16\rho_{overlap}$ and $\rho_p(r_p = 19$ nm$) = 0.32\rho_{overlap}$) only single colloids are present in solution, see Figure 6.10A and D, respectively. Upon increasing the depletant concentration the cluster size distribution shifts towards larger clusters with an exponential decay in the cluster size for $\rho_p(r_p = 8$ nm$) = 0.19\rho_{overlap}$ and $\rho_p(r_p = 19$ nm$) = 0.35\rho_{overlap}$ (Figure 6.10B and E). For the larger polymer with radius r_p=19 nm, the peak in the cluster distribution is observed around $n = 10$ for a polymer concentration of $\rho_p = 0.40\rho_{overlap}$ (Figure

6.10F). Cluster size distributions obtained from Monte Carlo simulations agree very well with the experiments for a polymer concentration $\rho_s(r_p = 19\text{ nm}) = 0.118\%\rho_{overlap}$ in the simulations. As described above, the large difference between the experimentally employed polymer concentration ($\rho_p(r_p = 19\text{ nm}) = 0.40\rho_{overlap}$) and the one found in computer simulations, $\rho_s(r_p = 19\text{ nm}) = 0.118\rho_{overlap}$, is likely due to the reduction of the depletion potential by a screened Coulomb repulsion, neglected in simulations for simplicity.

The simulations diverge, however, from experimental results on the smaller polymer with $r_p = 8$ nm. The peak in the simulated cluster size distribution is clearly found around $n = 10$, whereas the experimental size distribution ranges from $n \approx 5$ to $n \approx 15$. To reach equilibrium in simulations, roughly 10^9 Monte Carlo steps were necessary. This long equilibration times originate from the strong ($u_s = -11\ k_BT$), short range depletion attraction. In experiments, we observed that two days after mixing the cluster size distribution is spread out homogeneously from $n = 5$ to $n = 15$. (see Figure 6.11A). After 9 days, the size distribution shifted towards larger clusters, as shown in Figure 6.11B. Therefore, the cluster size distribution is still changing, and most likely not in equilibrium yet. The comparison with simulated data in Figure 6.10C supports this hypothesis as well: a growth of clusters around $n = 5$ will create a peak at higher values, while the relative probability for monomers will increase.

6.3.4. Micelle Model

The parallels between our experimental observations on clusters of colloidal dimers with one attractive patch and surfactant micelles lead us to apply a model inspired by micelle theory to describe the experimental cluster distributions. The density of clusters consisting of n colloids is found to be (see Appendix for derivation):

$$\rho(n) = \rho(1)^n v_{av}(n)^{n-1} e^{-c(n)u}. \tag{6.4}$$

Here, $v_{av}(n)$ is the volume available to the colloids within a cluster of size n, i.e., maintaining bonds with energy u (in units of k_BT), and $c(n)$ is the number of bonds between colloids in a cluster of size n. This bond distribution can be approximated by findings on clusters of spherical colloids interacting via short-range depletion interaction similar to the experiments on colloidal micelles.[**97**]

$$c(n) = \begin{cases} 0 & \text{for} \quad n = 1 \\ 1 & \text{for} \quad n = 2 \\ 3n - 6 & \text{for} \quad n = 3...9 \\ 3n - 5 & \text{for} \quad n > 9 \end{cases} \tag{6.5}$$

Clusters with $n > 9$ colloids form more bonds per colloid than smaller ones, in principle even exceeding the value of $3n - 5$ used here for $n > 10$ [**101**]. However, although these ground states with extra bonds occur more frequently than other cluster states

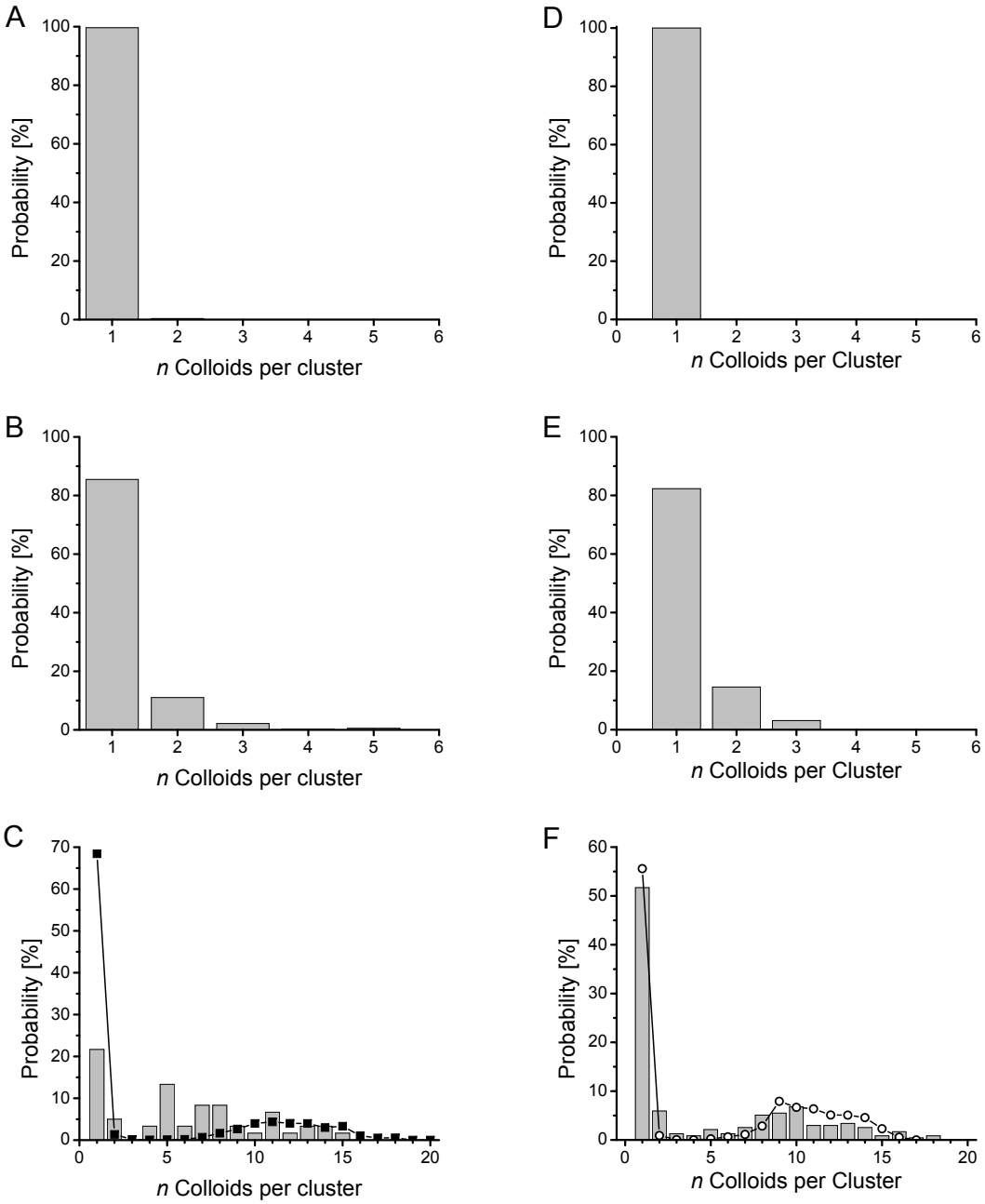

Figure 6.10. Cluster size distributions for experiments (bars) and simulations (symbol and line) for R(1.5)S(1.1) colloids with small smooth side and $r_p = 8$ nm polymer at increasing concentrations A) $\rho_p = 0.16\rho_{overlap}$, B)$\rho_p = 0.19\rho_{overlap}$ and C) $\rho_p = 0.22\rho_{overlap}$. The experimental cluster size distribution in C) ranges from $n = 5$ to $n = 15$, whereas simulations show a peak at $n = 10$. D), E) and F) For a larger polymer (r_p= 19 nm) a similar trend with increasing polymer concentration is observed: D) Single particles are present in solution at $\rho_p = 0.32\rho_{overlap}$, E) small clusters with an exponentially decaying size distribution for $\rho_p = 0.35\rho_{overlap}$, and F) for $\rho_p = 0.4\rho_{overlap}$ a clear peak in the cluster size distribution appears around $n = 10$, which agrees well with Monte Carlo simulations by Ni et al.

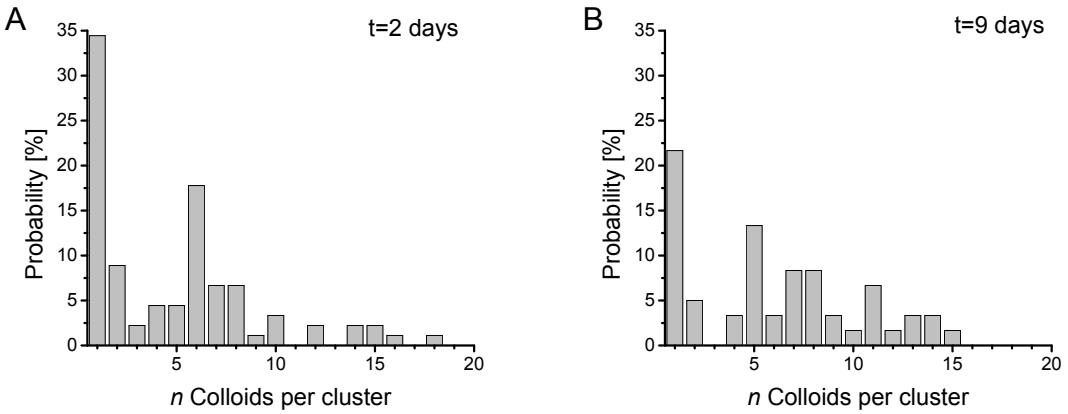

FIGURE 6.11. Cluster size distributions for the depletant with radius $r_p = 8$ nm and concentration $\rho_p = 0.22\rho_{overlap}$ A) 2 days on rotating stage, and B) 7 days later stored flat.

($n = 10$: 10%, $n = 11$: 20 %, $n = 12$: 30%, the majority of clusters with less bonds has a higher rotational entropy. Including this effect, that is, setting $c(11) = 29$ and $c(12) = 33$, does not significantly alter the results presented in the following. Instead of accounting for the large variety of different clusters, their degeneracies and bond numbers, we pragmatically employ the bond distribution given by eq. (6.5).

In the simplest case, each colloidal particle added to a cluster reduces the available volume per particle, v_{av}, by a factor $1/n_{max}$, where n_{max} is the maximum number of colloids in a cluster at which close-packing is reached. We can then approximate the accessible volume with (see also Appendix, eq. 6.14):

$$v_{av}(n) \approx 4\pi \left(1 - \frac{n-1}{n_{max}}\right) R^2 \xi. \tag{6.6}$$

Using this simple model for the available volume together with the bond number distribution in eq. (6.4), we can fit the experimental data as shown in Figure 6.12 A. We presumed a maximum cluster size of $n_{max} = 15$, and the bond energy u was set to -4.05 k_BT to obtain the best agreement between experiments and theoretical model (Figure 6.12A). This bond energy is low compared to values required for cluster formation in simulation, which were around -10 k_BT. However, considering the rather crude model for the available volume, these values are roughly in agreement. More importantly, the size distribution is well fitted, with a sharp peak located at $n = 10$. Also interesting to note is the sensitive dependence of the cluster distribution on the bond energy u. For slightly lower values of $u = -4$ k_BT, the fraction of monomers increases to 0.78, and for slightly higher values of $u = -4.2k_BT$ it decreased to 0.02. This is of course expected, because the bond energy u appears in the exponent of eq. (6.4). As discussed above, taking lower ground states, such as $3n - 4$ for $n = 11$ and $3n - 3$ for $n = 12$, in the bond distribution $c(n)$ into account, leads only to a slight shift of the peak towards

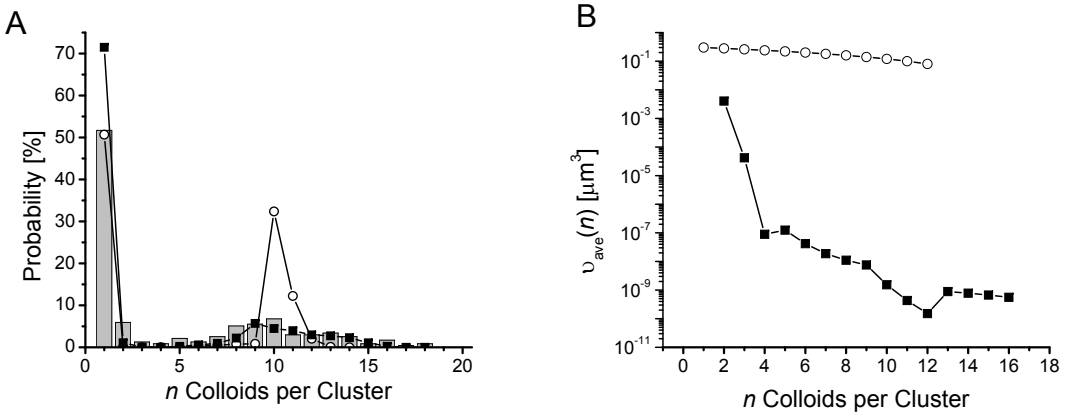

Figure 6.12. A) Comparison of experimental cluster size distribution with micelle model using the available volume calculated from a simple linear model, $v_{av} = 4\pi R^2\xi(1-(n-1)/15)$ and $u = -4.05$ k_BT (-○- line), and extracted from simulations (-■- line). B) Comparison between the simple linear model for $v_{av}(n)$ (-○- line) and $v_{av}(n)$ determined from cluster distribution from simulations (-■- line).

$n = 12$. Furthermore, we expect elongated structures to form at large n at high colloid concentrations, comparable to Bernal spirals.[**98**] Experimentally, we observed a transition towards more elongated clusters for larger n. The bond number in these Bernal spirals is $c(n) = 3n - 6$ for all particles, lower than our approximation made above in eq. (6.5), resulting in a peak of the cluster distribution at $n = 10$.

A more accurate model for the available volume is calculated with help of eq. (6.4) using the simulated cluster distribution. Figure 6.12B compares the values for $v_{av}(n)$ obtained from the simplified model (eq. (6.6)) to the available volumes extracted from the simulation data for $r_p = 19$ nm and $\phi = 0.4\phi_{overlap}$ (see also Figure 6.10D). Both functions decrease with the number of colloids in a cluster. However, especially at larger clusters n the available volume from simulations is several orders of magnitude lower than in our simplified model. In view of these large differences, it is actually quite surprising that a simple linear dependence on n for the available volume per particle can capture the essential features of the cluster size distribution. Employing $v_{av}(n)$ extracted from simulations the theoretical model has a broader peak around $n = 10$ and requires bond energies of $u = -11$ k_BT for good agreement with the experimental data. The latter agrees with values found in simulations.

6.3.5. Packing of Colloidal Particles at Air-Water Interfaces

During the experiments another intriguing observation was made. After a few days, colloidal R(1.2)S(1.7) particles spontaneously assembled at the air-water interface in the presence of dextran polymer. Multiple layers of particles were formed along the macroscopic interfaces with remarkable uniformity in their alignment, which reminds

of surfactants stabilizing an interface. For air-water interfaces curved towards the air phase, the colloids preferably aligned with their smaller, rough side to the air phase (Figure 6.13A, B for a larger view). Furthermore, when the packing of the colloidal particles at the interface is low, we observe a more random orientation of the colloids as shown in Figure 6.13C. Away from the glass surface, colloids were found to similarly lay flat on the air-water interface at low colloid concentrations. The curvature of the air-water interface is not influenced by the colloidal particles, but rather the curvature induces the packing. For an almost straight air-water interface, the colloidal particles seem to orient in such a way as to on average yield zero curvature (Figure 6.13D). Images were taken at different locations of the air-water meniscus, but at the glass interface, which might additionally forces parallel alignment of the length axis of the colloids with the glass surface. A schematic of the locations is shown in Figure 6.13E.

At this moment, we can only speculate what induces the alignment of the particles at the interface. Surfactants consist of a hydrophilic and a hydrophobic part, which leads to aggregates whose shape is determined by the packing parameter $P = V/(a_0 l_0)$, in the first place. [**102**] The rough-smooth particles have been suggested to have a similar property by Kim et al. [**103**], with the rough parts being more hydrophilic due to the integrated 3-(trimethoxysilyl) propyl ethyleneamine (TMSPA). However, the alignment observed in our experiments is opposite to this suggestion, with rough parts favoring the air phase.

A pure geometric packing argument is not sufficient for explaining the preferential parallel alignment between the colloidal particles since the curvature of the interface in Figure 6.13A is much lower than the curvature preferred by the colloidal particles would be. Hence, it would be expected to find also colloidal particles with an anti-parallel alignment, which would increase the packing fraction. Still, the site-specific depletion interaction induced by dextran polymer favors contacts between the larger, smooth sides of the particles. For anti-parallel aligned colloids, the smaller rough sides would stick to the water phase without increasing the packing fraction, because the breaking of the bonds between the smooth sides would be too costly. An example of a particle aligned in that fashion is seen in Figure 6.13B second and fifth from the right side.

The surfactant-like behavior exhibited by the R(1.2)S(1.7) particles does not seem to be induced by an amphiphilicity of the colloids for air and water, but rather a combination of depletion attraction between the smooth sides and the preference to adsorb at the interface. The preferential parallel alignment is not fully understood yet. Furthermore, the colloidal particles are not the only surface-active species present, and hence, they should not be considered to be colloidal surfactants. [**103**] Further investigations are necessary to determine the conditions at which this assembly takes place. The adsorption was often accompanied with a partial evaporation of the solution, which moved the air-water interface, possibly furthering particle adsorption. However, the

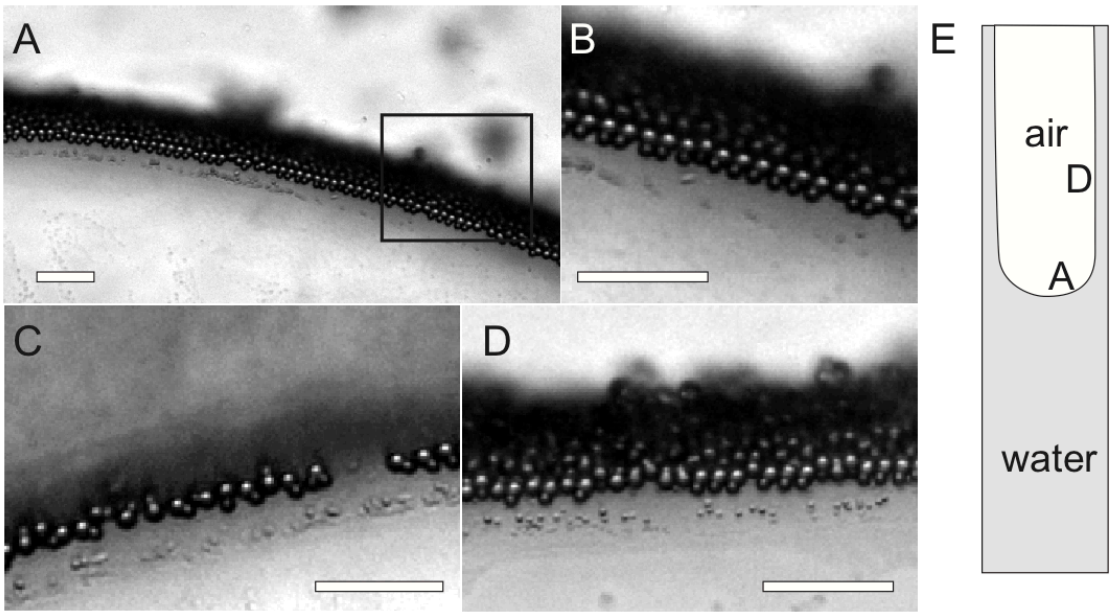

Figure 6.13. Spontaneous assembly of colloidal particles with large smooth and small rough side at the air-water interface (water: top, air: bottom phase). A) Curved interface with densely adsorbed layer of particles, B) inset of square in A), C) sparsely covered air-water interface with more randomly oriented colloids. D) Straight interface densely covered with colloidal particles. E) Schematic of a capillary with locations of shown light microscopy images. A indicates location of A,B, and C), and D location of a flat interface shown in D). Scale bars are 20 μm.

uniform alignment for dense packings according to the curvature of the interface points towards a packing optimization. It would be interesting to investigate the assembly at air bubbles with higher curvatures in addition to the macroscopic air-water interfaces presented here.

6.4. Outlook

The results on site-specific depletion interactions created by discrete surface roughness of colloidal particles can now be extended to other available experimental systems. Particles that posses not only one, but multiple smooth protrusion in a controlled arrangement may lead to exciting new structures, determined only by the positioning of the smooth spots on the particle surface. With the particle syntheses presented in Chapters 2, 3 and 4 we have very promising colloidal systems already at hand.

The synthesis for making rough-smooth colloidal particles presented here, can also lead to the formation of colloidal molecules through the fusion of the liquid protrusions (see Chapter 2 and 3). Such colloidal molecules consist of two or more rough seed particles, and a smooth side originating from the fused protrusions. For SEM images of

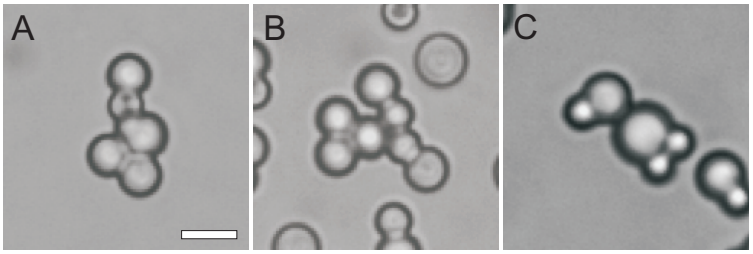

Figure 6.14. Clusters are also obtained between colloids with single protrusions and colloidal molecules made from fusion of liquid protrusions. Employed particles are A) and B) R(1.5)S(1.1) colloids, and C) R(1.2)S(1.7) colloids. The fused protrusions are smooth, while the seed particles are rough. Binding occurs with the smooth side made from fused protrusions.

smooth-rough colloidal molecules see 3.7. These colloidal molecules with multiple rough and one smooth side selectively bind at their smooth sides with other rough-smooth colloids in the presence of polymers, as shown in Figure 6.14. Further investigation of clustering of colloidal molecules of only one type could lead to interesting new types of clusters.

By making use of controlled formation of multiple protrusions on highly cross-linked seed particles and adsorption of secondary small particles created during polymerization, anisotropic particles with one, two, or three smooth protrusions can be made. Due to the well-controlled fabrication, high yields of either one of these particles can be obtained, a great advantage over other synthesis methods that either produce small quantities or require time-consuming and yield-reducing separation of the desired clusters. [**55, 12, 104**] Still, complex colloidal geometries may induce intricate new clustering behavior, and therefore are certainly interesting to be employed in site-specific depletion studies. Other colloidal assembly routes that, for example, employ Janus particles with hydrophilic-hydrophobic hemispheres ([**57, 87**]) are as well more restricted with the particle yield in the fabrication, and the patches can be arranged in only a limited fashion. Furthermore, depletion interactions have the advantage that their strength can be controlled even after sample preparation, for example by changing the size of the depletant, or by dilution. [**65, 51**]

We believe that the generality of our assembly approach together with the flexible particle synthesis presented in previous chapters is a promising route to controlled self-assembly of colloidal particles into larger structures with desired topology and properties.

6.5. Conclusions

By employing anisotropic dimer particles with two sides of distinctly different surface roughness, we demonstrated that we can create patchy particles making use of

depletion interaction. The short-ranged attraction between the smooth sides of the particles is stronger than between the rough sides due to a larger overlap volume, creating locally attractive patches. We showed that for short-ranged depletion potentials even a screened Coulomb potential may significantly reduce the total potential. At intermediate depletant concentrations, we find the formation of finite-sized clusters of rough-smooth particles, with the smooth particle sides oriented towards the inside. The clusters resemble colloidal micelles, with a well-defined peak in the cluster size distribution, that depends on the polymer size. Experimental observations on the clusters and the size distribution agree well with Monte-Carlo simulations. A theory inspired by surfactant micelles lead to qualitative agreement with the experimental cluster size distribution.

Acknowledgements

I thank Ran Ni, Michiel Hermes and Marjolein Dijkstra for performing computer simulations and discussions, and Kisun Yoon for insights into the synthesis of the colloidal particles. Alfons van Blaaderen is thanked for useful suggestions and discussion. I thank Jan Groenewold for theoretical considerations onthe cluster distribution.

Appendix - Micelle model

Here, we derive the equilibrium size distribution of colloidal clusters of size n, $N(n)$ or $\rho(n) = N(n)/V$, with V the system volume. In the general case of n colloids in equilibrium with clusters of size n, with $n \geq 1$, we have

$$\mu_n = n\mu_1. \tag{6.7}$$

Here, μ_n is the chemical potential of a cluster of size n. Note that a cluster of size $n = 1$ is a monomer. The chemical potentials are related to the 'molecular' partition functions, z_n, by

$$\beta\mu_n = -\ln \frac{z_n}{N(n)}, \tag{6.8}$$

where $\beta = 1/kT$ with k Boltzmann's constant and T absolute temperature. The z_n are defined by the canonical partition function $Z_n = \frac{z_n^{N(n)}}{N(n)!}$ and are coarse-grained partition functions. Assuming ideal behavior in terms of translation, they read

$$z_n = \frac{V}{\ell^3} z_{int}(n), \tag{6.9}$$

where ℓ^3 is on the order of the solvent molecular volume.[**105**] $z_{int}(n)$ takes into account all coarse-grained internal degrees of freedom of the cluster, that is, all translational degrees of freedom other than translations of the centers of mass of the clusters over the

volume V of the system. Inserting eqs. (6.8,6.9) into the equilibrium condition eq.(6.7) leads to

$$\rho(n)\ell^3 = \frac{z_{int}(n)}{z_{int}(1)^n}(\rho(1)\ell^3)^n. \tag{6.10}$$

Obviously, it must be that $z_{int}(1) = 1$. For $n > 1$, the internal partition function of clusters of size n is given by

$$z_{int}(n) = \frac{1}{n!}\int_{cluster\ volume} ... \int \frac{e^{-U(\vec{r}^{\,n})}}{\ell^{3(n-1)}} d\vec{r}^{\,(n-1)}. \tag{6.11}$$

The integral runs over $n-1$ coordinates, for one coordinate has already been consumed by the translations of the center of mass of the cluster. Even for a simple potential such as AO or a combination of that with screened - Coulomb, the integral eq.(6.11) is prohibitively difficult for the colloidal geometries studied here. We therefore simplify the situation by approximating the interaction potential as pairwise additive, i.e., $U(\vec{r}^{\,n}) \approx \Sigma_{i>j} u(r_{ij}) \approx c(n)u$ with $u(r_{ij})$ the (approximated as isotropic) pair energy in k_BT, $c(n)$ the number of contacts (or bonds) between colloids in a cluster of size n, and u the average energy per contact (bond). An isotropic $u(r_{ij})$ seems a reasonable approximation as long as the interactions between the (anisotropic) colloids are dominated by the smooth parts. Next, we allow the centers of mass of the colloids in the cluster to move in a volume determined by geometry and interaction range ξ. That is, we approximate $u(r_{ij})$ by a square well of range ξ and energy u located between (smooth) sphere radius R and $R + \xi$. Beyond the well, the potential is infinite. For the time being, let's designate the volume accessable to the colloids due to this construction as the 'available' volume $v_{av}(n)$. It depends on n by excluded volume effects. Finally, the coordinate of the center of mass of a clusters in eq. (6.11) is determined by the coordinates of the colloids $\vec{r_1}, \vec{r_2}, ..., \vec{r_n}$. Such configuration can be established in $n!$ ways. Including this degeneracy, eq.(6.11) becomes

$$z_{int}(n) \approx \frac{v_{av}(n)^{n-1}}{\ell^{3(n-1)}} e^{-c(n)u}. \tag{6.12}$$

The 'energy' here has been averaged over all available coordinates and formally is a potential of mean force. Inserting eq. (6.12) into eq. (6.10) leads to the size distribution of colloidal micelles,

$$\rho(n)v_{av}(n) = (\rho(1)v_{av}(n))^n\, e^{-c(n)u}. \tag{6.13}$$

Note that the coarse-grained length ℓ literally drops out of the equation. Naturally, ξ is the diameter of the depletant. If we had two single smooth spheres, we would have $v_{av} = 4\pi R^2\xi$. Taking into account the geometry of our dimers, and assuming close-packing is reached at $n = n_{max}$, then, in the simplest case, each added dimer reduces the available volume per dimer by a factor $1/n_{max}$. And therefore,

$$v_{av}(n) \approx 4\pi\left(1 - \frac{n-1}{n_{max}}\right) R^2\xi. \tag{6.14}$$

Note that $v_{av}(n)$ is only defined for $1 < n < n_{max}$ being the range of 'compact' clusters. The result is easily generalized for, e.g., cylindrical or helical aggregates. In that case, to a good approximation $v_{av}(n)$ is a constant function of n.

Furthermore, from the concentration of monomers, that is, $n = 1$, we can estimate the bond energy u. The equilibrium constant for the multichemical equilibrium given by eq. (6.7) is

$$K_n = \frac{\rho(n)}{\rho(1)^n} = v_{av}^{n-1} e^{-c(n)u} \tag{6.15}$$

where eq. (6.13) was used. Then, the critical micelle concentration (cmc) of the colloidal particles is given as

$$\rho_0 = K_n^{1/(1-n)} = v_{av}(n)^{-1} e^{c(n)u/(n-1)}. \tag{6.16}$$

considering the equilibrium between monomers and the most probable cluster size n^* we have:

$$\rho_0 \approx v_{av}(n^*)^{-1} e^{c(n^*)/(n^*-1)u}. \tag{6.17}$$

Part 3

Thermodynamically Stable Pickering Emulsions

7

Conditions for Equilibrium Solid-Stabilized Emulsions

Abstract

Particular types of solid-stabilized emulsions can be thermodynamically stable as evidenced by their spontaneous formation and monodisperse droplet size, which only depends on system parameters. Here, we investigate the generality of these equilibrium solid-stabilized emulsions with respect to the basic constituents: aqueous phase with ions, oil, and stabilizing particles. From systematic variations of these constituents, we identify general conditions for the spontaneous formation of monodisperse solid-stabilized emulsions droplets. We conclude that emulsion stability is achieved by a combination of solid particles as well as amphiphilic ions adsorbed at the droplet surface, and low interfacial tensions of the bare oil-water interface of order 10 mN/m or below. Furthermore, preferential wetting of the colloidal particles by the oil phase is necessary for thermodynamic stability. We demonstrate the sufficiency of these basic requirements by extending the observed thermodynamic stability to emulsions of different compositions. Our findings point to a new class of colloid-stabilized meso-emulsions with a potentially high impact on industrial emulsification processes due to the associated large energy savings.

7.1. Introduction

Emulsions stabilized by solid particles, also called Pickering emulsions,[**73**] were for a long time believed to be thermodynamically unstable.[**72, 74, 106**] They do not form spontaneously but require energy input due to an increase in surface free energy upon droplet breakup. By adsorption of colloidal particles to the droplet surface the energetically unfavorable oil-water interface is reduced and a mechanical barrier that retards the coalescence of the emulsions droplets is created. In the long term, oil and water phase separate again, and hence the emulsions are considered to be only of kinetic, but not of thermodynamic stability.

A thermodynamically stable emulsion in contrast,[**48, 107**] forms spontaneously without any additional input of energy such as shaking or ultrasonication. The size of the emulsion droplets depends only on the components that determine the thermodynamic state of the system. Traditionally, only microemulsions, namely oil-water mixtures stabilized by surfactants and possibly cosurfactants, were considered to be thermodynamically stable. Only recently, a specific type of Pickering emulsion was discovered that exhibits thermodynamic stability. In the initial experiments, it was found that mixtures of a particular oil (3-(Methacryloxypropyl) trimethoxysilane, TPM), water, and magnetite particles roughly 11 nm in size, spontaneously formed oil-in-water emulsions with the solid particles adsorbed at the interface.[**48**] Later, spontaneous emulsification was also demonstrated for colloidal cobalt ferrite and Ludox silica.[**108**] Thermodynamic stability was deduced from mixing two emulsions with different droplet sizes that spontaneously evolved into a single emulsion with an intermediate droplet size. Furthermore, the monodisperse droplet size ranges between 30 and 150 nm and is determined by the mass ratio of TPM and colloidal particles. Upon increase of the oil-colloid weight ratio, the droplet size grows linearly at first. Above a certain oil-colloid weight ratio the droplet size reaches a constant value. Additional oil is expelled as a separate phase, in analogy to microemulsions.[**107**]

The late finding, historically speaking, of thermodynamically stable meso-emulsions poses the question whether the stability is due to a specific chemical composition, and therefore unique for a TPM oil phase and certain stabilizing colloids in aqueous media, or, whether it can be described in terms of more general physical parameters. In consideration of the wide range of possible applications and impact on energy efficiency of emulsification processes on industrial scales, a thorough understanding of the generality of the spontaneous emulsification is desirable.

Therefore, this chapter aims to elucidate the molecular origins of the thermodynamic stability of these Pickering emulsions, investigate the effect of the different components on the stability in detail, and compare experimental results with theoretical predictions. Specifically, we focus on the following issues:

1. emulsion stability in absence of colloidal particles;
2. ions present in the aqueous phase;
3. nature of colloidal particles that are adsorbed onto the oil-water interface;
4. the nature of the oil.

We first review the current knowledge of the thermodynamically stable Pickering emulsions to motivate this choice of investigated parameters. Then, we describe the conducted experiments, discuss the results, and draw conclusions with respect to the basic requirements for thermodynamic stability.

7.2. Previous Work

Emulsification of a macroscopic oil and water phase into small droplets significantly enlarges the interfacial area between the oil and water phase. Adsorption of colloidal particles onto the droplet surface partially decreases this interfacial area, reducing the energy necessary to create such an interface. However, at least 10% of the interfacial area remains uncovered. The energy required to create that bare interface depends on the interfacial tension between oil and water phase. Previously, it was measured that the bare oil-water interfacial tension is as low as 3 mN/m,[**109**] much higher than the ultralow interfacial tensions of microemulsions, but still low compared to common oil-water interfacial tensions, being typically 50 mN/m. The low interfacial tension between TPM-oil and water phase is achieved by partial hydrolysis of the alkoxy moieties of TPM, a process catalyzed in alkaline environment. Alkalinity is a result of the complete dissociation of the quaternary ammonium salt tetramethylammonium hydroxide (TMAH) present in the aqueous colloidal suspension. Trialkoxysilanes such as TPM undergo hydrolysis in dilute aqueous solutions via a series of consecutive reactions, of which the first one is

$$\mathrm{R{-}Si(OR')_3 + H_2O \rightleftharpoons}\ k_1\mathrm{R{-}Si(OR')_2OH + R'OH} \tag{7.1}$$

where in the case of TPM, $\mathrm{R = H_2CC(CH_3)CO_2(CH_2)_3}$, and $\mathrm{R' = CH_3}$. Consecutive hydrolysis steps take place at a slower rate than the first.[**110**] The reaction product methanol in TPM hydrolysis in the presence of TMAH was detected by NMR measurements.[**109**] After formation, the weakly acidic silanol groups can dissociate according to

$$\mathrm{R{-}Si(OR')_2OH \rightleftharpoons}\ k_2\mathrm{R{-}Si(OR')_2O^- + H^+} \tag{7.2}$$

creating negatively charged molecules that are surface active due to their amphiphilic nature. The adsorption to the interface was verified by observing a decrease in the interfacial tension between TPM and aqueous 6 mM TMAH from 8 mN/m down to 3 mN/m over the course of 24 h. Furthermore, self-condensation between the modified TPM molecules might play an undesired role in the stability. However, condensation of hydrolyzed TPM is a much slower process than the initial hydrolysis. Addition of

NaCl salt to an equilibrated emulsion in the presence of an excess oil phase increased the droplet size significantly, hinting at a charge induced preferred curvature of the droplets. [**48**]

Due to these very specific requirements, it is as of yet unclear whether the thermodynamic stability of solid-stabilized emulsions can be extended to other oils and colloidal particles. Recently, theoretical progress has been made on describing the underlying physics in two distinct regimes of emulsion stability.[**111, 112**] The models are complementing each other as they are applicable to the one-phase and the two-phase region, that is, in the absence and presence of excess oil, respectively.

In the linear growth regime and absence of excess oil Zwanikken et al. concluded that spontaneous emulsification is possible for hydrophobic, charge-stabilized colloidal particles, amphiphilic salt ions and hydrolyzable oil.[**112**] The adsorption of charged colloidal particles to the oil-water interface can compensate the surface charge of the bare oil-water interface created by dissociated, hydrolyzed TPM molecules. Positive ions (TMA^+) are assumed to preferentially adsorb onto the colloidal particles, whereas the reactivity of the oil creates negatively charged molecules adsorbed at the oil-water interface. As long as the net surface charge of the droplet remains low, the surface tension can decrease even to negative values. A finite droplet radius and thermodynamic stability of the solid-stabilized droplets is found at an optimal value for the ratio of colloid surface in contact with water over free oil interface.[**112**]

For the two-phase regime, Kegel et al. proposed that adsorption of hydrophobic colloids that preferably are wetted by the oil phase to the oil-water interface releases ions from the chargeable groups of the colloidal surface.[**111**] Compared to the immersion in the oil phase, the ion dissociation yields an entropic contribution to the free energy of the droplets which can balance the unfavorable free energy necessary for creating bare oil-water interface. At surface tensions of bare oil-water interface on the order of 1 mN/m a global minimum in the free energy was found for a finite droplet size. The subtle balance in the interfacial tensions between colloids and oil, γ_{co}, colloids and water, γ_{cw}, and oil and water, γ_{ow} , determines droplet stability. Thermodynamic stability is achieved for $-0.4 \leq (\gamma_{co} - \gamma_{cw})/\gamma_{ow} \leq -0.2$. Furthermore, an upper limit for the particle size that yields emulsion stability was predicted.

Both models take negatively charged colloidal particles that have a preference for the oil phase, and low interfacial tensions between the bare oil-water interface, into account.

This incomplete picture of spontaneous emulsification into solid-stabilized oil droplets motivated us to systematically investigate the different constituents.

First, we investigate whether thermodynamic stability of the emulsions can be obtained in the absence of the colloidal particles, by mixing TPM and water containing TMAH salt.

To examine the influence of TMAH, and salts in general, on the stability, we use dialyzed colloidal silica with different types of salts added in a controlled manner.

Subsequently, we explore emulsion stability with respect to different colloidal particles, ranging from nanometer-sized gold colloids to silica colloids of up to roughly 200 nm in diameter. Here, size, charge, and material of the colloids are considered when drawing conclusions on thermodynamic stability.

Finally, the specificity of the molecular structure of the oil phase that is required to obtain thermodynamically stable emulsion droplets is studied by systematically varying the different moieties of the trialkoxysilane oil as well as by employing linear alkanes and cycloalkanes. Conclusions on the conditions of thermodynamic stability are employed to find emulsions composed of different oil phase, counterions, and colloidal particles that still exhibit thermodynamic stability. Given the various experiments that corroborated thermodynamic stability in these Pickering emulsions,[**48, 109, 108**] we limit ourselves to testing the emulsions for stable monodisperse droplet sizes.

7.3. Experimental

7.3.1. Colloidal Dispersions

Magnetite colloids Colloidal magnetite dispersions (Fe_3O_4) were prepared following a precipitation method described by Massart.[**113**] 40 mL of a 1 M aqueous solution of $FeCl_3$ and 10 mL of an acidic (2 M HCl) aqueous solution of 2 M $FeCl_2$ were combined and quickly added to 500 mL of 0.7 M NH_4OH under vigorous stirring. The immediately precipitated black magnetite was collected with a magnet, decanted, and redispersed overnight in 50 mL of a 1 M solution of a quaternary ammonium salt. To vary the type of ions present in the colloidal dispersion, magnetite dispersions were prepared with either a tetramethylammonium hydroxide (TMAH) or tetraethylammonium hydroxide (TEAH) solution. The magnetite particles were subsequently transferred to Millipore water via magnetic decantation. The final dispersion contained nonaggregated, negatively charged magnetite colloids with an average diameter of 11 ± 28% nm (TMAH stabilized) and 12 ± 30% nm (TEAH stabilized). Aqueous magnetite is known to oxidize to maghemite in time. Even though no influence on emulsion stability could be detected and therefore no measures were taken to control the oxidation state, it may be useful to use a standard oxidation state in future experiments.[**114**]

Cobalt ferrite colloids Similarly, aqueous dispersions of cobalt ferrite ($CoFe_2O_4$) nanoparticles of 20 nm ± 27% were prepared by the co-precipitation of iron chloride and cobalt chloride salts, as described by Claesson et al.,[**114**] based on the procedure developed by Tourinho et al..[**115**] First, 2.38 g (0.01 mol) of $CoCl_2 \cdot 6\,H_2O$ was dissolved in a solution of 1 mL of HCl (37%) and 4 mL of water, and 5.406 g (0.02 mol) of $FeCl_3 \cdot 6\,H_2O$ was dissolved in 40 mL of water. These solutions were both heated

to 50 °C, and subsequently mixed and quickly added to a 200 mL solution of boiling 1.0 M aqueous NaOH under vigorous stirring. After stirring for 30 min at 100 °C the black mixture was cooled down to room temperature. The particles precipitated within minutes and were collected with a magnet, the supernatant was decanted, and the black sediment was redispersed in 100 mL H_2O. This procedure was used to rinse the particles 4 times with 100 mL of H_2O. The resulting sediment was redispersed in 30 mL of 2.0 M HNO_3 and stirred for 5 min, upon which 30 mL of 0.35 M $Fe(NO_3)_3 \cdot 9\,H_2O$ was added. The reaction mixture was refluxed for 45 min, after which it was cooled down to room temperature. After sedimentation of the particles with a magnet and removal of the supernatant, they were redispersed in 50 mL of 1 M tetramethylammonium hydroxide (TMAH) overnight under stirring. Finally, the particles were sedimented on a magnet to remove the excess of TMAH and redispersed in approximately 60 mL of H_2O.

Silica colloids Ludox AS-40 silica dispersions (DuPont) containing 50% w/w amorphous colloidal silica with a diameter of 25 nm ± 18% in an aqueous ammonium hydroxide solution were diluted with Millipore water to 10.36% w/w. A 100 mL volume of this silica dispersion was dialyzed against demi water for 5 days during which the water was changed four times. After filtration through 0.2 μm Millipore filters and further dilution an aqueous dispersion of 2.85% w/w nonaggregated silica was obtained.

Bindzil 30/360 colloidal silica dispersion containing particles 5-8 nm in diameter at 30% w/w was obtained from EKA, Akzo Nobel. The Bindzil dispersion was diluted to 2.33% w/w for emulsion experiments.

Furthermore, a silica dispersion containing particles with a diameter of 203 nm ± 4.7% was synthesized in ethanol according to the Stöber method.[**116**] After transfer to Millipore water, the dispersion was prepared at volume fractions of 1.0% w/w.

Polystyrene colloids Polystyrene particles of 113 nm (7% w/w, 3% w/w divinylbenzene) were prepared by emulsion polymerization in aqueous solution as described previously (see Chapter 2). A fraction of the polystyrene particles was subsequently coated with vinyl acetate to render them more hydrophilic.[**33, 28**]

Gold colloids A colloidal dispersion containing gold colloids of about 20 nm in diameter was made via the Turkevich-Frens method.[**117, 118**] For this, 250 mL of a 0.01% w/w $HAuCl_4$ aqueous solution was brought to the boil under vigorous stirring. When boiling, 3.8 mL of a 1% w/w sodium citrate ($C_6H_5Na_3O_7$) aqueous solution was added and boiling was continued for approximately 5 min during which the solution turned dark purple. The final suspension contained 0.09% w/w colloidal gold (20 nm diameter). The dispersion was dialyzed against demi water, and the pH of the colloidal dispersion was raised to 7 with TMAH.

Furthermore, a dispersion of colloidal gold capped with 4-mercaptobenzoic acid (4-MBA) was prepared following a modified method of Buining,[**119**] Reincke,[**120**] and Brust.[**121**] For this, 10.0 mL Millipore water was mixed with 200 μL aqueous $HAuCl_4$ solution (4.61 mg/mL) and 200 μL 4-MBA in ethanol (0.233 mg/mL). Under vigorous stirring, the hydrogen tetrachloroaureate was reduced by addition of 200 μL of a 100 mM aqueous sodium borohydrate solution ($NaBH_4$). The pH was adjusted by addition of aqueous TMAH to pH 9. The final suspension contained 1.4% w/w colloidal gold with a diameter of 3.5 $\pm$ 1.5 nm.

7.3.2. Emulsion Preparation

General procedure for emulsion preparation. Unless stated otherwise, the components were added in no specific order as the final state of a thermodynamically stable system is only depending on the relative amounts of the components and not on the sequence of addition.[**48**] After preparation the samples were stored on a vibration-free table in a dark, temperature controlled room. Especially when oils containing an acrylic group, such as 3-(Methacryloxypropyl) trimethoxysilane (TPM, Acros Organics, used as received), were used as the oil phase, exclusion of light as well as elevated temperatures are important in order to avoid spontaneous polymerization upon exposure to UV light or heat.

Polymerization of the particle stabilized TPM droplets was done either by addition of potassium persulfate (0.5 mL of 23 mg/mL aqueous KPS per 3 mL of emulsion) at 70 °C or by exposure to UV light (180 W, λ=365 nm, Fluolink Flex, New Bruinswick; 100 min exposure, samples placed in optical glass cuvettes with 10 mm thickness) in the presence of 2% w/w Irgacure ((2,4,6-trimethylbenzoyl, Ciba) in the TPM phase at room temperature. Furthermore, acidic as well as strong alkaline conditions above pH 10 are to be avoided because they lead to rapid self-condensation reactions of the oil and, in the case of solid silica particles, significant dissolution of colloidal silica for pH¿9. All samples were polymerized by radical initiation through KPS unless mentioned otherwise.

Mixtures of TPM and TMAH in the absence of colloids. The necessity of colloidal particles for the emulsion formation was investigated by addition of different aliquots of TPM oil (50 μL, 100 μL, 150 μL, 200 μL and 250 μL) to 10.0 mL of a 6 mM TMAH in Millipore water solution. The concentration of TMAH corresponds to pH 9 as measured.

Different colloidal particles. Emulsions containing TPM and colloidal particles of different sizes and materials at colloid concentrations mentioned above were prepared

to investigate the influence of size and material of the colloidal particles.

Nature of salt. To investigate the effect of the nature of ions present in the system, we prepared several series containing dialyzed Ludox silica colloids (12.0 g of 1% w/w colloidal silica per sample) as well as either 1 mL Millipore water, 1 mL 0.1 M NaOH, 1 mL 0.1 M TMAH, 1 mL 0.1M TEAH or 1 mL 0.1 M tetrapropylammonium hydroxide (TPAH). These salts were chosen in order to test whether hydroxide molecules that hydrolyze TPM, and thereby induce low interfacial tensions, are sufficient for emulsion stability. The concentrations of ions were chosen such that the pH in the final solution was 9 to 10. For each series we prepared four samples with increasing concentrations of TPM, such that the weight ratios $m_{\text{oil}}/m_{\text{colloid}}$ were 0.9, 1.5, 2.2, and 2.9.

Nature of oil.

3-(Methacryloxypropyl) trimethoxysilane (TPM) was used as received from Acros Organics in different concentrations as described in the respective experiments. Besides TPM, other oils were used to explore the influence of different chemical moieties on the thermodynamic stability of the emulsions. In TPM, the methacrylate allows for polymerization of the oil by radical initiators or UV light. The methoxy groups can be hydrolyzed in the presence of hydroxide to render the silane group negatively charged, thereby creating an amphiphilic molecule. All oils used in mixtures with TPM were tested for macroscopic mixing with TPM to exclude possible phase separation of the two oils.

Dodecane/Octane/Cyclohexane. TMAH-magnetite stabilized emulsions were prepared with dodecane (99%, used as received from Acros Organics), octane (99%, used as received from Acros Organics) and cyclohexane (p.a., used as received from Mallinckrodt Baker) as the respective oil phases at an oil-colloid weight ratio $m_{\text{TPM}}/m_{\text{colloid}} = 7$. These experiments were conducted to determine whether alkane and cycloalkanes can form thermodynamically stable emulsions. DLS measurements were performed 1 day after preparation. Then, 10% w/w TPM with respect to the total oil mass was added to the emulsions. DLS measurements were performed again after one and six days of equilibration.

(3-Methacryloxypropyl) triethoxysilane (MPTES). We furthermore used MPTES as received from ABCR, an oil with a chemical structure equivalent to TPM, but with three ethoxy groups instead of three methoxy groups attached to the silane moieties (see also Table 1, Appendix). The ethoxy groups of the oil are more resistant to hydrolysis while MPTES is still having a chemical structure similar to TPM. From these experiments the influence of the hydrolyzation product on thermodynamic stability can be determined.

(3-Mercaptopropyl) trimethoxysilane. In addition, emulsions were prepared from (3-Mercaptopropyl) trimethoxysilane (Sigma Aldrich, used as received) and 10.00 g

0.125% w/w TMAH stabilized magnetite dispersion to obtain an oil-colloid weight ratio $m_{\text{oil}}/m_{\text{colloid}} = 6.4$. (3-Mercaptopropyl) trimethoxysilane has chargeable trimethoxysilane and apolar propyl group in common with TPM, but contains a mercapto instead of the methacryloxy group (see also Supp. Info.). Here, the influence of the molecular specificity of the apolar tail group was investigated.

(3-Mercaptopropyl) triethoxysilane Similarly, emulsions were also prepared from (3-Mercaptopropyl) triethoxysilane (tech., > 80%, Sigma Aldrich, used as received) and 10.00 g 0.125% w/w TMAH stabilized magnetite dispersion to obtain an oil-colloid weight ratio $m_{\text{oil}}/m_{\text{colloid}} = 6.4$. (3-Mercaptopropyl) triethoxysilane is an oil with a chemical structure similar to that of (3-Mercaptopropyl) trimethoxysilane with only the methoxy groups exchanged for ethoxy groups. Combined with the experiment on (3-Mercaptopropyl) trimethoxysilane, use of this oil should elucidate any correlation between emulsion stability and the mercapto group, as well as the necessity of the methoxy-/ethoxy group for thermodynamic stability, respectively. Please refer to the Appendix for tables with the chemical formulas of the different oils (Table 1, Appendix) and salts (Table 2, Appendix) used in this chapter.

7.3.3. Characterization

Microscopy. Polymerized emulsion droplets were imaged by transmission electron microscopy (TEM, TECNAI 10 or TECNAI 12, Philips). Samples were prepared by drying drops of diluted dispersions on polymer coated copper TEM grids. Dynamic light scattering (DLS). Dynamic light scattering was performed on diluted emulsions at 25 °C using an argon ion laser ($\lambda = 641.7$ nm, 400 mW, Spectra Physics). Samples were diluted immediately before measurement to minimize any effect of dilution on the thermodynamic state of the emulsion.

Zeta potential. Zeta potentials were measured on diluted emulsions with a Malvern Zetasizer Nano NS at 25 °C.

Interfacial tension. The surface tensions of various oils embedded in a 6 mM aqueous TMAH phase were determined at 25 °C using a spinning-drop tensiometer. The samples were prepared by first filling glass tubes with the denser phase, after which droplets of the lighter phase were injected. For mixtures of TPM/MPTES 10/90 50% D_2O was used in the aqueous phase to obtain a density of 1.05 g/cm^3. The angular velocity of the spinning tube was measured using an optical sensor. The droplet size was measured by observation through a microscope. The surface tension was determined from the droplet deformation in the centrifugal field as a function of the rotational speed, using the Vonnegut equation: $\gamma = \Delta\rho\omega^2 r^3/4$, which is valid if $l > 8r$. Here, $\Delta\rho$ is the density difference between the heavy and the light phase, r is the droplet

radius perpendicular to the axis of rotation, and l is the droplet length along the axis of rotation. The change in density upon addition of ions was taken into account.

7.4. Results and Discussion

7.4.1. Emulsion Stability in the Absence of Colloidal Particles

Solid-stabilized emulsions consist of four constituents: an aqueous phase containing dissolved salts, an oil phase and solid colloidal particles. To test for the necessity of colloidal particles in the stabilization of the emulsion droplets, we first investigated the behavior of mixtures of TPM and aqueous TMAH without colloidal particles. The presence of TMAH furthers hydrolysis of TPM not only by shifting the pH towards alkaline conditions but it probably acts as a catalyst in the reaction. In kinetic studies of the hydrolysis of TPM triethylamine, similar in chemical structure to the positive tetramethyl ammonium ion, was found to catalyze the hydrolysis, but also to speed up the self-condensation reaction of the formed silanols into siloxane linkages.[**122**] Hydrolyzed TPM molecules can dissociate forming negatively charged silane groups that consecutively lower the interfacial tension between the oil and the water phase. Samples containing different volume fractions of TPM (between 0.5 and 2.5% v/v) at a fixed concentration of TMAH (6 mM), but without colloidal particles, turned turbid within a day after gentle mixing. The turbidity increased with the TPM volume. After several days, the emulsions became unstable and phase separation occurred as shown in Figure 7.1. TEM measurements on TPM droplets polymerized one day after preparation show large, highly polydisperse TPM droplets (Figure 7.1B-D).

Despite the system being a thermodynamically unstable emulsion, at a given point in time before phase separation, the average droplet size increases linearly with the volume fraction of TPM, ϕ, as shown in 7.1. We can even conclude that the average droplet size increases linearly with the ratio of the concentration of TPM to TMAH in the absence of stabilizing solid particles. Since the concentration of TMAH was equal in all experiments, the concentration of the hydroxide ions, [OH−], and hence the concentration of hydrolyzed TPM is in first approximation constant throughout the series. Then, the oil-water interfacial area A_{oil} that can be occupied by surface-active TPM molecules obtained from hydrolysis is constant as well, and the radius of the droplets should scale linearly with the volume of the TPM phase, since $R = 3V_{oil}/A_{oil}$. Indeed, this can be seen in Figure 7.1. Why the system chooses this unusual path of emulsification and phase separation is unclear. A possible mechanism could be self-emulsification induced, for example, by local supersaturation or preferential diffusion of hydrolyzed TPM molecules into the water phase. Emulsions formed by self-emulsification are generally metastable.[**123**] In contrast, in the presence of colloidal particles, significantly smaller monodisperse and stable droplets were found. Thermodynamic stability was

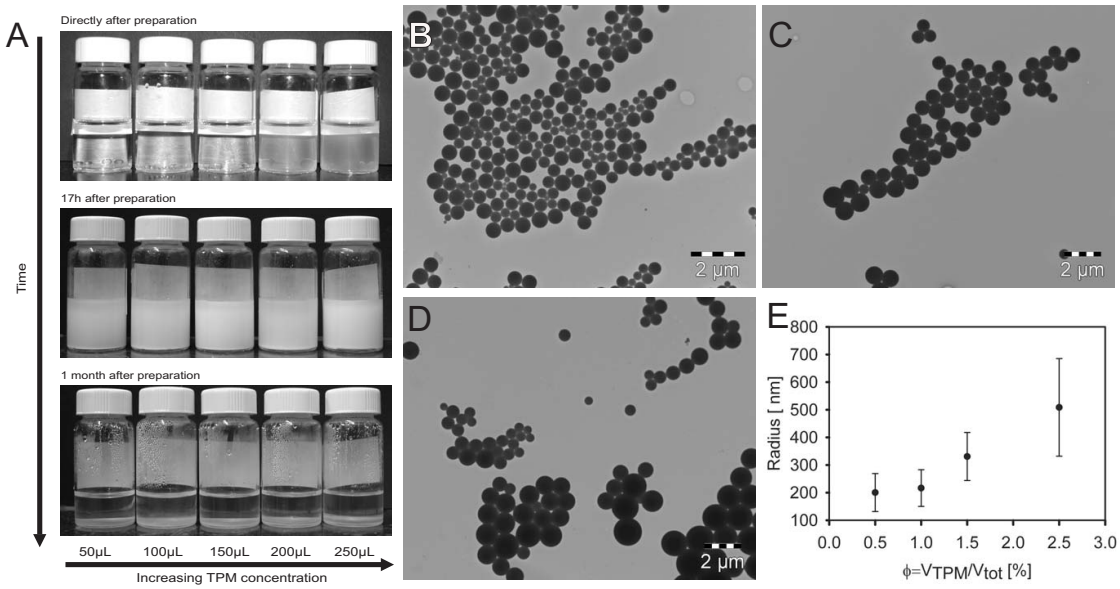

Figure 7.1. Even though mixtures of TPM in 6 mM aqueous TMAH solution are not stable, emulsion droplets show an approximately linear increase with the TPM concentration 1 day after mixing. A) Photographs of samples containing different amounts of TPM in aqueous TMAH solution at different times. TEM micrographs of polymerized samples containing B) 50μL, C) 150 μL and D) 250 μL TPM. E) Droplet size as a function of TPM concentration.

demonstrated by spontaneous formation of intermediate droplet sizes from two emulsions with different average droplet sizes.[**48**] We therefore conclude that for the formation of equilibrium solid-stabilized emulsions self-emulsification may play a role in the initial emulsification, but is not the reason for its thermodynamic stability. Yet, for stability another component than just hydrolyzing ions, and an oil and aqueous phase, is required.

7.4.2. Ions Present in the Aqueous Phase

Tetramethylammonium ions have been hypothesized to play a role in emulsion stabilization, [**109**] not only by raising the pH and catalyzing hydrolysis of TPM, but possibly also by adsorbing onto the colloidal particles and the oil-water interface.[**112**]

To investigate the significance of salts on thermodynamic stability, we dialyzed Ludox silica colloids and prepared emulsions with these colloids containing no salt, 7.7 mM NaOH, TMAH, TEAH, or TPAH, respectively. The samples with salts had pH 9, whereas the sample without salt was at neutral pH. This pH value was chosen because it induces hydrolysation of TPM on the time scale of 24 h without leading to rapid self-condensation reactions of the oil and, in the case of solid silica particles, significant dissolution of colloidal silica. In the presence of the quaternary ammonium salts

(TMAH, TEAH and TPAH) the mixtures quickly turned turbid indicating emulsification. The sample containing sodium hydroxide only slightly increased turbidity of the liquid phase, and had a clear phase consisting of TPM at the bottom of the flask. In the absence of any of those salts, and therefore at a neutral pH, no emulsification occurred, which is clearly visible by the transparent white aqueous phase and the white TPM phase at the bottom. Photographs of the samples that illustrate the effect of the presence and type of salt during emulsification are shown in Figure 7.2A. After polymerization of a fraction of the top phase we imaged all samples with a transmission electron microscope (TEM).

In the absence of salt, we find many free silica particles as well as small clusters (Figure 7.2C). With sodium hydroxide in the aqueous phase the silica colloids are either free, clustered or attached to small droplets (Figure 7.2D). In the presence of quaternary ammonium salts (TMAH, TEAH and TPAH) we have never observed free silica particles in solution. All colloids are adsorbed onto emulsion droplets (Figure 7.2C, D, Supp. Info. Figure S2 and S3). Even though the pH in all samples containing salts were equal, only the ones containing quaternary ammonium salts emulsified significantly. The hydroxide molecules present are hydrolyzing TPM into surface active molecules as described by the net reaction (1). However, this experiment shows clearly that hydroxide molecules alone are insufficient for stabilization. Surface tension measurements between TPM and water containing either NaOH or TMAH showed no significant difference 24 h after preparation (Table 7.2). Both lie around 10 mN/m. Even if TMAH acts as a catalyst in hydrolysis of TPM it does not lead to a difference in the interfacial tension on the time scale of emulsion formation. Similarly, mixtures of Bindzil colloids with 7.7 mM NaOH and 7.7 mM TMAH were prepared and monodisperse emulsion droplets that formed spontaneously were observed only in the presence of TMAH (see Appendix, Figure A.5).

Due to their amphiphilic nature, the positively charged tetramethylammonium ions are more likely to adsorb on the interface. As a result, they reduce both the negative colloidal as well as interfacial charge from surface-active TPM molecules more efficiently than ions in solution alone. This behavior is not expected for sodium ions and could therefore explain the difference in stability.

Another interesting observation is that the silica covered TPM droplets stabilized by quaternary ammonium salts change size depending on the oil-colloid weight ratio $m_{\text{oil}}/m_{\text{colloid}}$ (Figure 7.2B) in the single-phase region. The linear size increase with the oil-colloid weight ratio is in contrast to previous observations on Ludox silica colloids in an aqueous ammonium hydroxide solution used as received.[**108**] There, emulsification occurred spontaneously above a threshold ratio $m_{\text{oil}}/m_{\text{colloid}} = 1.3$, and the droplet size remained constant upon further increase of the oil concentration. Below an oil-colloid weight ratio of 1.3 electron micrographs showed uncovered TPM droplets and

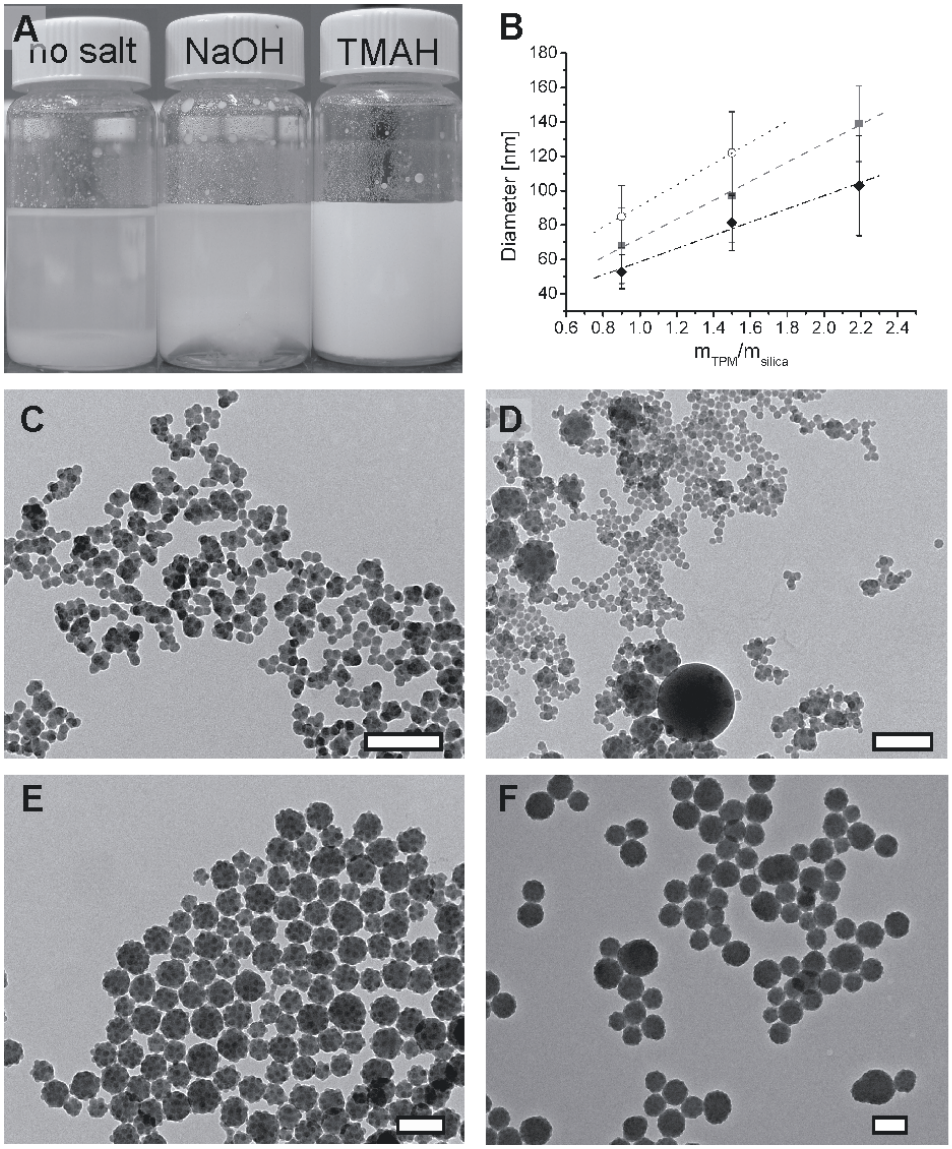

Figure 7.2. A) Mixtures of dialyzed Ludox AS 40 silica colloids, TPM and either water, NaOH, or TMAH. Without ions a white sediment is observed, whereas for NaOH most of the oil remains on the bottom of the flask. In the presence of TMAH emulsification is observed, indicated by an increase in turbidity. B) Linear dependence of the droplet diameter on the oil (TPM)-silica ratio as a function of added quaternary ammonium salt: 7 mM ⋄ TMAH, ■ TEAH and ∘ TPAH. With increasing length of the alkyl group the droplet size increases at a given oil-colloid weight ratio. Emulsions of 2.85% w/w dialyzed Ludox silica dispersions and TPM were prepared using C) no salt, D) 7.7 mM NaOH, E) 7.7 mM TMAH, or F) 7.7 mM TEAH. Emulsions are formed in the presence of the quaternary ammonium salts (E, F), but not without salt or with NaOH (C, D). Transmission Electron micrographs shown are for a TPM-silica mass ratio 2.2. Scale bars are 200 nm.

free silica colloids. Using silica colloids with salt added after dialysis, we also found spontaneous emulsification at a ratio $m_{\text{oil}}/m_{\text{colloid}} = 0.9$ (Supp. Info. Figures S2, S3 and S4). The linear size increase with the oil-colloid weight ratio is analogous to previous results obtained for TPM droplets stabilized by colloidal magnetite in the presence of TMAH in the single phase region.

Furthermore, note that, at a given oil-colloid weight ratio, the droplet size increases with the length of the alkyl group of the ions. A longer alkyl group implies stronger amphiphilicity of the ion, which apparently is more efficient in reducing the negative charge of the colloidal particles and surface-active TPM molecules upon adsorption at the interface. The better the charge between the colloidal particles is screened, the smaller the surface area they occupy is and the larger the droplet size at equal oil volumes must be. However, the net surface charge of the emulsion droplets remains low. For a magnetite stabilized TPM emulsion (oil-colloid mass ratio of 10, diameter 152 ± 3 nm) the zeta potential was measured to be -1.5 $k_B\text{T}/e$. That equals to roughly 350 negative elementary charges for an ionic strength of 7 mM. For further images and electron micrographs on experiments with dialyzed Ludox and Bindzil silica particles, see Figures A.2,A.3, A.5, and A.4, Appendix. Such direct comparisons between different batches of magnetite or cobalt ferrite stabilized by TMAH and TEAH cannot be made due to the insufficient control over ion removal during magnetic decantation: different batches can contain different concentrations of quaternary ammonium salts. Zeta potential measurements give information on the charge of the colloidal particles and therefore indirectly on the concentration of stabilizing salt. For magnetite (TMAH and TEAH stabilized) and cobalt ferrite (TMAH stabilized) colloids the zeta potential was measured to be -1.6 ± 0.3 $k_B\text{T}/e$, -2.0 ± 0.3 $k_B\text{T}/e$, and -2.2 ± 0.4 $k_B\text{T}/e$, respectively. Qualitatively, the increase in droplet size as a function of the oil-colloid mass ratio is always the same, as depicted in Figure 7.3. However, the slope of the increase in the droplet size with the oil volume and the droplet size in the presence of an excess oil phase may vary. In the one-phase region the slope of the droplet size increase as a function of the oil-colloid mass ratio is larger for TMAH than for TEAH stabilized magnetite colloids.

7.4.3. Type of Stabilizing Colloidal Particles

To achieve thermodynamically stable Pickering emulsions, different types of colloidal particles were used in TPM-water systems: TMAH stabilized magnetite and cobalt ferrite, and commercial Ludox AS 40 silica.[**108**] However, it is still unknown how broad a range in material, size, and properties of the colloidal particles can be used to stabilize these emulsions. This is both interesting with respect to possible applications as well as for the understanding of the mechanism of emulsification. We used different colloidal particles with a variety of materials, sizes and stabilizing ions in emulsion

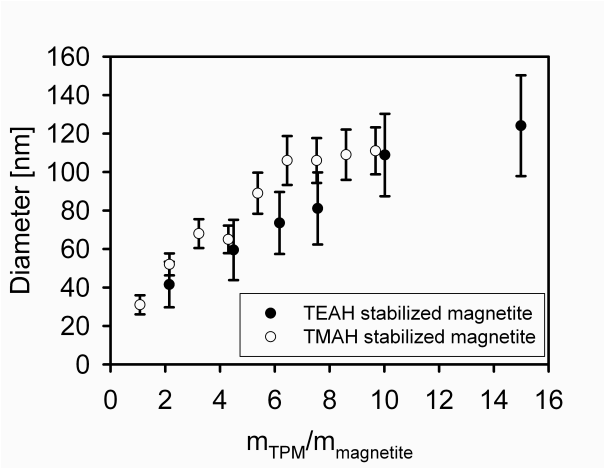

Figure 7.3. Emulsion droplet size of magnetite stabilized TPM droplets as a function of the oil-colloid mass ratio for magnetite dispersions stabilized by TMAH and TEAH.

experiments with TPM as the oil phase: 11 nm TMAH- and 12 nm TEAH-stabilized magnetite, TMAH-stabilized cobalt ferrite of 20 nm, Ludox AS 40 silica of 25 nm, Bindzil 30/360 silica colloids of 5-8 nm, Stöber silica of 203 and 310 nm, polystyrene of 226 nm, both pure polystyrene as well as with a hydrophilic coating of vinyl acetate, and gold colloids 20 nm in diameter with citrate capping as well as gold colloids of 3.5 nm with 4-mercaptobenzoic acid (4-MBA) capping.

Without any additions to the colloidal suspensions as obtained from synthesis mixtures containing magnetite, cobalt ferrite and Ludox silica colloids were found to form monodisperse, stable emulsions. However, droplet stability could not be obtained by Bindzil silica, Stöber silica, polystyrene or gold colloids in aqueous solution. Whereas the 25 nm Ludox silica particles formed stable emulsions, the smaller Bindzil and the larger Stöber silica particles were incapable of achieving this despite the similarity in material. Emulsification failure might be due to the absence of TPM hydrolyzing molecules that lower the oil-water interfacial tension by creating surface-active molecules. As previously shown for dialyzed Ludox silica, colloidal particles suspensions alone that do not contain hydrolyzing agents such as TMAH (magnetite and cobalt ferrite) or ammonia (Ludox silica) are not sufficient for droplet stability. Therefore, we prepared emulsions of TPM and colloidal particles in aqueous 6 mM TMAH solution that previously did not spontaneously emulsify. In the case of uncapped gold colloids, polydisperse droplets are seen on TEM images of polymerized emulsions. Small droplets contain only one or few gold colloids, whereas the larger droplets do often not have any gold particles attached (Figure 7.4A). 4-MBA capped gold colloids exhibit bidisperse TPM emulsion droplets sparsely covered with colloidal particles (see Figure 7.4B). The inset shows that the smaller droplet species resembles typical stable Pickering emulsions. The large

Colloidal material	Colloidal diameter	Stable emulsion?
4-MBA capped Gold	3.5 ± 43% nm	Yes
Citrate capped Gold	20 nm	No
Magnetite stabilized by TMAH	11 ± 28% nm	Yes
Magnetite stabilized by TEAH	12 ± 30% nm	Yes
Cobalt ferrite stabilized by TMAH	20 ± 27% nm	Yes
Bindzil Silica 30/360	5-8 nm	Yes
Ludox Silica AS	25 ±18% nm	Yes
Stöber Silica	203 ± 4.7% nm	No
Sulfated Polystyrene	226 ± 2.5% nm	No
Vinyl-acetate coated Polystyrene	222 ± 2.5% nm	No

Table 7.1. Emulsion stability for different types of colloidal particles, 6 mM TMAH (unless mentioned otherwise) and TPM.

uncovered droplets may be due to an excess of TPM. This improvement in stabilizing capability compared to the citrate capped gold colloids could be due to the more hydrophobic 4-MBA coated surface.

No emulsification was obtained with Stöber silica and polystyrene particles. TEM pictures of polymerized samples show polydisperse TPM droplets and free silica particles, with only few colloids adsorbed to emulsion droplets (Figure 7.4D). For sulfated and vinyl-acetate coated polystyrene particles emulsification was not obtained either (Figure 7.4E, F). On the other hand, emulsions containing TEAH stabilized magnetite colloids readily emulsified as supported by TEM images of polymerized samples (Figure 7.4C). Dialyzed Bindzil colloidal particles readily form emulsions in the presence of 7.7 mM TMAH (Figure 7.4H), whereas polydisperse droplets and free silica particles are observed in the presence of NaOH (Figure 7.4G, and Appendix, Figure A.5). Hematite spindles stabilized with TMAH and with a long axis of 250 nm were also found to spontaneously induce emulsification, but did not exhibit thermodynamic stability.[**109**] It was theoretically predicted that a condition for thermodynamically stable emulsions is that colloidal particles though initially dispersed in the aqueous phase are preferentially wetted by the oil phase.[**112, 111**] Preferential wetting of magnetite particles by the oil phase was also found previously in wetting experiments with water and TPM on a macroscopic polished magnetite surface.[**48**] Besides, colloidal particles that do achieve emulsification, such as magnetite, cobalt ferrite, silica, and 4-MBA-capped gold, are more hydrophobic than the ones that failed emulsification, such as citrate-capped gold, sulfated and vinyl-acetate coated polystyrene. Furthermore, we have observed that colloidal particles with which stable emulsions are achieved transfer into the oil phase on the time scale of days to weeks.[**124**] This is possibly caused by a slow chemical

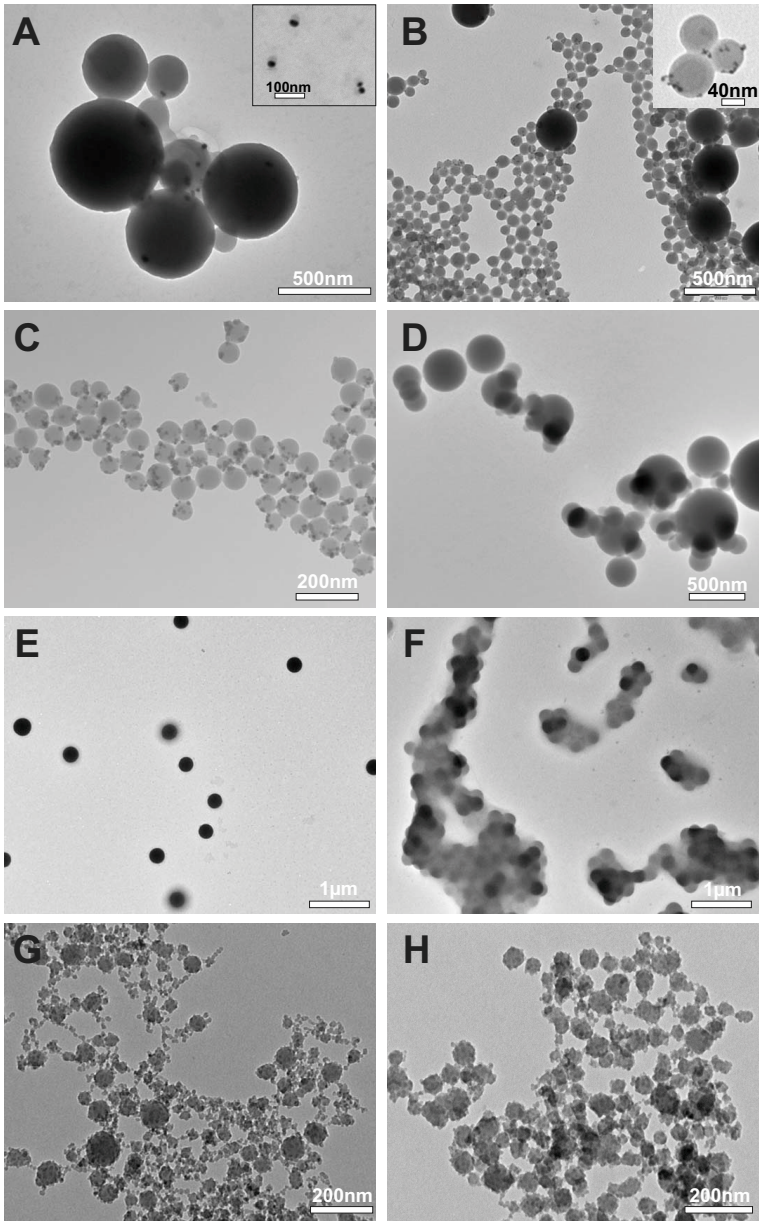

Figure 7.4. Polymerized samples of mixtures of TPM with different stabilizing colloidal particles. A) Polydisperse emulsion droplets with each only one adsorbed citrate capped gold colloid. Inset shows small droplets that were frequently observed (scale is 100 nm). B) Bidisperse droplets are visible after polymerization when 4-MBA coated gold colloids are mixed with TMAH and TPM. Inset shows a blow up of the smaller species with gold colloids adsorbed to the interface. C) TEAH stabilized magnetite readily emulsifies TPM into monodisperse emulsion droplets. D) Stöber silica colloids adsorb at the interface of TPM droplets, but do not form monodisperse emulsion droplets. E) Sulfated polystyrene colloids in 6 mM TMAH and mixed with TPM lead to growth of the individual particles, but not to emulsion droplets. F) Vinylacetate coated sulfated polystyrene colloids in 6 mM TMAH and mixed with TPM are aggregating, but do not show monodisperse droplet sizes. G) Similarly to Ludox silica as shown in Figure 7.2, mixtures of Bindzil silica colloids in 7.7 mM NaOH and TPM contained polydisperse droplets as well as free silica colloids. H) In the presence of 7.7 mM TMAH, Bindzil silica colloids and TPM form stable emulsion droplets.

Oil phase	γ_{ow} [mN/m]	$\gamma_{ow-Salt}$ [mN/m]		Salt	Stable emulsion?[a] (within 24 h)
		0 h	24 h		
Cyclohexane	44	42	42	6 mM TMAH	No
Dodecane	45	41	41	6 mM TMAH	No
Octane	46	45	45	6 mM TMAH	No
TPM[b]	8.2	8.5	5.8	6 mM TMAH	Yes
TPM[b]	8.2	8.5	6.9	6 mM NaOH	No
TPM[c]	11	11	10	6 mM TMAH	Yes
TPM[c]	11	11	11	6 mM NaOH	No
MPTES	19	17	7.0	6 mM TMAH	No
McTMS	7.3	7.6	3.1	6 mM TMAH	Yes
McTES	3.0	3.8	too turbid	6 mM TMAH	No

[a] in the presence of colloidal particles

[b] bottle open for 6 months

[c] fresh bottle

Table 7.2. Interfacial tensions of different oils against water (γ_{ow}) or water containing 6 mM salt ($\gamma_{ow-Salt}$) measured immediately (0 h) and 24 h after mixing of oil and water phase by a spinning drop tensiometer. To test for spontaneous emulsification colloidal magnetite was used in all cases except for TPM against NaOH where dialyzed Ludox silica colloids were employed.

process such as self-condensation of TPM on the particle surface and happens on a different time scale (see also Chapter 8).[**124**] Moreover, formation of stable monodisperse emulsions was found only for negatively charged particles that do not exceed 203 nm in diameter. Zeta potentials for magnetite and cobalt ferrite were around $-2\ k_BT/e$, as mentioned earlier.

7.4.4. Nature of the Oil

TPM plays an important role in the spontaneous emulsification because the molecules exposed to the aqueous TMAH phase are hydrolyzed and consecutively charged by dissociation. Next, we investigate whether the thermodynamic stability is specific to the chemical structure of TPM or if a common physical property can be identified. In the case of the latter, other oils with similar properties should also lead to spontaneous emulsification into monodisperse particle-covered emulsion droplets. First, mixtures consisting of TMAH-stabilized magnetite dispersions and alkane (octane and dodecane) or cycloalkane (cyclohexane) oils were investigated. Within 24 h the samples did not exhibit the for successful emulsification characteristic turbidity. They remained phase

Oil phase		γ_{ow} [mN/m]		$\gamma_{ow-\text{TMAH}}$ [mN/m]		Stable emulsion?[a]
		0 h	24 h	0 h	24 h	
Cyclohexane / TPM	90/10	18	18	18	9.6	Yes
Dodecane / TPM	90/10	16	16	11	8.7	Yes
Octane / TPM	90/10	18	18	11	9.6	Yes
MPTES / TPM	90/10	17	15	17	9.8	Yes

[a] in the presence of colloidal magnetite stabilized by TMAH.

Table 7.3. Interfacial tensions of different oils plus 10% w/w TPM against water (γ_{ow}) or 6 mM aqueous TMAH ($\gamma_{ow-\text{TMAH}}$) measured immediately (0 h) and 24 h after mixing of oil and water phase by a spinning drop tensiometer.

separated with a separate oil phase floating on the dispersion. To enhance emulsification, the samples were gently agitated and then stored without disturbance. After one day dynamic light scattering was performed on diluted samples. As expected from the macroscopic appearance, all samples contained polydisperse droplets, indicating a thermodynamically unstable emulsion (Figure 7.5A). None of these oils can form charged amphiphilic molecules by hydrolysis or dissociation, and surface tensions against water therefore are above 40 mN/m (see Table 7.2), even in the presence of 6 mM TMAH in the aqueous phase. For comparison, surface tensions of TPM against water and 6 mM aqueous TMAH was measured to be 8.2 and 5.8 respectively. The emulsification failure at such high surface tensions is also in agreement with theoretical predictions.[**111**] If low surface tensions are caused by hydrolysis of the methoxy groups and subsequent adsorption of the resulting amphiphilic molecule, slower emulsification should occur for (3-methacryloxypropyl) triethoxysilane (MPTES). MPTES has a similar molecular formula as TPM, but with ethoxy instead of methoxy groups. For an overview of molecular structures and chemical properties of the oils employed, please refer to the Appendix. Those groups are undergoing partial hydrolysis much less readily and are therefore an ideal test for the impact of the hydrolysis product on the thermodynamic stability. Indeed, MPTES mixed with TMAH stabilized magnetite suspension did not form stable emulsions within 24 h. Surface tension measurement against water and 6 mM aqueous TMAH yielded 19 mN/m and 17 mN/m immediately after preparation of the samples. Within 24 h the interfacial tension decreased to 7 mN/m in the presence of TMAH. Yet, no emulsification was observed on the same time scale in the presence of magnetite colloids. This difference may be due to better mixing and therefore a larger contact area between the oil and the water phase during spinning drop measurements which speeds up hydrolysis. This agrees with the significantly larger time of 7 days necessary for spontaneous emulsification.

Further support comes from emulsification experiments with (3-mercaptopropyl) trimethoxysilane (McTMS) and TMAH stabilized magnetite particles. McTMS is an oil with hydrolysable trimethoxysilane moiety, but a mercaptopropyl group as the apolar tail. After 1 day the mixture showed a significant increase in turbidity and DLS measurements on an unpolymerized sample revealed droplet sizes of 43 nm (Figure 7.5C). Surface tension between the oil and aqueous TMAH was as low as 3.1 mN/m after 24 h, supporting the correlation between low surface tensions and emulsion stability further. Again exchanging the methoxy for ethoxy groups, that is using (3-mercaptopropyl) triethoxysilane (McTES) as the oil phase together with TMAH-stabilized magnetite particles, did not show increased sample turbidity. DLS measurements indicated polydisperse droplets, further corroborating the absence of thermodynamic stability (Figure 7.5C). Even though McTMS can form partially hydrolyzed molecules that exhibit surface-active properties due to the chargeable silane group and the mercaptopropyl tail much faster than the ethoxy variant of the oil, surface tension of McTES in the presence of TMAH was measured to be 3.8 mN/m immediately after mixing. However, within a few hours the sample turned very turbid making surface tension measurements after 24 h impossible.

From the emulsification experiments and surface tension measurements, we conclude that even though low surface tensions play an important role as emulsification was never observed for surface tensions above roughly 10 mN/m, they are in itself not sufficient for stability. The quaternary ammonium ions only have a small effect on the surface tension in the absence of colloidal particles. Surface tensions of alkanes and cyclohexane against aqueous TMAH were slightly lower than against pure water. Yet, only the combination of colloidal particles, quaternary ammonium ions, and the surface-active TPM molecules is sufficient for emulsion stability. We propose that a collective effect between those three components leads to much lower surface tension and therefore stability, than is expected from the sum of the individual components. This collective effect is in analogy to significantly lower interfacial tensions achieved by a combination of surfactants and cosurfactants in microemulsions. Theoretical frameworks that find an equilibrium droplet size explicitly consider this adsorption of quaternary ammonium ions at the interface in the single-phase region.[**112**] Also, in the presence of an excess oil phase this collective effect can be understood as follows:[**111**] a decrease in the net surface charge by adsorption of the positively charged quaternary ammonium ions allows for further ion dissociation from the colloidal particles. The dissociation yields a gain in ion entropy that can compensate for the more unfavorable oil-water tensions.

Note that the time a bottle of TPM has been opened and therefore exposed to humidity plays a small role in the surface tensions. Surface tension measurements of fresh TPM against water and 6 mM TMAH were found to be 11 mN/m instead of 8.2 mN/m and 10 mN/m instead of 5.8 mN/m. Yet, emulsification was observed with

both, indicating that surface tensions around or below 10 mN/m are sufficient to induce spontaneous emulsification in the presence of colloidal particles.

If only the partially hydrolyzed and dissociated molecules are playing a significant role in lowering the surface tensions, then stabilization should also be achieved in the presence of a small number of such molecules that adsorb at the oil-water interface. This can be tested by using oil mixtures of an oil that does not spontaneously emulsify and one that does, for example, TPM.

Therefore, we added 10% w/w TPM to the emulsions containing dodecane, octane, or cyclohexane, agitated the samples gently, and remeasured the droplet size with DLS after one day. All droplet sizes became monodisperse and significantly decreased (see Figure 7.5B). The sample containing an oil mixture of cyclohexane and 10% w/w TPM was remeasured after 4 days. The emulsion droplet size decreased further to 35 nm. Also, a mixture of MPTES and 8% w/w TPM spontaneously emulsified in the presence of magnetite colloids, yielding a droplet size of 64 ± 2 nm by DLS. Emulsion stability for all mixtures of an inert oil and 10% w/w TPM agrees with significantly smaller surface tensions against an aqueous TMAH phase on the order of 10 mN/m (Table 7.3 and 7.2) compared to surface tensions of the inert oil phase against aqueous TMAH.

Without TPM, surface tensions are roughly 45 mN/m for octane, dodecane, and cyclohexane, and 19 mN/m for MPTES. The lower surface tensions and observed spontaneous emulsification into monodisperse droplets clearly link hydrolysis and subsequent dissociation of TPM into surface-active molecules with emulsion stability. However, no stability is achieved in the absence of colloidal particles (see section 7.4.1). Only a combination of low surface tensions, amphiphilic ions, and colloidal particles yields equilibrium solid-stabilized emulsions. Note also that weak acidity of the oil may be a requirement for the emulsion stability. Strong acids completely dissociate, leading to very low interfacial tensions and probably a micellar solution rather than emulsions. Still, a small quantity of a strong acid may be employed in combination with an inert oil to achieve spontaneous emulsification.

With these minimum requirements in mind, it is straightforward to consider other liphophilic ionizable oils, such as fatty acids, for use as the oil phase in colloidally stabilized emulsions. Indeed, preliminary experiments on stearic acid and TMAH-stabilized magnetite particles yielded spontaneous emulsification into roughly 150 nm sized droplets as measured by DLS. We are currently investigating the stability of emulsions made from various fatty acids, in analogy with trialkoxysilane-stabilized emulsions.

7.5. Conclusions and Outlook

Understanding the basic requirements for stable Pickering emulsions is a stepping stone for the development of mesoscopic equilibrium particle stabilized emulsions. From systematic variations of the main components of a Pickering emulsion, colloids, oil

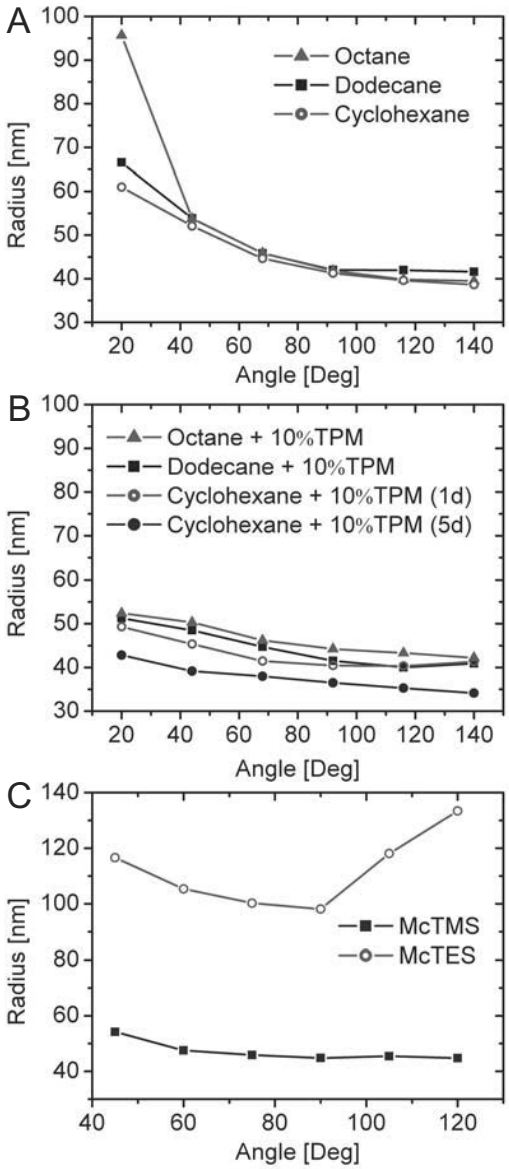

Figure 7.5. Dynamic light scattering (DLS) data showing the radii of the emulsion droplets as a function of the scattering angle. (A) Radii for magnetite stabilized emulsions containing dodecane, octane and cyclohexane measured 1 day after mixing of the components. Emulsion droplets are polydisperse in all cases. (B) Addition of 10% w/w TPM to the emulsions leads to monodisperse emulsion droplets after 1 day as measured by DLS. C) DLS data for magnetite stabilized emulsions containing McTMS and McTES. The oil containing methoxy groups, McTMS, forms monodisperse emulsions whereas the ethoxy group containing McTES shows polydisperse droplets.

phase, and dissolved ions in the water phase, we have deduced the conditions necessary for spontaneous emulsification into a thermodynamically stable system. Successful oil-in-water emulsion stabilization requires a combination of three conditions: low interfacial tensions between the oil-water interface below 10 mN/m, amphiphilic ions that can adsorb at the droplet interface, and colloidal particles (Figure 7.6). Particle-stabilized emulsions were not obtained in the absence of one of those components.

In the initial experiments on thermodynamically stable Pickering emulsions a low interfacial tension was obtained by use of a particular oil (TPM) that hydrolyzes in the presence of quaternary ammonium salts. After dissociation, hydrolyzed TPM is an amphiphilic and therefore surface-active molecule. These molecules adsorb at the interface thereby lowering the interfacial tension significantly. By systematically changing the moieties of TPM, we could attribute emulsification to the hydrolyzable part of the molecules. However, this is just one way of obtaining low interfacial tensions and not required for spontaneous emulsification. Using mixtures of hydrolyzable and inert oils in combination with a hydrolyzing agent and colloidal particles we obtained stable emulsions for a variety of oil mixtures. As long as both oils mix, the chemical nature of the inert oil is of no influence on emulsion stability. Only interfacial tensions lower than 10 mN/m are required, independent of the chemical composition of the oil, furthermore supported by surface tension measurements on pure and mixed systems. However, low interfacial tensions of the oil-water interface in the absence of colloids are not sufficient for spontaneous emulsification. In theoretical models, even surface tensions below 2-3 mN/m were required for thermodynamic stability of the emulsions. Emulsion stability also requires the presence of surface-active ions such as quaternary ammonium ions as emulsification was not achieved at low surface tensions in the presence of sodium hydroxide. We therefore suggest that a collective effect of quaternary ammonium ions and colloids leads to a stronger release of counterions. This implies that the presence of colloidal particles yields much lower surface tensions than the oil aqueous TMAH interface. Furthermore, stabilization is only obtained by negatively charged colloidal particles with a diameter below 203 nm. Possibly the maximum particle diameter with which stabilization still can be obtained is even smaller. Preferential wetting by the oil phase was found to be another common property of colloids achieving stabilization.[**124**] The detailed nature of the colloidal bulk material is not playing an essential role, as long as the colloidal surface has a preference for the oil phase. It is unclear as of yet whether size and hydrophobicity are only helpful or essential for stable emulsions. Furthermore, it still remains a challenge to make a thermodynamically stable water-in-oil Pickering emulsion. A schematic that summarizes these requirements is shown in Figure 7.6. We propose that only the collective effect of adsorption of colloidal particles, low surface tensions and amphiphilic ions leads to emulsion stability. This general mechanism

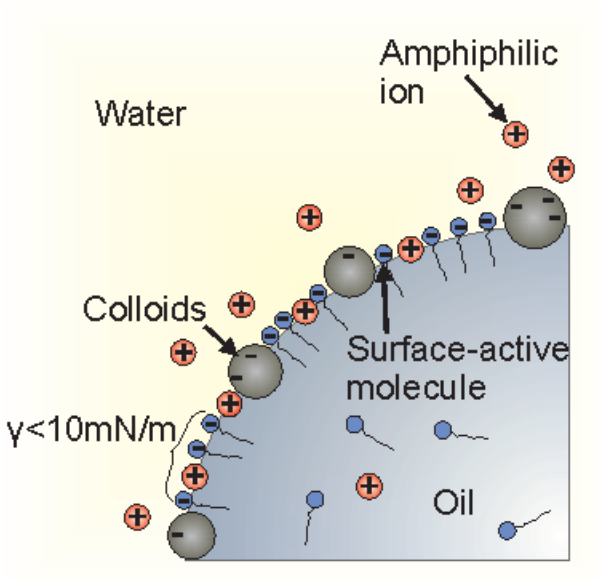

Figure 7.6. Schematic of the constituents necessary to achieve thermodynamically stable Pickering emulsions. Adsorption of negatively charged colloidal particles, surface-active molecules, and amphiphilic ions at the oil-water interface, leads to stable emulsions.

was found in many different oil-colloid systems, pointing to a new class of equilibrium solid-stabilized emulsions.

The two theoretical frameworks proposed by Zwanikken et al. and Kegel et al. are compatible with the experimental findings in previous work and described in this article. Both models take the basic requirements of low interfacial tensions, amphiphilic ions, and colloidal particles into account while finding an equilibrium droplet radius. Furthermore, they predict a preference of the colloidal particles for the oil phase as well as a maximum colloid size that still induces spontaneous emulsification.

Spontaneous emulsification into particle-stabilized oil-in-water droplets is not only fascinating from an academic viewpoint but may have an impact on emulsion fabrication because of the significant energy savings. The knowledge obtained on the minimum requirements of these Pickering emulsions may be applied to other oils and colloidal particles, with possibly industrial applications in food or material science. Not only oils that create their own surfactants by hydrolysis and dissociation but also oils that achieve similar surface-active molecules in other ways are expected to be used for spontaneous emulsification.

Acknowledgements

I thank Stefano Sacanna, Bob Luigjes and Sonja Castillo for collaboration on many experiments. Julius de Folter is thanked for surface tension measurements. Bob Luigjes, Albert Philipse and Willem Kegel have contributed significantly to the understanding

of the thermodynamic stability through many discussions. Also, I thank Jos Zwanniken and René van Roij for discussions as well as the fruitful collaboration that lead to a theoretical framework. This chapter is the unedited author's version of a Submitted Work that was subsequently accepted for publication in The Journal of Physical Chemistry B, copyright American Chemical Society after peer review. To access the final edited and published work, see http://pubs.acs.org/doi/abs/10.1021/jp102659b.

8

Evolution of Equilibrium Pickering Emulsions - A Matter of Time Scales

Abstract

A new class of equilibrium solid-stabilized oil-in-water emulsions harbors a competition of two processes on disparate time scales that affect the equilibrium droplet size in opposing ways. The aim of this chapter is to elucidate the molecular origins of these two time scales and demonstrate their effects on the evolution of the emulsion droplet size. Firstly, spontaneous emulsification into particle-covered droplets occurs through *in situ* generation of surface-active molecules by hydrolysis of molecules of the oil phase. We show that surface tensions of the oil-water interfaces in the absence of stabilizing colloidal particles are connected to the concentration of these surface-active molecules, and hence, also to the equilibrium droplet size in the presence of colloids. As a consequence, the hydrolysis process sets the timescale of formation of these solid-stabilized emulsions.

A second timescale is governing the ultimate fate of the solid-stabilized equilibrium emulsions: by condensation of the *in situ* generated amphiphilic molecules onto the colloidal particles their wetting properties change, leading to a gradual transfer from the aqueous to the oil phase via growth of the emulsion droplets. This migration is observed macroscopically by a color change of the water and oil phases, as well as by electron microscopy after polymerization of the oil phase in a phase separated sample. Surprisingly, the relative oil volume sets the timescale of particle transfer. Phase separation into an aqueous phase and an oil phase containing colloidal particles is influenced by sedimentation of the emulsion droplets. The two processes of formation of surface-active molecules

through hydrolysis and condensation thereof on the colloidal surface have opposite influence on the droplet size. By their interplay, a dynamic equilibrium is created where the droplet size always adjusts to the thermodynamically stable state.

8.1. Introduction

Two classes of emulsions are known to exhibit thermodynamic stability at present: microemulsions[**107**], and a special class of Pickering emulsions.[**48, 125**] Their equilibrium state is determined by the volume fractions of the basic components, oil and aqueous phase, the type and amount of stabilizer, the temperature and the pH. For stabilization surfactants, cosurfactants, solid particles and salt, and combinations thereof may be employed. Thermodynamic stability in microemulsions is provided by very low interfacial tensions created by adsorption of surfactants and possibly cosurfactants at the oil-water interface.[**107**] In the only recently discovered special class of Pickering emulsions, a combination of interfacial tensions of the bare oil-water interface below 10 mN/m, stabilizing colloids smaller than 200 nm, and amphiphilic ions leads to thermodynamic stability.[**125**] A systematic study of this system is described in detail in a previous publication, see [**125**]. The term Pickering emulsion generally refers to solid stabilized emulsions that were first discovered by Pickering and Ramsden at the beginning of the 20th century.[**73, 72**] Notably, apart from the system we focus on in this chapter, all other Pickering are only of kinetic and not thermodynamic stability.[**74**] To make the distinction between common, meta-stable Pickering emulsions, and the special type of thermodynamically stable Pickering emulsions investigated here, the latter ones are also sometimes termed solid-stabilized equilibrium emulsions.[**125**]

In contrast to other oil-water systems which require significant energy input for their formation, for example by mechanical mixing, thermodynamically stable emulsions form spontaneously upon mixing of the components. Their final state, such as the droplet size or whether an oil-in-water or a water-in-oil emulsion is formed, is determined only by the concentrations of the components and the type of emulsifiers added. In solid-stabilized equilibrium emulsions, for example, the droplet size in the absence of an excess oil phase increases roughly linearly with the oil-colloid mass ratio.[**48**] Mixing two emulsions with different average droplet sizes results in an intermediate droplet size.[**48**] Generally, when mixing two emulsions that are thermodynamically stable, the intermediate state is obtained corresponding to the new concentrations of the components. This also implies that the order of mixing of the constituents does not affect the state of the emulsion.

Not only deliberate changes in the composition may induce an adaption of the emulsion system to the new conditions, but also chemical processes, though unreported as of yet, should trigger a spontaneous response and alter the state of the emulsion. Here we report on thermodynamically stable Pickering emulsions in which a slow chemical change competes with the generally much faster formation of the solid-stabilized emulsion. The primary goal of this article is to explain the observed changes in the emulsion droplet size by the underlying molecular processes. We first investigate the role that

in situ generation of surface-active molecules plays on spontaneous emulsion formation. Then, we explore the reasons that lead to emulsion droplet size growth. Intriguingly, these competing time scales govern the evolution of the emulsion droplet size. We find that the droplet size always adapts to the lowest free energy state as defined by the emulsion conditions, leading to a dynamic equilibrium.

8.2. Experimental

8.2.1. Colloidal dispersions

Magnetite colloids Colloidal magnetite dispersions (Fe_3O_4) were prepared following a precipitation method described by Massart.[**113**] 40 mL of a 1 M aqueous solution of $FeCl_3$ and 10 mL of an acidic (2 M HCl) aqueous solution of 2 M $FeCl_2$ were combined and quickly added to 500 mL of 0.7 M NH_4OH under vigorous stirring. The immediately precipitated black magnetite was collected with a magnet, decanted and redispersed overnight in 50 mL of a 1 M solution of a quaternary ammonium salt. To vary the type of ions present in the colloidal dispersion, magnetite dispersions were prepared with either a tetramethyl ammonium hydroxide (TMAH) or tetraethyl ammonium hydroxide (TEAH) solution. The magnetite particles were subsequently transferred to Millipore water via magnetic decantation. The final dispersion contained non-aggregated, negatively charged magnetite colloids with an average diameter of 11 ± 28% nm (TMAH stabilized) and 12 ± 30% nm (TEAH stabilized). Aqueous magnetite is known to oxidize to maghemite in time. Even though no influence on emulsion stability could be detected and therefore no measures were taken to control the oxidation state, it may be useful to use a standard oxidation state in future experiments.[**114**]

Cobalt ferrite colloids Similarly, aqueous dispersions of cobalt ferrite ($CoFe_2O_4$) nanoparticles of 20 nm ± 27% were prepared by the co-precipitation of iron chloride and cobalt chloride salts, as described by Claesson et al.,[**114**] based on the procedure developed by Tourinho et al..[**115**] First, 2.38 g (0.01 mol) of $CoCl_2 \cdot 6\,H_2O$ was dissolved in a solution of 1 mL of HCl (37%) and 4 mL of water, and 5.406 g (0.02 mol) of $FeCl_3 \cdot 6\,H_2O$ was dissolved in 40 mL water. These solutions were both heated to 50 °C, subsequently mixed and quickly added to a 200 mL solution of boiling 1.0 M aqueous NaOH under vigorous stirring. After stirring for 30 minutes at 100 °C the black mixture was cooled down to room temperature. The particles precipitated within minutes and were collected with a magnet, the supernatant was decanted, and the black sediment was redispersed in 100 mL H_2O. This procedure was used to rinse the particles 4 times with 100 mL of H_2O. The resulting sediment was redispersed in 30 mL of 2.0 M HNO_3 and stirred for 5 minutes, upon which 30 mL of 0.35 M $Fe(NO_3)_3 \cdot 9\,H_2O$ was added. The reaction mixture was refluxed for 45 minutes, after which it was cooled down to room temperature. After sedimentation of the particles with a magnet and removal

of the supernatant, they were redispersed in 50 mL of 1 M tetramethylammonium hydroxide (TMAH) overnight under stirring. Finally, the particles were sedimented on a magnet to remove the excess of TMAH, and redispersed in approximately 60 mL of H_2O.

Silica colloids Ludox AS-40 silica dispersions (DuPont) containing 50% w/w amorphous colloidal silica with a diameter of 25 nm ± 18% in an aqueous ammonium hydroxide solution were diluted with Millipore water to 10.36% w/w. A 100 mL volume of this silica dispersion was dialyzed against demi water for five days during which the water was changed four times. After filtration through 0.2 μm Millipore filters and further dilution an aqueous dispersion of 2.85% w/w non-aggregated silica was obtained.

8.2.2. Emulsion Preparation

General procedure for emulsion preparation. The components were added in no specific order as the final state of a thermodynamically stable system only depends on the relative amounts of the components and not on the sequence of addition. Colloidal suspensions were diluted with Millipore water to the mentioned weight fractions. The oil phase consists, unless stated otherwise, of (3-methacryloxypropyl) trimethoxysilane (TPM, Acros Organics, used as received, stored at 4 °C), a polymerizable trialkoxysilane that can form surface-active molecules through hydrolysis and dissociation of weakly acid silanol groups. After preparation the samples were stored on a vibration-free table in a dark, temperature-controlled room.

Polymerization of the particle stabilized TPM droplets was achieved by addition of potassium persulfate (0.5 mL of 23 mg/mL aqueous KPS per 3 mL of emulsion) at 70 °C.

Stability at high TPM concentrations. A series of magnetite-stabilized TPM emulsions was prepared to investigate the emulsion stability at high oil concentrations. Each sample contained 2.0 g of a 0.125% w/w magnetite dispersion and different TPM volumes, such that the corresponding mass ratios $m_{\text{oil}}/m_{\text{colloid}}$ were 100, 150, 200, 250, 300, 350, 400, 500, 600 and 1000. The samples were gently homogenized several times a day during the first three days to separate emulsion stability from effects due to sedimentation. Furthermore, three samples containing 2.0 g of a 0.125% w/w magnetite dispersion with mass ratios $m_{\text{oil}}/m_{\text{colloid}}$ of 160, 240 and 400 were prepared. These samples were not shaken during the observation.

Long-term emulsion stability. Two emulsions were prepared by the addition of 0.104 g and 0.466 g of TPM to 44.45 g and 42.17g of 1.2 g/L cobalt ferrite dispersions in water, to obtain oil-colloid weight ratios $m_{\text{oil}}/m_{\text{colloid}}$ of 2.0 and 9.2, respectively. The emulsions were monitored for 20 days by visual observation, and aliquots of 1.5 mL

were taken and polymerized for investigation by TEM. The emulsion was homogenized by shaking before a sample was taken.

(3-Methacryloxypropyl) triethoxysilane. We used (3-methacryloxypropyl) triethoxysilane (MPTES, used as received from ABCR), an oil with a chemical structure equivalent to TPM, but with three ethoxy groups instead of three methoxy groups attached to the silane moieties. The ethoxy groups of the oil are more resistant to hydrolysis while MPTES is still having a chemical structure similar to TPM. From these experiments the influence of the surface-active molecules generated through hydrolysis on thermodynamic stability can be determined. Besides using pure MPTES in the oil phase, we also prepared emulsions with different ratios of TPM and MPTES at a fixed oil-colloid weight ratio of 5. For each sample we added 0.11 g oil to 10.5 g of a 0.2% w/w magnetite dispersion. By doing so we investigated whether fractions of TPM in the oil phase provide sufficient surface-active molecules to induce stability.

8.2.3. Characterization

Electron microscopy Polymerized emulsion droplets were imaged by transmission electron microscopy (TEM, TECNAI 10 or TECNAI 12, Philips). Samples were prepared by drying drops of diluted dispersions on polymer coated copper TEM grids. Polymerized sediment was sputter coated with platinum/palladium prior to imaging by scanning electron microscopy (SEM XL FEG 30).

Dynamic Light Scattering Dynamic light scattering was performed on diluted emulsions at 25 °C using an argon ion laser ($\lambda = 641.7$ nm, 400 mW, Spectra Physics). Samples were diluted immediately before measurement to minimize any effect of dilution on the thermodynamic state of the emulsion.

Interfacial tension The surface tensions of various oils embedded in a 6 mM aqueous TMAH phase were determined at 25 °C using a spinning-drop tensiometer.[**126**] The samples were prepared by first filling glass tubes with the denser phase, after which droplets of the lighter phase were injected. Mixtures of MPTES and TPM at 70/30, 50/50, and 30/70 with densities close to 1 g/cm^3 were measured against an aqueous phase containing 75% w/w D_2O (density of the mixture 1.08 g/cm^3). For mixtures of 10/90 TPM/MPTES 50% D_2O was used in the aqueous phase to obtain a density of 1.05 g/cm^3. The angular velocity of the spinning tube was measured using an optical sensor. The droplet size was measured by observation through a microscope. The surface tension was determined from the droplet deformation in the centrifugal field as a function of the rotational speed, using the Vonnegut equation:[**126**] $\gamma = \Delta\rho\omega^2 r^3/4$, which is valid if $l > 8r$. Here, $\Delta\rho$ is the density difference between the heavy and the

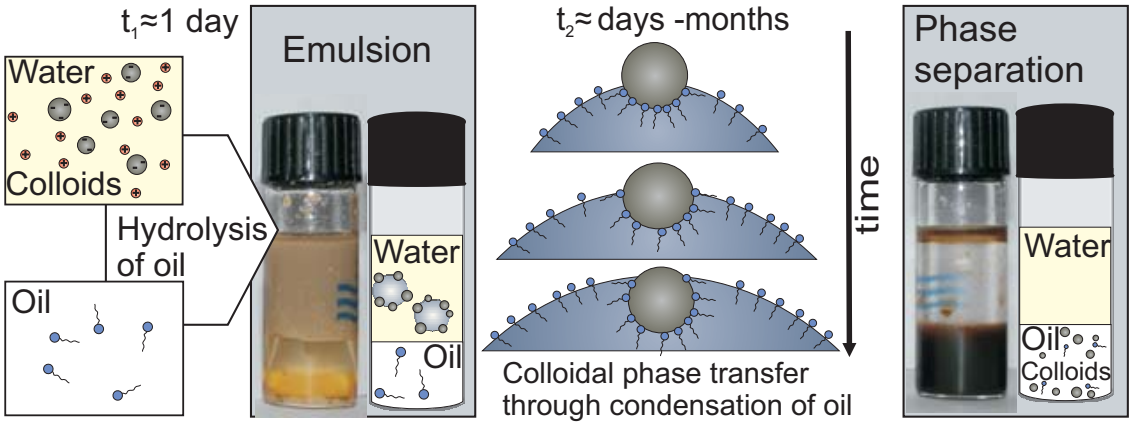

Figure 8.1. Schematic drawing of the two processes of hydrolysis and condensation occurring in the emulsion system. Hydrolysis leads to spontaneous emulsification on the time scale of a day. Gradual coating of the colloidal particles by condensation of hydrolyzed oil molecules transfers them to the oil phase, with phase separation as the final state.

light phase, r is the droplet radius perpendicular to the axis of rotation, and l is the droplet length along the axis of rotation. The change in density upon addition of ions was taken into account.

8.3. Results and Discussion

Upon mixing of aqueous colloidal suspensions and a particular oil, (3-methacryloxypropyl) trimethoxysilane (TPM), emulsification into monodisperse oil droplets covered with colloidal particles is observed. Direct evidence for this spontaneous emulsification was provided by confocal microscopy of water and TPM containing fluorescent dye.[**108**] In the absence of colloidal particles, oil droplets undergo coarsening, whereas in the presence of magnetite colloids the oil droplets shrink in size. Within two hours a large fraction of TPM is dispersed into droplets covered by solid particles. Chain formation of the droplets in a magnetic field confirms that the magnetite colloids are adsorbed onto the droplet interface. Ludox silica stabilized emulsions are forming on the time scale of two days as indicated by the angle-independent size measured by Dynamic Light Scattering (DLS).[**108**] Other stabilizing colloidal particles, such as Bindzil silica, cobalt ferrite, and gold, also induce emulsification within a day.[**125, 108**]

The time scale for the formation of these solid-stabilized emulsions is linked to the timescale of partial hydrolysis and subsequent dissociation of the TPM molecules in the oil phase (Figure 8.1). The dissociated, hydrolyzed TPM molecules are amphiphilic and hence adsorb at the oil-water interface, lowering the interfacial tension.[**125**], [**109**] In the presence of 6 mM aqueous tetramethylammonium hydroxide (TMAH) the interfacial tension continuously decreases from 8 mN/m to 3 mN/m over the course of

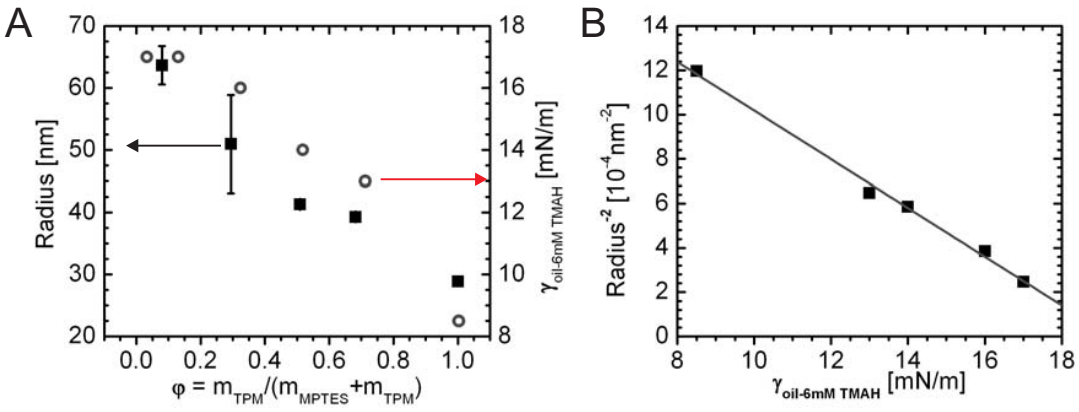

FIGURE 8.2. Emulsions containing magnetite particles and an oil phase consisting of MPTES and TPM show a correlation between surface tension of the bare oil-water interface and emulsion droplet size. No excess oil phase was present in these samples. A) Radii of emulsion droplets measured by Dynamic Light Scattering (DLS) as a function of the relative amount of TPM in the oil phase (left), and surface tension of TPM-MPTES mixtures against 6 mM aqueous TMAH as measured by spinning drop tensiometry in the absence of colloidal particles (right). B) The inverse droplet size scales quadratically with the surface tension of the bare oil-water interface (fit: $R^{-2} = 2.12 \cdot 10^{15}\mathrm{m}^{-2} - 1.1 \cdot 10^{17}\mathrm{J}^{-1}\gamma$).

24 h.[**109**] Therefore, using an oil with the much less readily hydrolyzing ethoxy[**127**] instead of methoxy groups, (3-methacryloxypropyl) triethoxysilane (MPTES), does not yield emulsification within a few days. The interfacial tension between MPTES and 6 mM aqueous TMAH is 17 mN/m immediately after mixing (Table 8.1); too high for spontaneous emulsification in the presence of colloidal particles.[**125**] Within 24 h the interfacial tension decreases down to 7 mN/m, even though no stable emulsions are obtained on that time scale. Emulsification occurs one week after mixing of the components, which is in line with the 6-10 times longer time scale of hydrolysis. [**127**]

Mixtures of MPTES and TPM have interfacial tensions in between the values of pure TPM and pure MPTES (Figure 8.2 A, Table 8.1). This indicates that the oils mix on the molecular level with compositions of TPM and MPTES on the droplet surface equaling the bulk composition. For an oil phase comprised of a mixture of MPTES and TPM, spontaneous emulsification occurs at all volume ratios in the presence of TMAH stabilized magnetite colloids. DLS measurements 5 days after mixing show that the droplet radius decreases with an increasing percentage of TPM in the oil phase, $\phi = m_{TPM}/(m_{TPM} + m_{MPTES})$ (see Figure 8.2). The sample with the smallest fraction of TPM, $\phi = 0.08$, was measured again 15 days after mixing. The droplet size slightly decreased over this period of 10 days from 64 ± 2 nm to 59 ± 1 nm. This decrease

Oil phase	γ_{OW} [mN/m]		γ_{OT} [mN/m]	
	0 h	24 h	0 h	24 h
TPM	8.2	-	8.5	5.8
MPTES/TPM 10/90	9.9	7.0	6.4	6.4
MPTES/TPM 30/70	15	-	13	9.9(4 h)
MPTES/TPM 50/50	15	12	14	10(2 h)
MPTES/TPM 70/30	17	14	16	9.0
MPTES/TPM 90/10	17	15	17	9.7
MPTES	19	16	17	7.0

Table 8.1. Interfacial tensions of different oils against water (γ_{OW} or 6 mM aqueous TMAH (γ_{OT}) measured immediately and 24 h (exceptions where indicated) after mixing of oil and water phase by a spinning drop tensiometer.

in droplet size might be due to the onset of the slower partial hydrolysis of MPTES. The droplet size and surface tension measurements on TPM-MPTES mixtures further support the hypothesis that the hydrolyzed fraction of TPM molecules forms surface-active molecules that consecutively occupy the droplet surface. The larger the fraction of TPM in the bulk oil phase the more hydrolyzed TPM molecules are generated, and the lower the surface tension of the bare oil-water interface is. Hence, more interface between oil and water can be created and the droplets shrink. Fitting the data presented in Figure 8.2B we find a linear relation between the inverse square of the radius and the bare oil-water interfacial tension, $R^{-2} = 2.12 \cdot 10^{15}\mathrm{m}^{-2} - 1.1 \cdot 10^{17} J^{-1}\gamma$. This indicates indeed, that more total droplet surface area, which scales with R^{-2}, can be created when the interfacial tension between oil and water phase is lower.

The contribution of the bare oil-water interface to the formation energy of one droplet would be $4\pi R^2(1-s)\gamma_{ow}$, where R is the radius of the droplet, s is the fraction of the droplet surface covered with colloidal particles, and γ_{ow} is the surface tension of the bare oil-water interface. Filling in typical values for such an emulsion, $R = 30$ nm, $s = 0.7$, and $\gamma_{ow} = 10$ mN/m, the energy per droplet would be on the order of $10^5 k_B T$ - way larger than the thermal energy which should be the dominating energy scale. Therefore, we conclude that the surface tension of the emulsion interface in the presence of colloidal particles, surface-active TPM molecules and surface-active quaternary ammonium ions is orders of magnitude lower than between TPM and aqueous TMAH only. Preliminary surface tension measurements on an aqueous droplet containing magnetite stabilized emulsions against TPM confirmed significantly lower surface tensions. We conjecture a collective effect between the colloidal particles, surface-active molecules and ions in analogy to microemulsions. [**125**]

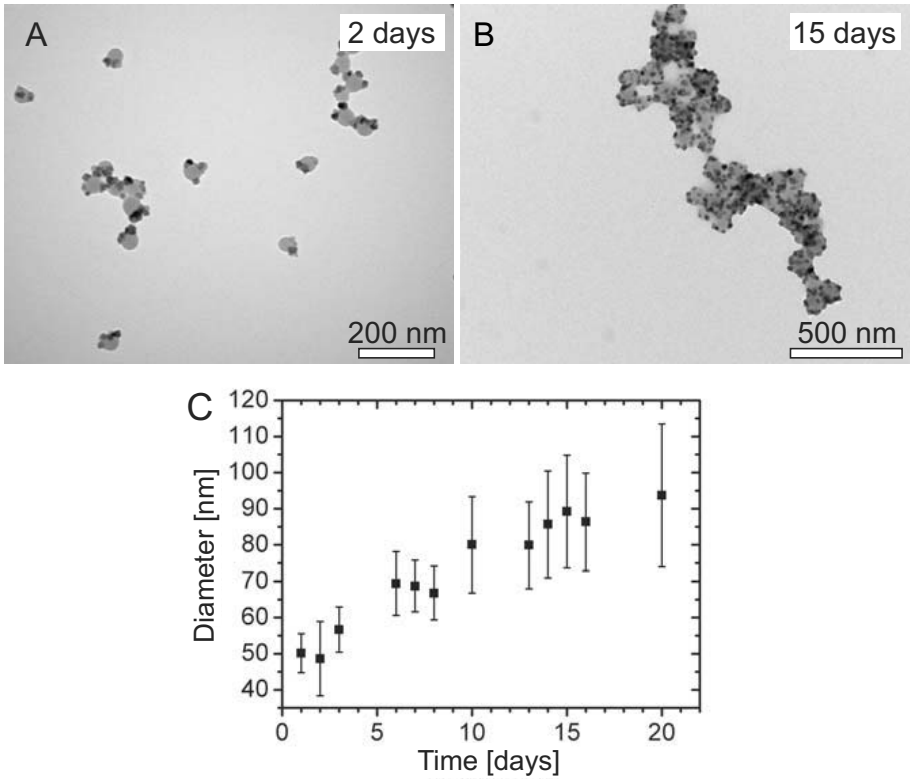

Figure 8.3. Over the course of 20 days, the emulsion droplet size grows linearly up to double the diameter without a significant increase in polydispersity. TEM images of polymerized aliquots after A) 2 days and B) 15 days. C) Diameter of cobalt ferrite stabilized TPM emulsion droplets as measured from TEM images of polymerized samples.

After formation the equilibrium Pickering emulsions can remain stable for days to months, with the time scale of stability depending on the specific composition of the emulsion. Macroscopically, a change in the droplet size can be noticed by the color of the emulsions turning lighter, manifesting larger light scattering objects and thus growth of the emulsion droplets. An emulsion consisting of TPM and cobalt ferrite colloids at oil-colloid weight ratio $m_{\text{oil}}/m_{\text{colloid}}$ of 2 turns from black/grey to grey/brown within 20 days (Figure 8.4). From TEM images of polymerized aliquots of this emulsion we quantified the size increase in time. Over the course of 20 days, the size of these emulsion droplets increases roughly from 50 to 90 nm, whereas polydispersity increases only slightly (see Figure 8.3A). TEM images after 2 and after 15 days show that the size of the droplets increased while the effective surface area per colloidal decreases from $3.2{\cdot}10^3$ nm^2 after 2 days to $2.3{\cdot}10^3$ nm^2 after 20 days (Figure 8.3 B, C). In other words, the colloidal particles are more closely packed at the interface after 20 than after 2 days. This denser surface occupation implies that the charge of the colloidal particles has decreased allowing for closer approach which in turn leading to droplet

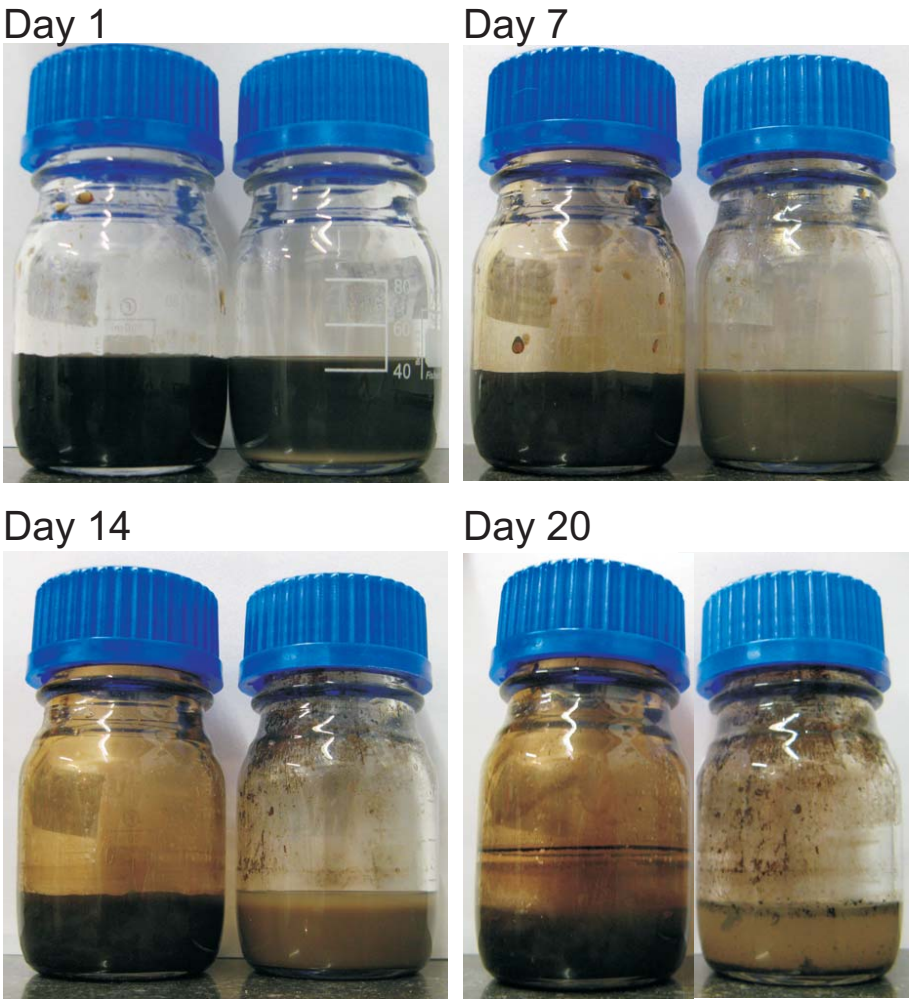

Figure 8.4. Cobalt ferrite stabilized TPM emulsions in time. Left: $m_{\text{oil}}/m_{\text{colloid}}$=2. Right: $m_{\text{oil}}/m_{\text{colloid}}$=9.

growth because the colloidal particles can stabilize less oil-water surface area. If this droplet size increase would be due to Ostwald ripening,[**128, 129**] the radius should scale as $r \propto t^{1/3}$. Fitting the experimental data with $r = a \cdot t^b$ yields $a = 44$ nm and $b = 0.25 \pm 0.02$, which makes Ostwald ripening not likely to be the mechanism for the size increase. We have observed droplet growth in time in various solid-stabilized equilibrium emulsions. Also for a cobalt ferrite stabilized TPM emulsion with an oil-colloid weight ratio of $m_{mboxoil}/m_{\text{colloids}} = 9$, that is in the presence of an excess phase, the average droplet diameter increased from 80 ± 15 nm to 191 ± 73 nm over the course of two weeks.

Eventually, the emulsions become unstable and form brown sediment. By polymerizing a magnetite as well as a cobalt ferrite emulsion that had been allowed to settle to the bottom of the flask we could image the sediment with scanning electron microscopy (SEM). The sediment consists of a continuous phase with attached and partly coalesced

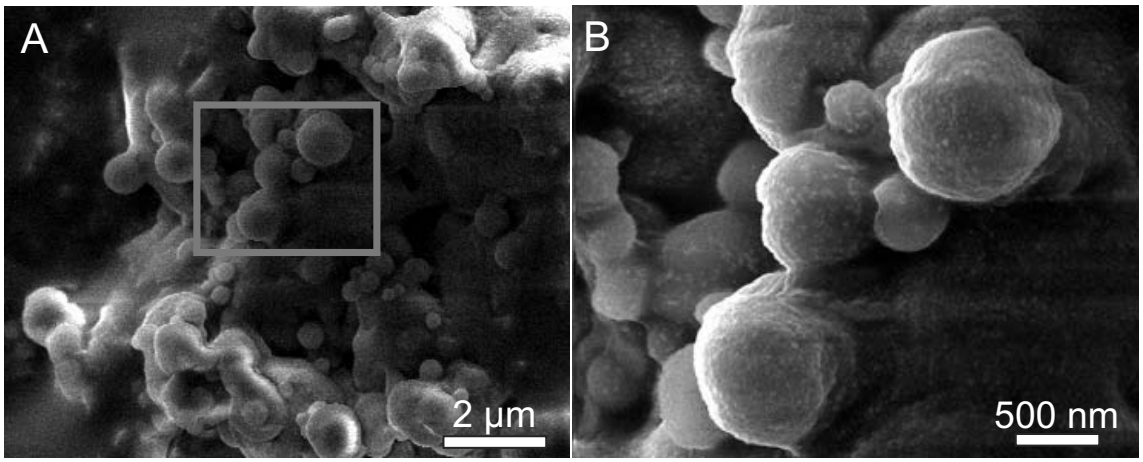

Figure 8.5. SEM micrographs of polymerized sediment of a magnetite stabilized TPM emulsion. A) A continuous phase with attached and partly coalesced droplets is visible. B) Magnified image of rectangle in A): the surface is covered with magnetite colloids.

droplets as can be seen in Figure 8.5. Droplets and continuous phase are covered with magnetite colloids. The color of the macroscopic sediment was identical to that of the colloidal suspension, whereas the supernatant became fully transparent. Similar experiments with cobalt ferrite colloids lead to comparable observations.

The time scale of sedimentation and coalescence, and ultimately transfer of magnetite to the oil phase, is linked to the relative amounts of oil and colloidal particles. To illustrate this dependence we prepared a series of magnetite stabilized TPM emulsions with oil-colloid mass ratios ranging from 100 to 1000 and observed the transfer macroscopically in time (Figure 8.6, see also Appendix Figure A.1 for more images). All samples contained an equal volume of a 0.125% w/w magnetite colloidal suspension, yet different volumes of TPM. 10 h after preparation of the samples all flasks exhibit two distinguishable phases: an aqueous upper phase consisting of colloid stabilized oil droplets and an excess oil phase on the bottom of the sample flask. The oil phase of samples with mass ratio $m_{\text{oil}}/m_{\text{colloid}}$ =400 and above appears slightly brownish, whereas samples below 400 exhibit a transparent oil phase. Since TPM by itself is a colorless liquid, the brown color of the oil phase indicates the presence of magnetite colloids. This is corroborated further by the response of the emulsion and excess phase to the presence of a magnet. After 2 days, the bottom phase of the sample with oil-colloid mass ratio 250 does not yet strongly respond to the magnet, whereas the sample with oil-magnetite mass ratio 500 does (Figure 8.8A and B, respectively). After 5 days the transfer of magnetite particles has proceeded to the point that the oil phase of all samples has turned brown/black and is magnetically responsive (Figure 8.6 B and 8.8D). Note, that before particle migration, the magnet attracts the magnetite stabilized emulsion phase more strongly (Figure 8.8C). Homogenization of the system

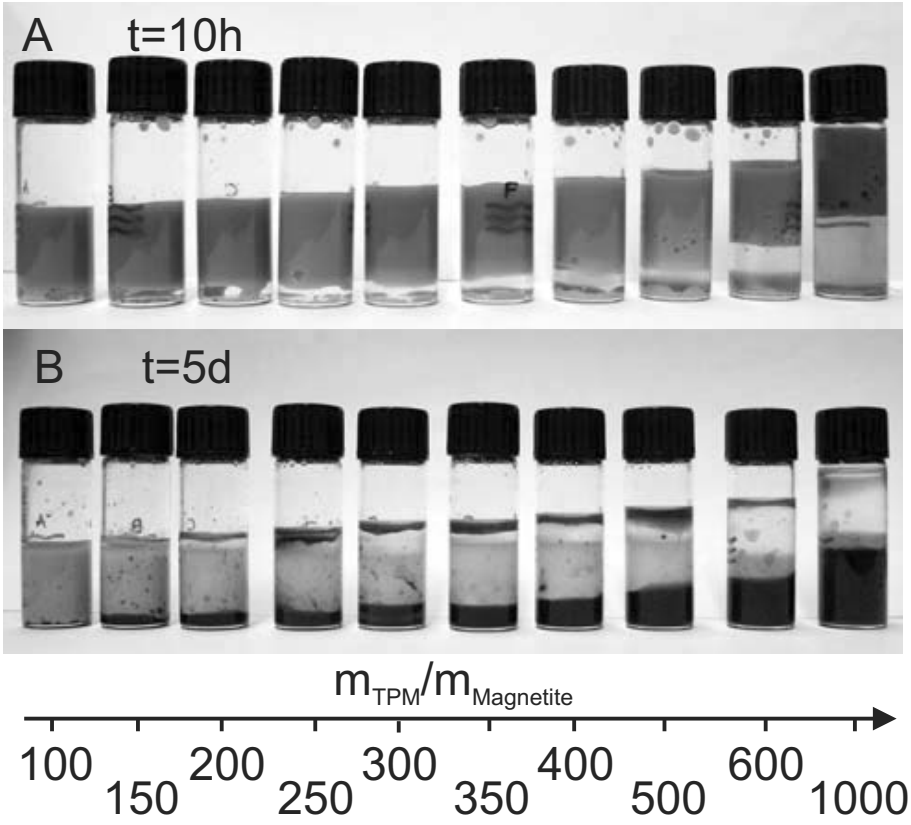

Figure 8.6. Emulsions containing magnetite colloidal particles and increasing volumes of TPM in the presence of an excess oil phase. A) After 10h emulsification of the aqueous (top) phase is indicated by increased turbidity. Samples above a TPM-magnetite mass ratio of 400 already show coloring of the bottom (TPM) phase due to migration of magnetite. B) After 5 days, most of the magnetite particles have transferred to the bottom phase, indicated by the brown color. In the upper phase emulsion droplets sediment with a sharp interface. Sedimentation occurs the faster the larger the relative oil volume is.

by gentle shaking several times a day does not influence the relative time scales of particle transfer: the colloids migrate more quickly to the oil phase with higher relative oil volumes (Figure 8.7). However, the regularly mixed samples show with increasing oil volume a less abrupt transition between an emulsified and a phase separated state than the undisturbed samples. Possibly this difference originates from sedimentation of the emulsion droplets to the excess oil phase, which is prohibited by shaking. Furthermore, the overall magnetite migration took place faster for the gently homogenized samples. Shaking not only prevents sedimentation of the droplets to the interface but also alleviates diffusion limitations within the aqueous phase for example for dissolved TPM molecules, and may increase the oil surface exposed to the aqueous phase leading to more hydrolyzed TPM molecules.

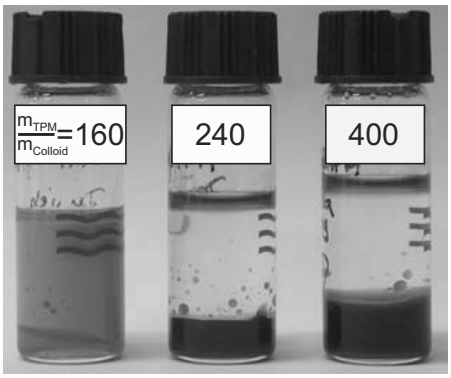

Figure 8.7. Samples of TPM and magnetite in different oil-colloid mass ratios that were not homogenized by gentle shaking.

For much smaller relative oil volumes the timescale of particle transfer lengthens significantly. Magnetite emulsions have been reported to be stable for months[**48**] and the cobalt ferrite stabilized TPM emulsion with oil-colloid mass ratio of 2 (Figure 8.3A) still exhibit emulsion droplets with a uniform size after 20 days (Figure 8.3C). For cobalt-ferrite emulsions with oil-colloid mass ratio of 9 (Figure 8.4) phase transfer has completed after 20 days as indicated by the black sediment on the bottom of the flask. The gradual emergence of the magnetic feature of the TPM phase at different times in the samples again demonstrates the oil volume dependent time scale of colloidal migration to the oil phase.

The colloidal transfer from the aqueous to the oil phase is not restricted to magnetite or cobalt ferrite stabilized TPM emulsions, but was also observed for Ludox silica particles in combination with TPM, as well as magnetite colloids in combination with fatty acids.[**130**] The latter are currently under investigation with respect to their similarities with TPM emulsions. In all cases, the transfer from the aqueous to the oil phase was observed to be faster with a higher relative oil volume.

The migration of colloidal particles to TPM likely occurs because of a slow condensation of hydrolyzed TPM molecules on the colloidal surface, rendering the colloids gradually more hydrophobic over the course of time. Silica particles deliberately coated with TPM support this scenario: the colloids were found to be stable in organic solvents, yet less stable in weakly polar organic solvents and unstable in water.[**131**] Self-condensation of alkoxysilanes is known to happen on oxides of iron, such as magnetite, and certainly is expected for silica surfaces.[**131, 132, 133**] Indications for this condensation reaction were found in infrared absorbance spectra on colloidal magnetite that was removed from a stable TPM emulsions by washing with ethanol.[**75**] Infrared absorbance spectra show a strong absorbance peak typical for TPM, indicating that TPM is still present on the magnetite surface. Furthermore, colloidal magnetite in ethanol as well as in TPM forms a stable dispersion, suggesting steric stabilization by the adsorbed

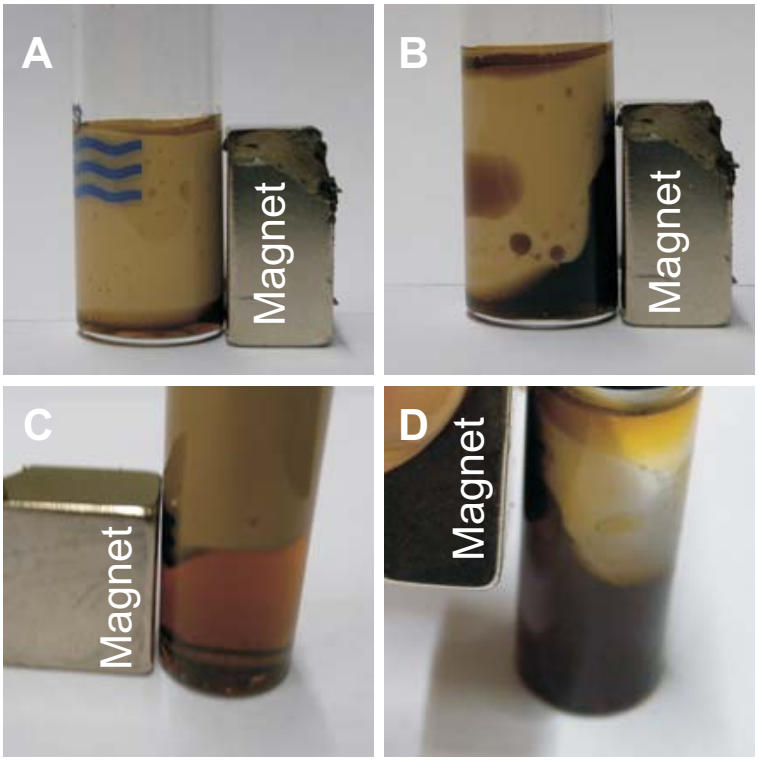

Figure 8.8. 2 days after preparation emulsions with A) an oil-magnetite mass fraction of 250 do not show significant attraction of the bottom phase to the magnet, whereas B) the dark brown oil phase of an emulsion with an oil-magnetite mass ratio of 500 strongly reacts to the magnet. C) Before migration the magnetite stabilized aqueous emulsion phase gets attracted more strongly to the magnet than the oil phase ($m_{\text{oil}}/m_{\text{colloid}} = 1000$). D) After phase separation (5 days) the oil phase is strongly magnetic.

TPM. The time scale governing the emulsion droplet growth therefore is comparable to the one governing the condensation of TPM on the colloidal particles. The time scale of condensation is set by various factors, such as temperature and pH.[**132, 122**], If the coating renders the colloidal particle sufficiently hydrophobic the particle migrates to the oil phase (see Figure 8.1 for schematic drawing). Therefore, the eventual phase separation into a transparent aqueous and an oil phase containing colloidal particles is a consequence of particle transfer to TPM.

Nevertheless, it is surprising that the migration of colloidal particles is faster with increasing relative oil volume. A likely scenario for explaining this behavior is that the number of hydrolyzed TPM molecules is higher for larger relative oil volumes, for example due to more oil-water interfacial contact, or dissolution of water molecules in the oil phase. If more hydrolyzed TPM molecules are dissolved in the aqueous phase, faster coverage of the colloidal surface and therefore transfer to the oil phase is expected.

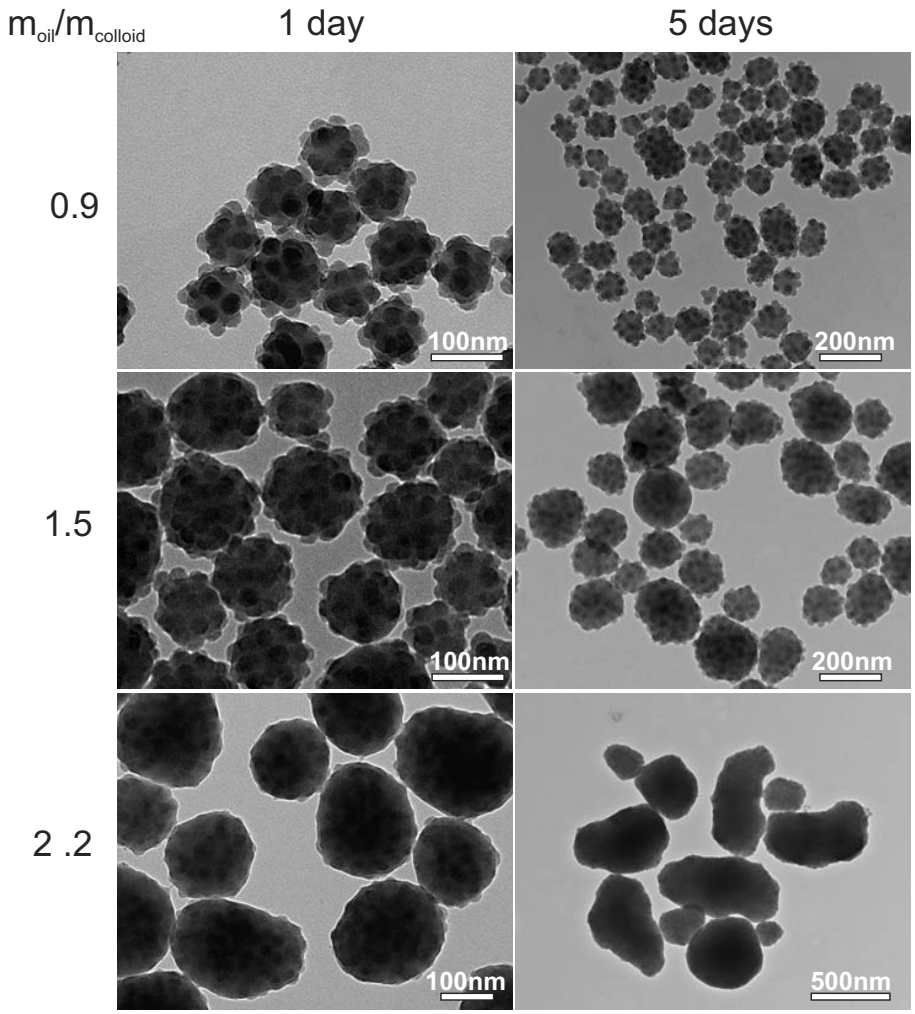

Figure 8.9. TEM micrographs of Ludox silica stabilized TPM emulsions at different oil-colloid concentrations ($m_{\text{oil}}/m_{\text{colloid}}$ from 0.9 to 2.2 top to bottom, no excess oil phase) and polymerized one and five days after mixture of the components.

The volume dependent time scale of particle coating has another surprising consequence: in the magnetite stabilized TPM emulsions with large excess oil phase sedimentation of the emulsion droplets of the aqueous upper phase occurs with a sharp interface between the transparent aqueous phase and the turbid light brown emulsion phase. The larger the relative oil volume, the faster the emulsion sediments, and hence the larger the emulsion droplets must be. This observation is surprising, because the solid-stabilized emulsions, in analogy with the preferred curvature of microemulsions, are expected to have a constant droplet size in the presence of an excess oil phase, independent of the volume thereof.[**48, 134**] However, through faster condensation of TPM on the particle surface, the charge on the colloidal particles decreases,[**111**] relieving the charge induced bending of the interface and leading to a lower preferred curvature

of the droplets. Therefore, the emulsion droplets grow despite the presence of an excess oil phase with an increasing oil volume.

Also in the absence of an excess oil phase, the coating with TPM leads to droplet growth in time (Figure 8.3 and 8.9). Here, it is not a preferred curvature that determines the droplet size, because of a shortage of oil volume. The radius of the droplets is given by the total oil volume, V_{oil}, and surface, A_{tot}, as $R = 3V_{oil}/A_{tot} = 3V_{oil}/(\sigma_{col}N_{col}))$. From this relationship, droplet growth in time can be explained by either a decrease in the number of colloidal particles at the interface, N_{col}, or the effective surface area per colloid, σ_{col}. For cobalt ferrite stabilized emulsions, the droplet radius slowly increases while the effective surface area of the colloidal particles continuously decreases in time as mentioned earlier (Figure 8.3A). From the TEM images we deduce that it is rather a lowering of the colloidal charge by coating with TPM that induces an effectively smaller area per colloidal particle than transfer of whole particles to the oil phase that accounts for the droplet growth.

One of the consequences of the gradual coating of the stabilizing colloidal particles with TPM is that the wetting angle between the colloids and the aqueous and the oil phase continuously changes in time. This can best be seen in Ludox silica stabilized TPM emulsions, where the change of the wetting angle occurs both with the available oil volume and with time, though the electron microscope images allow for a rough characterization only (Figure 8.9). At an oil-colloid ratio of 0.9 the silica particles have a wetting angle smaller than 90° (measured through the aqueous phase) which increases to values above 90° for an oil-colloid ratio of 2.2, and possibly even 180°. Four days later TEM micrographs show furthermore that the droplets have grown in size and that the droplet shape is less uniformly spherical. The first observation can only partially be explained by a decrease in the colloidal charge by coating with TPM, because the colloids were already closely packed one day after emulsion preparation. We conclude that in this case it is not the effective interface per colloidal particle that decreases, but rather the number of stabilizing particles adsorbed at the droplet interface. After five days, a fraction of the silica colloids is fully immersed in the oil droplets leading to less total available surface area and droplet growth as a consequence. The droplet deformation could be due to an inhomogeneous distribution of wetting angles or a more rigid oil surface due to self-condensation of TPM.

From our observations on droplet size growth and chemical changes leading to different wetting properties of the stabilizing particles, thermodynamic stability of the Pickering emulsions may come into question. However, there are convincing experiments that demonstrate thermodynamic stability and point to a more intricate equilibrium: spontaneous emulsification occurs only in the presence of colloidal particles[**125**] and reproducibly leads to a specific droplet size depending on the oil volume relative to the number of colloidal particles.[**48**] Even more so, an intermediate droplet size is obtained

from mixing two emulsions with a different equilibrium droplet size.[**48**] Also, the order of addition of the constituents does not influence the outcome. These observations strongly suggest that a thermodynamic equilibrium exists towards which the system develops depending on the total amounts of the components.

Along that line, we consider this system to be thermodynamically stable, despite the slow chemical changes taking place over time. By definition, thermodynamic equilibrium exists if changes in an equilibrated system are much slower than an experimental observation time. The slow process here is formation and condensation of surface-active molecules onto the particles surfaces. This changes the particle wetting properties and the system moves to a new equilibrium state. If another oil-colloid system is found that does not rely on in situ generation of surfactants that can condense on the particle surface, the change in the wetting properties of the colloids due to the chemical processes of hydrolysis and condensation will be prevented. In the presented oil-colloid system, the emulsion adapts to the change in the wetting properties of the colloids. Yet, it does so in a controlled way, that is, the droplets collectively grow in size without becoming polydisperse. The latter suggests a minimum in the free energy, which determines the state towards which the emulsion evolves. Hence, the presented type of stable Pickering emulsions exhibits an intricate equilibrium emulsion whose formation and evolution depends on two time scales that are linked to the chemical processes hydrolysis and condensation of the oil molecules.

8.4. Conclusions and Outlook

Intriguingly, the solid particle stabilized equilibrium emulsions always adjust to the slow changes in the system parameters. At first, the droplet size decreases due to hydrolysis-mediated formation of surface-active molecules on the time scale of a day. Surface tension of the bare oil-water interface is inversely related to the square of the emulsion droplet size. Subsequently, the emulsion droplets slowly grow again due to the gradual coating of the stabilizing particles by self-condensation of the hydrolyzed trialkoxysilane molecules on the surface. The coating of the colloids occurs more rapidly with larger fractions of TPM because of larger numbers of dissolved hydrolyzed TPM molecules, and leads to droplet growth in time, both in the absence and presence of excess oil. In both cases the colloidal charge decreases, leading to closer approach of the colloids and less coverable interface in the absence of excess oil, and a decreased preferred curvature of the emulsion droplets in the presence of excess oil. Ultimately, the colloidal particles migrate into the oil phase and the emulsions phase separate into a colloid rich oil phase and an aqueous phase. While undergoing change in the chemical composition through formation of surface-active oil molecules and condensation thereof on the colloidal surface, the solid-stabilized emulsions always adapt their equilibrium size to the physical conditions created by the chemical process.

Here, we also note an analogy of this dynamic equilibrium with living polymers that spontaneously respond to changes in the amount of available monomer. We propose therefore to term this type of stable Pickering emulsions that respond to changes in the wetting properties of the stabilizing particles living Pickering emulsions.

As a consequence, simply increasing the oil volume fraction does not achieve emulsion inversion into water-in-oil Pickering emulsions because the particles quickly transfer to the oil phase. So far, we have not succeeded in creating water-in-oil emulsions despite a variety of approaches. It would also be interesting to test for emulsification in the presence of colloidal particles that are originally dispersed in the oil phase. Such experiments could lead to a Pickering emulsion that does not undergo changes in the wetting properties of the colloidal particles and therefore stays uniform in time. This remains a challenge and motivation for future work on this system.

Acknowledgements

I thank Bob Luigjes for the experiments on cobalt ferrite and and Julius de Folter for surface tension measurements. Bob Luigjes, Albert Philipse and Willem Kegel are thanked for discussions on the intricate equilibrium presented in this chapter. This chapter is the unedited author's version of a Submitted Work that was subsequently accepted for publication in The Journal of Physical Chemistry B, copyright American Chemical Society 2010 after peer review. To access the final edited and published work, see http://pubs.acs.org/doi/full/10.1021/jp104662g.

9

First Experiments on Pickering Emulsions from Fatty Acids

Abstract

We explore the possibility to induce spontaneous formation of solid-stabilized oil-in-water emulsions using fatty acids and magnetite colloidal particles. Different types of fatty acids have been studied with respect to their potential to form emulsion droplets without the necessity for mechanical agitation. By dynamic light scattering we find objects on two distinct sizes, namely between 50 and 100 nm, and between 140 and 300 nm, to be present in solution. Electron microscopy confirms the presence of aggregates of magnetic particles. In the absence of stabilizing particles, spontaneous emulsification was observed as well. However, in that case, droplet sizes were on significantly larger, and with higher polydispersity. We investigate their similarities and differences with thermodynamically stable Pickering emulsions based on trialkoxysilanes.

9.1. Introduction

A fundamental feature of the particle-stabilized emulsions investigated in chapters 7 and 8 is their thermodynamical stability, which is in contrast to other solid-stabilized emulsion systems known. As shown in chapter 7, certain minimum requirements need to be fulfilled to obtain these stable equilibrium Pickering emulsions. Charged colloidal particle smaller than $\approx$ 200 nm in diameter are just one crucial factor required for thermodynamic stability. Additionally, low bare oil-water surface tensions $\leq$ 10 mN/m and amphiphilic ions in aqueous solution are necessary to accomplish a collective effect that lowers the overall "effective" surface tension below values that induce spontaneous emulsification and stability.

The conclusions on the requirements for thermodynamically stable Pickering emulsions were achieved by variation of the moieties of (3-Methacryloxypropyl) trimethoxysilane, or TPM, the oil with which the original experiments were conducted. Successful emulsification was found for molecules that *in situ* generate surface-active molecules through hydrolysis and dissociation. Adsorption of the surface active molecules at the oil-water interface reduces the interfacial tensions of the bare interface, thereby fulfilling the criterion that interfacial tensions have to be below $\approx$ 10 mN/m. Due to their preferential adsorption at the interface, small quantities of these molecules are sufficient for lowering the interfacial tension of water-oil interfaces. The latter finding extended the selection of oils that can be implemented in equilibrium solid-stabilized emulsions towards oils that mix with any of the functional trialkoxysilanes. [**125**] Yet, for further validation of our previously distinguished requirements, [**125**] it would be desirable to find stable emulsions that are free of trialkoxysilanes. Furthermore, particle migration from the aqueous to the oil phase observed in trialkoxysilane emulsions [**124**] may be prevented by use of different oils that do not undergo a condensation reaction on the particle surface. Stable emulsions based on oils other than trialkoxysilanes is also advantageous for many applications of emulsions, such as in food products, due to the possible health risks of trialkoxysilanes.

In situ generation of surface-active molecules can be achieved more directly by dissociation of, for example, a proton, avoiding the intermediate hydrolysis step. A straightforward choice for such molecules are fatty acids. Their properties are well characterized and they are widely used in industrial scale emulsifications, for example in food processing. Fatty acids are carboxylic acids with a long aliphatic chain (see Appendix for chemical structures). In aqueous solution, their carboxylic head group gets negatively charged by dissociation of a proton, yielding an amphiphilic molecule. The degree of amphiphilicity, or the hydrophilic-liphobilic balance (HLB), of fatty acids is conveniently tunable by the length of the carbon chain.

In this chapter, we study the spontaneous formation of Pickering emulsions from fatty acids in the presence of magnetite particles stabilized by tetramethylammonium hydroxide (TMAH). We vary the chain length of saturated fatty acids from 12 to 20 carbon atoms. Furthermore, a dicarboxylic acid is investigated with respect to spontaneous emulsification. We compare our experimental results obtained from dynamic light scattering and electron microscopy to the well-studied TPM system, and find both similarities as well as differences. In particular, the aim of this chapter is to compare the fatty acid emulsions to trialkoxysilane based emulsions with respect to the following characteristics: spontaneous formation of monodisperse oil-in-water (o/w) emulsion droplets in the absence and presence of colloidal TMAH-stabilized magnetite, droplet sizes with polydispersity of around 10%, droplet size dependence on the oil-colloid mass ratio $m_{oil}/m_{colloid}$, emulsion stability over time, migration of colloidal particles to the oil phase, and, thermodynamic stability.

9.2. Experimental

9.2.1. Emulsion Components

Saturated fatty acids. A variety of saturated fatty acids was tested for emulsification in the presence of TMAH stabilized colloidal magnetite. Different lengths of the aliphatic chain were employed: lauric acid ($CH_3(CH_2)_{10}COOH$, 99.5+%, Acros Organics), palmitic acid ($CH_3(CH_2)_{12}COOH$, Sigmaultra, Sigma Aldrich), stearic acid ($CH_3(CH_2)_{16}COOH$, Acros Organics), and arachidic acid ($CH_3(CH_2)_{18}COOH$, Sigma Aldrich). The melting points of the saturated fatty acids increase with the carbon chain length, and range between 42.2 °C (lauric acid) and 75.5 °C (arachidic acid). For an overview over the chemical structure formula and properties of chemicals used in this chapter see Appendix of Part 2.

Sebacic acid. Furthermore, sebacic acid ($(HOOC)(CH_2)_8(COOH)$, 99%, used as received from Sigma Aldrich), a dicarboxylic acid, was used as the oil phase. The molecule can dissociate up to two protons from opposite ends.

Colloidal magnetite. Colloidal magnetite (Fe_3O_4)was prepared following Massart's method[**113**] as described in chapter 7. The resulting magnetite particles are stabilized by tetra methyl ammonium hydroxide (TMAH) and have an average diameter of 11 ± 28% nm. Magnetite dispersions were placed in an ultrasonic bath for 20 mins before use

9.2.2. Emulsion Preparation

Fatty acids were placed in the sample flasks as solid flakes at room temperature. Colloidal magnetite at a dilution of 1.2 g/L was subsequently added to the fatty acids

and sample flasks were well sealed with PTFE tape. Consecutively, the samples were heated to 80 °C in a thermostat controlled oil bath. The temperature was chosen to be above the melting temperature of the carboxylic acids.

Samples at different oil-colloid mass ratios $m_{\text{oil}}/m_{\text{colloid}}$ were prepared to investigate any influence thereof on emulsion droplet sizes. Every 24 h aliquots of the samples were taken for investigation by dynamic light scattering and electron microscopy. The sample aliquots were stored at room temperature, which 'freezes-in' the state of the emulsions and prevents further evolution thereof.

To test for emulsification in the absence of colloidal particles 32.6 mg stearic acid and 5.02 g 6 mM TMAH were mixed and stored in an 80 °C oil bath for 24 h.

9.2.3. Characterization

Dynamic light scattering (DLS). Dynamic light scattering measurements were performed on diluted emulsions. Samples were diluted immediately before measurement to minimize any effect of dilution on the thermodynamic state of the emulsion. Multiple angle DLS measurements were carried out at 25 °C using an argon ion laser ($\lambda = 641.7$ nm, 400 mW, Spectra Physics). Furthermore, DLS measurements at a scattering angle of 176 °C were conducted by a Malvern Zetasizer Nano NS in a glass cuvette with square aperture at 25, 70 and 80 °C. To allow for temperature equilibration samples were kept at least 30 min. at the elevated temperatures before measuring.

Microscopy. Diluted samples were dried on polymer-coated carbon sputter copper grids. Samples were imaged using a transmission (TEM, Technai 12, 120 kV, Philips) and a scanning electron microscope (SEM XL FEG 30, Philips). The dried samples of particles were sputter coated with 4 nm platinum/palladium prior to imaging.

9.3. Results and Discussion

9.3.1. Spontaneous Emulsification

In this study, we explored the possibility of using different types of fatty acids to promote the spontaneous emulsification of fatty acid-water mixtures into particle stabilized droplets. After combining the fatty acids with colloidal magnetite and heating to 80 °C to induce melting of the fatty acids, the samples turned slightly turbid (see Figure 9.1 for examples). Turbidity was less pronounced than in the case of TPM-like oils, but still clearly discernible. Dynamic light scattering (DLS) measurements on mixtures of stearic acid and TMAH-stabilized magnetite colloids at various oil-colloid mass ratios, $m_{oil}/m_{colloid}$, are presented in Figure 9.2. For all oil-colloid mass ratios diameters between 150 and 320 nm were found after 2 days, suggesting spontaneous emulsification. The droplet size remained constant over the course of at least 10 days. Next to these sizes, smaller droplet diameters around 40 to 100 nm sometimes appeared as plotted in

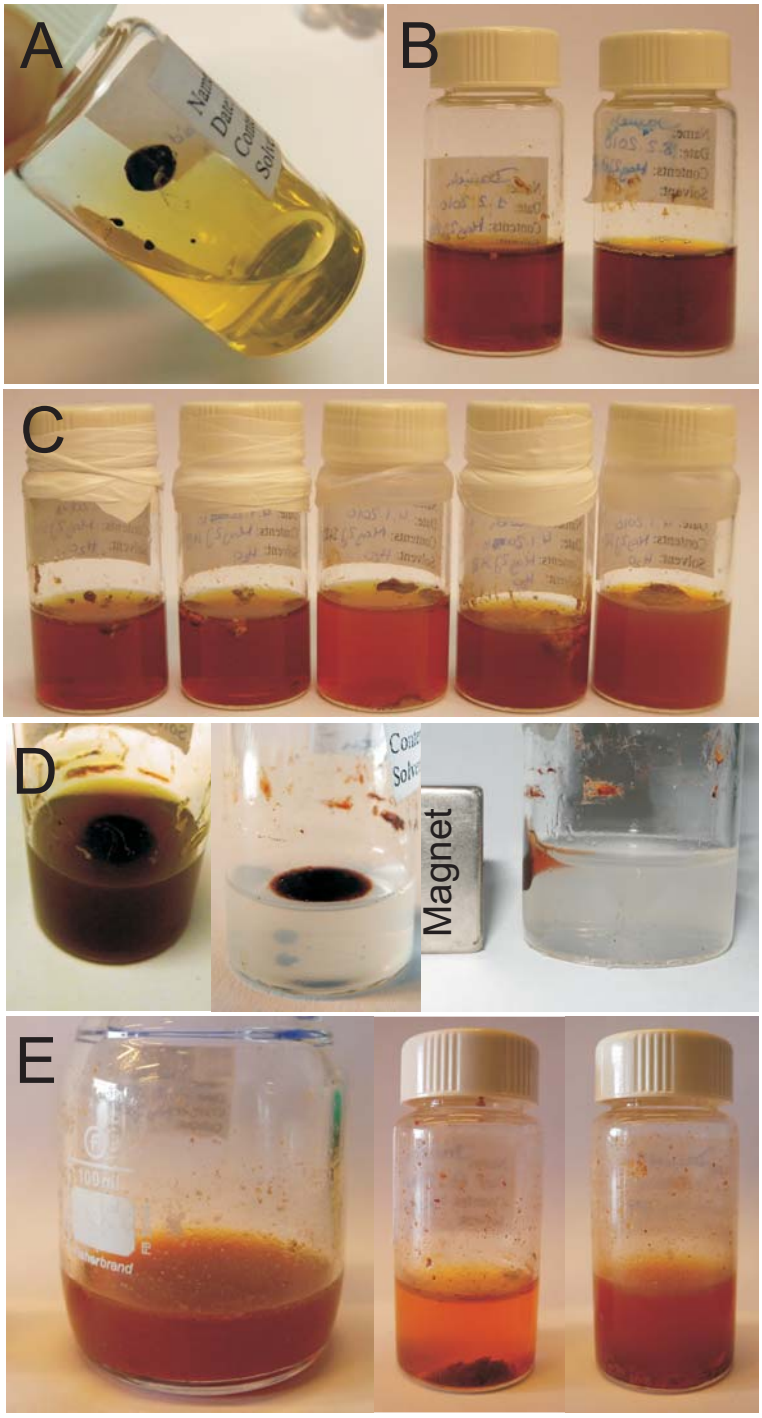

Figure 9.1. Emulsions made from saturated fatty acids and magnetite colloids before (turbid samples) and after particle transfer to the oil phase. After phase transfer, sample flasks contain a transparent aqueous phase and a dark fatty acid phase containing magnetite colloids. The samples shown contain A) lauric acid (1 h after preparation), B) palmitic acid (3 days heated, left $m_{\text{oil}}/m_{\text{colloid}} = 0.67$, right $m_{\text{oil}}/m_{\text{colloid}}$=2.6), C) stearic acid (3 days heated, left to right: $m_{\text{oil}}/m_{\text{colloid}}$=1.8, 4.5, 6.0, 8.5, 11.3), D) stearic acid (8 days heated, responds to magnet) and E) arachidic acid (4 days heated, left to right: $m_{\text{oil}}/m_{\text{colloid}}$=0.6, 1.2, 2.6.

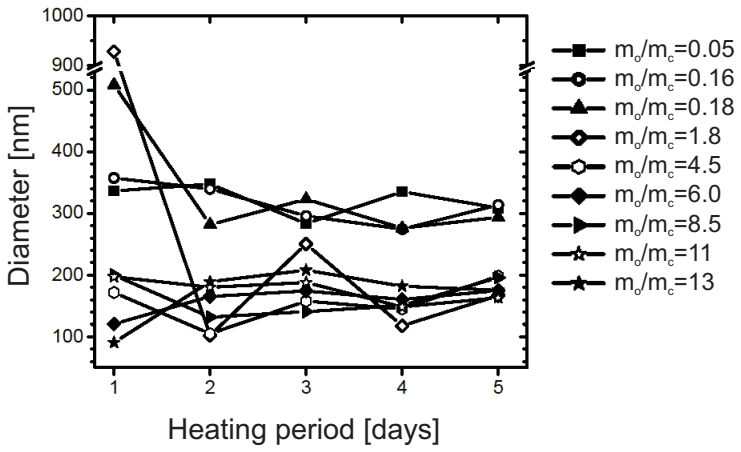

Figure 9.2. DLS measurements of droplet diameters of emulsions containing stearic acid as a function of time for different oil-colloid ratios $m_{\text{oil}}/m_{\text{colloid}}$.

Figure 9.6. We associate these secondary small diameters to free magnetite particles in solution, because the diluted magnetite dispersion yields an average diameter of 54 ± 20 nm by DLS. We note that this value is significantly larger than the single magnetite particles seen under TEM. The discrepancy is possibly due to magnetic attraction between the particles, and hence dimer or trimer formation, as radii of gyration were generally observed to be larger than radii seen in TEM for magnetite and cobalt ferrite dispersions.

Similarly, for arachidic acid, average diameters were found to be between 130 and 240 nm for oil-colloid mass ratios 1.2, 1.4, 2.6 and 3.3 (Figure 9.3). For the sample with the lowest amount of oil ($m_{\text{oil}}/m_{\text{colloid}}$=0.62) the diameter in the first three days also fell within that range, but increased to 280 nm on the fourth day. The cause of this size increase is still unclear. Furthermore, samples containing palmitic acid and magnetite colloids exhibited diameters ranging between 81 and 142 nm after 24 h storage at 80 °C. All DLS measurements presented here were associated with a significant polydispersity, with the polydispersity index ranging between 0.15 to 0.25. Therefore, no error bars were included in the plots of values obtained. Furthermore, we corroborated the high polydispersity by performing dynamic light scattering at various angles ranging between 48 and 140 ° on a sample of stearic acid. The average radii ranged between 107 and 72 nm for 48 and 140 °, respectively, indeed confirming polydisperse droplets.

By storing the fatty acid based emulsions at room temperature the oil phase solidifies, "freezing-in" the emulsion droplet, such that they can be imaged by electron microscopy. We validated the assumption that solidification of the fatty acid phase does not influence the droplet size by performing DLS at various temperatures, shown in Figure 9.4.

Transmission electron microscopy (TEM) images of fatty acid mixtures with colloidal magnetite indeed show clusters of magnetic colloids (see Figure 9.5), quite different from

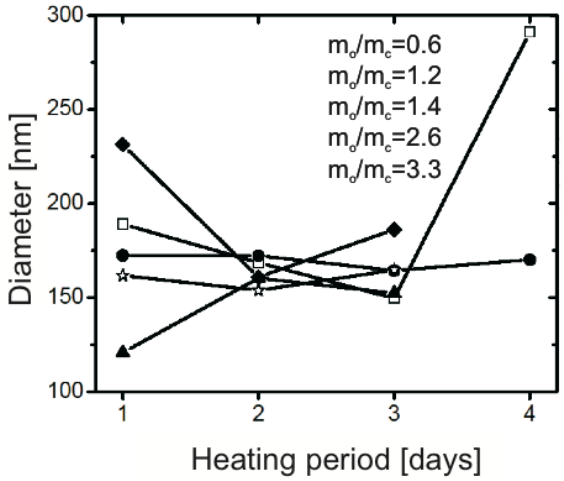

Figure 9.3. DLS measurements of droplet diameters containing arachidic acid as a function of time for different oil-colloid ratios $m_{\text{oil}}/m_{\text{colloid}}$.

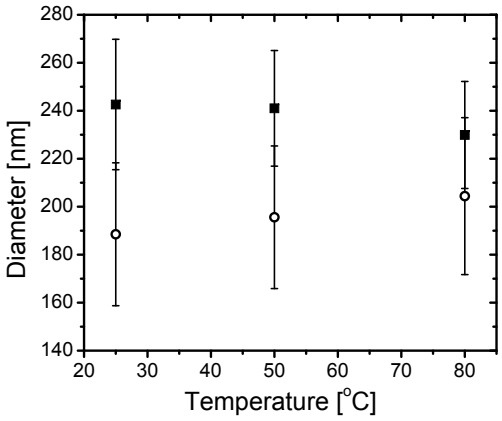

Figure 9.4. DLS measurements of droplet diameters containing stearic acid as a function of temperature.

TEM micrographs of magnetite colloidal dispersions. In all emulsified samples clusters of magnetite particles between 40 and 170 nm were present. Furthermore, seemingly unattached, or, "free" magnetite colloids are seen next to waxy non-spherical spots (see arrows in Figure 9.5, which possibly originate from excess oil. Free colloidal magnetite was not seen in TPM-like oils, yet free Ludox silica colloids have been observed. [**108**] However, excess oil was present in these fatty acid emulsions, raising the question why the free particles did not induce emulsification of the excess oil phase. Figure 9.5 A-C shows images of stearic acid stabilized by magnetite particles. Clearly visible are clusters of colloidal magnetite as well as some free particles and waxy spots. In Figure 9.5C, larger objects with a low difference in contrast and surrounded by magnetite particles are visible next to the magnetite clusters depicted in A) and B). Their size is on the

order of 250-300 nm making them candidates for the larger length scale measured by DLS. However, this stearic acid sample was the only sample where such objects could be seen. For arachidic and palmitic acid, similar clusters of colloidal magnetite with high polydispersity as well as free magnetite particles and waxy spots were observed (Figure 9.5D, E, and F. No waxy spots surrounded by magnetite particles could be find in these samples.

A possible scenario that reconciles the clusters of colloidal magnetite of around 100 nm with the larger size measured by DLS could be the following: during drying of diluted emulsion samples for TEM a part of the fatty acids is evaporated, creating deformed and smaller droplets dense in colloidal magnetite. The singular appearance of larger waxy object surround by colloidal particles (Figure 9.5C) would than have to be attributed to either an accidentally well-conserved emulsions, or to contaminations of the TEM grids.

Another explanation would be to associate the smaller lengths scales seen in DLS not with free magnetite in solution, but with these dense clusters. It would not be possible to distinguish between the clusters and free, yet attractive magnetite by light scattering, because they are of comparable size. However, this scenario does not explain the larger sizes measured by DLS, except for one stearic acid sample depicted in Figure 9.5C. To resolve the question about the in-solution state of these solid-covered droplets with certainty cryo-TEM could be employed in the future.

9.3.2. Effect of the Oil-Colloid Mass Ratio on Emulsion Droplet Size

One of the striking characteristics of thermodynamically stable Pickering emulsions based on trialkoxysilanes is their size dependence on the oil-colloid mass ratio, $m_{\mathrm{oil}}/m_{\mathrm{colloid}}$. Increasing this ratio first leads to a linear growth of the emulsion droplet size, and, probably after reaching the preferred curvature, remains roughly constant (see for example Figure 7.3). Oil in excess of the maximum total droplet volume set by the preferred curvature and the total number of colloids is expelled from the droplet and forms a separate phase. This size dependence on the oil-colloid mass ratio also forms the basis for the proof of thermodynamic stability of the emulsion.[**48**] Through mixing of two emulsions with different average droplet sizes it can be tested whether the equilibrium state is set by the total amounts of the constituents, and therefore thermodynamic stability. Indeed, an intermediate droplet size developed from emulsions with disparate droplet sizes.

In Figure 9.6 DLS measurements on stearic acid for various oil-colloid ratios are presented. Clearly, no linear dependence of the droplet diameter was found for low oil-colloid ratios. We did, however, observe an excess oil phase in samples exceeding $m_{\mathrm{oil}}/m_{\mathrm{colloid}}$=1.8. Lower ratios do not seem to lead to a decrease in the average droplet size, as would be expected in experiments on TPM, but rather a slight increase.

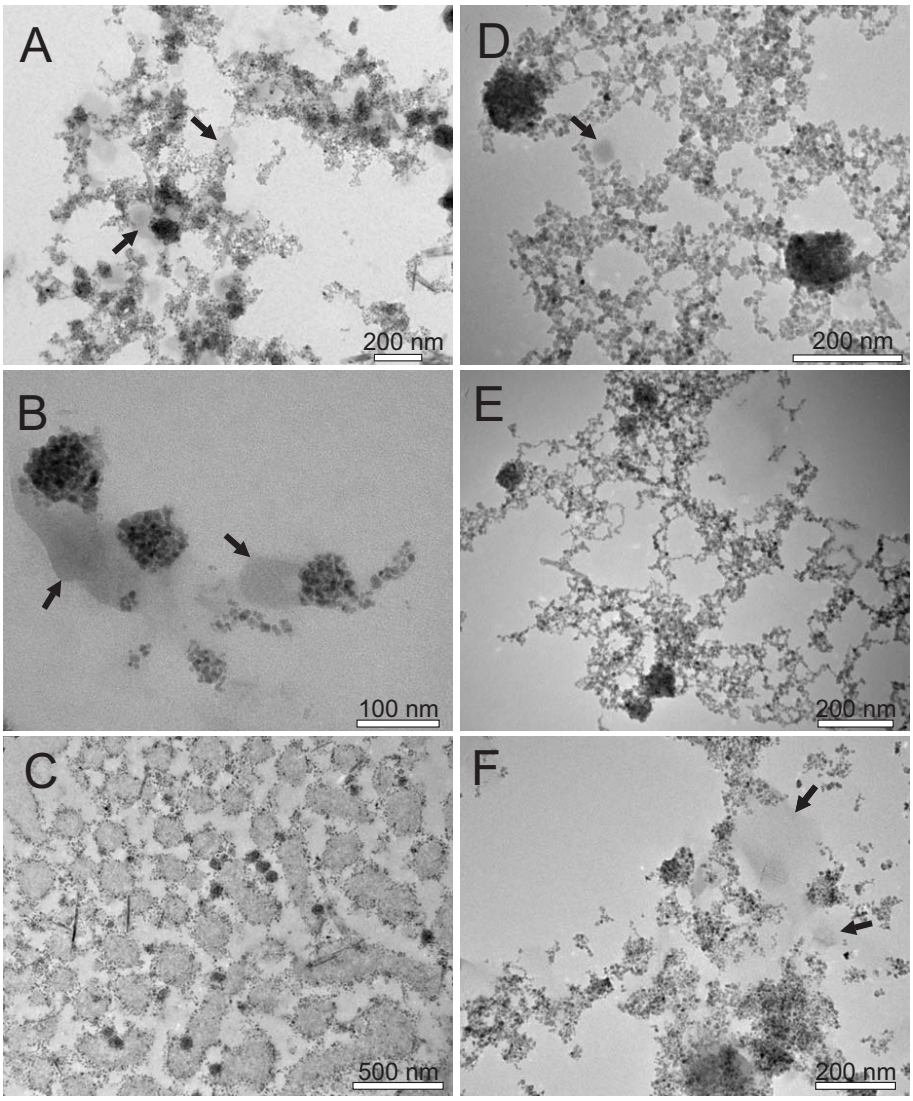

Figure 9.5. TEM micrographs of samples containing magnetite particles and various fatty acids. Arrows indicate waxy spots that are possibly originating from excess fatty acid. TEM micrographs shown are for samples consisting of mangetite colloids and A)-B) stearic acid after 8 days ($m_{\text{oil}}/m_{\text{colloid}}$=3), C) stearic acid after 5 days ($m_{\text{oil}}/m_{\text{colloid}}$=13), D) arachidic acid after 3 days ($m_{\text{oil}}/m_{\text{colloid}}$=0.54), E) arachidic acid after 4 days ($m_{\text{oil}}/m_{\text{colloid}}$=1.2), F) palmitic acid after 1 day ($m_{\text{oil}}/m_{\text{colloid}}$=1.0)

Still, an increase in turbidity with increasing relative weight of stearic acid can be noticed. Error bars shown are standard deviations from averaging over 10 measurements. Droplet size polydispersity is significantly higher, with polydispersity indices ranging between 0.1 and 0.3 as mentioned previously.

The finding of rather polydisperse emulsion droplets is not in conflict with thermodynamic stability. Within the theoretical framework proposed by Kegel and Groenewold

[**111**] the droplet size found to minimize the free energy is not sharply defined at one value, but allows for a broad emulsion droplet size distribution.

9.3.3. Different Time Scales of Colloidal Phase Transfer

Originally, trialkoxysilanes have been designed to condense on surfaces, for instance glass or nanoparticles, after hydrolysis and dissociation, thereby applying a multilayer coating with the desired properties to the surface.[**133**] Unavoidably, the use of trialkoxysilanes in a solid stabilized emulsion leads to coating of the nanoparticles with hydrolyzed and dissociated TPM molecules. The coating renders the particles more hydrophobic over time, leading to droplet growth, and, eventually, phase separation. This process has been investigated in detail in chapter 8.

Fatty acids, such as oleic acid, are known to have a strong affinity for magnetite particles, which may transfer directly from an aqueous to an oleic acid phase. [**130**] Similarly, mixtures of lauric acid and magnetite colloids lead to particle transfer to the lauric acid phase within one hour after preparation. The transfer can be observed directly by a change in color of the aqueous and the oil phase, the first turning more transparent, the latter turning black over time, indicating the presence of colloidal magnetite (see Figure 9.1A). As expected, the oil phase responded to a magnet upon turning black.

Similarly, for other (di-)carboxylic acids employed in the emulsion study, colloidal transfer took place, though at longer time scales than for lauric acid. For palmitic, stearic and arachidic acid, transfer was detected after roughly 3, 8, and 4 days, respectively. For stearic acid, a sample after 8 days of heating is shown in Figure 9.1D. However, one has to be careful with assigning definite timescales of transfer, as it depends on the relative oil volume as in the case of TPM-like oils, and is not unequivocally determinable. Over the course of time, the excess phase gradually turns more brownish, while the emulsion size measured by DLS remains more or less constant (see Figure 9.6). For small oil volumes, a dark, granular sediment, that can be easily redispersed by gentle agitation, emerges after roughly 10 days of heating for emulsions based on stearic acid. Again, the emulsion droplet size remains constant, which is a clear difference with trialkoxysilanes as the oil phase. The quicker transfer for samples may be due to the higher solubility of lauric acid in the aqueous environment due to the shorter carbon chain of the molecule. However, the trend is not clear from other fatty acids.

In trialkoxysilanes, coating of the stabilizing colloids leads to gradual transfer and droplet growths. As noted earlier, seemingly, not all magnetite colloids are integrated in the emulsification process of fatty acids. If those colloids that participated in the emulsions in the first place get coated by fatty acids and expelled towards the excess oil phase, other, free magnetite colloids can take their place, possibly leading to magnetite covered droplets highly loaded with fatty acid coated magnetite. This gradual coating

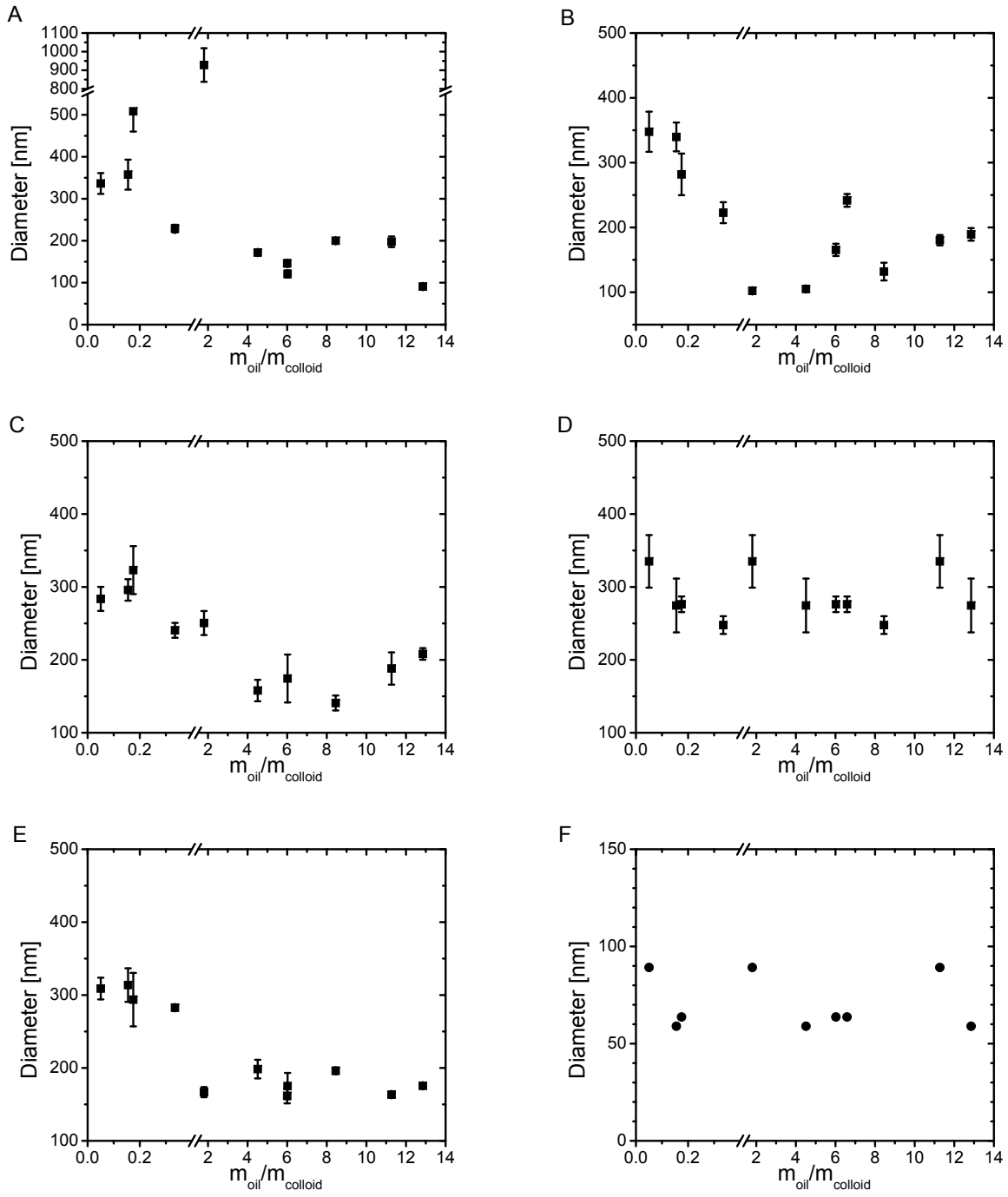

Figure 9.6. Diameter of emulsion droplets as a function of the oil-colloid ratio $m_{\text{oil}}/m_{\text{colloid}}$ as measured by DLS after A) 1 day, B) 2 days, C) 3 days, D) 4 days, and E) 5 days of heating to 80 °C. Error bars represent a standard deviation from averaged values of the diameter. F) Size of secondary smaller objects as measured by DLS after 4 days of heating.

would be an alternative explanation for the origin of the dense clusters of colloidal magnetite. In either case, it is clear, that a somewhat different emulsion mechanism compared to that of trialkoxysilane oils is at work here.

Furthermore, we found that, as in the case of TPM, the time scale of transfer depends on the relative oil volume. An example is shown in Figure 9.1E for arachidic acid. Similar observations were made for stearic and palmitic acid. Generally, the transfer took place at a slower rate in the presence of lower relative oil volumes, in analogy to observations on trialkoxysilanes (see Chapter 8). However, the transfer time does not always consistently scale with the oil volume as is the case for TPM: the sample with oil-colloid mass ratio of 1.2 exhibits clear phase separation, whereas the one with mass ratio 2.6 still contains a turbid aqueous phase next to the excess oil phase (Figure 9.1E).

9.3.4. Emulsification in the Absence of Stabilizing Particles

To check for the necessity of stabilizing colloidal particles for emulsification, a mixture of stearic acid and 6 mM TMAH aqueous solution was prepared. After storage for 24 h at 80 °C DLS measurements were performed at 25, 50, 75, and 80 °C . Analysis of DLS data yields a polydisperse size distributions around 0.87±0.1 μm, much larger than the objects detected in the presence of colloidal magnetite. Consistently, TEM images show waxy, vague shapes several micrometer in size (Figure 9.7). Just as for TPM, emulsification of stearic acid in the presence of 6 mM TMAH occurs spontaneously. Such spontaneous emulsification is known to be induced by, for example, local supersaturation or preferential diffusion of one component from one phase to the other.[**135, 123**] Yet, to obtain emulsion droplets 100-300 nm in diameter colloidal particles are required. The prerequisite of stabilizing particles for emulsion stability is in analogy with trialkoxysilane based emulsions.

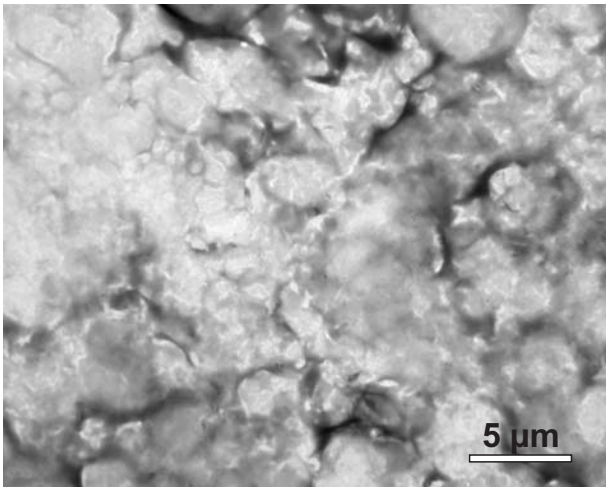

Figure 9.7. TEM image of a sample containing stearic acid and 6 mM TMAH.

9.4. Conclusions and Outlook

We have presented first indications for the spontaneous formation of Pickering emulsions from fatty acids and colloidal magnetite. Dynamic light scattering measurements indicated two characteristic lengths scales to be present in solution: one around 40-100 nm, the other between 150 and 320 nm. From DLS measurements on colloidal magnetite, we associated the lower length scale to free magnetite particles, which is also supported by free particles observed on transmission electron micrographs. The larger length scale is attributed to magnetite covered fatty acid emulsions. We propose that the dense clusters of colloidal magnetite seen in TEM originate from these Pickering emulsions after partial evaporation of the fatty acid component. Successful emulsification was observed for palmitic, stearic and arachidic acid. Lauric and sebacic acid cause very rapid transfer of colloidal particles to the fatty acid phase. Similarly, also palmitic, stearic and arachidic acid lead to particle transfer, though on a longer timescale. We qualitatively found that smaller relative volumes of fatty acid delay the particle transfer. However, the transfer time is difficult to pin down, as the transfer seems to occur in a gradual fashion without leading to an increasing emulsion droplet size.

Similar to trialkoxysilanes, spontaneous emulsification occurs without mechanical agitation of the samples. For larger oil-colloid mass ratios, an excess oil phase is observed. However, the characteristic dependence of the droplet size on the oil-colloid mass ratio was found for emulsions of fatty acids. As a consequence, it is not possible to probe thermodynamic stability by investigating droplet size adjustment to changes in the composition. Not all colloidal particles took part in stabilizing fatty acid emulsions, whereas free magnetite was never found in TPM emulsions. Ludox silica colloids, however, have been found to be free in solution for low oil-colloid mass ratios. Eventually, phase transfer of the colloidal particles to the oil phase took place, comparable to that of TPM. Yet, no increase in the droplet diameter occurred while particles progressively migrated to the oil phase. In TPM, migration happens uniformly for all colloidal particles, leading to a gradual droplet size increase. The difference in behavior may be explained by the fact that not all magnetite particles are employed in stabilization of the fatty acid emulsion. A non-uniform transfer of colloidal particles therefore may be the reason for the observed difference.

Acknowledgement

I thank Albert Philipse for discussions and useful suggestions.

A

Pickering Emulsions

Systematic name and Chemical formula	Structural formula	Code
(3-Methacryloxy propyl) trimethoxysilane $H_2C{=}C(CH_3)CO_2(CH_2)_3Si(OCH_3)_3$	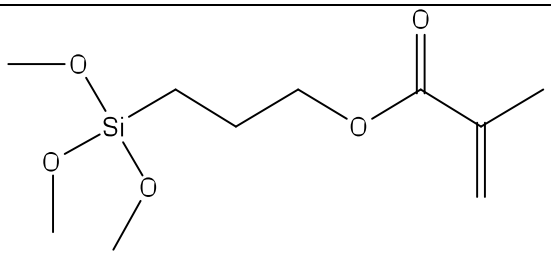	TPM
(3-Methacryloxy propyl) triethoxysilane $H_2C{=}C(CH_3)CO_2(CH_2)_3Si(OCH_2CH_3)_3$	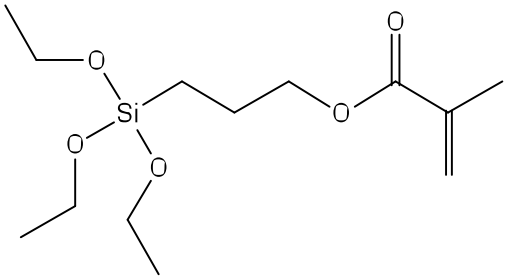	MPTES
(3-Mercapto propyl) trimethoxysilane $HS(CH_2)_3Si(OCH_3)_3$	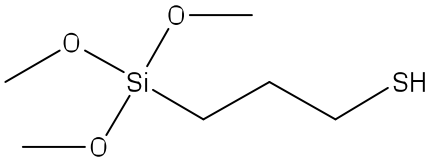	McTMS
(3-Mercapto propyl) triethoxysilane $HS(CH_2)_3Si(OCH_2CH_3)_3$	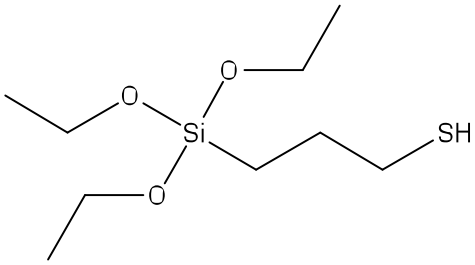	McTES
Octane	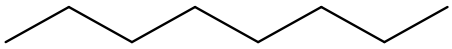	
Dodecane	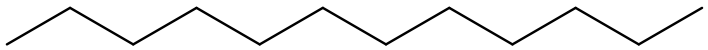	
Cyclohexane	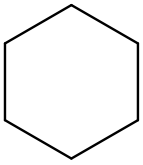	

Table A.1: Overview over oils used for the emulsion experiments

Systematic name and Chemical formula	Structural formula	Melting point
Lauric acid $CH_3 (CH_2)_{10}COOH$	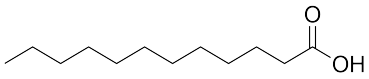	43-46 °C
Palmitic acid $CH_3 (CH_2)_{14}COOH$	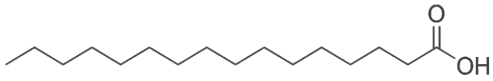	61-62.5 °C
Stearic acid $CH_3 (CH_2)_{16}COOH$	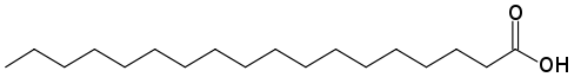	67-72 °C
Arachidic acid $CH_3 (CH_2)_{18}COOH$	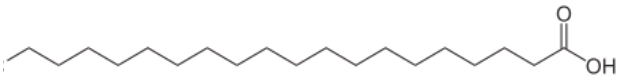	74-76 °C
Sebacic acid $(CH_2)_8(COOH)_2$	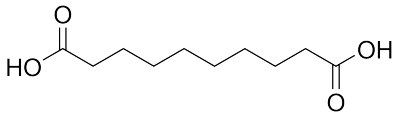	133-137 °C

Table A.2: Overview over fatty acids used for the emulsion experiments

Salt	Chemical formula	Emulsion stability?
NaOH	Na^+ OH^-	No
Tetra methyl ammonium hydroxide $(CH_3)_3NOH$	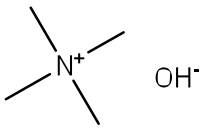	Yes
Tetra ethyl ammonium hydroxide $(CH_2CH_3)_3$ NOH	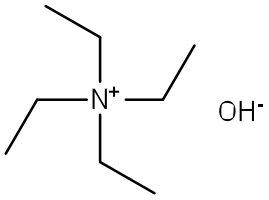	Yes
Tetra propyl ammonium hydroxide $(CH_2CH_2CH_3)_3$ NOH	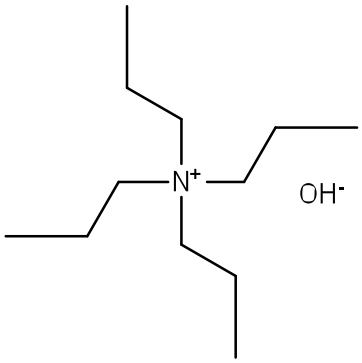	Yes

Table A.3: Systematic name, chemical and structural formula of the different salts used in the experiments on Pickering emulsions; emulsion stability in the presence of Ludox silica colloids is indicated in the last column.

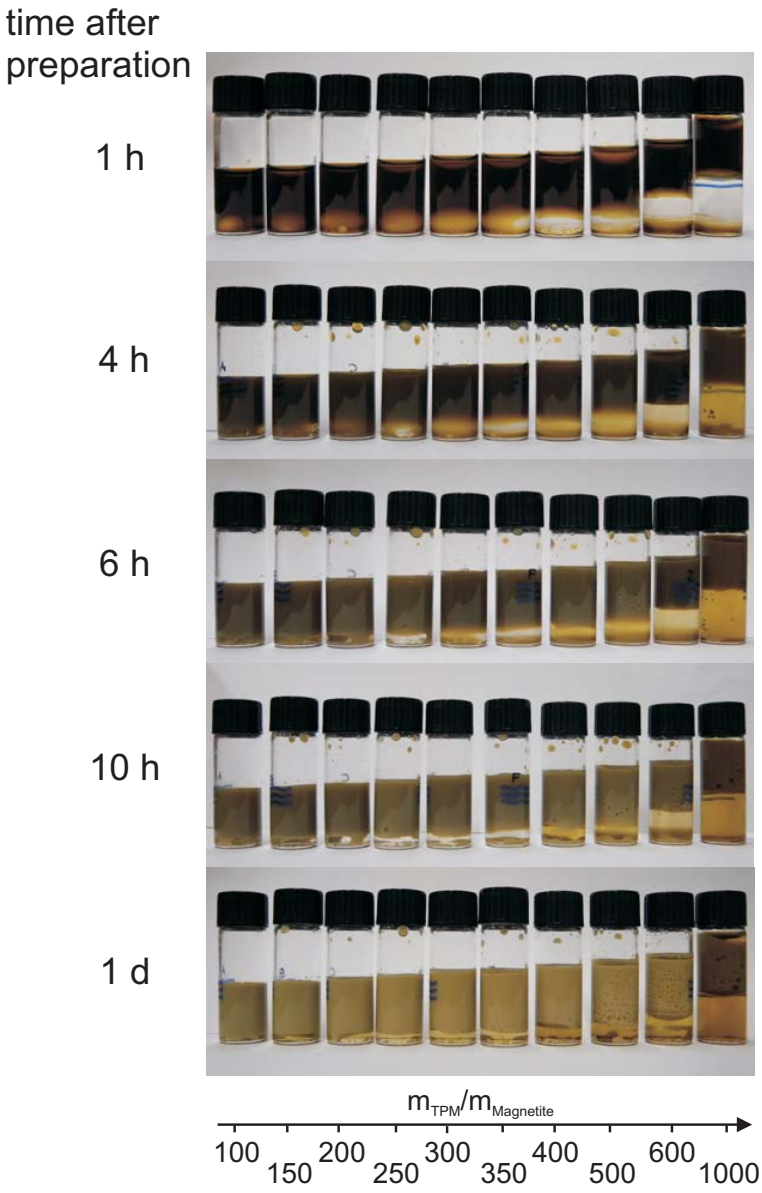
time after preparation
1 h
4 h
6 h
10 h
1 d
$m_{TPM}/m_{Magnetite}$
100
150
200
250
300
350
400
500
600
1000

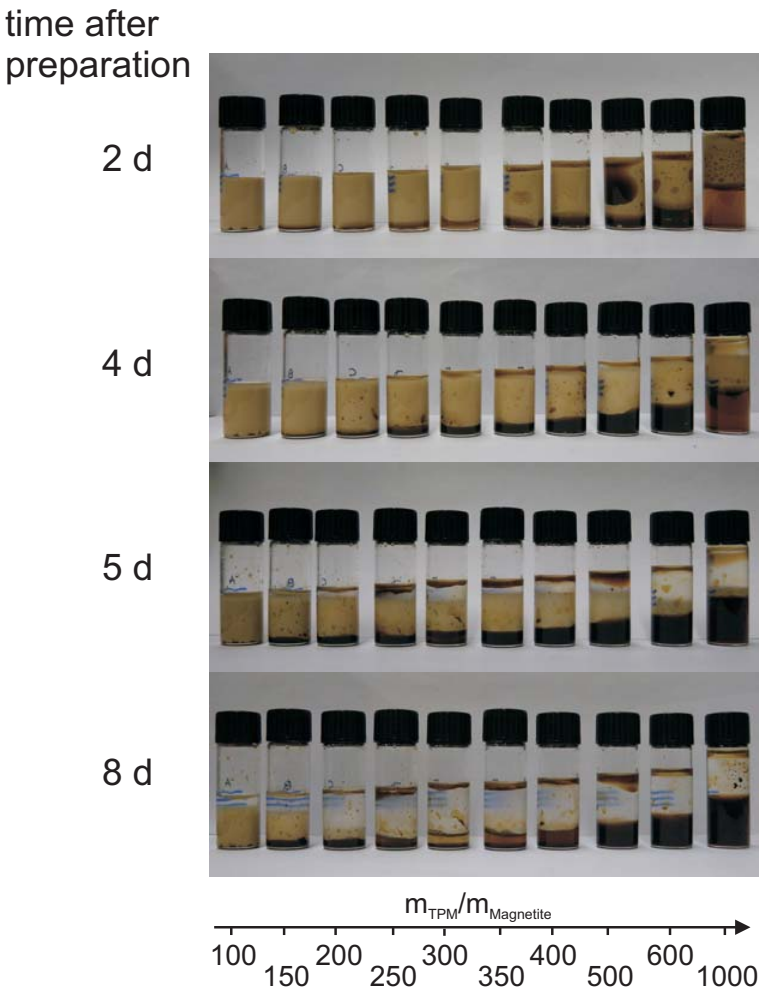

Figure A.1. Magnetite stabilized TPM emulsions containing equal volumes of a 0.125% w/w magnetite suspension at different TPM concentrations in time. Samples were gently homogenized several times a day.

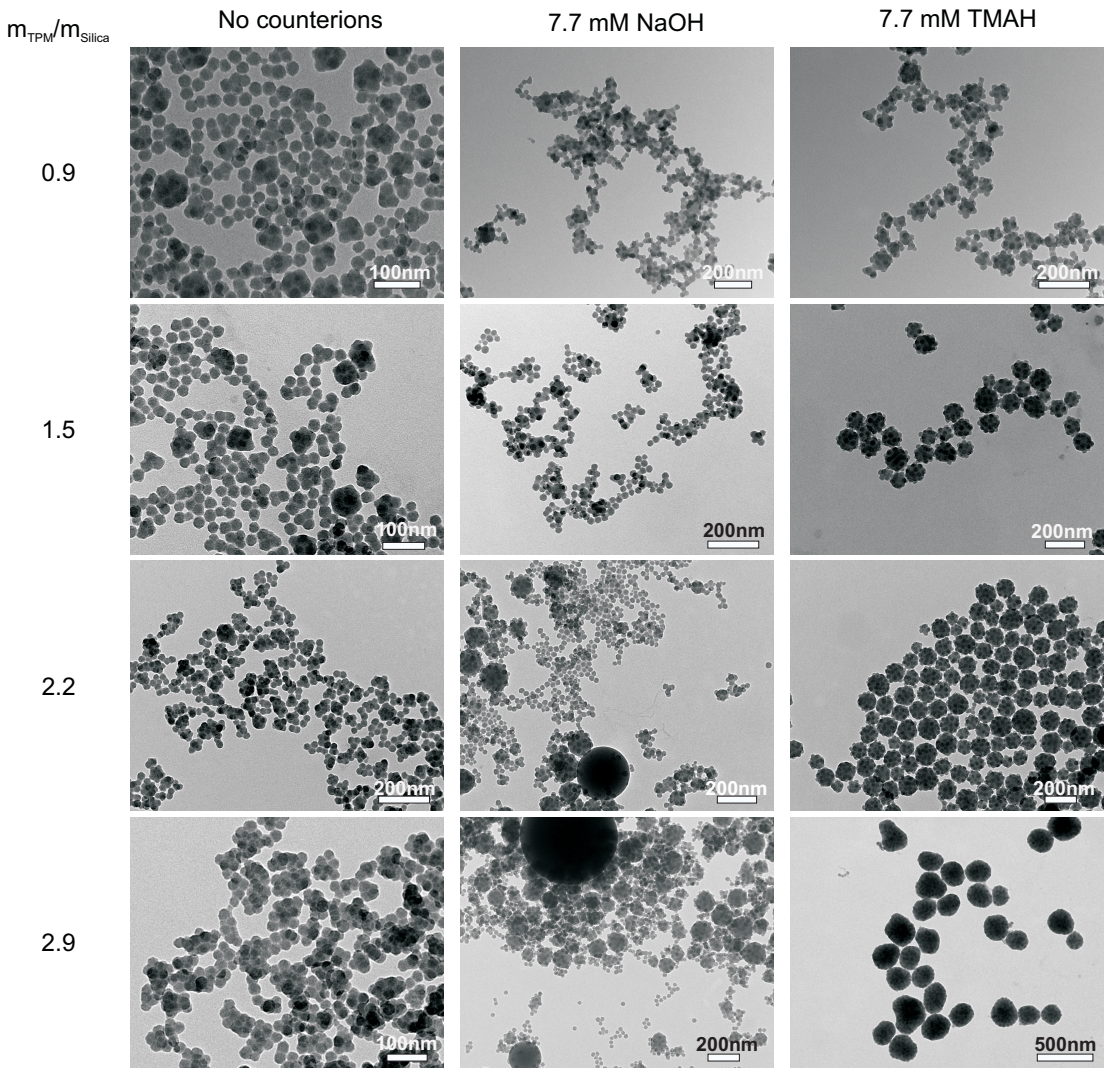

Figure A.2. TEM micrographs of polymerized TPM emulsions (one day after preparation) stabilized by dialyzed Ludox AS 40 silica in the presence of different counterions.

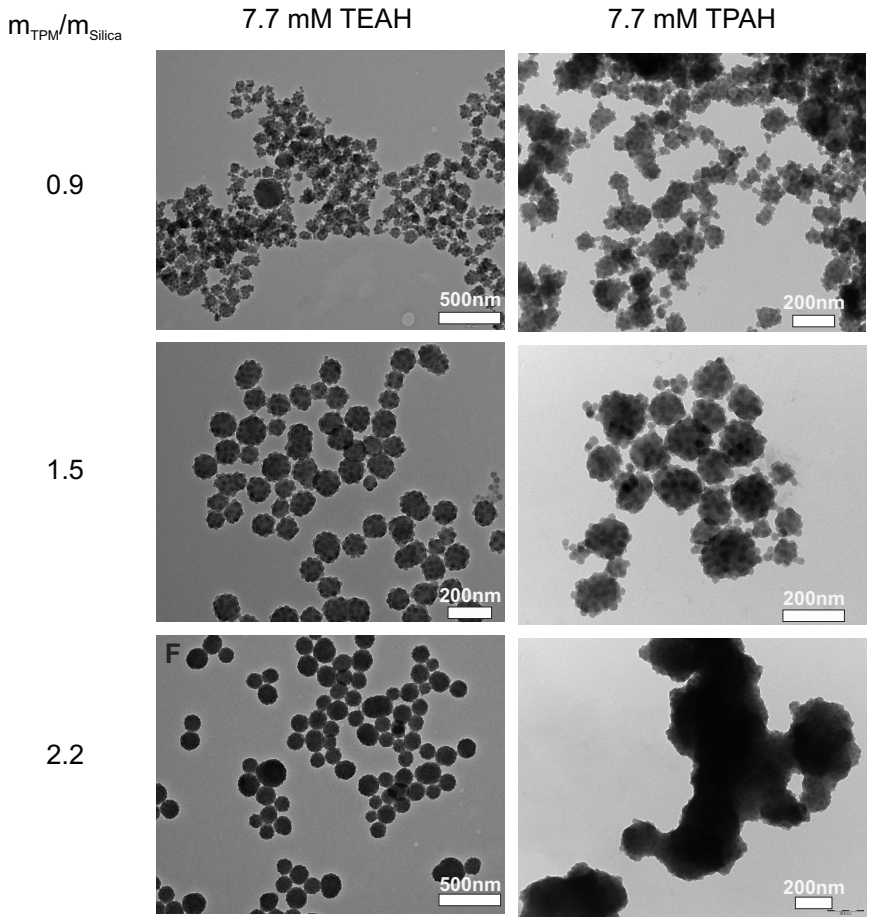

Figure A.3. TEM micrographs of polymerized TPM emulsions (one day after preparation) stabilized by dialyzed Ludox AS 40 silica in the presence of different counterions.

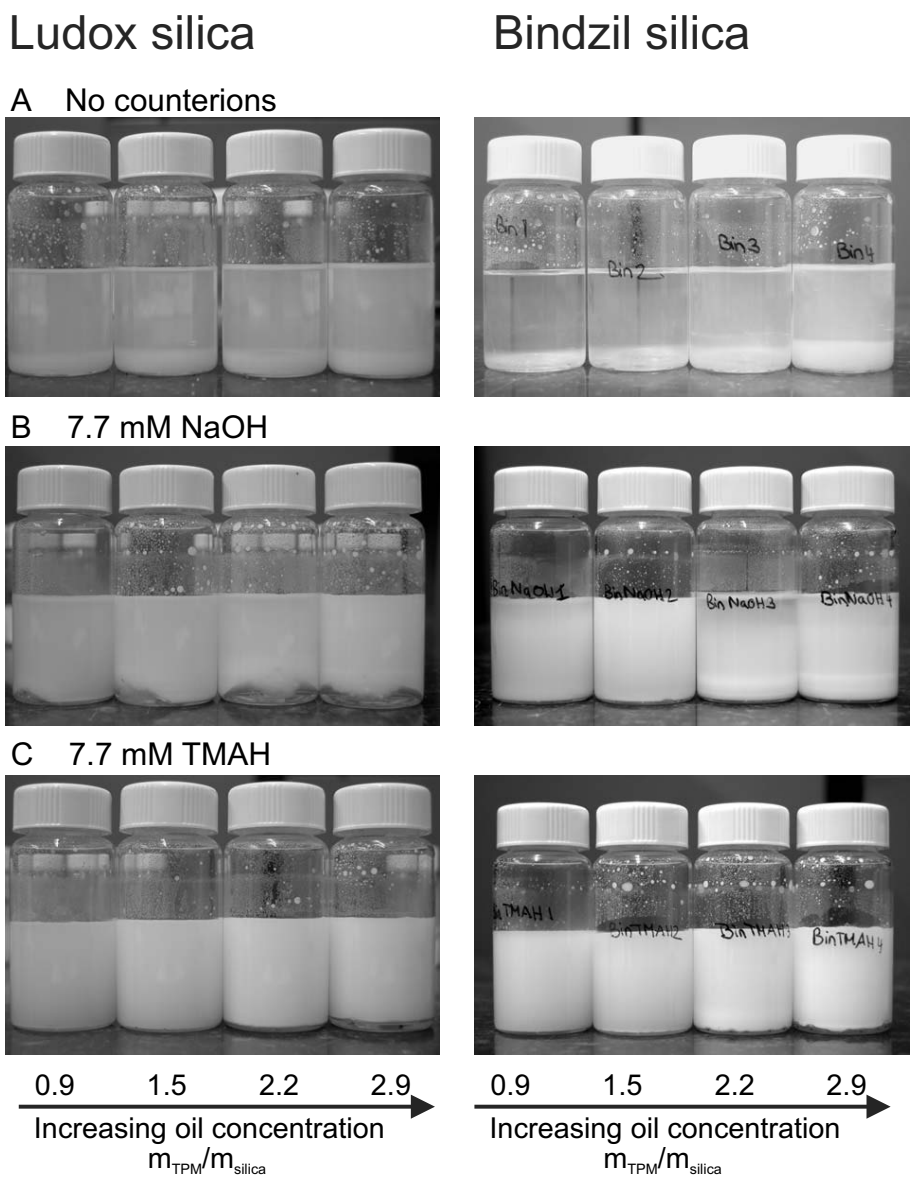

Figure A.4. Photographs of samples containing TPM emulsions stabilized by Ludox (left) and Bindzil (right) colloids in the presence of different counterions one day after preparation.

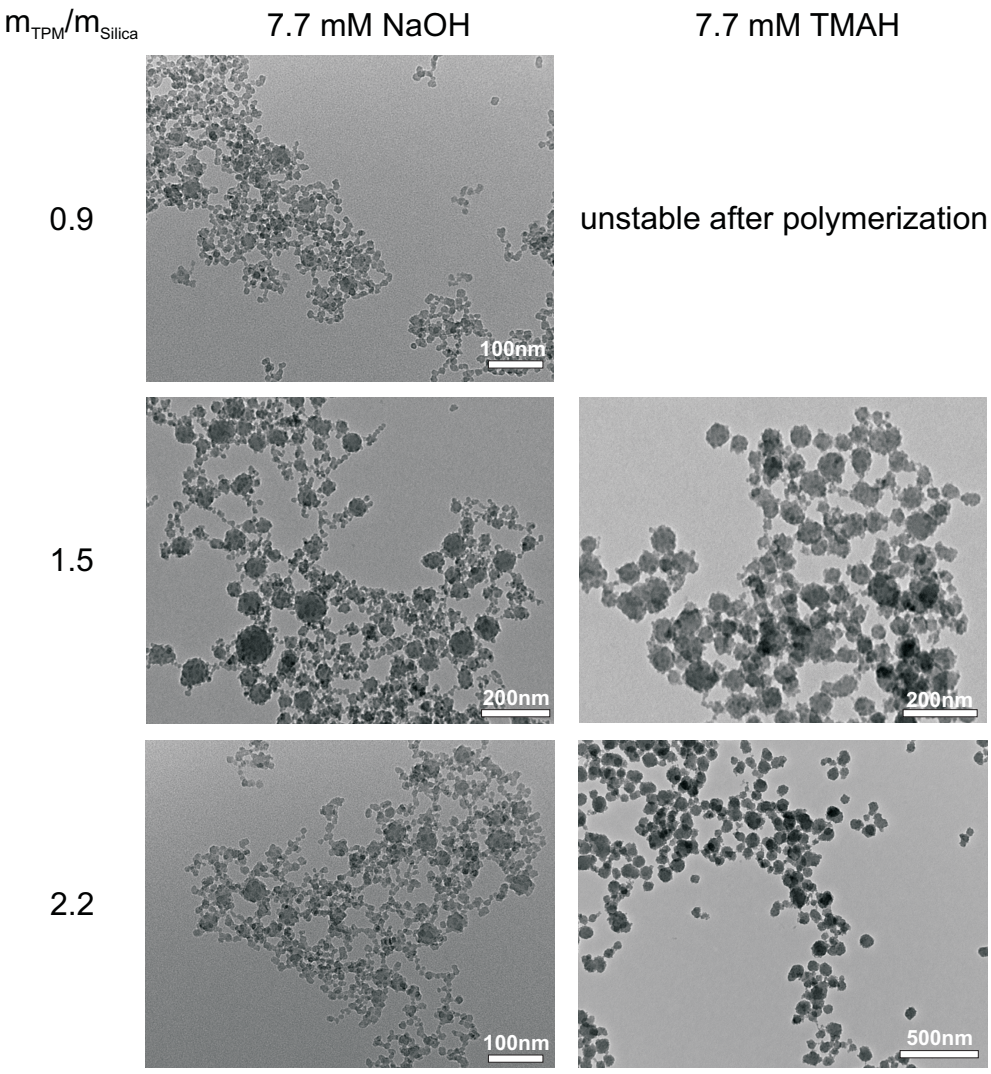

Figure A.5. TEM micrographs of polymerized TPM emulsions (one day after preparation) stabilized by dialyzed Bindzil 30/360 silica in the presence of different counterions.

Part 4

Kinetic Zipper Model for the Assembly of Tobacco Mosaic Virus

10

Kinetic Zipper Model for the Self-Assembly of Tobacco Mosaic Virus

Abstract

We apply a modified Zipper model in order to describe the statics and dynamics of the spontaneous reconstitution of rod-like tobacco mosaic virus particles in solutions containing the so-called double-disk structures of 34 coat proteins and the single-stranded RNA of the virus. An important ingredient of our model is the conformational switching of a bilayer disk to a helical structure, necessary for the binding of the first protein unit to the origin-of-assembly domain of the viral RNA. The subsequent addition and conformational switching of coat proteins to the growing capsid, we believe is catalyzed by the presence of the helical arrangement of bound proteins to the RNA, a form of allosteric action. The model explains why the formation of complete viruses is favored over incomplete ones, even though the process is quasi one-dimensional in character, and hence should be dominated by fluctuations. We numerically solve the relevant kinetic equations and show that time evolution is different for the assembly and disassembly of the virus, the former exhibiting a time lag. We find the late-stage assembly kinetics in the presence of excess protein to be governed by a single-exponential relaxation, which agrees with available experimental data. We suggest that the combination of conformational switching and template-assisted self-assembly is not specific to the *in-vitro* assembly of tobacco mosaic virus, but may apply to other viruses and protein-macromolecule binding processes as well.

10.1. Introduction

Arguably, virology as a field of study in biology started in 1898 with a publication of Beijerinck on a communicable disease afflicting tobacco plants, causing lesions in and curling of the leaves detrimental to crop yields.[**136**] He showed that the disease was caused by neither a bacterium nor any other microscopic organism, but by a contagious fluid that reproduces itself in diseased plants. This contagious fluid contains what we now know to be tobacco mosaic virus particles. Beijerink quite correctly speculated at the time that other diseases of unknown origin may also be caused by a similar contagious fluid.

Tobacco mosaic virus, or TMV for short, is a rod-shaped virus consisting of a single-stranded RNA molecule of 6395 nucleotides and 2130 identical protein subunits. The latter are helically arranged around the RNA molecule, producing a particle that measures approximately 300 nm in length and 18 nm in width.[**137**] It has a characteristic cylindrical cavity about 4 nm wide that runs through the entire length of the rod; the RNA is locked in the protein body of the cylinder about 2 nm from the cavity. Each coat protein binds to three nucleotides via a combination of hydrogen-bonding, hydrophobic and electrostatic interactions.[**91**]

TMV was not only the first virus to be discovered, it was also the first one to be reconstituted in vitro. In 1955, Fraenkel-Conrat and Williams showed that infectious virus particles self assemble if solutions containing only the coat protein and the RNA are mixed under appropriate physicochemical conditions.[**138**] A vast body of literature has since been appeared on the *in-vitro* assembly of TMV, work that has been pivotal in drawing attention to the importance of self-assembly in biology and the role of physical interactions therein.[**139**] To this day, TMV remains to play a role of some importance, e.g., in studies of host-pathogen interactions and cellular trafficking,[**140**] as a model system in colloid science,[**141, 142, 143**] in expressing pharmaceutical proteins in plants, and for improving cryo-electron microscopy techniques in structural biology.[**144**]

Although superficially TMV appears like a simple and somewhat unremarkable virus, the molecular processes involved in its assembly from the protein and RNA constituents are far from that.[**145**] Indeed, despite half a century of research there are still many open questions and we refer to a recent review of the assembly kinetics by Butler, one of the exponents in the field.[**137**] An important issue still under discussion in the assembly of TMV is the precise role of an intermediate aggregate structure known as the disk. The disk is a two-ring structure of 34 coat proteins that self-assembles under conditions of (near) neutral pH and for concentrations in excess of a critical aggregation concentration, the latter depending on the temperature and salinity.[**146**]

The first step, referred to as the nucleation step in the assembly of TMV, is the insertion of a stem-loop-type origin-of-assembly sequence (OAS) into the cavity in the center of the disk. The OAS is located at about 1000 nucleotides from the 3' end of the RNA. Following the insertion into the cavity, the stem-loop structure interacts with what are known as the flexible loops of the coat protein that become helical upon binding and that lock the OAS in between the double disk structure. In this process, the disk undergoes a major conformational change to a proto-helix called the lock washer.[**147**] The stem of the OAS melts and presumably positions itself in the protein proto-helix, while a loop sticks out of the other end of the cavity. Both the 3' and 5' portions of the remainder of the RNA extend out of the other end of the proto-helix.

The elongation of the virus seems to involve the sequential binding and helical conformational switching of disks onto the RNA loop-side of the lock washer. It is plausibly driven by a combination of protein-protein interactions and binding to the exposed loop that in the process draws in more RNA through the cavity. This way, the viral RNA, of which in free solution between 30 and 70 percent of nucleotides are involved in base paring, is straightened out so the growing virus particle acts as a helicase. This kind of "running-loop" or "inside-out"[**148**] assembly of virus particle is very fast indeed, and for this reason it has been suggested that the assembly process via an unstable intermediate lock washer structure, instead of single coat protein units, not only secures specificity through the required binding of the OAS but also speed.[**137**]

Although the elongation pathway is contested and supposed to involve the addition of single coat proteins rather than disks, there is little doubt that the initial conformational switching associated with the conversion to the lock washer structure is crucial to an efficient and successful assembly of the virus. Indeed, the concept of "autosteric control", in which conformational switching is used as a regulatory control mechanism in biology and which was put forward by Caspar 30 years ago, was inspired by assembly studies on TMV.[**149**] Strong support for the importance of conformational switching for self-assembly of viruses is not restricted to TMV, but extends to icosahedral viruses, e.g., the plant virus CCMV and the phage MS2.[**150, 151**]

Here, we argue that some sort of conformational switching is not only advantageous to the assembly of viruses like TMV but in fact a bare necessity. The reason is that the self-assembly of molecular building blocks (coat proteins) onto a linear template molecule (a single-stranded RNA molecule) is dominated by fluctuations as this constitutes in essence a quasi one-dimensional process. Fluctuations imply imperfect coverage of the template molecule, which arguably is detrimental to the survival of the virus as the coat protects the genome from, e.g., the attack of nucleases. Indeed, recent experiments on the reversible, Langmuir-type adsorption of naphtalene derivatives to single-stranded, homopolymeric DNA molecules support this: for this kind of system full coverage is almost impossible to attain.[**152**]

We base our conclusions on the application of a model inspired by the well-known Zipper model for the melting of DNA.[**153**] We specifically model the self-assembly of the virus from the OAS in the 5' direction and for simplicity ignore the finalization of it in the 3' direction. The latter process is slower, it involves a relatively small portion of the RNA and much less is known about it [**137**]. We find that the combination of conformational switching and the sequential assembly from an OAS strongly favors either complete assembly towards the 5' end, or no assembly at all. Incompletely covered RNAs are thus strongly suppressed, which we believe is of evolutionary advantage to the virus. A kinetic version of the Zipper model is proposed to describe the kinetics of reversible assembly. We find that conformational switching introduces nucleation-type kinetics, and an inherent asymmetry in the assembly and disassembly kinetics. Although highly idealized, our model quite successfully describes available experimental data on the encapsulation of both native and synthetic RNAs.

In the remainder of this paper, we first describe our equilibrium statistical mechanical model in section 10.2. We present our predictions for the coverage of the RNA template molecule as a function of the relevant binding energies and of the concentrations of both coat protein and RNA. The role of stoichiometry is highlighted and shown to be very important in creating sufficiently cooperative binding. Next, we present our kinetic model in section 10.3, which we solve numerically. We find that the lag time that we find before assembly commences depends strongly on the free energy difference between the disk and lock washer structures, but that the late-stage kinetics is virtually independent of it, and can be described by a single relaxation time. We compare the model to experimental data available from literature in section 10.4, and end this paper, in section 10.5, with a discussion and summary of our main findings.

10.2. Equilibrium Assembly Model

In our model for the assembly of TMV virus particles in a solution containing single-stranded RNAs and disks, we presume that the assembly can only commence by the binding of a disk to one end of the template molecule. This mimics the action of the OAS. Binding to the template necessitates a conformational change of the proteins in the disk to accommodate a helical structure. The latter we presume to be a high-energy structure. This is plausible because in free solution proto-helices (lock washers) are not stable under conditions of neutral pH and physiological ionic strength. Indeed, recent calculations put the free energy difference between the disk and proto-helix under those conditions as large as 34 k_BT, with k_B Boltzmann's constant and T the absolute temperature.[**91**] This might seem like a huge free energy difference, but in fact amounts to only 1 k_BT per protein involved.

We assume that the conformational switching of the second, third, etc. protein disks is catalyzed by the presence of the first, second, etc., and costs much less free energy

than that of the first. For simplicity we put this free energy cost equal to zero.* That way, we incorporate allosteric binding in our model. Clearly, binding of the first and of each subsequent disks after that, shown schematically in Figure 10.1, also liberates free energy. This free energy is in part needed to allow for the conformational switching of the first disk (and/or the proteins in this disk) upon binding. There are two obvious sources of binding free energy: that of the interaction of the proteins with the RNA, and that of the protein-protein contacts in the growing helix. The latter binding energy is taken relative to that between the proteins in the disks in free solution, and involves changes in interactions between pairs of neighboring proteins as well as of a larger number of such contacts. For a more detailed discussion of this, we refer to recent work of Kegel and van der Schoot[**91**].

Parenthetically, we note that the binding free energy related to interactions between proteins and RNA has very recently been measured using an atomic force microscopy tip to pull the TMV RNA out of a fully assembled virus, and was determined to be around 30 $k_{\mathrm{B}}T$ per protein subunit.[**154**] This value for the RNA-protein binding strength is rather high considering that there are 34 protein subunits in one protein disk. On the other hand, the measured value is a binding energy between RNA nucleotides and proteins and does not include the free energy cost for melting the secondary structure of the RNA in solution, i.e, removing the intra-molecular base pairing.

Given these assumptions, we can now make the model more explicit. Let each viral RNA strand present in the solution act as a template that can accommodate a maximum of q protein disks. Considering a total of N RNA strands in the system therefore corresponds to Nq binding sites for disk material. If the total amount of protein material present in the solution corresponds to M disks, we can define the stoichiometry between available binding sites and disks as $\lambda \equiv Nq/M$. It turns out useful to work not in a canonical but grand canonical ensemble, in which case N and M are expectation values. The quantity of interest describing the thermodynamic state of the solution then is the grand potential.

Let Ω denote a dimensionless grand potential density† of coat protein disks, RNA molecules and partially assembled viruses in an ideal solution of volume V. The only interactions we account for are those involved in the binding of disks onto RNA binding sites. The grand canonical potential then consists of several contributions, including that of the translational entropy of protein disks in solution, the RNA strands with n adsorbed protein disks, the chemical potentials of RNA molecules, μ_R, and of the free and adsorbed protein disks, μ_D. There is also a contribution accounting for the

*Formally, this contribution can be absorbed in the free energy gain of binding.

†The grand potential is scaled by the thermal energy, and multiplied by the ratio of a molecular volume and the system volume.

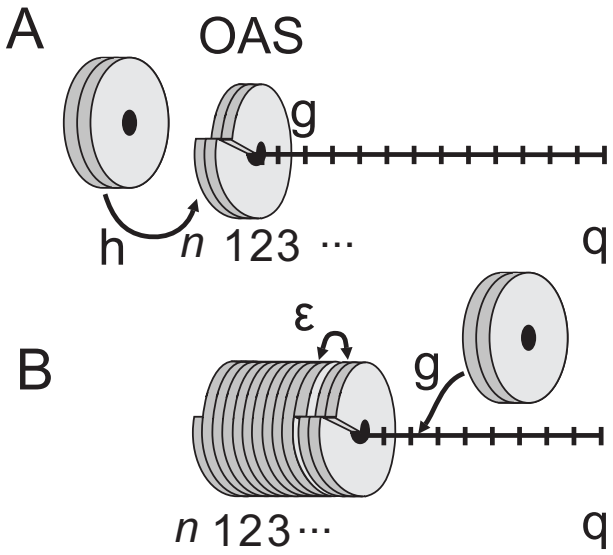

Figure 10.1. Schematic representation of our kinetic zipper model for the assembly of Tobacco Mosaic Virus from protein disks onto RNA templates with q binding sites. Elongation of the rod-like virus particles starts at the Origin of Assembly (OAS) region by conformational switching of the double disk to a proto-helix, which requires an energy h. Binding of protein helix onto the RNA molecule yields a binding free energy g, and the binding between two protein disks is associated with an interaction free energy ϵ. This guarantees sequential assembly commencing at the OAS.

different configurations of bound protein disks on RNA, expressed in an intra-chain partition function $Z(n)$.

If the dimensionless number densities of the coat proteins and partially assembled viruses, i.e., RNA molecules with n adsorbed protein units ($0 \leq n \leq q$), are defined as ρ_D and $\rho_R(n)$, then we have

$$\begin{aligned} \Omega &= \sum_{n=0}^{q} \rho(n)_R \left[\ln \rho_R(n) - 1 - \ln Z(n) - \mu_R - n\mu_D\right] \\ &\quad + \rho_D \left(\ln \rho_D - 1 - \mu_D\right) \end{aligned} \tag{10.1}$$

Under conditions of thermodynamic equilibrium, the optimal number densities of the RNA molecules and the free disks minimize the grand potential. Hence, we set $(\partial\Omega/\partial\rho_R(n))_{\mu_R,n\mu_D,V,T} = 0$, and find,

$$\rho_R(n) = Z(n) \exp\left(\mu_R + n\mu_D\right), \tag{10.2}$$

for the number density of chains that have n bound disks. Similarly, we set $(\partial\Omega/\partial\rho_D)_{\mu_R,\mu_D,V,T} = 0$, to find for the equilibrium number density of free protein disks,

$$\rho_D = \exp\left(\mu_D\right). \tag{10.3}$$

It is clear that the level of coverage of the RNAs in the protein solution is set by the chemical potentials of both components, as well as by the partition function of the protein-RNA complexes. The latter quantity acts like an equilibrium binding constant and within our model is a function of three free energies. Adsorption of the first disk onto the OAS costs conformational free energy, defined as $h > 0$, for switching from the double disk to the proto-helix. We take all energies to be in units of the thermal energy, k_BT. As for the subsequently adsorbed protein disks, we presume that the switching is catalyzed by the growing helix starting at the OAS, and we set $h = 0$ for these. Adsorption of the protein onto the RNA liberates a binding free energy, $\epsilon < 0$, presumed equal for all disks. Furthermore, sequential binding of disks to previously adsorbed ones produces an additional protein-protein interaction free energy, $g < 0$. The dimensionless free energy $F(n)$ of n disks adsorbed to one RNA can thus be written as

$$\begin{aligned} F(n) &= -h - \epsilon(n-1) - gn, && \text{for } n \geq 1 \\ F(0) &= 0, && \text{for } n = 0. \end{aligned}$$

In essence, our model is equivalent to the well-known zipper model for the melting of DNA,[**153**] in our case describing the elongation of the virus capsid from the OAS onwards. The model does not allow for random adsorption onto different sites of the template, for this is not seen in Nature.[**155, 148**] It turns out useful not to focus on the canonical partition function $Z(n) = \sum_{n=0}^{q} \exp[-F(n)]$, but rather on the semi-grand canonical partition function $\Xi(\mu_D) = \sum_{n=0}^{q} \exp[-F(n)] \exp(n\mu_D)$, that is, the sum over all possible configurations of bound protein disks onto RNA. This quantity is easily calculated using equation 10.4 and reads

$$\Xi = 1 + \sigma s \left[\frac{1 - s^q}{1 - s} \right], \tag{10.4}$$

where we have defined $s \equiv \exp(-\epsilon - g + \mu_D) = \rho_D \exp(-\epsilon - g)$, and $\sigma \equiv \exp(-h + \epsilon)$. Here, the quantity s is a measure for the affinity of protein disks for RNA molecules, combining the binding free energy between the disks and that to the RNA with the number density of free protein disks. The effect of nucleation and allostery is captured in the quantity σ, a measure for the net free energy cost of adsorption of the first disk as described in the introduction. If σ is small, then the binding of the first disk to the template constitutes a high-energy state.

From the semi-grand partition function of the RNA molecules, we can now calculate the average level of their coverage by the coat proteins, $\langle\theta\rangle = \sum_{n=0}^{q} n\rho_R(n)/q \sum_{n=0}^{q} \rho_R(n)$ $= q^{-1} \left(\partial \ln \Xi / \partial \mu_D\right)_{\mu_R,V,T}$, and find

$$\langle\theta\rangle = \frac{\sigma}{q} \cdot \frac{s}{1-s} \cdot \frac{1 - (q+1)\, s^q + q s^{q+1}}{1 - s + \sigma s \left(1 - s^q\right)}. \tag{10.5}$$

Equation (10.5) shows that by increasing the affinity of the protein for the RNA, that is, by increasing the value of s for example by changing the pH [**91**] or the concentration

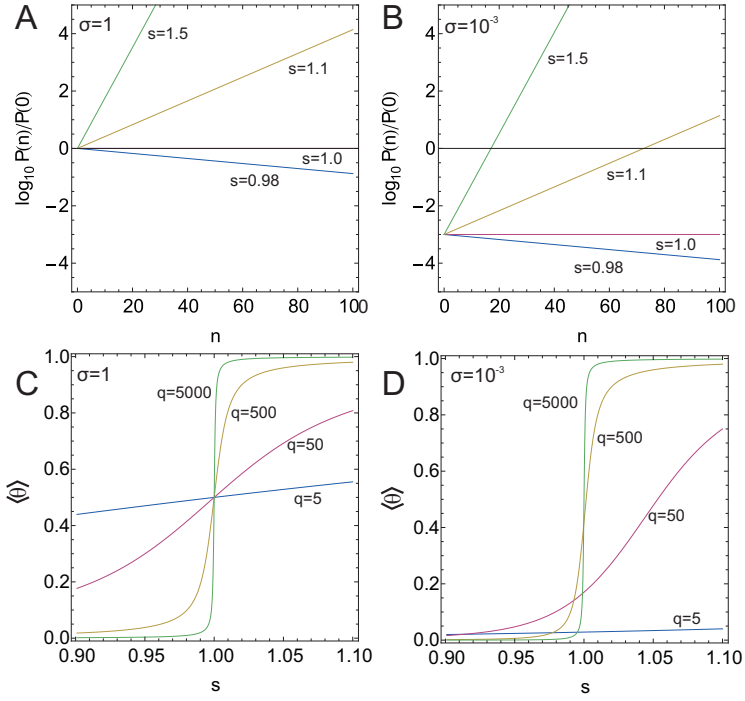

FIGURE 10.2. Ratio of probabilities $P(n)/P(0)$ for an RNA molecule to be coated by n protein disks as a function of the affinity s, A) in the absence of allostery ($\sigma = 1$), and B) in the presence of allosteric effects ($\sigma = 10^{-3}$). The average fraction of binding sites occupied by protein disks, $\langle\theta\rangle$, for C) $\sigma = 1$ and D) $\sigma = 10^{-3}$ also as a function of the affinity s. For the number of binding sites on each polymeric template we set $q = 63$.

of free protein disks in the solution, can only lead to full encapsidation of the viral RNA and $\langle\theta\rangle \to 1$ if $s \gg 1$. For $s \ll 1$, $\langle\theta\rangle \to 0$, and RNA molecules and protein disks then remain freely dispersed in solution.

Before explaining how we can link the affinity, s, to experimentally relevant control parameters, we note that the transition from free RNA and protein disks to fully functional TMV particles occurs for a value close to $s = 1$ and becomes sharper with increasing template lengths. This is shown in Figure 10.2A and B. Allostery causes the point where half of the RNA molecules are on average covered with protein disks to shift towards larger values of s, while at the same instance sharpening the transition, see Figure 10.2 C and D.

It is of interest how precisely the average coverage is achieved, that is, whether the mean coverage applies to the individual RNA molecules or whether there are great differences in coverage between different ones. To find this out it is necessary to consider the equilibrium distribution of RNAs occupied by n protein disks, defined as $P(n) =$

$\rho_R(n)/\sum_{n=0}^{q}\rho_R(n)$. Hence, we find

$$\begin{array}{rcll} P_{eq}(0) & = & \frac{1}{\Xi} & \text{for} \quad n=0 \\ P_{eq}(n) & = & \frac{\sigma s^n}{\Xi} & \text{for} \quad n>0 \end{array} \tag{10.6}$$

From Figure 10.2 C and D, we conclude that allostery plays an important role in strongly favoring fully over partially covered RNA molecules. For $\sigma = 1$, that is, in the absence of allosteric effects, RNA molecules coated with n protein disks obey an exponential distribution in n, leading to partially covered TMV particles of all intermediate lengths n for $s > 1$ albeit favoring the completely filled one for $n = q$. When allostery does come into play and $\sigma \ll 1$, the probability for coverage of RNA with protein disks below a critical value $n^* = -\ln\sigma/\ln s$, yet larger than zero, is much lower than that of the empty RNAs (with $n = 0$). Only above n^*, substantial coverage of RNA with protein disks occurs, producing either empty or what in essence are fully covered viruses, in particular if σ is sufficiently small.

We now return to the issue of linking the affinity, s, to an experimentally controllable quantity. Let ϕ_D denote the overall (dimensionless) concentration of proteins present in the solution. From the condition of the conservation of mass of the protein disks we have,

$$\phi_D = \rho_D + \sum_{n=0}^{q} n\rho_R(n) = \rho_D + q\,\langle\theta\rangle\,\rho_R, \tag{10.7}$$

where $\rho_R = \sum_{n=0}^{q}\rho(n)$ is the dimensionless RNA concentration. Hence,

$$S = s + S\lambda\,\langle\theta\rangle\,, \tag{10.8}$$

with $\lambda = q\rho_R/\phi_D$ the earlier defined stoichiometric ratio and $S \equiv \phi_D \exp(-\epsilon - g)$ a "bare" affinity. The bare affinity is the product of the overall protein concentration ϕ_D, which is a known quantity, and a binding constant associated with the two free energies ϵ and g. Clearly, equation 10.8 is an implicit expression that needs to be solved for s. For the case of excess protein $\lambda \to 0$ we obviously have the identity $s = S$. In the other limit, for concentrations of RNA binding sites far in excess of that of protein disks in the solution, $\lambda \to \infty$ and $s \to 0$, implying low average RNA coverage.

We conclude that to fully cover *all* the RNA molecules present in the solution, such that $\langle\theta\rangle = 1$, we need an amount of protein far in excess of the number of binding sites, qN. This can also be deduced from Figure 10.3, where we plot the mean fraction of occupied sites as a function of the bare affinity, S, and of the stoichiometry, λ. Apparently, the level of cooperativity of the binding of the proteins to the RNA strongly decreases with increasing stoichiometry.

In the next section we investigate how a new equilibrium state is reached if we suddenly change S, e.g., by a temperature jump. As we shall see, the assembly and disassembly kinetics are quite different from each other.

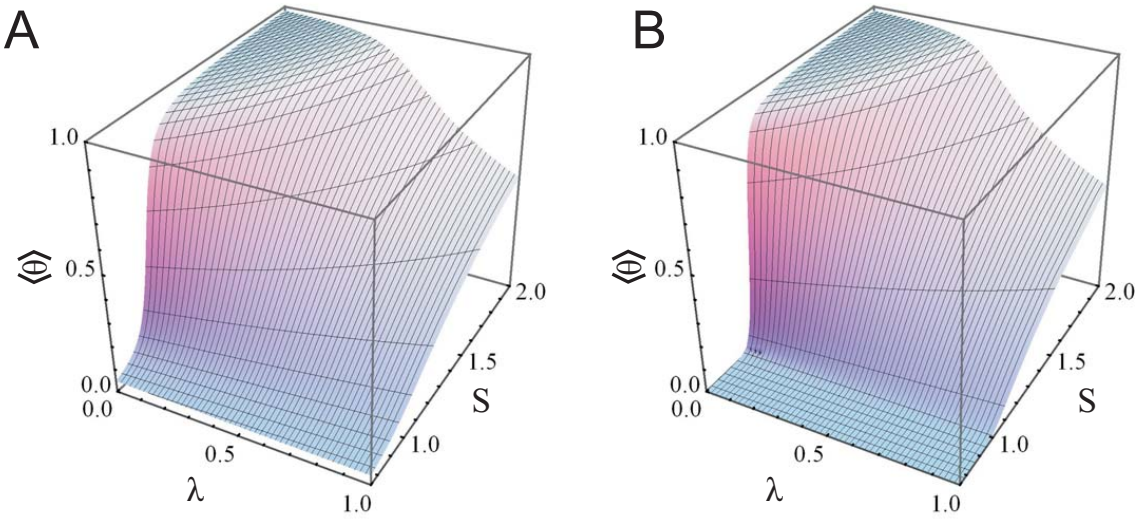

Figure 10.3. The average level of coverage of RNA strands by coat proteins $\langle\theta\rangle$ as a function of the bare affinity S, A) in the absence of allostery ($\sigma = 1$), and B) in the presence of allosteric effects ($\sigma = 10^{-3}$). The effective number of binding sites equals $q = 63$.

10.3. Kinetic Model

To extend our equilibrium model towards a description of the dynamics of the assembly and disassembly of the rod-like virus capsids, we consider a reversible sequential association or dissociation of disks, with adsorption rates $k_+(n)$ and desorption rates $k_-(n)$ that depend on how many disk-equivalents n are bound onto the RNA. From this, we obtain a set of kinetic equations for the probabilities $P(n,t)$ that RNA molecules are occupied by n protein disks at time t.

In the following, we for convenience imply the time dependence of the occupation probabilities by writing $P(n) = P(n,t)$, and distinguish these from the equilibrium distribution written as $P_{eq}(n)$. The set of kinetic equations is

$$\frac{\partial P(0)}{\partial t} = -k_+(0)P(0) + k_-(1)P(1) \tag{10.9}$$

$$\frac{\partial P(m)}{\partial t} = -k_+(m)P(m) + k_-(m+1)P(m+1) - k_-(m)P(m) + k_+(m-1)P(m-1)$$
$$\text{for } 0 < m < q \tag{10.10}$$

$$\frac{\partial P(q)}{\partial t} = -k_-(q)P(q) + k_+(q-1)P(q-1), \tag{10.11}$$

where the first and last equation involve the empty and fully bound RNAs, respectively. In time, the system evolves towards its equilibrium state as discussed in section 10.2, and hence $\lim_{t\to\infty} P(n,t) = P_{eq}(n)$ and $\lim_{t\to\infty} \partial P(n,t)/\partial t = 0$. With these conditions, the disassembly rates $k_-(n)$ can be expressed by the assembly rates $k_+(n)$ and the

equilibrium probabilities $P_{eq}(n)$ as

$$k_-(n) = k_+(n-1)P_{eq}(n-1)/P_{eq}(n), \tag{10.12}$$

where the equilibrium distribution $P_{eq}(n)$ is given by eq.(10.6) for our Zipper model.

Following the adsorption of the first disk onto the OAS with a rate $k_+(0)$, the adsorption kinetics of subsequent protein disk should not differ significantly from each other. We therefore presume that the on rates are independent of the number of previously adsorbed protein disks, so $k_+(n) = k_+$, at least for $n > 1$. Then, it makes sense to relate the on rate of the first disk to that of the others, $k + (0) \equiv \kappa k_+$. Here, κ is a measure for how much faster or slower binding of the first disk is relative to that of the subsequent ones.

Clearly, if $\kappa \ll 1$ we expect assembly to be slowed down drastically as the binding of the first disk will become rate limiting. However, as we shall see below, for the viruses to assemble we anyway need to pass a free energy barrier if $\sigma \ll 1$. The reason is of course that assemblies of size $0 < n < n^*$ are high-energy structures, as discussed in the preceding section. This implies that in practice it will be difficult to distinguish between kinetic and "thermodynamic" nucleation, although their effect on the disassembly kinetics turns out to be quite different.

If we in addition substitute $k_+t \equiv \tau$ and $0 \leq f(n) \equiv P(n)/P_{eq}(n) \leq 1$, we obtain the following set of kinetic equations

$$\begin{aligned}
\frac{\partial f(0)}{\partial \tau} &= -\kappa\left[f(0) - f(1)\right] && (10.13)\\
\frac{\partial f(1)}{\partial \tau} &= -f(1) + f(2) + \frac{\kappa}{\sigma s}\left[f(0) - f(1)\right] && (10.14)\\
\frac{\partial f(m)}{\partial \tau} &= -f(m) + f(m+1) + \frac{1}{s}\left[f(m-1) - f(m)\right], \text{ for } 1 < m < q && (10.15)\\
\frac{\partial f(q)}{\partial \tau} &= \frac{1}{s}\left[f(q-1) - f(q)\right], && (10.16)
\end{aligned}$$

where we see that the second equation depends on the ratio of κ and σ. The former is a measure for the importance of kinetic nucleation and the latter for thermodynamic nucleation. Note that κ occurs in the first equation independently of σ, yet the ratio of κ and σ occurs in the kinetic equation of RNA molecules with one bound protein disk.

The set of kinetic equations can be simplified further if written in vector notation, $\dot{\bar{f}} \equiv \partial \bar{f}/\partial t = \overline{\overline{M}} \cdot \bar{f}$, where $\bar{f} = (f(0), f(1), \ldots, f(q))$ is a vector of length $q+1$, describing the distribution of partially covered RNA molecules compared to their equilibrium

values, and $\overline{\overline{M}}$ is a tri-diagonal $(q+1)\times(q+1)$ matrix describing the model dynamics,

$$\overline{\overline{M}} = \begin{pmatrix} -\kappa & \kappa & 0 & 0 & \cdots & 0 \\ \frac{\kappa}{\sigma s} & -1-\frac{\kappa}{\sigma s} & 1 & 0 & \cdots & 0 \\ 0 & \frac{1}{s} & -1-\frac{1}{s} & 1 & 0 & 0 \\ & & & \vdots & & \\ 0 & \cdots & 0 & \frac{1}{s} & -1-\frac{1}{s} & 1 \end{pmatrix}. \tag{10.17}$$

Solving the time-dependent equations in principle yields the complete dynamics of TMV assembly and disassembly upon variation of the co-operativity σ and/or the affinity s. Recall that s becomes equal to the measurable quantity S in the limit of excess protein. Unfortunately, we found an analytical solution of the characteristic equation to remain elusive. Therefore, we employed a classical fourth-order Runge-Kutta method to numerically solve the kinetic equations for protein concentrations in excess of the number of binding sites, i.e., $\lambda \to 0$ or $S = s$, and investigate the characteristics of dynamics of assembly and disassembly of our model that way.

As discussed in the preceding section, assembly from nearly empty to fully covered RNA molecules requires a deep quench in the affinity S, for example by a sudden change in pH or temperature, or by a sudden addition of proteins to a solution of RNA molecules. Upon a quench from, say, conditions where $\langle\theta\rangle = 1.0\cdot 10^{-4}$ to those with $\langle\theta\rangle = 0.99$, assembly occurs via unstable intermediates towards the stable equilibrium distribution. See Figure 10.4. In this case, the majority of RNA molecules, roughly 95%, is covered with more than 60 protein discs after assembly has completed, if we presume $q = 63$ and $\sigma = 0.01$. For these values of σ and q, the affinities $s = 0.35$ and $s = 2.6$ correspond to values of the affinity s for the initial and final coverage.

The rate-determining step for assembly is the adsorption and conformational switching of the first protein disk, as indicated by the slow decrease in concentration of empty RNA molecules, $P(0)$. See Figure 10.4A. After nucleation has occurred and the highly unfavorable intermediate states have been populated temporarily, assembly occurs quickly towards fully assembled virus particles. If allosteric effects were not important and $\sigma = 1$, $P(0)$ decreases significantly more quickly than if $\sigma \ll 1$. If $\sigma = 1$, the distribution of partially assembled viruses is much wider than in the allosteric case where $\sigma \ll 1$, as expected. So, whilst allostery helps to completely cover the RNAs, it does so at the cost of slowing down the assembly kinetics.

Not surprisingly, the disassembly is not delayed by a sluggish nucleation process and therefore the fraction of fully assembled viruses quickly decreases upon a downward quench of the affinity s. This does not mean that σ has no influence on the disassembly kinetics, as is shown in Figure 10.5 B, although its effect is subtle. According to our model, disassembly is quite a bit swifter than assembly. Unfortunately, we have not been able to find results of *in-vitro* disassembly studies in the literature, so whether

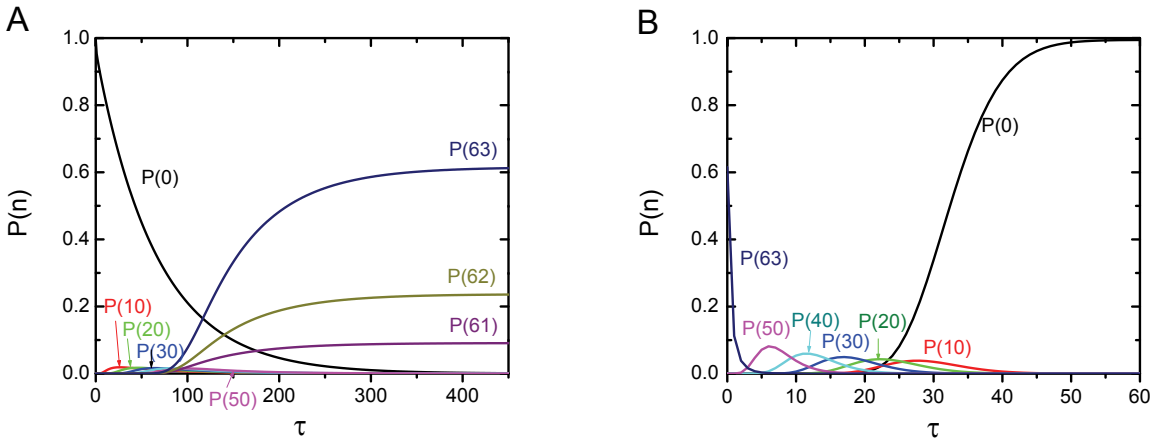

Figure 10.4. A) Assembly following a sudden quench from affinities $s_1 = 0.35 \rightarrow s_2 = 1.6$ and B) disassembly after the quench $s_2 = 1.6 \rightarrow s_1 = 0.35$. Shown are the probabilities $P(n)$ of n protein disks on RNA molecules consisting of 63 binding sites as a function of the dimensionless time τ. Here, $s_1 = 0.35$ corresponding to a coverage of $\langle\theta\rangle = 10^{-4}$ and $s_2 = 2.6$ corresponding to $\langle\theta\rangle = 0.99$, and the level of allostericity of the binding is set by the parameter $\sigma = 0.01$. All on rates are equal, implying $\kappa = 1$. See also the main text.

this prediction holds any water remains unclear. It is true that in *in-vivo* experiments, disassembly from the 5′ to the 3′ end occurs rapidly in 2-3 minutes.[**156, 157, 158**]. *In-vitro* assembly into full viruses occurs on the time scale of 6 to 10 minutes, which would support our prediction.[**137**] However, disassembly *in vivo* is thought not to proceed via spontaneous processes, but rather by cotranslational disassembly.[**159**]

As we have seen, allostery, expressed in the parameter σ, plays an important role not only in determining the equilibrium distribution of partially covered RNA strands but also in the dynamics of assembly. Decreasing the value of this parameter σ increases the influence of allosteric effects in the binding of protein to the RNA. As can be seen from Figure 10.5A, the average coverage by protein disks creates a lag time in the early-stage kinetics due to the nucleation step that strongly influences the overall rate of assembly. The rate of disassembly is decreased as well by a stronger allosteric effect as is shown in Figure 10.5B. Here, assembly and disassembly were chosen between a coverage of $\langle\theta\rangle = 0.001$ and of $\langle\theta\rangle = 0.9$. It implies that different quench depths Δs were employed because the coverage depends on σ.

The disassembly rates for deep quenches of equal quench depth are essentially equivalent for different values of σ, except for the very late stages (see Figure 10.5C). For shallow quenches in the affinity s, the rates are indeed different as we shall see below. This qualitatively different behavior for shallow and deep quenches originates from the variation of $\langle\theta\rangle$ with the affinity s. For deep quenches in s, $\langle\theta\rangle$ does not significantly

change with different σ. For shallow quenches $\langle\theta\rangle$ varies strongly as a function of σ, which translates itself in different rates of assembly and disassembly.

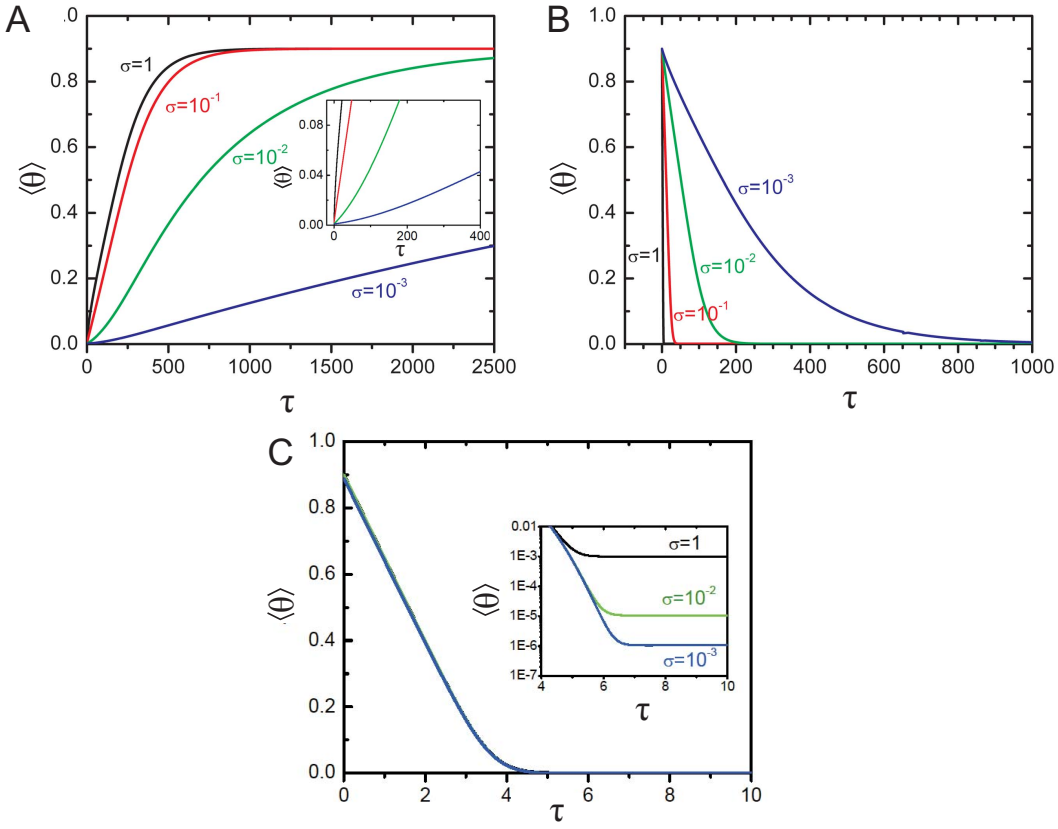

Figure 10.5. A) Assembly and B) disassembly kinetics of tobacco mosaic virus as modeled by a kinetic zipper for different values of the allosteric parameter σ presuming 63 binding sites for each RNA molecul. The quenches are between average surface coverages $\langle\theta\rangle = 0.001 \rightarrow \langle\theta\rangle = 0.9$ and $\langle\theta\rangle = 0.9 \rightarrow \langle\theta\rangle = 0.001$. The inset in A shows an expanded view of the onset of assembly, to point out the lag time introduced by the allosteric factor σ. All on rates are presumed equal. C) Disassembly kinetics for quenches from $s = 1.1586$ to $s = 0.05923$ for different values of σ.

In Figure 10.4 and 10.5, the assembly rates for adsorption of the first and subsequent protein disks were taken to be equal, i.e., $\kappa = 1$ so $k_+(0) = k_+$. The observed nucleation-type assembly kinetics originates in solely from the costly conformational switching of the first adsorbed protein disk into a proto-helix and the melting of the RNA strand. By taking a different assembly rate for the adsorption of the first disk into account, implying $\kappa \neq 1$, or, in other words, $k_+(0) \neq k_+$, we find an even stronger delay of the assembly the smaller κ is, and the slower the first step is in comparison with subsequent steps. See Figure 10.6A. This is of course to be expected, given our discussion above.

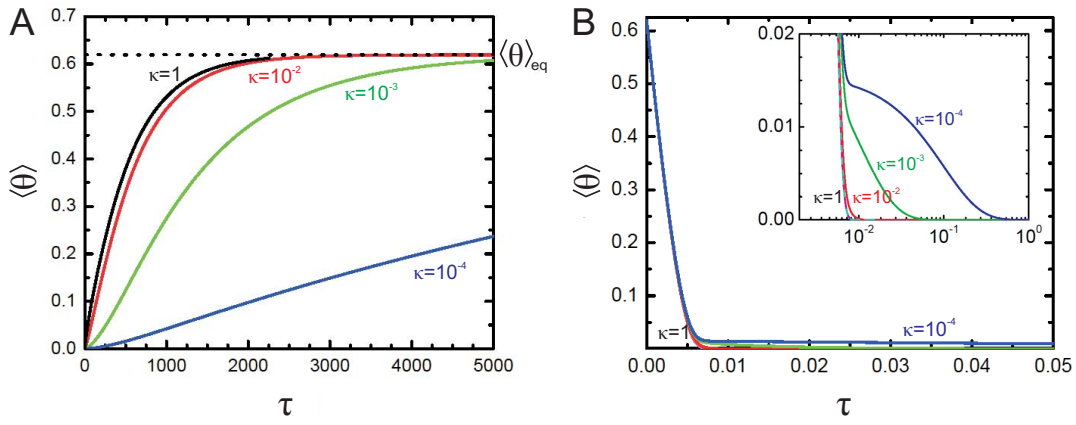

Figure 10.6. Numerical results for the average RNA coverage $\langle\theta\rangle$ as a function of time for different ratios of the assembly rates, $\kappa = k_+(0)/k_+$, A) assembly from the affinity $s = 10^{-4}$ to $s = 1.03$, and B) disassembly from $s = 1.03$ to $s = 10^{-4}$, and $\sigma = 0.1$. The number of binding sites is presumed to be equal to 63.

The disassembly kinetics of the removal of all but the last disk turns out to be unaffected by the parameter choice of $\kappa \ll 1$. This can be easily understood by considering that κ, just like σ, influences the rate of nucleation of assembly. We have seen that lowering the value of κ or σ introduces a lag time and slows down the rate of assembly. Disassembly, however, is not affected by the choice of the actual values for lower values of κ as well as σ. Only the late stage kinetics are dominated by desorption rate of the last protein disk as shown in Figures 10.5C and 10.6B. As the ratio of κ and σ occurs in the kinetic equations, it might be expected that the effect of lowering one value should be equal to increasing the other. Yet, κ also occurs in the equation for the adsorption/desorption of the first/last protein disk and this process seems to dominate over the appearance of κ in the kinetic equation for the probability of one bound protein disk.

We also note that an increase in the rate of adsorption of the first protein disk and setting $\kappa > 1$ does *not* influence the assembly and disassembly kinetics to any discernible level. This, we believe is caused by the presence of the high-energy intermediates, and hence to be an effect of the allostery. As the assembly kinetics are already well captured with the introduction of the allosteric factor σ, it seems sensible to set $\kappa = 1$ in the remainder of our discussion.

It is instructive to probe the assembly dynamics following a shallow quench of the affinity s around the value $s_{1/2}$, defined as that value of s for which $\langle\theta\rangle = 0.5$, see Figure 10.7C. Our choice of reference value of $\langle\theta\rangle = 0.5$ is no coincidence of course, as it is the value at the transition point from largely assembled to largely disassembled

conformational states. The quench $\Delta s_{1/2}$ is taken symmetrically around $s_{1/2}$, with $\Delta s_{1/2} > 0$ a quench promoting assembly and $\Delta s_{1/2} < 0$ promoting disassembly. Because a significant fraction of RNA molecules has more than a single protein disk adsorbed if the coverage is around 50%, no lag time is observed for small symmetric quenches around $s_{1/2}$.

Of interest is the half-coverage time $\tau_{1/2}$, i.e., the time required to achieve a coverage of 50 %, or $\langle\theta\rangle = 0.5$, for different values of the allosteric parameter σ. See Figure 10.7A. On account of the fluctuation dissipation theorem, the relaxation time $\tau_{1/2}$ probes the regression time of spontaneous fluctuations of the coverage of the RNAs, at least in the limit $\Delta s_{1/2} \to 0$. See Figure 10.7B. We find that this half-coverage time $\tau_{1/2}$ depends on both the magnitude and sign of the quench depth $\Delta s_{1/2}$, i.e., whether we take an assembly quench or a disassembly quench.

For assembly, $\tau_{1/2}$ is only weakly dependent on the quench depth, at least for the (small) values probed. Even though the driving force towards assembly must be stronger with increasing quench depth, which naively should lead to a decrease in assembly times, the nucleation step apparently predominates the overall rate of assembly. See also our discussion above. This is much less so for disassembly, where we do see a strong effect of quench depth, that is, a strong decrease of disassembly times with increasing quench depth. As a consequence, the disassembly rates are always larger than the ones for assembly. Not surprisingly, the asymmetry in assembly and disassembly rates increases with decreasing values of σ, i.e., with increasing allostery.

We also note that the relaxation time $\tau_{1/2}$ increases with decreasing values of σ both for assembly and disassembly, as in fact is to be expected in view of our earlier findings on the influence of κ presented in Figure 10.6A. When fitting $\tau_{1/2}(\sigma)$ with a power law for $\sigma < 1$, we find $\tau_{1/2} \approx 46.1 \cdot \sigma^{-0.667}$. From this it seems reasonable to assume that in the limit $\sigma \to 0$ the assembly time $\tau_{1/2}$ diverges. This would correspond to the phenomenon of critical slowing down, although in our case a true phase transition occurs only in the limit $q \to \infty$.[‡]

Finally, we find that the late stage kinetics of assembly and disassembly can be described quite well by a single exponential decay with a time constant τ_{exp}, as is illustrated in Figure 10.7A for shallow quenches. Just as is the case for the time $\tau_{1/2}$, the relaxation time τ_{exp} for shallow quenches scales with a power of $\sigma < 1$. We find $\tau_{exp} \propto \sigma^{-0.67}$. For deeper quenches, the mean fraction of occupied binding sites on the RNA also follows a single exponential decay function reasonably well. In this case $\tau_{exp} \propto \sigma^{-0.75}$. It is not clear what causes the difference in the scaling exponent.

[‡]From classical nucleation theory we expect the relevant time scale for crossing the nucleation barrier to scale as $1/s\sigma$. This time scale also diverges in the limit $\sigma \to 0$.

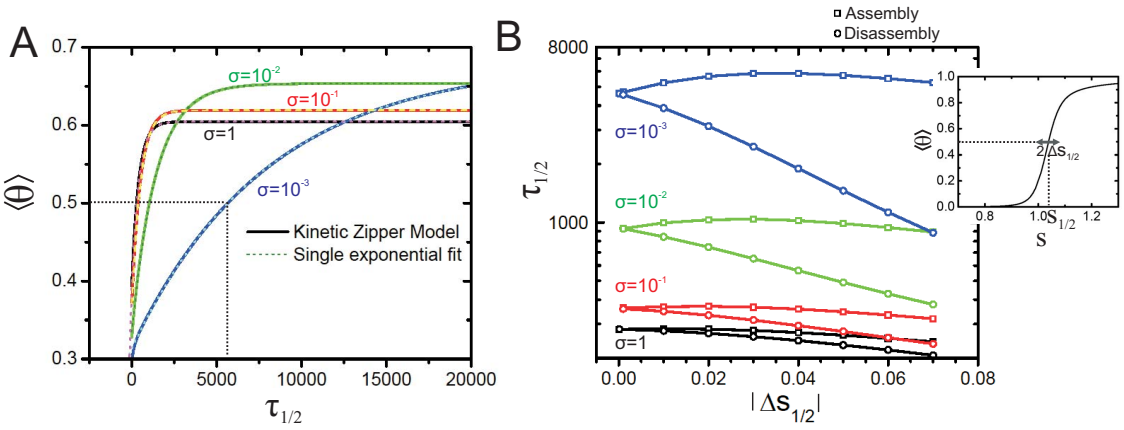

Figure 10.7. A) Average coverage $\langle\theta\rangle$ as a function of dimensionless time τ for symmetric quenches around $s_{1/2}$ and different degrees of allostery, σ. $\tau_{1/2}$ is the dimensionless time needed to obtain half coverage, $\langle\theta\rangle = 0.5$ ($\Delta s_{1/2} = 0.02$); B) $\tau_{1/2}$ for assembly and disassembly as a function of the symmetric quench depth $\Delta s_{1/2}$ around $s_{1/2} = s(\theta = 0.5)$ for different values of σ. $s_{1/2}$ is the value of s at which $\langle\theta\rangle = 0.5$. (Inset, $\sigma = 0.01$.)

In the following section we apply our kinetic zipper model to experimental data. As we shall see, even though our description is highly idealized, it quite accurately describes a broad range of experimental observations.

10.4. Comparison with Experimental Data

To compare our model with available experimental data, we set the length of the template equal to the effective number of binding sites per disk on the viral RNA. Because each coat protein binds to three nucleotides, this corresponds to the $q = 63$ binding sites used in our calculations of the previous sections. We furthermore presume for simplicity that the addition rate of the first disk is equal to that for all subsequent protein disks, so we set $\kappa = 1$. As we have seen in the previous section, even if in reality this is not quite true and, say, $\kappa < 1$, then the nucleation-type of kinetics that this produces cannot easily be distinguished from that resulting from the effects of allostery. For this reason, by setting $\kappa = 1$ we absorb potential kinetic effects into the thermodynamics of allostery, i.e., into the value of σ that becomes an effective one.

The most detailed experimental data we confront our theory with are those of Butler and Finch [**160**], who, in 1973, studied the reconstitution of Tobacco Mosaic Virus particles by mixing solutions of TMV RNA and protein disks. In these experiments, protein disks were added to the RNA molecules in excess of the number of binding sites on the RNA with a stoichiometry of $\lambda = 0.45$. The length distribution of the assembled structures was recorded as a function of time and corrected for the effects of the degradation of RNA molecules, presumably due to the presence of nucleases in the

solution. Partially assembled rods shorter than 20 nm were ignored due to limitations of the electron microscopy that was used to determine the size distribution.

The best fit to the data, presented in Figure 10.8, we found by setting $\sigma = 0.1$, and presuming a quench from an affinity of $s = 0.312$ to that of $s = 1.159$. This corresponds to bare values of the affinities of $S = 0.312$ and $S = 1.95$. Following the experiments, we left out partially assembled rods shorter than 20 nm, equivalent to $0 \leq n \leq 3$, from the analysis, and we renormalized the probabilities such that they to add up to 1 again. The time scale $\tau = 45t[\text{min}]$ we set equal to the actual time in minutes $t[\text{min}]$ to obtain the best fit, giving an add-on rate of $k_+ = 45[\text{min}^{-1}]$. Here, we presumed that the experimental data at $t = 0$ min indeed corresponds to the beginning of the assembly process, that is, $t_0 = 0$ min. We note however, that the sample preparation might have introduced a delay time between the moment the sample was taken from the protein RNA solution, and the time at which the assembly actually was stopped in the sample taking. Because the allostery parameter σ in particular influences the in initial stages of the virus particle growth, a somewhat different choice of "zero time" may lead to a smaller value for σ than we estimated from our curve fitting. In our comparisons we presumed that indeed $t = 0$ min corresponds to the zero time t_0.

Butler and Finch [**160**] divided the experimental data for the time evolution of the various levels of completion of the encapsulation of the RNA into bins of multiples 40 nm particle lengths, ignoring, again, for technical reasons, the contribution from particles shorter than 20 nm. As is clear from Figure 10.8, our kinetic zipper model describes the time dependence of the entire population of TMV particles of different states of completion reasonable well. In the late stages, i.e., after 10 minutes, still a very large fraction of almost complete TMV particles with an average length of 240 ± 20 nm remains, which does not quite agree with our predictions as is evident from Figure 10.8.

Although Butler and Finch did correct their data for growth termination due to degraded RNA, it is reasonable to assume that in the late assembly stages distinguishing discontinued growth of the 240 ± 20 nm particles for thermodynamic reasons from that due to broken RNA molecules is not possible. The latter is of course not accounted for in our model. From the best fit to the experimental data, we conclude that the assembly has not completed at the point when the experiments halted (Figure 10.8 bottom right). Hence, a part of the fraction of TMV particles with average length 240 ± 20 nm could be due to degraded RNA molecules.

Another explanation may be that the elongation of the virus is bidirectional: assembly from the origin of assembly region on towards the $5'$ end of the viral RNA completes much more rapidly than the assembly in the direction of the $3'$ end. The latter plausibly occurs by the addition of A-proteins (a mixture of small protein aggregates) rather than protein disks.[**161**] If the assembly in the $5'$ direction is completed the virus particles

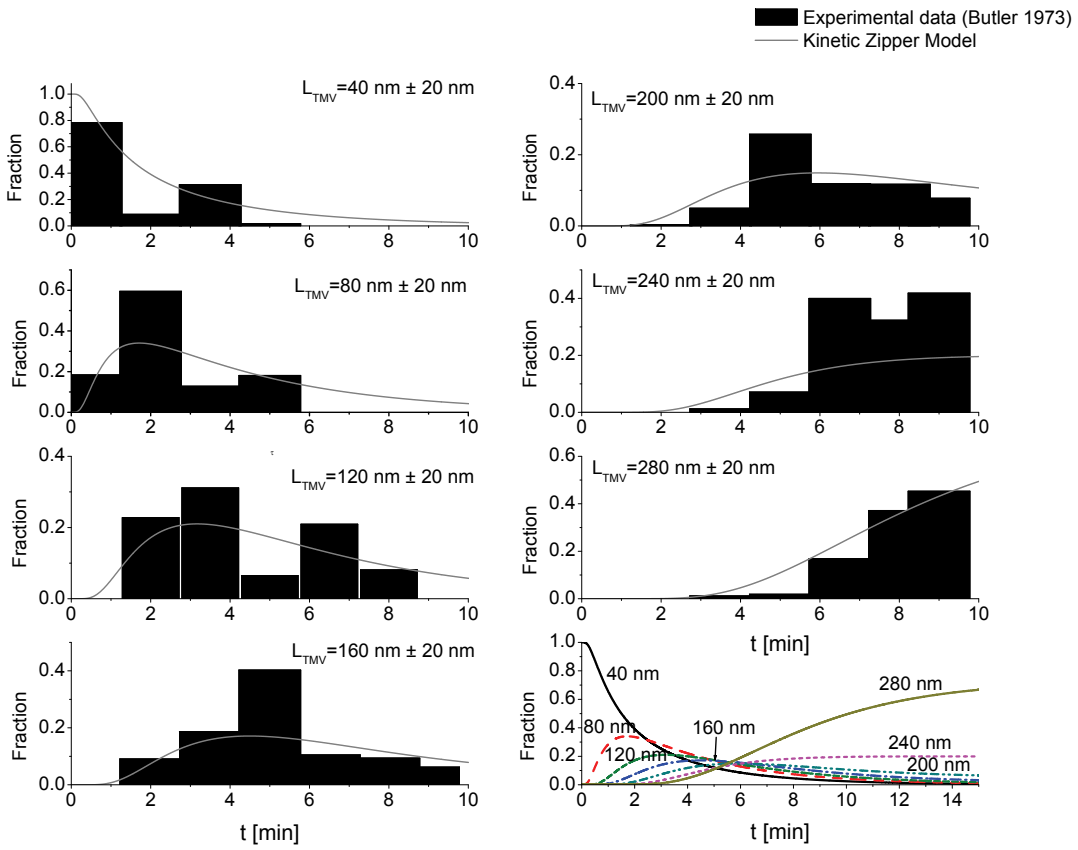

FIGURE 10.8. Comparison of the predictions of the kinetic zipper model with the experimental data of Butler and Finch on the reconstitution kinetics of TMV [**160**]. Shown are fractions in percentile units of binned length ranges as a function of dimensionless time τ. To obtain a good fit, we set the model parameters described in the main text at $\sigma = 0.1$ and $\kappa = 1$, and presumed a quench from $s_1 = 0.312$ to $s_2 = 1.159$.

are roughly 260 nm in length, which is in good agreement with the large fraction of almost fully complete viruses 240 ± 20 nm in length seen in experiments. It seems that the discrepancy between our model and the experimental data in the late stages of the assembly may well be due to the much slower assembly mode from the $5'$ to the $3'$ end, not captured by our model.

The relatively large value that we find for σ is somewhat of a surprise, given the estimate of the 34 k_BT involved in the conformational switching of a disk that we mentioned in the introduction. This parameter determines in particular the duration of the begin period following the instantaneous quench where not much happens. To get a good estimate of this lag time, the "zero time" must be known to reasonable accuracy as discussed above. Here, there is some ambiguity in zero time because of the way the experiments were done. Also, as we have seen in section 10.2, the larger

the stoichiometry the smaller effective degree of co-operativity, i.e., the larger the σ we expect to obtain from our fitting to the zero-stoichiometry calculation. Obviously, this by no means explains the large difference in the value for σ that we find from the experiments and that deduced from theory.[**91**]

In spite of all this, it seems that our model captures the main elements of the assembly kinetics of TMV, certainly that of in the direction of the 5' end. As a further test, we compared our model with reconstitution data obtained by means of SAXS, i.e., small angle x-ray scattering [**162**], and turbidity measurements [**163**]. In both these studies, experiments were conducted with just as many coat proteins as RNA binding sites available implying that $\lambda = 1$. Strictly speaking, our numerical model does not apply for this stoichiometric ratio as we presumed $\lambda \ll 1$, except in the initial stages. The reason is that then only a small fraction of disks is incorporated into growing virus particles, and the solution concentration of free disks then remains close to its initial value. Our predictions for the late stages may be more tenuous because then initial and final concentrations of disk protein are no longer approximately the same.

The mean radius of gyration, R_g, of the assembling virus particles, extracted from (time-resolved) static radiation scattering experiments, is a so-called z-average of all particles in the population and related to the z-averaged particle length, L, via

$$R_{g,z}^2 = \frac{1}{12}\langle L^2\rangle_z = \frac{1}{12}\sum_{n=1}^{q} P(n)L(n)^4 / \left(\sum_{n=1}^{q} P(n)L(n)^2\right),$$

where $L(n) = l \times n$ obviously depends on how many disk equivalents n of length l have adsorbed onto the RNA [**164**]. In Figure 10.9A we fit the theory of the SAXS data of Sano et al. [**162**], where we set $q = 63$, $l = 4.76$nm, $\sigma = 0.1$ and $k_+ = 23[\text{min}^{-1}]$ and presume a quench from $\langle\theta\rangle = 0$ to $\langle\theta\rangle = 0.9$. The value of the add-on rate k_+ that we now find is smaller by a factor 2 than the one we found previously, but this may of course be due to different solution conditions. Since the "zero time" is not precisely known in these experiments either, we set the assembly to commence at $t_0 = -4$ min in our model to obtain good agreement with the experimental data.

Quite similar results for the size of the growing rods may be obtained from turbidity measurements. The turbidity is proportional to the scattered total intensity that within the Rayleigh-Debye-Gans approximation scales as the *weight* average of the rod length, $\langle L\rangle_w$
$= \sum_{n=1}^{q} P(n)L(n)^2/(\sum_{n=1}^{q} P(n)L(n))$.[**165**] By setting $\sigma = 0.1$, $k_+ = 60[\text{min}^{-1}]$, $t_0 = 0$ min, and presuming the assembly proceeds from a coverage of $\langle\theta\rangle = 0$ to that of $\langle\theta\rangle = 0.9$, we find good agreement between the experimental data, as is shown in Figure 10.9B.

We finally compare the *static* version of our zipper model to the binding of the movement protein P30 to TMV RNA. Cell to cell transport of TMV particles is mediated by this protein. The binding of P30 to TMV RNA is strong, highly cooperative and

seems to be sequence non-specific [**166**], implying that the OAS probably does not promote binding of the P30 proteins. Still, the high co-operativity expresses itself in the observed "all or nothing" adsorption of P30 proteins, similar to the binding of TMV protein disks onto RNA. This makes it an interesting candidate for comparison with our model.

Experiments have been conducted by incubating a solution of TMV RNA with increasing amounts of P30 protein [**166**]. We fixed the maximum number of P30 proteins that can be bound to the TMV RNA to $q = 40$, because experiments indicated 26-45 P30 proteins per RNA molecule at maximum coverage.[**166**] Complexes of P30 and RNA were resolved by gel retardation. In Figure 10.9C we compare the equilibrium values found for the coverage as a function of the (reciprocal) stoichiometry, so $\langle\theta\rangle(\lambda^{-1})$, with the results from the zipper model. We took for the affinity $S = 10$, which is sufficiently large to get complete coverage in excess P30. Agreement with the data is best if we presume there is no allostery involved, so $\sigma = 1$. Apparently, the binding co-operativity is driven by protein-protein interactions alone, yielding good agreement with our model as shown in Figure 10.9C.

10.5. Conclusions

In summary, we have presented a kinetic zipper model to describe the statics and dynamics of the assembly and disassembly of tobacco mosaic virus particles in solutions containing protein disks and RNA molecules. The model is in essence based on the "inside-out" or "running loop" model proposed some time ago by Butler [**147, 137**]. A key ingredient of our theory is the integration of allostery: only the binding of the first disk and concomitant conformational switching to the helix structure is penalized by a free energy cost. The conformational switching of subsequent disks (or single proteins) bound to the RNA is catalyzed by the already present helical arrangement of proteins.

The model explains the main features of the *in vitro* reconstitution of TMV particles as observed in experiments. We find that allostery, if sufficiently strong, leads to "all-or-nothing" behavior in the assembly. This means that rather than incompletely encapsulating all RNAs in the solution, there is a strong driving force to (nearly) completely cover a fraction of RNAs, while keeping the remainder naked. Arguably, this "all-or-nothing" coverage enhances the survival probability of the virus, because the exposed ("naked") RNA of an incomplete viruses is susceptible to attack, e.g., by nucleases.

We find that the co-operative assembly of fully covered RNA molecules, i.e., intact virus particles, is strongly influenced by the stoichiometric ratio that is proportional to the number of nucleotides and proteins in the solution. Only for the case where protein is available vastly in excess of the total number of nucleotides, full coverage can be achieved. Often, experiments are done at the in some sense ideal stoichiometry

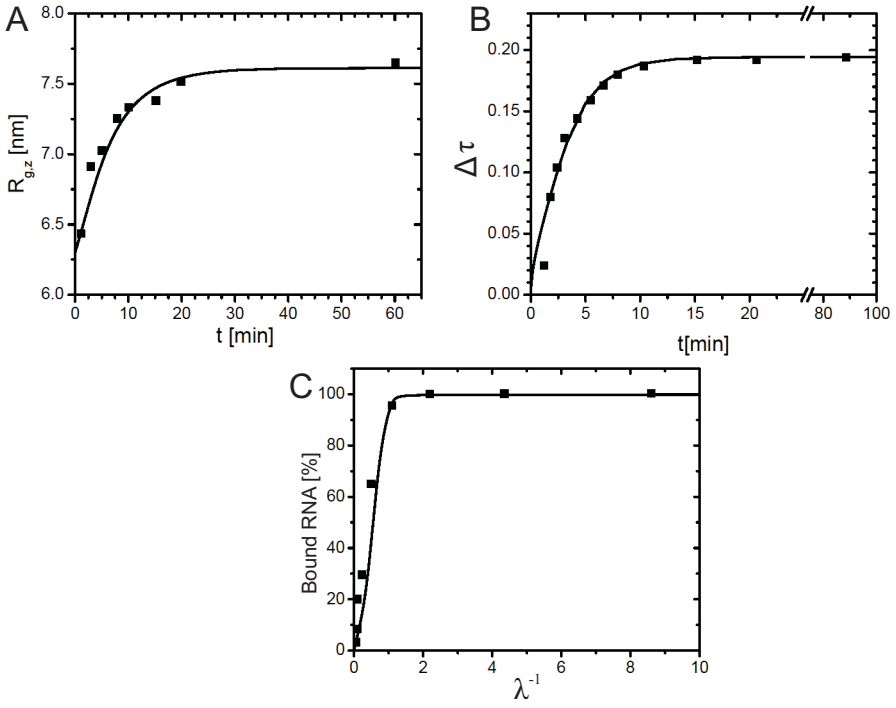

Figure 10.9. Comparison between experimental results probing some average of the size of the growing virus particles in TMV assembly experiments and the kinetic zipper model. A) Radius of gyration as obtained by SAXS versus time; symbols: experimental data [**162**], drawn line: theory. B) Assembly kinetics followed by the increase in turbidity upon mixing TMV protein disks with TMV RNA [**163**]. C) Equilibrium coverage $\langle\theta\rangle$ fractions of TMV RNA molecules by bound P30 movement protein as a function of the reciprocal stoichiometric ratio λ^{-1}. Symbols: experimental data[**166**], drawn line: theory for $\sigma = 1$.

corresponding to that of the complete virus where exactly as many protein disks are used as available binding spots on the RNA molecules. This stoichiometry turns out not so ideal after all, because complete coverage of the RNA is in this case difficult to obtain according to our calculations, unless the binding is very strong.

If allostery is indeed an important mechanism in virus assembly, as we believe is the case, then our calculations show that the assembly kinetics must occur via high-energy intermediate states that are present only in low concentrations. This makes the nucleation process the rate-limiting step. The associated lag time before assembly commences seems to be influenced by both the relative rate of adsorption of the first disk and the extent of allostery. For the opposite case of the disassembly of the virus, these parameters only influence desorption of the last protein disk and hence not the overall rate of disassembly.

The late-stage assembly and the early-stage disassembly kinetics we find to be governed by a single-exponential relaxation, at least for the situation of excess protein. Comparison of our quite simple model with available experimental data shows remarkably good agreement. From our curve fitting, we obtain estimates for the allostery parameter of $\sigma \approx 0.1$. This is perhaps not as small as we would expect and may be related to the difficulty of establishing zero time and/or a stoichiometry ratio that is not sufficiently small. Clearly, more experiments are needed to resolve this issue, as is an analysis of the kinetic model that deals with more realistic stoichiometries. The latter is left for future work.

Acknowledgements

I am grateful for having had the opportunity to work with Paul van der Schoot (TU Eindhoven and Utrecht University) on the results presented in this chapter.

Bibliography

[1] G. Whitesides and M. Boncheva, "Beyond molecules: self-assembly of mesoscopic and macroscopic components," *P Natl Acad Sci Usa*, vol. 99, no. 8, p. 4769, 2002.

[2] J. D. Halley and D. A. Winkler, "Consistent concepts of self-organization and self-assembly," *Complexity*, vol. 14, pp. 10–17, Nov 2008.

[3] H. Benard, "The cellular whirlpools in a liquid sheet transporting heat by convection in a permanent regime," *Ann Chim Phys*, vol. 23, pp. 62–101, Jan 1901.

[4] L. Rayleigh, "On convection currents in a horizontal layer of fluid, when the higher temperature is on the under side," *Philos Mag*, vol. 32, pp. 529–546, Jan 1916.

[5] R. Zhang and B. Shklovskii, "Phase diagram of aggregation of oppositely charged colloids in salty water," *Phys Rev E*, vol. 69, p. 021909, Feb 2004.

[6] G. Zhang, D. Wang, and H. Möhwald, "Decoration of microspheres with gold nanodots-giving colloidal spheres valences," *Angew. Chem.*, pp. 7767–7770, Nov 2005.

[7] A. W. Wilber, J. P. K. Doye, A. A. Louis, E. G. Noya, M. A. Miller, and P. Wong, "Reversible self-assembly of patchy particles into monodisperse icosahedral clusters," *J Chem Phys*, vol. 127, p. 085106, Jan 2007.

[8] A. W. Wilber, J. P. K. Doye, and A. A. Louis, "Self-assembly of monodisperse clusters: Dependence on target geometry," *J Chem Phys*, vol. 131, p. 175101, Jan 2009.

[9] E. Bianchi, P. Tarlaglia, E. Zaccarelli, and F. Sciortino, "Theoretical and numerical study of the phase diagram of patchy colloids: Ordered and disordered patch arrangements," *J Chem Phys*, vol. 128, p. 144504, Jan 2008.

[10] G. Doppelbauer, E. Bianchi, and G. Kahl, "Self-assembly scenarios of patchy colloidal particles in two dimensions," *J. Phys.: Condens. Matter*, vol. 22, pp. 1–12, Feb 2010.

[11] S. C. Glotzer and M. J. Solomon, "Anisotropy of building blocks and their assembly into complex structures," *Nature Materials*, vol. 6, pp. 557–562, Jan 2007.

[12] A. B. Pawar and I. Kretzschmar, "Fabrication, assembly, and application of patchy particles," *Macromol. Rapid Commun.*, pp. 150–168, Jan 2010.

[13] A. van Blaaderen, "Colloidal molecules and beyond," *Science*, vol. 301, pp. 470–471, Jan 2003.

[14] Z. Zhang and S. Glotzer, "Self-assembly of patchy particles," *Nano Lett*, vol. 4, pp. 1407–1413, Jan 2004.

[15] S. C. Glotzer, "Some assembly required," *Science*, pp. 419–420, Oct 2004.

[16] E. W. Edwards, D. Wang, and H. Möhwald, "Hierarchical organization of colloidal particles: From colloidal crystallization to supraparticle chemistry," *Macromol Chem Physic*, vol. 208, pp. 439–445, Jan 2007.

[17] T. Chen, Z. Zhang, and S. C. Glotzer, "Simulation studies of the self-assembly of cone-shaped particles," *Langmuir*, pp. 6598–6605, Jan 2007.

[18] E. Bianchi, J. Largo, P. Tartaglia, E. Zaccarelli, and F. Sciortino, "Phase diagram of patchy colloids: Towards empty liquids," *Phys Rev Lett*, vol. 97, p. 168301, Oct 2006.

[19] J. P. K. Doye, A. A. Louis, I.-C. Lin, L. R. Allen, E. G. Noya, A. W. Wilber, H. C. Kok, and R. Lyus, "Controlling crystallization and its absence: proteins, colloids and patchy models," *Phys Chem Chem Phys*, vol. 9, pp. 2197–205, Jun 2007.

[20] Z. Zhang, A. Keys, T. Chen, and S. C. Glotzer, "Self-assembly of patchy particles into diamond structures through molecular mimicry," *Langmuir*, vol. 21, pp. 11547–11551, Jan 2005.

[21] T. Ngo, C. Liddell, M. Ghebrebrhan, and J. Joannopoulos, "Tetrastack: Colloidal diamond-inspired structure with omnidirectional photonic band gap for low refractive index contrast," *Appl Phys Lett*, vol. 88, p. 241920, Jan 2006.

[22] V. N. Manoharan, M. Elsesser, and D. J. Pine, "Dense packing and symmetry in small clusters of microspheres," *Science*, vol. 301, pp. 483–487, Jan 2003.

[23] N. Sloane, R. Hardin, T. Duff, and J. Conway, "Minimal energy clusters of hard spheres," *Discrete Comput Geom*, vol. 14, pp. 237–259, Jan 1995.

[24] Y. Cho, G. Yi, J. Lim, S. Kim, V. N. Manoharan, D. J. Pine, and S. Yang, "Self-organization of bidisperse colloids in water droplets," *J Am Chem Soc*, vol. 127, pp. 15968–15975, Jan 2005.

[25] S.-H. Kim, G.-R. Yi, K. H. Kim, and S.-M. Yang, "Photocurable pickering emulsion for colloidal particles with structural complexity," *Langmuir*, vol. 24, pp. 2365–2371, Jan 2008.

[26] H. Sheu, M. S. El-Aasser, and J. Vanderhoff, "Uniform nonspherical latex particles as model interpenetrating polymer networks," *Journal of Polymer Science: Part A: Polymer Chemistry*, vol. 28, pp. 653–667, Jan 1990.

[27] H. Sheu, M. El-Aasser, and J. Vanderhoff, "Phase-separation in polystyrene latex interpenetrating polymer networks," *J Polym Sci Pol Chem*, vol. 28, pp. 629–651, Jan 1990.

[28] E. B. Mock, H. D. Bruyn, B. Hawkett, R. G. Gilbert, and C. F. Zukoski, "Synthesis of anisotropic nanoparticles by seeded emulsion polymerization," *Langmuir*, vol. 22, pp. 4037–4043, Jan 2006.

[29] C. Paquet, M. Allard, G. Gledel, and E. Kumacheva, "Guest-host colloid crystals: Experimental study and simulations," *Journal of Physical Chemistry B*, vol. 110, pp. 1605–1613, Jan 2006.

[30] W. K. Kegel, D. Breed, M. Elsesser, and D. J. Pine, "Formation of anisotropic polymer colloids by disparate relaxation times," *Langmuir*, vol. 22, pp. 7135–7136, Aug 2006.

[31] J.-W. Kim, R. J. Larsen, and D. A. Weitz, "Synthesis of nonspherical colloidal particles with anisotropic properties," *J Am Chem Soc*, pp. 14374–14377, Nov 2006.

[32] G.-R. Yi, V. N. Manoharan, E. Michel, M. T. Elsesser, S.-M. Yang, and D. J. Pine, "Colloidal clusters of silica or polymer microspheres," *Adv Mater*, pp. 1204–1208, Jul 2004.

[33] D. J. Kraft, W. S. Vlug, C. M. van Kats, A. van Blaaderen, A. Imhof, and W. K. Kegel, "Self-assembly of colloids with liquid protrusions," *J Am Chem Soc*, vol. 131, pp. 1182–1186, Jan 2009.

[34] A. van Blaaderen, "Materials science - colloids get complex," *Nature*, vol. 439, pp. 545–546, Jan 2006.

[35] F. Sciortino, E. Bianchi, J. F. Douglas, and P. Tartaglia, "Self-assembly of patchy particles into polymer chains: A parameter-free comparison between Wertheim theory and Monte Carlo simulation," *J Chem Phys*, vol. 126, p. 194903, Jan 2007.

[36] A. Hynninen, J. H. J. Thijssen, E. C. M. Vermolen, M. Dijkstra, and A. van Blaaderen, "Self-assembly route for photonic crystals with a bandgap in the visible region," *Nature Materials*, vol. 6, pp. 202–205, Jan 2007.

[37] C. Liddell and C. Summers, "Monodispersed ZnS dimers, trimers, and tetramers for lower symmetry photonic crystal lattices," *Adv Mater*, vol. 15, pp. 1715–1719, Jan 2003.

[38] C. E. Snyder, A. M. Yake, J. D. Feick, and D. Velegol, "Nanoscale functionalization and site-specific assembly of colloids by particle lithography," *Langmuir*, vol. 21, pp. 4813–4815, May 2005.

[39] A. M. Yake, R. A. Panella, C. E. Snyder, and D. Velegol, "Fabrication of colloidal doublets by a salting out-quenching-fusing technique," *Langmuir*, pp. 9135–9141, Jan 2006.

[40] J.-W. Kim, R. J. Larsen, and D. A. Weitz, "Uniform nonspherical colloidal particles with tunable shapes," *Adv Mater*, vol. 19, pp. 2005–2009, Jan 2007.

[41] R. Fitch, *Polymer Colloids*. Academic Press, 1997.

[42] D. Nagao, M. Hashimoto, K. Hayasaka, and M. Konno, "Synthesis of anisotropic polymer particles with soap-free emulsion polymerization in the presence of a reactive silane coupling agent," *Macromol. Rapid Commun.*, vol. 29, pp. 1484–1488, Jan 2008.

[43] M. Okubo, "Micron-sized, monodisperse, snowman/confetti-shaped polymer particles by seeded dispersion polymerization," *Colloid Polymer Science*, pp. 1041—1045, May 2005.

[44] Y.-S. Cho, G.-R. Yi, S.-H. Kim, S.-J. Jeon, M. T. Elsesser, H. K. Yu, S.-M. Yang, and D. J. Pine, "Particles with coordinated patches or windows from oil-in-water emulsions," *Chem Mater*, vol. 19, pp. 3183–3193, Jan 2007.

[45] C. E. Snyder, M. Ong, and D. Velegol, "In-solution assembly of colloidal water," *Soft Matter*, pp. 1263–1268, Mar 2009.

[46] P. Pieranski, "Two-dimensional interfacial colloidal crystals," *Phys Rev Lett*, vol. 45, pp. 569–572, Jan 1980.

[47] A. Hurd, "The electrostatic interaction between interfacial colloidal particles," *J Phys A-Math Gen*, vol. 18, pp. 1055–1060, Jan 1985.

[48] S. Sacanna, W. K. Kegel, and A. P. Philipse, "Thermodynamically stable Pickering emulsions," *Phys Rev Lett*, vol. 98, pp. 158301–158304, Jan 2007.

[49] R. Holyst, D. Plewczynski, A. Aksimentiev, and K. Burdzy, "Diffusion on curved, periodic surfaces," *Phys Rev E*, vol. 60, pp. 302–307, Jan 1999.

[50] D. Edwards and C. Bonilla, "Viscosity of liquid styrene and butadiene," *Ind Eng Chem*, vol. 36, pp. 1038–1040, Jan 1944.

[51] S. Sacanna, W. T. M. Irvine, P. M. Chaikin, and D. J. Pine, "Lock and key colloids," *Nature*, vol. 464, pp. 575–578, Mar 2010.

[52] C. Zoldesi and A. Imhof, "Synthesis of monodisperse colloidal spheres, capsules, and microballoons by emulsion templating," *Adv Mater*, vol. 17, pp. 924–928, Jan 2005.

[53] D. J. Kraft, J. Groenewold, and W. K. Kegel, "Colloidal molecules with well-controlled bond angles," *Soft Matter*, vol. 5, pp. 3823–3826, Jan 2009.

[54] S. C. Glotzer, M. J. Solomon, and N. A. Kotov, "Self-assembly: From nanoscale to microscale colloids," *AIChE Journal*, vol. 50, pp. 2978–2985, Nov 2004.

[55] A. M. Yake, C. E. Snyder, and D. Velegol, "Site-specific functionalization on individual colloids: Size control, stability, and multilayers," *Langmuir*, pp. 9069–9075, Jan 2007.

[56] A. B. Pawar and I. Kretzschmar, "Patchy particles by glancing angle deposition," *Langmuir*, vol. 24, pp. 355–358, Jan 2008.

[57] L. Hong, A. Cacciuto, E. Luijten, and S. Granick, "Clusters of amphiphilic colloidal spheres," *Langmuir*, vol. 24, pp. 621–625, Jan 2008.

[58] S. Gangwal, O. J. Cayre, and O. D. Velev, "Dielectrophoretic assembly of metallodielectric Janus particles in AC electric fields," *Langmuir*, vol. 24, pp. 13312–13320, Jan 2008.

[59] S. K. Smoukov, S. Gangwal, M. Marquez, and O. D. Velev, "Reconfigurable responsive structures assembled from magnetic Janus particles," *Soft Matter*, vol. 5, pp. 1285–1292, Jan 2009.

[60] J. Ge, Y. Hu, T. Zhang, and Y. Yin, "Superparamagnetic composite colloids with anisotropic structures," *J Am Chem Soc*, pp. 8974–8975, Jul 2007.

[61] J.-G. Park, J. D. Forster, and E. R. Dufresne, "High-yield synthesis of monodisperse dumbbell-shaped polymer nanoparticles," *J Am Chem Soc*, vol. 132, pp. 5960–5961, Jan 2010.

[62] J.-G. Park, J. D. Forster, and E. R. Dufresne, "Synthesis of colloidal particles with the symmetry of water molecules," *Langmuir*, vol. 25, pp. 8903–8906, Jan 2009.

[63] S. Badaire, C. Cottin-Bizonne, J. W. Woody, A. Yang, and A. D. Stroock, "Shape selectivity in the assembly of lithographically designed colloidal particles," *J Am Chem Soc*, vol. 129, pp. 40–41, Jan 2007.

[64] S. Badaire, C. Cottin-Bizonne, and A. D. Stroock, "Experimental investigation of selective colloidal interactions controlled by shape, surface roughness, and steric layers," *Langmuir*, vol. 24, pp. 11451–11463, Oct 2008.

[65] K. Zhao and T. Mason, "Directing colloidal self-assembly through roughness-controlled depletion attractions," *Phys Rev Lett*, vol. 99, p. 268301, Dec 2007.

[66] K. Zhao and T. Mason, "Suppressing and enhancing depletion attractions between surfaces roughened by asperities," *Phys Rev Lett*, vol. 101, p. 148301, Sep 2008.

[67] R. Pelton and P. Chibante, "Preparation of aqueous latices with N-isopropylacrylamide," *Colloids and Surfaces*, pp. 247–256, Jun 1986.

[68] W. McPhee, K. C. Tam, and R. Pelton, "Poly(N-isopropylacrylamide) latices prepared with sodium dodecyl sulfate," *Journal of Colloid and Interface Science*, pp. 24–30, Dec 1993.

[69] J. Zhang, S. Xu, and E. Kumacheva, "Polymer microgels: Reactors for semiconductor, metal, and magnetic nanoparticles," *J Am Chem Soc*, vol. 126, pp. 7908—7914, Mar 2004.

[70] M. Okubo, "Production of anomalously shaped carboxylated polymer particles by seeded emulsion polymerization:," *Colloid Polym Sci*, vol. 265, pp. 876–881, Mar 1987.

[71] D. J. Kraft, J. Hilhorst, M. Heinen, M. Hoogenraad, B. Luigjes, and W. K. Kegel, "High yield synthesis of anisotropic patchy polymer particles," *accepted for publication in The Journal of Physical Chemistry B*, 2010.

[72] W. Ramsden, "Separation of solids in the surface-layers of solutions and 'suspensions' (observations on surface-membranes, bubbles, emulsions, and mechanical coagulation)," *Proceedings of the Royal Society of London*, vol. 72, pp. 156–164, Jan 1903.

[73] S. Pickering, "Emulsions," *J Chem Soc*, vol. 91, pp. 2001–2021, Jan 1907.

[74] R. Aveyard, B. Binks, and J. Clint, "Emulsions stabilised solely by colloidal particles," *Adv Colloid Interfac*, vol. 100, pp. 503–546, Jan 2003.

[75] S. Sacanna and A. P. Philipse, "Preparation and properties of monodisperse latex spheres with controlled magnetic moment for field-induced colloidal crystallization and (dipolar) chain formation," *Langmuir*, vol. 22, pp. 10209–10216, Jan 2006.

[76] S. Sacanna and A. P. Philipse, "A generic single-step synthesis of monodisperse core/shell colloids based on spontaneous Pickering emulsification," *Adv Mater*, vol. 19, pp. 3824–3826, Jan 2007.

[77] D. Suzuki, S. Tsuji, and H. Kawaguchi, "Janus microgels prepared by surfactant-free Pickering emulsion-based modification and their self-assembly," *J Am Chem Soc*, vol. 129, pp. 8088–8089, Jan 2007.

[78] O. D. Velev, K. Furusawa, and K. Nagayama, "Assembly of latex particles by using emulsion droplets as templates. 1. microstructured hollow spheres," *Langmuir*, pp. 1–11, Feb 1996.

[79] A. D. Dinsmore, M. Hsu, M. Nikolaides, M. Marquez, A. Bausch, and D. A. Weitz, "Colloidosomes: Selectively permeable capsules composed of colloidal particles-supp info," *Science*, vol. 298, pp. 1006–1009, Jan 2002.

[80] M. Hsu, M. Nikolaides, A. D. Dinsmore, A. Bausch, V. Gordon, X. Chen, J. Hutchinson, and D. A. Weitz, "Self-assembled shells composed of colloidal particles: Fabrication and characterization," *Langmuir*, vol. 21, pp. 2963–2970, Jan 2005.

[81] M. J. Bowick, D. R. Nelson, and A. Travesset, "Interacting topological defects on frozen topographies," *Physical Review B*, pp. 8738–8751, Sep 2000.

[82] A. Bausch, M. Bowick, A. Cacciuto, A. D. Dinsmore, M. Hsu, D. Nelson, M. Nikolaides, A. Travesset, and D. A. Weitz, "Grain boundary scars and spherical crystallography," *Science*, vol. 299, pp. 1716–1718, Jan 2003.

[83] M. Nikolaides, A. Bausch, M. F. Hsu, A. Dinsmore, M. Brenner, D. Weitz, and C. Gay, "Electric-field-induced capillary attraction between like-charged particles at liquid interfaces," *Nature*, vol. 420, pp. 299–301, Jan 2002.

[84] M. Nikolaides, A. Bausch, M. Hsu, A. D. Dinsmore, M. Brenner, C. Gay, and D. A. Weitz, "Like-charged particles at liquid interfaces - reply," *Nature*, vol. 424, pp. 1014–1014, Jan 2003.

[85] S. Arditty, C. Whitby, B. Binks, V. Schmitt, and F. Leal-Calderon, "Some general features of limited coalescence in solid-stabilized emulsions," *Eur Phys J E*, vol. 11, pp. 273–281, Jan 2003.

[86] K. J. Stebe, E. Lewandowski, and M. Ghosh, "Oriented assembly of metamaterials," *Science*, vol. 325, pp. 159–160, Jan 2009.

[87] F. Sciortino, A. Giacometti, and G. Pastore, "A numerical study of one-patch colloidal particles: from square-well to Janus.," *Phys Chem Chem Phys*, vol. 12, pp. 11869–11877, Aug 2010.

[88] F. Romano, E. Sanz, and F. Sciortino, "Phase diagram of a tetrahedral patchy particle model for different interaction ranges," *J. Chem. Phys.*, vol. 132, p. 184501, Jan 2010.

[89] L. Hong, A. Cacciuto, E. Luijten, and S. Granick, "Clusters of charged Janus spheres," *Nano Lett*, pp. 1–5, Jan 2006.

[90] S. Jiang, Q. Chen, M. Tripathy, E. Luijten, K. S. Schweizer, and S. Granick, "Janus particle synthesis and assembly," *Adv Mater*, vol. 22, pp. 1060–1071, Jan 2010.

[91] W. K. Kegel and P. van der Schoot, "Physical regulation of the self-assembly of tobacco mosaic virus coat protein," *Biophys J*, vol. 91, pp. 1501–1512, Aug 2006.

[92] S. Asakura and F. Oosawa, "Interaction between particles suspended in solutions of macromolecules," *J Polym Sci*, vol. 33, pp. 183–192, Jan 1958.

[93] A. Vrij, "Polymers at interfaces and the interactions in colloidal dispersions," *Pure Appl. Chem*, Jan 1976.

[94] H. Lekkerkerker, W. Poon, P. Pusey, A. Stroobants, and P. Warren, "Phase-behavior of colloid plus polymer mixtures," *Europhys Lett*, vol. 20, pp. 559–564, Jan 1992.

[95] M. Hermes and M. Dijkstra, "in preparation," *see chapter 8 PhD thesis, M Hermes*, 2010.

[96] E. Verwey and J. Overbeek, *Theory of the stability of lyophobic colloids: the interaction of sol particles having an electric double layer*. Elsevier, Jan 1948.

[97] G. Meng, N. Arkus, M. P. Brenner, and V. N. Manoharan, "The free-energy landscape of clusters of attractive hard spheres," *Science*, vol. 327, pp. 560–563, Jan 2010.

[98] J. Bernal, "Bakerian lecture 1962 - structure of liquids," *Proc R Soc Lon Soc-A*, vol. 280, pp. 299–322, Jan 1964.

[99] A. Campbell, V. Anderson, J. V. Duijneveldt, and P. Bartlett, "Dynamical arrest in attractive colloids: the effect of long-range repulsion," *Phys Rev Lett*, vol. 94, no. 20, p. 208301, 2005.

[100] F. Sciortino, P. Tartaglia, and E. Zaccarelli, "One-dimensional cluster growth and branching gels in colloidal systems with short-range depletion attraction and screened electrostatic repulsion," *J. Phys. Chem. B*, vol. 109, no. 46, pp. 21942–21953, 2005.

[101] N. Arkus, V. N. Manoharan, and M. P. Brenner, "Minimal energy clusters of hard spheres with short range attractions," *Phys Rev Lett*, vol. 103, p. 118303, Jan 2009.

[102] J. Israelachvili, *Intermolecular and Surface Forces*. Academic Press, 2nd ed., 1991.

[103] J.-W. Kim, D. Lee, H. C. Shum, and D. A. Weitz, "Colloid surfactants for emulsion stabilization," *Adv Mater*, vol. 20, pp. 3239–3243, Sep 2008.

[104] M. D. McConnell, M. J. Kraeutler, S. Yang, and R. J. Composto, "Patchy and multiregion Janus particles with tunable optical properties," *Nano Lett*, vol. 10, pp. 603–609, Feb 2010.

[105] H. Reiss, W. Kegel, and J. Groenewold, "Length scale for configurational entropy in microemulsions," *Berichte der Bunsengesellschaft für physikalische Chemie*, vol. 100, no. 3, pp. 279–295, 1996.

[106] F. Leal-Calderon and V. Schmitt, "Solid-stabilized emulsions," *Curr Opin Colloid In*, vol. 13, pp. 217–227, Jan 2008.

[107] W. K. Kegel, G. Overbeek, and H. Lekkerkerker, "Thermodynamics of microemulsions I," *Handbook of microemulsion science and technology*, Jan 1999.

[108] S. Sacanna, W. K. Kegel, and A. P. Philipse, "Spontaneous oil-in-water emulsification induced by charge-stabilized dispersions of various inorganic colloids," *Langmuir*, vol. 23, pp. 10486–10492, Jan 2007.

[109] S. Sacanna, L. Rossi, and A. P. Philipse, "Oil-in-water emulsification induced by ellipsoidal hematite colloids: Evidence for hydrolysis-mediated self-assembly," *Langmuir*, vol. 23, pp. 9974–9982, Jan 2007.

[110] G. Kozerski, R. Gallavan, and M. Ziemelis, "Investigation of trialkoxysilane hydrolysis kinetics using liquid chromatography with inductively coupled plasma atomic emission spectrometric detection and non-linear regression modeling," *Anal Chim Acta*, vol. 489, pp. 103–114, Jan 2003.

[111] W. K. Kegel and J. Groenewold, "Scenario for equilibrium solid-stabilized emulsions," *Phys Rev E*, vol. 80, p. 030401, Jan 2009.

[112] J. Zwanikken, "Chapter 8," *PhD thesis*, 2010.

[113] R. Massart, "Preparation of aqueous magnetic liquids in alkaline and acidic media," *IEEE Transactions on Magnetics*, Jan 1981.

[114] E. Claesson and A. Philipse, "Monodisperse magnetizable composite silica spheres with tunable dipolar interactions," *Langmuir*, vol. 21, pp. 9412–9419, Jan 2005.

[115] F. Tourinho, R. Franck, and R. Massart, "Aqueous ferrofluids based on manganese and cobalt ferrites," *J Mater Sci*, vol. 25, pp. 3249–3254, Jan 1990.

[116] W. Stöber, A. Fink, and E. Bohn, "Controlled growth of monodisperse silica spheres in micron size range," *J Colloid Interf Sci*, vol. 26, pp. 62–&, Jan 1968.

[117] J. Turkevich, P. Stevenson, and J. Hillier, "A study of the nucleation and growth processes in the synthesis of colloidal gold," *Discuss Faraday Soc*, pp. 55–75, Jan 1951.

[118] G. Frens, "Controlled nucleation for the regulation of the particle size in monodisperse gold suspensions," *Nature Physical Science*, pp. 1–3, Oct 1973.

[119] P. A. Buining, B. M. Humbel, A. P. Philipse, and A. J. Verkleij, "Preparation of functional silane-stabilized gold colloids in the (sub)nanometer size range," *Langmuir*, vol. 13, pp. 3921–3926, Aug 1997.

[120] F. Reincke, W. K. Kegel, H. Zhang, M. Nolte, D. Wang, D. Vanmaekelbergh, and H. Möhwald, "Understanding the self-assembly of charged nanoparticles at the water/oil interface," *Physical Chemistry Chemical Physics*, vol. 8, pp. 3828–3835, Jan 2006.

[121] M. Brust, M. Walker, D. Bethell, D. J. Schiffrin, and R. Whyman, "Synthesis of thiol-derivatised gold nanoparticles in a two-phase liquid-liquid system," *Journal of the Chemical Society*, pp. 801–802, Oct 1994.

[122] M.-C. B. Salon, P.-A. Bayle, M. Abdelmouleh, S. Boufi, and M. N. Belgacem, "Kinetics of hydrolysis and self condensation reactions of silanes by NMR spectroscopy," *Colloid Surface A*, vol. 312, pp. 83–91, Jan 2008.

[123] J. Sjöblom, ed., *Emulsions and emulsion stability*, vol. 132. Boca Raton, FL: Taylor and Francis, 2006.

[124] D. J. Kraft, B. Luigjes, J. W. J. de Folter, A. P. Philipse, and W. K. Kegel, "Evolution of equilibrium Pickering emulsions - a matter of timescales," *Journal of Physical Chemistry B*, vol. 114 (38), pp. 12257–12263, 2010.

[125] D. J. Kraft, J. W. J. de Folter, B. Luigjes, A. P. Philipse, and W. K. Kegel, "Conditions for equilibrium solid-stabilized emulsions," *Journal of Physical Chemistry B*, vol. 141, pp. 10347–10356, 2010.

[126] B. Vonnegut, "Rotating bubble method for the determination of surface and interfacial tensions," *Review of Scientific Instruments*, vol. 13, pp. 6–9, Jan 1942.

[127] B. Arkles, J. Steinmetz, J. Zazycyny, and P. Mehta, "Factors contributing to the stability of alkoxysilanes in aqueous-solution," *J Adhes Sci Technol*, vol. 6, pp. 193–206, Jan 1992.

[128] W. Ostwald, "On the assumed isomerism of red and yellow mercury oxide and the surface-tension of solid bodies," *Zeitschrift für Physikalische Chemie-Stochiometrie und Verwandtschaftslehre*, vol. 34, pp. 495–503, Jan 1900.

[129] I. Lifshitz and V. Slyozov, "The kinetics of precipitation from supersaturated solid solutions," *J Phys Chem Solids*, vol. 19, pp. 35–50, Jan 1961.

[130] G. van Ewijk, G. Vroege, and A. P. Philipse, "Convenient preparation methods for magnetic colloids," *J Magn Magn Mater*, vol. 201, pp. 31–33, Jan 1999.

[131] A. P. Philipse and A. Vrij, "Preparation and propertiesof nonaqueous model dispersions of chemically modified, charged silica spheres," *J Colloid Interf Sci*, vol. 128, pp. 1–16, May 1988.

[132] E. P. Plueddemann, *Silane Coupling Agents*. Plenum Press: New York, 1982.

[133] B. Arkles, "Tailoring surfaces with silanes," *Chemtech*, vol. 7, p. 766, 1977.

[134] H. Lekkerkerker, "Contribution of the electric double layer to the curvature elasticity of charged amphiphilic monolayers," *Physica A*, vol. 159, p. 319, 1989.

[135] N. Shahidzadeh, D. Bonn, J. Meunier, M. Nabavi, M. Airiau, and M. Morvan, "Dynamics of spontaneous emulsification for fabrication of oil in water emulsions," *Langmuir*, vol. 16, pp. 9703–9708, Jan 2000.

[136] M. Beijerinck, "On a contagium vivum fluidum causing the spotdisease of the tobacco-leaves," *Koninklijke Nederlandse Akademie van van Wetenschappen Proceedings*, vol. 1, pp. 170–176, 1898.

[137] P. Butler, "Self-assembly of tobacco mosaic virus: the role of an intermediate aggregate in generating both specificity and speed," *Philos T Roy Soc B*, vol. 354, pp. 537–550, Jan 1999.

[138] H. Fraenkel-Conrat and R. Williams, "Reconstitution of active tobacco mosaic virus from its inactive protein and nucleic acid components," *P Natl Acad Sci Usa*, vol. 41, pp. 690–698, Jan 1955.

[139] K. Scholthof, J. Shaw, M. Zaitlin, and L. Sindelar, *Tobacco mosaic virus: one hundred years of contributions to virology*. APS press, 1999.

[140] K. Scholthof, "Tobacco mosaic virus: A model system for plant biology," *Annu Rev Phytopathol*, vol. 42, pp. 13–34, Jan 2004.

[141] S. Fraden, "Phase transitions in colloidal suspensions of virus particles," *NATO ASI Series C Mathematical and Physical Sciences-Advanced Study Institute*, vol. 460, pp. 113–164, 1995.

[142] M. Adams, Z. Dogic, S. Keller, and S. Fraden, "Entropically driven microphase transitions in mixtures of colloidal rods and spheres," *Nature*, vol. 393, pp. 349–352, Jan 1998.

[143] M. Young, D. Willits, M. Uchida, and T. Douglas, "Plant viruses as biotemplates for materials and their use in nanotechnology," *Annu Rev Phytopathol*, vol. 46, pp. 361–384, Jan 2008.

[144] C. Sachse, J. Z. Chen, P.-D. Coureux, M. E. Stroupe, M. Faendrich, and N. Grigorieff, "High-resolution electron microscopy of helical specimens: A fresh look at tobacco mosaic virus," *J Mol Biol*, vol. 371, pp. 812–835, Jan 2007.

[145] A. Klug, "The tobacco mosaic virus particle: structure and assembly," *Philos T Roy Soc B*, vol. 354, pp. 531–535, Jan 1999.

[146] A. Durham, "Cause of irreversible polymerization of tobacco mosaic virus protein," *Febs Lett*, vol. 25, pp. 147–152, Jan 1972.

[147] P. Butler, "The current picture of the structure and assembly of tobacco mosaic-virus," *J Gen Virol*, vol. 65, pp. 253–279, Jan 1984.

[148] G. Lebeurier, A. Nicolaieff, and K. Richards, "Inside-out model for self-assembly of tobacco mosaic-virus," *P Natl Acad Sci Usa*, vol. 74, pp. 149–153, Jan 1977.

[149] D. L. Caspar, "Movement and self-control in protein assemblies - quasi-equivalence revisited," *Biophys J*, vol. 32, pp. 103–138, Jan 1980.

[150] E. C. Dykeman and R. Twarock, "All-atom normal-mode analysis reveals an RNA-induced allostery in a bacteriophage coat protein," *Phys Rev E*, vol. 81, p. 031908, Jan 2010.

[151] L. Liepold, J. Revis, M. Allen, L. Oltrogge, M. Young, and T. Douglas, "Structural transitions in cowpea chlorotic mottle virus (CCMV)," *Phys Biol*, vol. 2, pp. S166–S172, Jan 2005.

[152] P. G. A. Janssen, S. Jabbari-Farouji, M. Surin, X. Vila, J. C. Gielen, T. F. A. de Greef, M. R. J. Vos, P. H. H. Bomans, N. A. J. M. Sommerdijk, P. C. M. Christianen, P. Leclere, R. Lazzaroni, P. van der Schoot, E. W. Meijer, and A. P. H. J. Schenning, "Insights into templated supramolecular polymerization: Binding of naphthalene derivatives to ssDNA templates of different lengths," *J Am Chem Soc*, vol. 131, pp. 1222–1231, Jan 2009.

[153] C. Kittel, "Phase transition of a molecular zipper," *Am J Phys*, vol. 37, pp. 917–920, Jan 1969.

[154] N. Liu, B. Peng, Y. Lin, Z. Su, Z. Niu, and Q. Wang, "Pulling genetic RNA out of tobacco mosaic virus using single-molecule force spectroscopy," *Journal of the American Chemical Society*, vol. 132 (32), pp. 521–522, 2010.

[155] D. Gallie, K. Plaskitt, and T. Wilson, "The effect of multiple dispersed copies of the Origin-of-Assembly sequence from TMV RNA on the morphology of pseudovirus particles assembled in vitro," *Virology*, vol. 158, pp. 473–476, Jan 1987.

[156] X. Wu, Z. XU, and J. Shaw, "Uncoating of tobacco mosaic-virus RNA in protoplasts," *Virology*, vol. 200, pp. 256–262, Jan 1994.

[157] X. Wu and J. Shaw, "Bidirectional uncoating of the genomic RNA of a helical virus," *PNAS*, vol. 93, pp. 2981–2984, Jan 1996.

[158] J. Shaw, "Tobacco mosaic virus and the study of early events in virus infections," *Philos T Roy Soc B*, vol. 354, pp. 603–611, Jan 1999.

[159] J. Culver, "Tobacco mosaic virus assembly and disassembly: Determinants in pathogenicity and resistance," *Annu Rev Phytopathol*, vol. 40, pp. 287–308, Jan 2002.

[160] P. Butler and J. Finch, "Structures and roles of polymorphic forms of tobacco mosaic-virus protein .7. lengths of growing rods during assembly into nucleoprotein with viral-RNA," *J Mol Biol*, vol. 78, pp. 637–649, Jan 1973.

[161] G. Lomonossoff and P. Butler, "Assembly of tobacco mosaic-virus - elongation towards the 3'-hydroxyl terminus of the RNA," *Febs Lett*, vol. 113, pp. 271–274, Jan 1980.

[162] Y. Sano, H. Inoue, and Y. Hiragi, "Differences of reconstitution process between tobacco mosaic virus and cucumber green mottle mosaic virus by synchrotron small angle X-ray scattering using low-temperature quenching," *J Protein Chem*, vol. 18, pp. 801–805, Jan 1999.

[163] A. Schön and K. W. Mundry, "Coordinated two-disk nucleation, growth and properties, of virus-like particles assembled from tobacco-mosaic-virus capsid protein with poly(A) or oligo(A) of different length," *European Journal of Biochemistry*, pp. 1–9, Jul 1984.

[164] P. van der Schoot, "Structure factor of a semidilute solution of polydisperse rodlike macromolecules," *Macromolecules*, vol. 25, no. 11, pp. 2923–2927, 1992.

[165] P. J. Flory, *Principles of polymer chemistry*. Cornell University Press, Jan 1953.

[166] V. Citovsky, D. Knorr, G. Schuster, and P. Zambryski, "The P-30 movement protein of tobacco mosaic-virus is a single-strand nucleic-acid binding-protein," *Cell*, vol. 60, pp. 637–647, Jan 1990.

Summary

Self-assembly in nature has many facets and occurs on all length scales. This thesis deals with selected examples on the colloidal length scale, ranging from tobacco mosaic virus particles of 300 nm in length to colloidal micelles roughly 10 μm in diameter.

Part 1 of this thesis deals with the synthesis of anisotropic model colloids, utilizing self-assembly processes.

Colloids are often termed "model atoms", because both obey the laws of statistical thermodynamics. Yet colloids have advantages over atoms, namely by being "soft, slow and seeable" (W. Poon), as well as having tunable interaction potentials. Analogous to atoms that bind to form molecules, colloids with liquid patches can bind with each other forming "colloidal molecules" (**Chapters 2** and **3**). The self-assembly process leads to different clusters consisting of a central liquid droplet with various numbers of colloidal particles attached at the interface. By solidifying the liquid droplet that connects the colloidal particles complex anisometric particles are obtained that remind one of space-filled models of molecules, and hence, the name "colloidal molecules". Both highly symmetric clusters as well as clusters with a lower symmetry can be synthesized by tuning the relative size of the liquid patch. Furthermore, the number of patches per particles can be controlled as shown in **Chapter 4**, allowing for high yield syntheses of colloidal molecules with various shapes, as well as even more complex colloidal molecules after binding between their liquid patches. Partial particle roughness is introduced through adsorption of smaller colloids nucleated during the polymerization. These new anisotropic colloidal molecules have great potential for assembling into functional crystal structures or other finite sized structures. In the long term, the self-assembling process leads to large spherical droplets with many colloids adsorbed at the interface, also called Pickering emulsions (**5**). We analyze these structures with respect to their size, distribution of colloids at the interface, and formation of clusters and multilayered shells upon removal of the liquid droplets.

In **Part 2** the spontaneous formation of clusters of colloidal dimers with one attractive patch, also termed "colloidal micelles" is studied and compared to surfactant micelles.

One application of the anisotropic colloidal particles described in **Part 1** as a model system is presented in **Part 2**. In **Chapter 6** we show that dimers consisting of one smooth sphere and one rough sphere can be used as a model system for self-assembly of surfactant molecules into micelles. By using depletion forces which are proportional to the overlap volume, and hence stronger for the smooth sides of the

dimers than for the rough ones, site specific attraction is realized experimentally. This site-specific attraction leads to clusters of dimers with the smooth sides pointing inside. Intriguingly, at intermediate attractions, the size distribution of the clusters is peaked around a discrete value, also found in computer simulations. The similarities between the observed colloidal clusters and surfactant micelles are discussed and quantified by a theoretical model.

Part 3 is devoted to self-assembling, thermodynamically stable Pickering emulsions.

In **Chapter 7** the emulsion system is investigated with respect to its generality. By systematically varying the different components oil, water, colloids, and ions, we extract the minimum requirements for stability of these droplets covered with colloids. We find that low surface tensions of the bare oil-water interface, colloids smaller than 200 nm with a preference for the oil phase, and large, amphiphilic counterions are sufficient for the formation and stability of the Pickering emulsion. On longer time scales, the system exhibits an intricate dynamic equilibrium which is described in **Chapter 8**. Through a chemical process the hydrophilicity of the stabilizing colloidal particles gradually changes in time, leading to migration of the colloidal particles to the oil phase, and as a consequence, droplet growth. In **Chapter 9** we explore the possibilities of employing fatty acids as the dispersed phase in these spontaneously forming Pickering emulsions.

In **Part 4**, a theoretical model for the assembly of tobacco mosaic virus particles is developed.

In **Chapter 10** we describe the statics and dynamics of the spontaneous formation of tobacco mosaic virus particles from protein disks and single-stranded RNA by a modified Zipper model. The model explains why fully functional viruses are favored over partially completed ones by the self-assembly process. The model describes experimental results on the reconstitution of tobacco mosaic virus well.

Modelsystemen voor Zelf-Organisatie
Samenvatting voor Iedereen

Zelf-organisatie

Het spontaan ontstaan van geordende structuren uit chaos is een van de meest fascinerende fenomenen in de natuur. Voorbeelden kunnen overal gevonden worden: de regelmatige rimpels in het zand, wolkenbanden op gelijkmatige afstand, een zwerm vogels of een school vissen zijn alledaagse voorkomende vormen van het ontstaan van patronen. Op een kleinere schaal, maar niet minder fascinerend, ontstaat een compleet virus spontaan uit losse proteïnen (eiwitten) en erfelijk materiaal, DNA of RNA. Dit proces gebeurt spontaan en heeft niets anders nodig dan de bouwstenen (proteïnen en erfelijk materiaal) zelf. Dat betekent dat de manier waarop virussen opgebouwd worden al door de bouwstenen vast gelegd is. Het is ook een heel nauwkeurig proces: alle virussen van één soort hebben dezelfde vorm en grootte. Ze bestaan uit een eiwitjasje (het viruscapside), dat het erfelijk materiaal beschermt. Fouten in het jasje zouden fataal voor het virus zijn: dan zou de cel het vreemde materiaal onmiddellijk herkennen en afbreken. Zo'n proces waar uit ongeordende, chaotisch verdeelde bouwstenen een geordende structuur ontstaat, heet zelf-ordenend. De bouwstenen van de bovenstaande voorbeelden zijn zand korrels, water druppels, een vogel of vis, en proteïnen en erfelijk materiaal. In dit proefschrift staan verschillende modellen voor zelf-organiserende systemen beschreven.

Colloïden als modellen voor zelf-organiserende systemen

Veel zelf-organiserende systemen zijn zo klein, bijvoorbeeld virussen, dat ze ook met een optische microscoop niet gezien kunnen worden. Om toch een inzicht in zulke processen te krijgen, gebruiken we experimentele en theoretische model systemen. Een bijzonder goede keuze voor een experimenteel model systeem zijn colloïden.

Collïden zijn deeltjes of druppels, die in een ander medium, een gas, vloeistof of een vaste stof, fijn verdeeld zijn. Fijn verdeeld betekent hier, dat ze minstens een dimensie bezitten die tussen 1 nm en 1 μm groot is. Een micrometer (1 μm) is het zelfde als een duizendste millimeter. Een nanometer (1 nm) is nog duizend keer kleiner. Ter vergelijking: een menselijk haar is ongeveer 70 μm dik. Colloïden komen in de natuur overal voor, en vinden een toepassing in veel producten. Bijvoorbeeld vormen

de pigmenten in verf een colloïdale oplossing. Ook in schoonmaakproducten, cosmetica, klei, en levensmiddelen zoals boter of melk komen colloïden voor.

Vooral hun afmetingen maken colloïden een interessant model systeem voor onderzoek aan zelf-organisatie: ze zijn groot genoeg, om ze met een optisch microscoop te kunnen bestuderen, maar klein genoeg om in een vloeistof onregelmatige bewegingen uit te voeren, de "Brownse beweging". De oorzaak voor deze beweging zijn de moleculen waaruit die vloeistof bestaat, bijvoorbeeld water moleculen. Ze zijn continue in beweging en botsen tegen de veel grotere colloïden aan, die daardoor onregelmatig bewegen. De "Brownse bewegingen" zorgt ervoor, dat de colloïden goed gemengd worden en constant met elkaar wisselwerken, en daardoor de toestand van laagste energie kunnen vinden.

Bolvormige colloïden worden vaak artificiële atomen genoemd, omdat hun wisselwerkingen vergelijkbaar zijn met die tussen atomen. Onderzoek aan colloïden kan nieuwe inzichten in atomaire systemen, zoals bijvoorbeeld kristallen, opleveren. In tegenstelling tot atomen kunnen de wisselwerkingen in colloïdale systemen aangepast worden, bijvoorbeeld versterkt of juist afgezwakt, en bovendien kan de afstand waarover de colloïden wisselwerken beïnvloed worden.

Anisotrope Colloïden

De meest eenvoudige vormen van colloïden, zoals bollen of schijven, kunnen helaas vaak de ingewikkeldere bouwstenen van de natuur niet goed genoeg nabootsen. De proteïnen van het tabaksmozaïekvirus lijken bijvoorbeeld eerder op stukjes taart. Bolvormige, isotrope colloïden zijn kunnen ook voor andere complexe structuren zoals kristallen met bijzondere optische of mechanische eigenschappen niet gebruikt worden, omdat ze bij voorkeur zo efficiënt mogelijk gepakte structuren willen vormen. Deze heten hexagonale dichtste stapeling ("hexagonally close packed") en kubisch vlakgecentreerde stapeling ("face centered cubic"), en lijken op de structuur waarmee ook sinaasappelen op elkaar gestapeld kunnen worden. Om deze complexe structuren te kunnen maken, zijn anisotrope colloïden nodig. Deze kunnen zowel anisotroop in vorm als in hun wisselwerkingen zijn. Het is een uitdaging om de colloïden zo aan te passen dat een gewenste structuur verkregen kan worden.

Een bijzonder interessante, want breed toepasbare categorie van colloïden met anisotrope wisselwerkingen zijn "patchy particles", oftewel colloïden met goed gedefinieerde gebieden aan het oppervlak, die elkaar aantrekken of afstoten. Van bolvormige colloïden met attractieve "patches" wordt voorspeld dat ze nieuwe, door de posities van de "patches" vastgelegde structuren of kristallen kunnen vormen. Maar tegenwoordig bestaan er maar weinig methodes, om zulke deeltjes met gecontroleerde "patches" te maken.

Deel 1 - Colloïdale Moleculen en Clusters

In het eerste deel van dit proefschrift worden verschillende methodes gepresenteerd, om anisotrope deeltjes te maken die op moleculen lijken. Zoals eerder al genoemd, worden colloïden vaak als model atomen gebruikt, bijvoorbeeld voor onderzoek aan kristallen en vloeistoffen. In de hoofdstukken 2 en 3 laten we zien, dat deeltjes met druppels aan hun oppervlak met elkaar kunnen binden door de druppels met elkaar te laten samenvloeien. Aansluitend kunnen de druppels gepolymeriseerd worden, om vaste colloïden te verkrijgen. Dit zelf-organiserend proces is analoog aan atomen, die door een binding moleculen vormen. Zulke colloïden worden dan ook "colloïdale moleculen" genoemd. Men kan ze ook als een bijzondere vorm van "patchy particles" zien: als het materiaal van de colloïden en de druppels verschillend zijn, ontstaan er "patches" met andere eigenschappen. We kunnen de positie en de grootte van de "patches" controleren en zo bijvoorbeeld colloïden maken, die op watermoleculen lijken.

In hoofdstuk 4 wordt een andere methode geïntroduceerd, om colloïdale moleculen te maken. We laten zien, dat meerdere druppels aan de oppervlakte van de colloïden op een gecontroleerde manier verkregen kunnen worden. Het samenvloeien van de druppels aan de oppervlakte wordt beïnvloedt door de oppervlaktespanning en het volume van de druppels. Door polymerisatie van de druppels worden uniforme colloïdale moleculen in grote hoeveelheden verkregen.

Als het samenvloeien van de druppels niet door polymerisatie gestopt wordt, ontstaan er grote druppels met honderden tot duizenden colloïden aan de oppervlakte. In hoofdstuk 5 bestuderen we dit proces en analyseren wij de posities van de colloïden. We proberen verder om de druppels te verwijderen en verkrijgen daardoor clusters, dat betekent aggregaten van colloïden. We vinden dat de clusters vanaf een bepaalde grootte aan hol zijn.

Deel 2 - Colloïdale Micellen

De methoden uit deel 1 om colloïdale moleculen te maken zijn gebaseerd op een zelf-organiserend proces, namelijk het samenvloeien van de druppels aan het oppervlak van de colloïden. In hoofdstuk 6 realiseren we "patchy particles" door colloïden te gebruiken, die uit twee bolvormige onderdelen bestaan: de ene helft is glad, en de andere helft heeft een ruw oppervlak. Als polymeren aan de colloïdale oplossing toegevoegd worden, trekken de colloïden elkaar aan. Polymeren zijn eigenlijk lange moleculen, maar in oplossing lijken ze op wanordelijke kluwens. De polymeren botsen met de colloïden, totdat deze zo dicht bij elkaar zijn dat er geen polymeren meer tussen kunnen zitten. De zone, waar geen polymeren meer kunnen zitten, heet overlap volume. Omdat er polymeren vanuit elke richting behalve deze overlap zone tegen de colloïden botsen, drijven ze de colloïden naar elkaar toe en creëren dus een effectieve aantrekkingskracht.

Deze kracht wordt ook depletie interactie genoemd. Hoe groter het overlap volume tussen de colloïden des te sterk deze kracht is. Voor de gladde kant van de colloïden is deze daarom sterker dan voor de ruwe kant. Men verkrijgt daarom een attractieve "patch" aan de gladde kant! In oplossingen vormen deze colloïden bolvormige structuren, met de gladde kanten van de colloïden naar het midden en de ruwe kanten naar buiten gericht.

Onze keuze voor deze deeltjes was niet toevallig: zeep moleculen bestaan ook uit twee onderdelen, namelijk één kant, die graag in contact is met water, en één kant, die graag in contact is met olie. Men noemt zulke moleculen dan ook "amphiphil", van het oud griekse *amphi* = aan beide kanten, en *phil* = liefhebbend. In water vormen zij onder meer bolvormige structuren, waar de kant met een voorkeur voor olie naar binnen wijzen, om zo min mogelijk in contact met water en zo veel mogelijk in contact te zijn met olie liefhebbende onderdelen. Zulke structuren heten micellen. Onze colloïden met een ruwe en een gladde kant zijn dus een modellsysteem voor amphiphile molecule en vormen "colloïdale micellen".

DEEL 3 - EMULSIES

Emulsies zijn fijn verdeelde mengsels van twee eigenlijk niet mengbare vloeistoffen, bijvoorbeeld olie en water. Om een mengsel te verkrijgen, heeft men normaliter energie nodig. Een alledaags voorbeeld is sla saus, waar olie en water heftig gemengd moeten worden. Zonder stabilisatie van de emulsie druppels vloeien deze weer samen, totdat er twee aparte fasen, olie en water, ontstaan. In de hoofdstukken 7, 8 en 9 wordt een heel speciaal type van stabiele emulsies onderzocht. De olie druppels, die in de waterige fase fijn verdeeld zijn, zijn door colloïden aan de oppervlakte gestabiliseerd. Zulke emulsies heten ook Pickering emulsies, benoemd naar één van hun ontdekkers Spencer Pickering. De meeste Pickering emulsies zijn instabiel en ontmengen naar een tijdje. In tegenstelling daarmee zijn de emulsies die in dit proefschrift onderzocht worden thermodynamisch stabiel. Dat betekent, dat ze zich in de toestand met de laagste vrije energie bevinden, en spontaan ontstaan als men water, colloïden, en een speciale olie in contact met elkaar brengt. Dit is een duidelijk verschil met bijvoorbeeld slasaus, die pas door heftig roeren ontstaat en na enige tijd weer ontmengt. Deze bijzondere emulsies werden pas kort geleden door Stefano Sacanna, Willem Kegel en Albert Philipse in het Van 't Hoff laboratorium ontdekt, en het is tot nu toe nog onduidelijk, of het een heel speciaal systeem is of een generieke nieuwe soort emulsies.

In hoofdstuk 7 variëren we de verschillende onderdelen van de emulsies systematisch, om de minimale vereisten voor het verkrijgen van stabiele Pickering emulsies uit te zoeken. Uit deze experimenten blijkt, dat er inderdaad sprake is van een nieuwe soort stabiele Pickering emulsies.

Hoewel deze emulsies stabiel genoemd worden, verandert de druppel grootte met de tijd: binnen de eerste 24 uur worden de olie druppels kleiner (tot ongeveer 100 nm), en daarna groeien ze langzaam dagen tot maanden lang door. In hoofdstuk 8 beschrijven we dit subtiele evenwicht, dat geïnduceerd wordt door een chemische verandering van de stabiliserende colloïdale deeltjes.

In hoofdstuk 9 passen we onze kennis over deze emulsies op een nieuw systeem toe. We onderzoeken of ook vetzuren als olie fase in deze emulsies gebruikt kunnen worden. De motivatie daarvoor is ten eerste academischer natuur, namelijk of we in hoofdstuk 7 de goede vereisten hebben gevonden, en ten tweede zijn vetzuren van groot belang in industriële producten. Een voorbeeld is margarine, een emulsie van verschillende vetten en water, die veel energie kost om te maken. Een spontaan aflopend zelf-organiserende emulsificatie proces heeft geen energie nodig en is daarom interessant voor een goedkopere productie.

Deel 4 - Een theoretisch model voor de zelf-organisatie van tabaksmozaïekvirus

In hoofdstuk 10 wordt de reconstructie van proteïnen en erfelijk materiaal (RNA) in staafvormige tabaksmozaïekvirussen onderzocht. Het tabaksmozaïekvirus is het eerste virus, dat ontdekt werd, en staat dus aan het begin van het huidige onderzoeksveld virologie. Het virus bestaat uit een ongeveer 300 nm lang en 18 nm breed proteïn jasje, dat om de RNA gevouwen zit. Om het proces van de zelf-organisatie van het virus te beschrijven, maken we gebruik van een aangepast "Zipper"-Model. Dit model houdt in, dat de adsorptie van proteïnen op het vorige aansluit. We ontwikkelen het model voor het statische en het dynamische geval, en vergelijken de resultaten met experimenten uit de literatuur.

Modellsysteme für Selbstassemblierung Zusammenfassung

Selbstassemblierung

Das spontane Entstehen von geordneten Strukturen aus Chaos ist eines der faszinierendsten Phänomene in der Natur. Beispiele dafür findet man überall: die regelmäßigen Rippel im Sand, Wolkenbänder, die in gleichen Abständen aufeinanderfolgen, oder Schwärme von Vögeln und Fischen sind nur einige der alltäglich vorkommenden Formen von Strukturbildung. Ein nicht weniger faszinierendes Beispiel auf kleinerer Größenskala, ist das Zusammensetzen von Proteinen und Nukleinsäuremolekülen, d. h. DNA oder RNA, zu funktionsfähigen Viren. Dieser Prozess läuft spontan ab und benötigt nichts anderes als die Bausteine selbst. Das bedeutet, dass die Art und Weise, wie sich der Virus zusammensetzt, in den Bausteinen festgelegt ist. Dieser Prozess ist sehr akkurat: alle Viren eines Stammes haben die gleiche Form und Größe. Sie bestehen aus einer Proteinhülle, welche die die genetische Information, die in Form eines Nukleinsäuremolekuls darin aufbewahrt wird, beschützt. Fehler in der Proteinhülle wären fatal für das Virus, denn dann könnten Abwehrsysteme der befallenen Zellen die Moleküle, die die genetische Information enthalten, angreifen und zerstören. Ein solcher Prozess, bei dem aus ungeordneten, chaotisch verteilten Bausteinen eine geordnete Struktur entsteht, heißt Selbstordnung oder Selbstassemblierung. Die Bausteine in den oben genannten Beispielen sind Sandkörner, Wassertröpfchen, ein Vogel oder ein Fisch, und die Protein- (Eiweiß-) und Nukleinsäuremoleküle. Wenn ein solcher Prozess konstant Energie verbraucht, spricht man von Selbstordnung, andernfalls von Selbstassemblierung. In dieser Doktorarbeit werden verschiedene Modelle für selbstassemblierende Systeme beschrieben.

Kolloide als Modellsysteme für Selbstassemblierung

Viele solcher selbstassemblierender Systeme sind so klein, dass sie nicht direkt beobachtet werden können. Um dennoch Einblicke in die ablaufenden Prozesse zu bekommen, werden experimentelle oder theoretische Modellsysteme verwendet. Besonders gut sind Kolloide als experimentelle Modellsysteme geeignet.

Kolloide sind Teilchen oder Tröpfchen, die in einem anderen Medium, einem Gas, einer Flüssigkeit oder einem Festkörper fein verteilt sind. Fein bedeutet hier, dass sie

in mindestens einer Dimension zwischen 1 nm und 1 μm großsind. Ein Mikrometer (1 μm) entspricht einem Tausendstel Millimeter. Ein Nanometer (1 nm) ist noch 1000 mal kleiner. Zum Vergleich: ein menschliches Haar ist ungefähr 70 μm dick. Kolloide sind in der Natur weit verbreitet, und werden in vielen Produkten verwendet. Zum Beispiel formen die Pigmente in Farben und Lacken eine kolloidale Lösung. Auch in Reinigungsmitteln, Kosmetika, Ton, und Lebensmitteln wie Butter oder Milch kommen Kolloide vor.

Kolloide sind aufgrund ihre Größe besonders interessant für die Erforschung selbstassemblierender und selbstorganisierender Systeme: Sie sind großgenug, um mit einem Mikroskop beobachtet werden zu können, und klein genug, um in Flüssigkeiten unregelmäßige, zuckende Bewegungen auszuführen, die sogenannte "Brownsche Bewegung". Die Ursache dafür sind die Atome oder Moleküle, aus denen eine Flüssigkeit besteht, zum Beispiel Wassermoleküle. Sie sind bei einer gegebenen Temperatur konstant in Bewegung und stoßen permanent von allen Seiten gegen die wesentlich größeren Kolloide, die dadurch zuckende Bewegungen machen. Der Vorteil dieser "Brownschen Bewegung" ist, dass die Kolloide sich ständig mischen und miteinander wechselwirken, und dadurch den Zustand mit der niedrigsten Energie finden können.

Kugelförmige Kolloide werden oft als künstliche Atome bezeichnet, da ihre Wechselwirkungen untereinander vergleichbar mit denen von Atomen sind. Die Kolloid-Forschung kann deshalb neue Einsichten in atomare Systeme wie beispielsweise Kristalle liefern. Kolloidale Systeme sind allerdings noch wesentlich vielfältiger als die Atome, die in der Natur vorkommen: Ihre Wechselwirkungen können gezielt verändert, zum Beispiel verstärkt oder abgeschwächt werden, aber man kann auch die Reichweite der Wechselwirkung kann anpassen.

Anisotrope Kolloide

Die einfachsten kolloidalen Formen, beispielsweise Kugeln oder Plättchen, reichen oft nicht aus, um die komplizierten Bausteine der Natur nachzuahmen. Die Proteine der Tabakmosaikviren sehen zum Beispiel eher wie ein Tortenstück aus. Auch für andere komplexere Anordnungen, wie zum Beispiel Kristalle mit besonderen optischen Eigenschaften, sind kugelförmige Kolloide ungeeignet, da sie sich nur auf ganz bestimmte Art und Weise aufeinander stapeln lassen. Diese einfachen Kristallstrukturen nennt man hexagonal dichteste (hcp) und kubisch flächenzentrierte (fcc) Kugelpackung. Sie sind vergleichbar mit gestapelten Orangen im Supermarkt. Um komplexere Strukturen herstellen zu können, werden anisotrope Kolloide benötigt. Diese können sowohl anisotrop in ihrer Form, als auch in ihren Wechselwirkungen sein. Die Herausforderung besteht darin, die kolloidale Form und ihre Wechselwirkungen an die zu untersuchende Fragestellung anzupassen.

Eine besonders interessante, breit anwendbare Kategorie von Kolloiden mit anisotropen Wechselwirkungen sind sogenannte Teilchen mit "Patches", d.h. Kolloide mit gut definierten Gebieten an der Oberfläche, die einander anziehen oder abstossen. Kugelförmige Kolloide mit attraktiven "Patches" können neue, durch die Positionen der "Patches" festgelegte Strukturen oder Kristalle bilden. Allerdings gibt es gegenwärtig nur wenige Methoden, um solche anisotropen Teilchen mit kontrollierten "Patches" herzustellen.

Teil 1 - Kolloidale Moleküle und Cluster

In dieser Doktorarbeit werden verschiedene Methoden präsentiert, um anisotrope Teilchen herzustellen, die Modellen von Molekülen ähneln. Wie oben schon angedeutet, werden Kolloide oft als Modellatome verwendet, z.B. in der Forschung an Kristallen oder Flüssigkeiten. In den Kapiteln 2 und 3 zeigen wir, dass Kolloide mit Tröpfchen an der Oberfläche eine Bindung eingehen können, indem die Tröpfchen zusammenfließen. Anschließend können die Tröpfchen gehärtet ("polymerisiert") werden, um feste Kolloide zu erhalten. Dieser selbstassemblierende Prozess ist analog zu Atomen, die mittels einer Bindung Moleküle formen. Solche Kolloide werden dann auch "Kolloidale Moleküle" genannt. Man kann sie auch als eine besondere Form von "patchy" Teilchen sehen: Wenn das Material der Tröpfchen ein anderes ist als das der Kolloide, erhält man "Patches" mit anderen Oberflächeneigenschaften. Wir können die Positionen und Größe der Patches kontrollieren, und so zum Beispiel Kolloide herstellen, die Wassermolekülen ähneln.

Ein direkterer Weg, um kolloidale Moleküle herzustellen, wird in Kapitel 4 vorgestellt. Hier zeigen wir, dass mehrere Tröpfchen an der Oberfläche von Kolloiden erzeugt werden können. Die Verschmelzung der Tröpfchen an der Oberfläche wird beeinflusst durch die Oberflächenspannung und das Volumen der Tröpfchen. Mit der Polymerisation der Tröpfchen erhält man einheitliche kolloidale Moleküle in großer Anzahl.

Wenn man diesen Verschmelzungsprozess nicht durch die Polymerisation stoppt, entstehen große Tropfen mit vielen hunderten bis tausenden Kolloiden an der Oberfläche. In Kapitel 5 studieren wir diesen Prozess und analysieren die Positionen der Kolloide. Wir versuche des Weiteren, die Tropfen zu entfernen, und erhalten dadurch Cluster, d.h. eine Ansammlung von Kolloiden. Wir findens, dass diese Cluster ab einer bestimmten Größe Hohlräume besitzen, so dass man auch von kolloidalen Hüllen sprechen kann.

Teil 2 - Kolloidale Micellen

Die vorgestellten Methoden, kolloidale Moleküle herzustellen basieren auf einem selbstassemblierenden Prozess, nämlich der Verschmelzung von Tröpfchen an den Ober-

flächen der Kolloide. In Kapitel 6 verwenden wir die erhaltenen Kolloide, um "patchy" Teilchen zu realisieren. Dazu verwenden wir Kolloide die aus zwei kugelförmigen Hälften bestehen: die eine Hälfte ist glatt, die andere hat eine rauhe Oberfläche. Wenn Polymere zu der kolloidalen Lösung gegeben werden, entsteht eine Anziehungskraft zwischen den Kolloiden. Polymere sind eigentlich sehr lange Moleküle, aber in Lösung kann man sie sich als Wollknäuel vorstellen. Die Polymere treiben die Kolloide aufeinander zu, bis sie miteinander in Kontakt kommen und kein Polymerknäuel mehr dazwischen passt. Die Zone, in der keine Polymere mehr sein können, heißt auch Überlappungs-Zone. Weil die Polymere dennoch überall außer in der Überlappungs-Zone gegen die Kolloide stoßen, treiben sie die Kolloide auf einander zu und erzeugen dadurch eine effektive Anziehungskraft. Diese Kraft wird auch Verarmungs-Wechselwirkung ("depletion interaction") genannt. Sie ist umso stärker, je größer die Überlapp-Zone ist. Für die glatten Hälften der Kolloide ist sie deshalb stärker als für die rauhen Hälften. Man erhält einen attraktiven "Patch" an der glatten Seite der Kolloide! In Lösung formen diese Kolloide runde Strukturen, in deren Mitte die glatten Hälften der Kolloide sind. An der Außenseite sind die rauhen Hälften zu finden.

Unsere Wahl dieser Teilchen war nicht willkürlich: Seifenmoleküle bestehen auch aus zwei Hälften, nämlich aus einer Hälfte, die gerne in Kontakt mit Wasser ist, und einer Hälfte, die gerne in Kontakt mit Fett ist. Man nennt solche Moleküle "amphiphil", vom altgriechischen *amphi*=auf beiden Seiten und *phil*=liebend. In Wasser formen sie runde Strukturen, in denen die fettliebenden Hälften nach innen weisen, um so wenig wie möglich in Kontakt mit Wasser und so viel wie möglich in Kontakt mit anderen fettliebenden Molekülen zu sein. Man nennt solche Strukturen Mizellen. Unsere Kolloide mit einer rauhen und einer glatten Seite sind also ein Modellsystem für solche amphiphilen Moleküle, und formen "kolloidale Mizellen".

Teil 3 - Emulsionen

Emulsionen sind fein verteilte Gemische zweier eigentlich nicht mischbarer Flüssigkeiten, beispielsweise Öl und Wasser. Um diese Mischung zu erhalten, muss normalerweise Energie aufgewandt werden. Ein alltägliches Beispiel ist Salatsoße, für die man Öl mit Wasser mit einem Schneebesen vermengt. Ohne zusätzliche Stabilisierung der Emulsion fließen diese fein verteilten Tröpfchen wieder zusammen, bis sich zwei separate Phasen, Öl und Wasser, geformt haben. In den Kapiteln 7, 8 und 9 wird eine sehr spezielle Form von stabilen Emulsionen untersucht. Die Öltröpfchen, die in der wässrigen Phase fein verteilt sind, sind an der Oberfläche durch Kolloide stabilisiert. Man nennt solche Emulsionen auch Pickering-Emulsionen nach einem der Entdecker, Spencer Pickering. Auch die meisten Pickering-Emulsionen sind instabil und entmischen nach einiger Zeit. Die in dieser Doktorarbeit behandelten Emulsionen sind dagegen thermodynamisch stabil. Das bedeutet, dass sie sich in dem energetisch günstigsten Zustand

befinden und spontan entstehen, wenn man Wasser, Kolloide und ein spezielle Sorte Öl miteinander in Kontakt bringt. Ein klarer Gegensatz etwa zu Salatsoßen, die heftig gemischt werden müssen, bevor kleine Tröpfchen entstehen. Sie wurden erst vor kurzem von Stefano Sacanna, Willem Kegel und Albert Philipse im Van 't Hoff Laboratorium entdeckt, und es ist noch unklar, ob es sich um einen Einzelfall handelt, oder ob eine neue Klasse Emulsionen gefunden wurde.

In Kapitel 7 untersuchen wir, welche Minimalanforderungen gegeben sein müssen, um solche stabilen Pickering-Emulsionen zu erhalten. Die Resultate der systematischen Experimente liefern starke Indikationen, dass es sich hier um ein neue, stabile Klasse von Emulsionen handelt.

Obwohl diese Emulsionen als stabil bezeichnet werden, verändert sich die Tröpfchengröße mit der Zeit: in den ersten 24 Stunden schrumpfen die Tröpfchen auf circa 100 nm, bevor sie langsam über Tage bis Monate hinweg wieder wachsen. In Kapitel 8 beschreiben wir dieses subtile Gleichgewicht, das durch eine chemische Veränderung der stabilisierenden kolloidalen Teilchen induziert wird.

In Kapitel 9 wenden wir unsere erworbenen Kenntnisse auf ein neues System an. Wir untersuchen die Möglichkeit, Fettsäuren als Ölphase in diesen Emulsionen zu verwenden. Die Motivation dafür ist zum einen akademischer Natur, nämlich um herauszufinden, ob in Kapitel 7 die richtigen Minimalanforderungen identifiziert wurden. Zum anderen haben Fettsäuren große Bedeutung in industriellen Fertigungsprozessen. Ein Beispiel dafür ist Margarine, eine Emulsion aus verschiedenen Fetten und Wasser, für deren Herstellung viel Energie aufgewendet werden muss. Eine spontan ablaufende Emulsifikation benötigt keine Energie und ist daher von Interesse für eine kostengünstigere Herstellung.

Teil 4 - Ein theoretisches Modell für die Selbstassemblierung des Tabakmosaikvirus

Kapitel 10 befasst sich mit der Rekonstitution von Proteinen und einem Nukleinsäuremolekül (RNA) zum stabförmigen Tabakmosaikvirus. Das Tabakmosaikvirus ist das erste entdeckte Virus, und begründete somit das Feld der Virologie mit. Das Virus selbst besteht aus einer circa 300 nm langen und 18 nm dicken Proteinhülle, in der die RNA zwischen den Proteinen verborgen ist. Um den Prozess der Selbstassemblierung zu beschreiben, wird ein "Reißverschluss- (Zipper-)" Modell adaptiert. Das bedeutet, dass die Adsorption von Proteinmolekülen an der RNA nur in eine Richtung abläuft und am vorigen Proteinmolekül anschließt. Wir entwickeln das Modell für den statischen und dynamischen Fall, und vergleichen die Resultate mit Experimenten.

Acknowledgements

When I came to Utrecht for a PhD in experimental colloid science, I had a background as a physicist with a master thesis in theoretical plasma physics. But I was also fascinated by colloids and self-assembly. Many people have helped me to find my way around in this new research field, and contributed on a scientific and personal level to the success of my PhD.

Willem Kegel, my supervisor and mentor, gave me the opportunity to undertake this journey and guided me enthusiastically into the world of colloidal science and self-assembly. Your support and your encouragement to develop and realize my own ideas was invaluable. I very much appreciate the different angle you can give to science and life. I'm very thankful for the inspiring and great time I had as your PhD student. But also on a personal level, I couldn't have wished for a better "Doktorvater", and with Marianne Westendorp, for a better "Doktormutter". Thank you for everything!

Within the Van't Hoff laboratory and the Soft Condensed Matter group, many people have contributed directly and indirectly to this thesis: In a common effort the emulsion team consisting of Stefano Sacanna, Bob Luigjes, Julius de Folter, Sonja Castillo, and Albert Philipse unravelled the mystery of the stable Pickering emulsions leading to two publications and several theoretical and experimental follow-up studies. On the theoretical side Jos Zwanikken, and René van Roij at the ITF, as well as Jan Groenewold at the Van 't Hoff laboratory helped to develop a deeper understanding of the physical principles underlying the emulsions. Jan Groenewold contributed to many parts of this thesis with his questions and creative ideas during and outside the weekly brainstorm sessions. For input during these brainstorm sessions, I also thank Sandra Veen, Ethayaraja Mani, Mikal van Leeuwen, Laura Rossi, Soumyajit Roy, and Tian Hui Zhang. My students Sonja Castillo, Freddy Rabouw, Sandy Heinen, Suzanne Woudenberg, Mathijs Hoogenraad, and Vera Abramova I thank for their enthusiasm and their valuable contributions to this thesis.

Many thanks also go to all the researchers in the Van 't Hoof laboratory and the soft condensed matter groups of Alfons van Blaaderen, Marjolein Dijkstra, and Arnout Imhof, as well as the group of René van Roij at the ITF, for inspiring and insightful discussions, collaborations, and the occasional drinks. These collaborations especially involved Carlos van Kats, Wessel Vlug, Ni Ran, and Michiel Hermes, but also Laura Filion, Teun Vissers, Peter van Oostrum, Niels Boon, Rao Vutukuri, Ahmet Demirörs, Johan Stiefelhagen, Matthieu Marechal, Anke Kuik, Frank Smallenburg and Krassimir

Velikov. Paul van der Schoot, partially at TU Eindhoven and the ITF, has introduced me to the fascinating world of virus assembly. Your enthusiasm and knowledge were a great source of inspiration, scientifically and beyond. Kisun Yoon and Dave Weitz are thanked for the opportunity to work in their lab at Harvard University and sharing their insights into the synthesis of anisotropic colloids.

To make four years a success a good support crew is a necessity. Hans Meeldijk, Chris Schneijdenberg, and Matthijs de Winter, as well as Emile Bakelaar, Bonny Kuipers, Dominique Thies, Kanvaly Lacina, and Marina de Bulten-Weerensteijn have always had a helping hand and showed interest in my work. Thank you.

At and around work, many people contributed to nice atmosphere and a good time. I'd like to thank my office mates Volkert de Villeneuve, Mark Klokkenburg, Jan Hilhorst, Ethayaraja Mani and Janne-Mieke Meijer for all the laughs and discussions. I'd like to especially thank Sandra Veen, Maurice Mourad, Elif Karagoz, and Sandra Kling for the 'gezelligheid'. The people at the van 't Hoff lab Esther van den Pol, Lia Verhoeff, Suzanne van Berkum, Jos van Rijssel, Andrei Kyrylyuk, Dima Byelov, Dzina Kleshchanoc, Agniezka Paszun-Chojnicka, Andrei Petukhov, Ben Erné, Gert-Jan Vroege and Henk Lekkerkerker added in one way or the other to the success of my PhD.

I would also like to express my thanks to the friends that I've made over the past years. The extended "Dutch class of 2007": Jens Steffen, Chris Conolly, Ana Arda Freire, Jacques Doux, Lucie Khemtemourian, Laurie Palasse, Doug LaRowe, Takeshi Kuramochi, Iana Tsandev, José Mogollon, Andrea Gorlani, Emma Martinez Sanchez, Oscar Velazquez, Héctor Galué, Angelica Candido, Lavinia Opris, Emmanuelle Simili, Julie Melling, Saad Shah, and Pierre-Olivier Guerra. My volleyball team: Anke Leferink op Reinink, Liesbeth Kreuk, Annerie Overzet, Hester Blok, Maarten Blok, Wouter Nieuwenburg and Joost van Gijn. The physicists from Würzburg: Andreas Vernaleken, Christian Holzner, Christian Ott, Christian Kern, Philipp Ulrich, Simon Hame, Kirsten Viering, Tobias Bartsch, Roland Fäustlin, Thomas Greif, Max Riedel, and (in a wider sense) Frauke Schäfer and Caroline Günzel. Also, I'd like to mention Natalia Zibibbo and Anna Abelmann-Brockmann. Thank you all for the friendship over the years!

Michael Keller, thanks for the friendship, and for being my paranimf. I cannot imagine anyone better to stand behind me during my defense.

Rob, mit dir scheint die Sonne! Thank you so much for your support, being my paranimf, and the wonderful time we've spent together.

Vielen Dank an meine Familie, insbesondere an meine Eltern, Ursula und Wolfgang, und an meinen Bruder, Matthias, für Eure uneingeschränkte Unterstützung und Liebe.

Daniela.

Curriculum Vitae

Daniela Jutta Kraft was born February, 5 1983 in Würzburg, Germany. She graduated with a focus on physics and biology from the Riemenschneider Gymnasium in Würzburg in 2002 with a grade of 1.2 (where 1 is best, 6 is worst). From 2002 until 2004 she did her undergraduate studies in physics with a minor in chemistry at the Julius-Maximilians Universität, Würzburg, Germany. She received her Vordiplom (Bachelor equivalent) with honors in October 2000. The German National Academic Foundation (Studienstiftung des deutschen Volkes) awarded her a scholarship for graduate studies in physics at the Julius-Maximilians Universität Würzburg, with a minor in biophysics. From July 2005 on she was a graduate student in physics at The University of Texas at Austin, financially supported by a grant for studies abroad by the German National Academic Foundation, and the Paul C. Boner graduate fellowship for physics. Under supervision of Roger Bengtson and Boris Breizman she performed her master research project on modeling the propagation of electromagnetic waves through a cylindrical plasma. She graduated as a Master of Arts in physics from The University of Texas at Austin in August 2006 with a grade point average of 4.0. In October 2006 she started her PhD research at the Van 't Hoff Laboratory for Physical and Colloid Chemistry under supervision of Willem K. Kegel. She has presented her work at several national and international conferences, including physics@FOM, the 5th Dutch Soft Matter Meeting, the 83rd ACS Colloid and Surface Science symposium, the 'Amsterdam-New Amsterdam' meeting, the Jüelich Soft Matter Days, the 'Liquids and Interfaces' meeting, as well as the Gordon Research conference on 'Colloidal, Macromolecular and Polyelectrolyte Solutions'.